Gene pieces of the heart

Regulation of cardiac alternative splicing

Montañés Agudo, P.

Publication date
2023

Document Version
Final published version

GENE PIECES OF THE HEART

Regulation of Cardiac Alternative Splicing

Pablo Montañés Agudo

Gene Pieces of the Heart

Regulation of Cardiac Alternative Splicing

Pablo Montañés Agudo

ISBN: 978-94-93278-48-6

Cover design: Pablo Montañés Agudo
Layout and printing: Off Page, Amsterdam

Financial support by the Dutch Heart Foundation for the publication of this thesis is gratefully acknowledged. Additional financial support for printing of this thesis was kindly provided by BioSemi B.V.

Gene Pieces of the Heart
Regulation of Cardiac Alternative Splicing

ACADEMISCH PROEFSCHRIFT

ter verkrijging van de graad van doctor
aan de Universiteit van Amsterdam
op gezag van de Rector Magnificus
prof. dr. ir. P.P.C.C. Verbeek
ten overstaan van een door het College voor Promoties ingestelde commissie,
in het openbaar te verdedigen in de Agnietenkapel
op donderdag 29 juni 2023, te 16.00 uur

door Pablo Montañés Agudo
geboren te Zaragoza

Promotiecommissie

Promotor:	prof. dr. Y.M. Pinto	AMC-UvA
Copromotor:	dr. E.E.J.M. Creemers	AMC-UvA
Overige leden:	prof. dr. V.M. Christoffels	AMC-UvA
	prof. dr. J.R. de Groot	AMC-UvA
	dr. E.M. Lodder	AMC-UvA
	prof. dr. E. van Rooij	Universiteit Utrecht
	dr. D.G. Wansink	Radboudumc
	prof. dr. A.J. van Zonneveld	Universiteit Leiden

Faculteit der Geneeskunde

A mis padres

TABLE OF CONTENTS

CHAPTER 1

INTRODUCTION AND SCOPE OF THIS THESIS

INTRODUCTION

"Why genes in pieces?"

Most genes in the human genome are not continuous coding sequences of DNA, but are interrupted by "silent" DNA fragments. These "silent" pieces of DNA are named introns (from "intragenic region") and split genes into their actual protein-coding segments known as exons[1]. In order to generate a mature and functional RNA transcript, the entire gene is first transcribed into a continuous sequence of exons and introns. Introns must later be excised through a process named splicing to create a mature mRNA consisting solely of the remaining exons.

At first sight, introns may seem like a burden for the genome. Human genes are on average interrupted by 7.8 introns[2]. In certain genes, the number of introns can be massive. For instance, the gene titin (*TTN*), which encodes the protein that forms the molecular spring of the heart, is interrupted by 362 introns. Introns are also much longer than exons. While the average length of an exon is only 170 bp, introns are on average 5,419 bp long. That is the average, but when looking at specific introns they can reach enormous lengths, as ~5% of all the introns are larger than 200,000 bp[3]. In fact, when considering the entire human genome, exons only represent 1.1 % of the DNA, and introns account for 24%[4]. So, why are introns so common? Why are genes split into pieces[1]?

Introns are essential for eukaryotic genomes because they bring flexibility to genes. By splitting genes into exons, introns confer a modular structure. Exons can be assembled in different configurations to create alternative transcripts from a single gene. This mechanism, named alternative splicing, creates new RNA sequences with novel functions, such as encoding various protein isoforms or incorporating different regulatory elements. This way, alternative splicing greatly expands the coding potential of the genome. From the ~20,000 genes present in the human genome more than 100,000 alternative spliced transcripts are produced[2]. It is currently estimated that 95% of the human genes undergo alternative splicing[2]. All of this makes alternative splicing a crucial mechanism of gene regulation that determines the functioning of our cells and body.

In the heart, alternative splicing plays a crucial role in producing the specific cardiac isoforms required for the mechanical, electrical, and metabolic functions of cardiomyocytes[5,6]. Alternative splicing generates new isoforms for essential cardiac genes, including structural components of the sarcomeres like troponin T (*TNNT2*) or titin (*TTN*); ion channels like the voltage-gated sodium (*SCN5A*) and calcium (*CACNA1C*) channels; signaling proteins like Ca^{2+}/calmodulin-dependent protein kinase (*CAMK2D*), and many other regulators such as the transcription factors from the Myocyte Enhancer Factor 2 (MEF2) family. The alternative isoforms created by splicing display distinct features to the canonical one.

These differences range from minor changes in substrate affinity, to novel functional domains and even proteins with a completely opposite function. This is the case for the transcription factors MEF2A, MEF2C and MEF2D[6–8]. The alternative splicing of a single exon in these transcription factors creates isoforms that behave either as transcriptional activators or as transcriptional repressors. While isoforms including exon α2 behave as transcriptional activators, isoforms including α1 behave as repressors of transcription by recruiting histone deacetylases (HDAC4/9) to the same subset of target genes[9].

Alternative splicing is a fundamental mechanism regulating the function of the heart. During cardiac development, alternative splicing generates new isoforms to adapt the properties of the heart to the growing demands of the body[10–12]. During disease, alternative splicing responds to stressors by generating new isoforms to cope with the pathological challenge[13,14]. Defects in alternative splicing due to genetic mutations can also cause certain cardiomyopathies, such as the RBM20-related cardiomyopathy[15]. Therefore, understanding how alternative splicing is regulated in the heart can provide insights into the fundamental origins of cardiac function and disease.

This thesis aims to further expand our understanding of the molecular mechanisms and regulators of cardiac alternative splicing.

The splicing reaction, the spliceosome(s) and splicing factors

The first step in gene expression is the transcription of the entire sequence of the DNA into pre-mature mRNA (pre-mRNA). Along this process, multiple small nuclear RNAs (snRNAs) and proteins bind to the nascent pre-mRNA in order to process it into a mature mRNA. One of the main steps in this process is the removal of introns by the splicing reaction.

The splicing reaction is a two-steps reaction than removes an intron while ligating the two flanking splices sites together (**Figure 1A**)[16]. The catalyst of this reaction is a large RNA-protein complex named the spliceosome. The different snRNAs and protein components of the spliceosome assemble along the splicing sites of the intron in sequential steps in order to catalyze the splicing reaction (**Figure 1B**).

There are two different types of introns based on their consensus sequences (i.e. 5' splice site, branch point sequence, 3' splice site): major or U2-dependent introns and minor or U12-dependent intron (**Figure 1C**). The major and minor introns require different types of spliceosomes for excision: the major or U2-dependent spliceosome and the minor or U12-dependent spliceosome. Some of the core components of the spliceosome are shared between the two types of spliceosomes, but others are specific to each spliceosome.

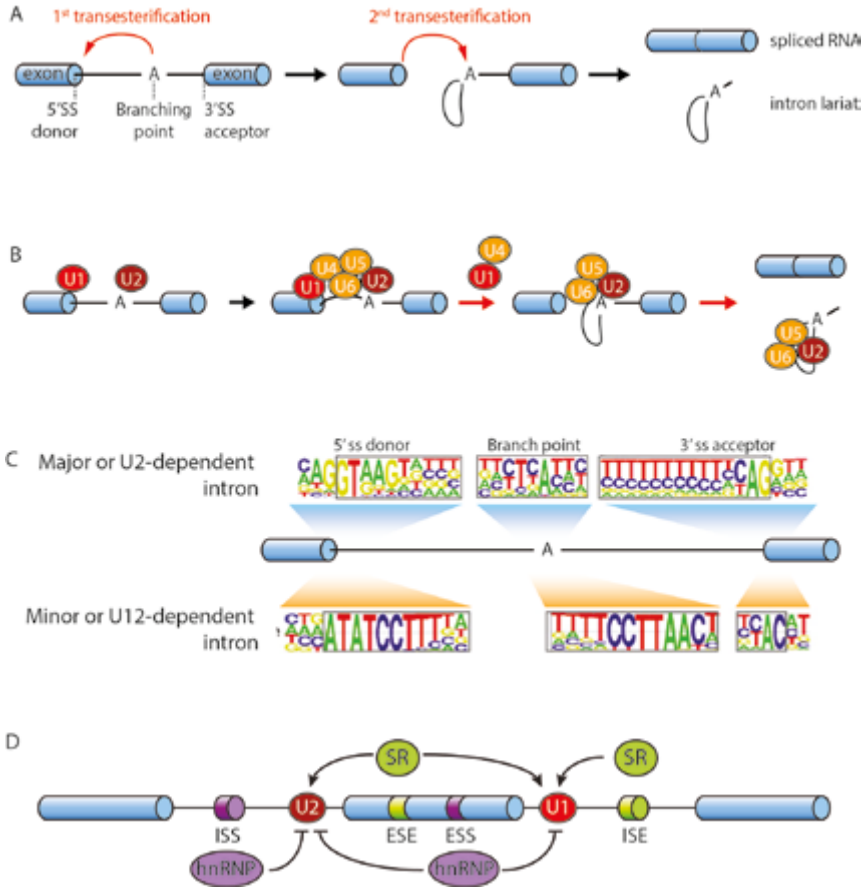

Figure 1. Basis of RNA splicing. (A) The splicing reaction links two exons in a two transesterification reaction. The first step is the nucleophilic attack of the 2′-hydroxyl group of an adenosine residue in the polypyrimidine region of the intron (i.e. the branch-point adenosine) to the phosphodiester bond of the 5' residue of the intron. This results in a intronic lasso structure (lariat intermediate) and a free exon with a 3′-hydroxyl group. The free exon (i.e. the donor exon) performs a second nucleophilic attack to the phosphodiester bond of the 3′ splice site (i.e. the acceptor exon). The end result is the ligation of the two exons and the release of the intron in the shape of a lariat[16]. (B) The spliceosome is a large RNA-protein complex that catalyzes splicing. snRNAs components build the core of the spliceosome and assemble the pre-mRNA in consecutive order to catalyze the splicing reaction. (C) Two different types of introns exist in eukaryotic genomes. They display unique sequences that are recognized by the major or minor spliceosome. Sequence logos adapted from (Akinyi et al, 2021)[17]. (D) Splicing factors bind to the pre-mRNA to regulate splicing. Typically, serine/arginine-rich (SR) proteins bind to exonic and intronic splicing enhancer sequences (ESE and ISE respectively) to activate splicing; and heterogeneous nuclear ribonuclear proteins (hnRNPSs) bind to exonic and intronic splicing silencer sequence (ISS and ESS) to repress it. Diagram adapted from (Kornblihtt et al, 2013)[18].

Since the vast majority of introns are major introns (>99%), and only a minority (<1%) represents minor introns, the expression levels of the major spliceosome components are larger than those of the minor spliceosome[19,20]. The reason why both major and minor introns exist in the human genome remains an enigma, but the enrichment of minor introns in specific gene families (e.g. voltage-gated Na^+ and Ca^{2+} channels) suggests that they control the expression of specific subsets of genes.

The regulators of splicing are splicing factors. These are proteins that bind to specific sequences of the nascent pre-mRNA (i.e. cis-regulatory sequences) to control where the spliceosome acts (**Figure 1D**). By controlling which splice sites react together, splicing factors control which alternative RNA sequence is formed. It is estimated that 300 to 400 splicing regulators exist in humans[21,22], and they regulate splicing through distinct mechanisms. For example, while the serine/arginine-rich splicing factors (SR proteins) generally favor exon inclusion by recruiting spliceosome components; splicing factors from the family of heterogeneous nuclear ribonucleoprotein (hnRNPs) mostly antagonize SR proteins. Many other splicing factors, such as Quaking (QKI) can act as positive or negative regulators of splicing depending on the location where they bind[23].

Alternative splicing generates novel RNA sequences carrying new functions

Alternative splicing unzips the full potential of genes by creating multiple combinations of exons. Introducing or skipping different exons enable the creation of new sequences encoding new protein isoforms with varying properties. New amino acid sequences of a protein can change its binding properties to substrates and to interactors, they can modify its enzymatic activity, they can alter the protein localization and stability, and they can introduce residues susceptible to post-translational modifications[6,24].

Up to seven different types of RNA splicing can be identified based on the exons and the splicing sites used in the splicing reaction (**Figure 2**)[13,25]. These modalities of alternative splicing, in combination with alternative promotor usage and alternative polyadenylation, give raise to the tremendous diversity of RNA transcripts and proteins observed in humans.

Splicing can also control gene expression by unproductive splicing: a modality of splicing in which the skipping of an essential exon, the inclusion of a "poison" exon, or the retention of an intron introduces a premature stop codon that target the mRNA for degradation by the nonsense-mediated mRNA decay (NMD) pathway[26]. This phenomenon has been observed to control the gene expression of SR splicing factors[26] and to prevent the expression of the *MYH7b* gene in the heart[27].

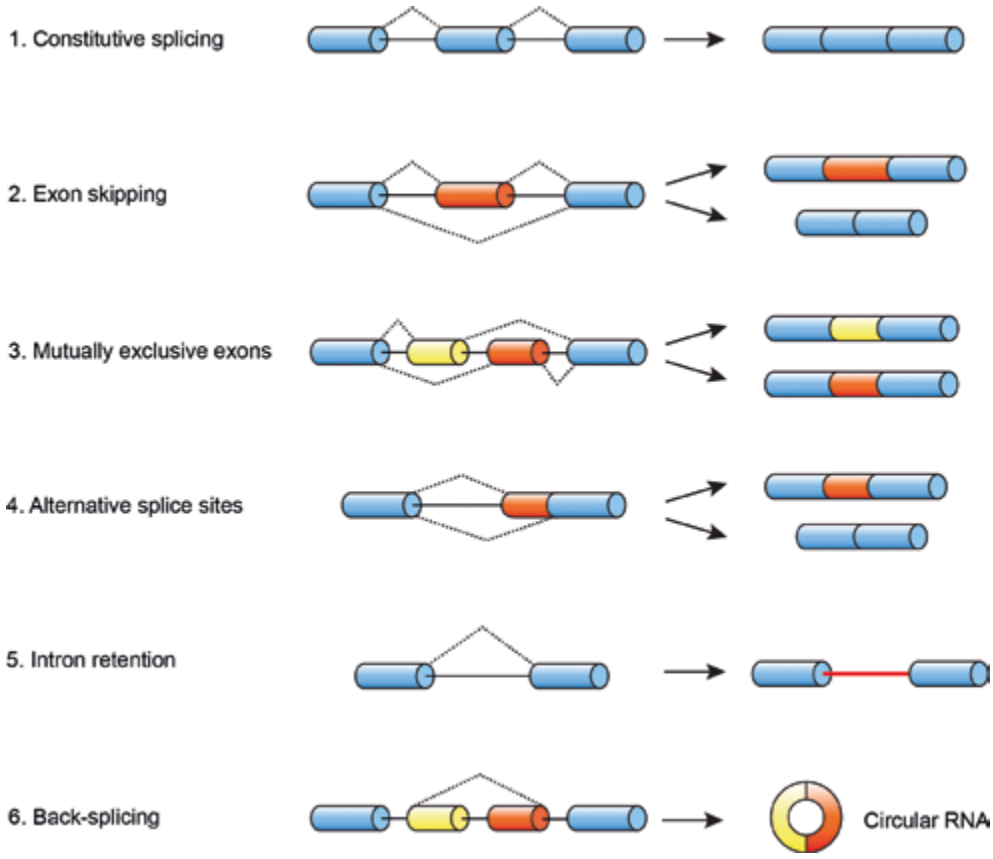

Figure 2. Modalities of RNA splicing found in mammalian cells. (1) **Constitutive splicing,** where all the exons of a gene are spliced in a consecutive manner**.** (2) **Exon skipping,** where one or more exons are not included in the final transcript. (3) **Mutually exclusive exons,** where only one or some exons of a region of the pre-mRNA can be included at the same time. (4) **Alternative splice sites,** where different splice sites from an exon can be used. Depending on the alternative splice sites, there is a distinction between 5' or 3' alternative splice site. This modality is also known as tandem splice sites, because the splice sites are disposed in a close tandem arrangement. (5) **Intron retention,** where an intron is not spliced out of the transcript. Retained introns often compromise the function of the transcript by impeding the translocation out of the nucleus and/or by introducing premature stop codons into the coding sequence. (6) **Back-splicing,** where the donor splice site is upstream to the acceptor. This disposition is opposite to linear splicing, and creates a new kind of RNA molecule with a covalently closed circular structure, a circular RNA (circRNA). (7) **Trans-splicing** (not shown), where exons from two different RNA transcripts are spliced together to form a new chimeric sequence. Although this phenomenon occurs in certain organisms, it does not occur naturally in mammalian cells, except in some human cancers.

Alternative splicing can also process long non-coding RNAs and non-coding sequences within mRNAs. Splicing of the 3' untranslated region (3'-UTR) can introduce miRNA binding sites or can affect the interaction of the mRNA with other elements, such as RNA-binding binding proteins[13]. A modality of splicing named back-splicing (**Figure 2**) creates circular RNAs (circRNAs), a new species of regulatory non-coding RNA with a circular structure. These circular transcripts are starting to gain attention for their regulatory roles in diverse pathophysiological processes. For example, circRNAs arising from the gene titin have been shown to act as miRNA sponges and as regulators of the splicing factors SRSF10 and RBM20[28].

Alternative splicing drive heart development

Each cell type presents a unique alternative splicing program that is determined by the specific combination of splicing factors expressed in that cell type. The splicing program of cells is dynamic and mostly changes during cellular differentiation. This is why the splicing pattern observed in each tissue of the body changes during embryonic development[10]. For example, throughout the course of myogenic differentiation, the expression of the splicing factor Quaking (QKI) increases while Polypyrimidine Tract Binding Protein (PTB) is reduced[29]. This shift in expression of splicing factors drives the upregulation of QKI-activated exons and the downregulation of PTB-repressed exons, thus making the proper switch of protein isoforms during myogenesis[29].

In the heart, the expression levels of many splicing factors change to adapt the splicing program to each developmental stage (e.g. CELF1, QKI, MBNL1-2, RBFOX1-2, RBM24)[11,30]. The most iconic splicing change in the heart takes place in the gene titin (*TTN*). TTN is a sarcomere protein that behaves as a molecular spring and confers elasticity to cardiomyocytes[31]. Changes in alternative splicing generates diverse TTN isoforms of varying length that determine the stiffness of the myocardium. The full length isoform of TTN is present in embryonic hearts and is compliant; the shorter isoforms N2BA and N2B isoforms are observed in adult hearts and they are stiffer. As a result of this splicing event, the stiffness of the myocardial wall adapts to the changing demands of the developing embryo. The main driver of this splicing change is the increasing expression of the splicing factor RBM20 during heart development. RBM20 acts as a splicing repressor, and prevents the inclusion of certain exons to switch from long and elastic TTN to short and stiff TTN[15,32].

Splicing changes upon cardiac stress

The alternative splicing program in the adult heart is not static. It constantly adapts to the changing (patho-)physiological demands of the heart. In human and rodent models, splicing changes have been observed under different types of stress and pathologies, such

as hypertrophy and heart failure[33–36]. A re-activation of the fetal splicing program occurs in mouse hearts in response to pressure overload, induced by the transverse aorta constriction (TAC) procedure[35]. Fetal splice isoforms are also observed in the context of human heart failure. Interestingly, the fetal splicing pattern is reversed after left ventricular assist device (LVID) implantation, which indicates that splicing may act as a compensatory mechanism to the changes in the mechanical forces that the heart faces[36].

These alterations in the alternative splicing program in cardiomyocytes result from changes in the expression of splicing factors and other regulators. The expression of certain splicing factors in the heart, like QKI[37], SLM2[38], RBFOX1[9] or RBFOX2[39], is altered in numerous pathological conditions, such as heart failure, hypertrophy or pressure overload. Post-translational modifications and changes in the intracellular location of splicing factors also participate in alterations of the splicing program[40,41]. For instance, the heterogeneous nuclear ribonucleoprotein C (hnRNPC) responds to mechanical stress during heart failure by relocating to the sarcomeric Z-disc. Even though hnRNPC expression is increased in disease, the translocation of hrRNPC from the nucleus to the sarcomere prevents its function as splicing factor and affects the splicing of many targets[42]. Other regulators of splicing, such as long non-coding RNAs (lncRNAs), also participate in tuning the splicing program. For example, the lncRNA triadin-antisense (*TRDN-AS*) regulates the balance between different isoforms of triadin during development and heart failure[43].

Defects in splicing can cause inherited cardiomyopathies

Defects in splicing can have serious consequences for gene expression. In the heart, they can translate to loss of cardiac isoforms and the development of severe cardiomyopathies. Mutations or variants in the cis-regulatory sequences of mRNAs can impair splicing. For instance, a disrupted spliced site or branch point site can induce intron retention or the skipping of an exon. Even if only one nucleotide is skipped, a frame shift can disrupt the entire amino acid sequence. In the best case scenario, this kind of mutation introduces a premature stop codon that targets the mutant coding sequence for the NMD pathway. In the worst case scenario, it creates a dominant negative protein that interferes with the remaining protein, derived from the healthy allele[44]. Variants in splice sites are common in humans. 9.4% of all the protein-coding variants found in the Genome Aggregation Database (gnomAD) correspond to splice site variants[45]. Some of these variants have been linked to cardiomyopathies. For example, splice variants in the genes *TTN*, *LMNA* and *DMD* have been linked to dilated cardiomyopathy (DCM); in *TTN*, *TNNT2* and *MYBPC* to hypertrophic cardiomyopathy (HCM); in *PKP2*, *JUP*, and *DSG2* to arrhythmogenic right ventricular cardiomyopathy; in *KCNH2* and *KCNQ1* to long QT syndrome; in *SCN5A* to Brugada syndrome; and in *GATA4* and *NR2F2* to congenital heart disease[46].

In addition to disrupting existing splice sites, mutations can also create new splice sites (i.e. activate cryptic splice site) in the middle of an exon or intron. This new splice site can change the splicing pattern of the transcript and disrupt the coding sequence[44]. It is estimated that 11% of de novo mutations are pathological due to the activation of a cryptic splice site in introns[47].

Mutations in splicing factors can also lead to disease. In the heart, mutations in the RNA-binding motif protein 20 (RBM20) account for 3% of the familial DCM cases[48]. The cardiac-specific splicing factor RBM20 participates in the splicing of multiple genes, including *TTN* and *CAMK2D*. Loss-of-function mutations can disrupt the entire RBM20 splicing network. As a result, RBM20 mutation carriers present a rapidly progressing heart failure and an increased risk of arrhythmias[48]. So far, no other therapy than heart transplant is available for these patients. Mutations in many other splicing factors have been linked to disease. Not specifically to cardiac disease, but to broad neuromuscular disorders that present cardiac symptoms among others. Patients with spinal muscular atrophy caused by mutations in the splicing factor survival motor neuron 1 (SMN1) also display bradycardia and premature heart failure[49]. These cardiac symptoms were thought to originate from innervation problems, but some *in vitro* models have shown that SMN1 is also important for cardiomyocyte function[50,51]. Mutations in the ubiquitously expressed RNA-binding protein FUS are responsible for amyotrophic lateral sclerosis (ALS), a neuromuscular disease in which patients also present an increased risk for arrhythmias and sudden cardiac death[52]. Core components of the spliceosome can also be mutated, and result in severe and pleiotropic syndromes. For example, mutations in the components of the minor spliceosome have been linked to complex neurological and growth disorders, in which sometimes there are also cardiac abnormalities[53].

Another splicing-related disease with a cardiac component is myotonic dystrophy (DM). DM is a neuromuscular disorder caused by expanded nucleotide repeats present in some mRNAs. These aberrant repetitions sequester splicing factors and interfere with their function. The main splicing effect observed during DM is the loss of function of the splicing factor MBNL and the increase of CELF (/CUG-BP). There are 2 types of DM depending on the nature of the repeats: DM1 (caused by the expansion of CUG repeats in the 3' UTR of the *DMPK* gene) and DM2 (caused by the expansion of CCUG-repeats in the intron 1 of *ZNF9*). Although different, these two diseases share molecular mechanisms and present common symptoms, such as myotonia, muscle weakness, cardiac conduction defects and arrhythmias[54].

Taken together, inherited cardiac diseases caused by splicing defects reveal the essential role of RNA splicing in heart function.

SCOPE OF THIS THESIS

In this thesis, we focus on the molecular mechanisms and regulators of cardiac alternative splicing.

In **Chapter 2,** we study the cardiac-enriched splicing factor quaking (QKI) in the developing and adult heart. To do so, we generated mice with conditional deletion of QKI in cardiomyocytes by the Cre-Lox system and we characterized them functionally. We performed RNA sequencing to assess changes in gene expression and exon usage to determine how QKI regulates alternative splicing in the heart.

In **Chapter 3**, we delve deeper into QKI-dependent splicing by focusing on back-splicing and circRNA formation. By using the QKI knock-out mouse model that we developed, we identified numerous circRNAs regulated by QKI in the heart. We assess how changes in these circRNAs relate to changes in linear splicing of the host genes. In addition, we compare circRNA formation changes occurring in this model with those occurring in RBM20 knock-out mice.

In **Chapter 4,** we re-examine several splicing factor knock-out mouse models that have been developed in the last decades. We retrieved and analyzed original RNA-sequencing data from eight published mouse models in which splicing factors have been genetically deleted (HNRNPU, MBNL1/2, QKI, RBM20, RBM24, RBPMS, SRSF3, SRSF4). We assess commonalities and differences between the splicing networks of these factors, and we show how changes in their expression correlate with changes in alternative splicing in a large cohort of heart failure patients.

In **Chapter 5,** we turn our attention to an unusual class of introns, namely minor or U12-dependent introns. Even though minor introns are enriched in crucial genes for cardiomyocytes (e.g. sodium and calcium channels, MAPKs, and calpains), little is known about their relevance in the (electro-)physiology of the heart. To study them, we inhibit minor splicing in cardiomyocytes by knocking downthe snRNA U6atac, and we examine the consequences on the expression and function of sodium and calcium channels.

In **Chapter 6,** we comment on a study investigating the role of the long non-coding RNA triadin-antisense in the regulation of cardiac splicing.

Finally, we conclude by summarizing the findings of this thesis and discussing the future directions in the field.

REFERENCES

1. Gilbert, W. Why genes in pieces? *Nature* **271**, 501–501 (1978).
2. Pan, Q., Shai, O., Lee, L. J., Frey, B. J. & Blencowe, B. J. Deep surveying of alternative splicing complexity in the human transcriptome by high-throughput sequencing. *Nat Genet* **40**, 1413–1415 (2008).
3. Sakharkar, M. K., Chow, V. T. K. & Kangueane, P. Distributions of exons and introns in the human genome. *In Silico Biol* **4**, 387–393 (2004).
4. Venter, J. C. *et al.* The Sequence of the Human Genome. *Science* **291**, 1304–1351 (2001).
5. Weeland, C. J., Hoogenhof, M. M. van den, Beqqali, A. & Creemers, E. E. Insights into alternative splicing of sarcomeric genes in the heart. *Journal of Molecular and Cellular Cardiology* **81**, 107–113 (2015).
6. Nakka, K., Ghigna, C., Gabellini, D. & Dilworth, F. J. Diversification of the muscle proteome through alternative splicing. *Skeletal Muscle* **8**, 8 (2018).
7. Cornwell, J. D. & McDermott, J. C. MEF2 in cardiac hypertrophy in response to hypertension. *Trends in Cardiovascular Medicine* (2022) doi:10.1016/j.tcm.2022.01.002.
8. Zhang, M., Zhu, B. & Davie, J. Alternative splicing of MEF2C pre-mRNA controls its activity in normal myogenesis and promotes tumorigenicity in rhabdomyosarcoma cells. *J Biol Chem* **290**, 310–324 (2015).
9. Gao, C. *et al.* RBFox1-mediated RNA splicing regulates cardiac hypertrophy and heart failure. *J Clin Invest* **126**, 195–206 (2016).
10. Mazin, P. V., Khaitovich, P., Cardoso-Moreira, M. & Kaessmann, H. Alternative splicing during mammalian organ development. *Nat Genet* **53**, 925–934 (2021).
11. Baralle, F. E. & Giudice, J. Alternative splicing as a regulator of development and tissue identity. *Nat Rev Mol Cell Biol* **18**, 437–451 (2017).
12. Wang, H. *et al.* Genome-wide analysis of alternative splicing during human heart development. *Sci Rep* **6**, 35520 (2016).
13. van den Hoogenhof, M. M. G., Pinto, Y. M. & Creemers, E. E. RNA Splicing. *Circulation Research* **118**, 454–468 (2016).
14. Martí-Gómez, C. *et al.* Functional Impact and Regulation of Alternative Splicing in Mouse Heart Development and Disease. *J. of Cardiovasc. Trans. Res.* **15**, 1239–1255 (2022).
15. Guo, W. *et al.* RBM20, a gene for hereditary cardiomyopathy, regulates titin splicing. *Nat Med* **18**, 766–773 (2012).
16. Will, C. L. & Lührmann, R. Spliceosome Structure and Function. *Cold Spring Harb Perspect Biol* **3**, a003707 (2011).
17. Akinyi, M. V. & Frilander, M. J. At the Intersection of Major and Minor Spliceosomes: Crosstalk Mechanisms and Their Impact on Gene Expression. *Frontiers in Genetics* **12**, (2021).
18. Kornblihtt, A. R. *et al.* Alternative splicing: a pivotal step between eukaryotic transcription and translation. *Nat Rev Mol Cell Biol* **14**, 153–165 (2013).
19. Montañés-Agudo, P. *et al.* Inhibition of minor intron splicing reduces Na+ and Ca2+ channel expression and function in cardiomyocytes. *J Cell Sci* **135**, jcs259191 (2022).
20. Baumgartner, M., Drake, K. & Kanadia, R. N. An Integrated Model of Minor Intron Emergence and Conservation. *Frontiers in Genetics* **10**, 1113 (2019).
21. Seiler, M. *et al.* Somatic Mutational Landscape of Splicing Factor Genes and Their Functional Consequences across 33 Cancer Types. *Cell Reports* **23**, 282-296.e4 (2018).
22. Fisher, E. & Feng, J. RNA splicing regulators play critical roles in neurogenesis. *WIREs RNA* **13**, e1728 (2022).
23. Fu, X.-D. & Ares, M. Context-dependent control of alternative splicing by RNA-binding proteins. *Nat Rev Genet* **15**, 689–701 (2014).
24. Marasco, L. E. & Kornblihtt, A. R. The physiology of alternative splicing. *Nat Rev Mol Cell Biol* 1–13 (2022) doi:10.1038/s41580-022-00545-z.
25. Beqqali, A. Alternative splicing in cardiomyopathy. *Biophys Rev* **10**, 1061–1071 (2018).
26. Lareau, L. F., Inada, M., Green, R. E., Wengrod, J. C. & Brenner, S. E. Unproductive splicing of SR genes associated with highly conserved and ultraconserved DNA elements. *Nature* **446**, 926–929 (2007).
27. Lee, L. A., Broadwell, L. J., Buvoli, M. & Leinwand, L. A. Nonproductive Splicing Prevents Expression of MYH7b Protein in

the Mammalian Heart. *Journal of the American Heart Association* **10**, e020965 (2021).

28. Tijsen, A. J. *et al.* Titin Circular RNAs Create a Back-Splice Motif Essential for SRSF10 Splicing. *Circulation* **143**, 1502–1512 (2021).
29. Hall, M. P. *et al.* Quaking and PTB control overlapping splicing regulatory networks during muscle cell differentiation. *RNA* **19**, 627–638 (2013).
30. Giudice, J. & Cooper, T. A. RNA-binding proteins in heart development. *Adv Exp Med Biol* **825**, 389–429 (2014).
31. Gigli, M. *et al.* A Review of the Giant Protein Titin in Clinical Molecular Diagnostics of Cardiomyopathies. *Front Cardiovasc Med* **3**, 21 (2016).
32. Maatz, H. *et al.* RNA-binding protein RBM20 represses splicing to orchestrate cardiac pre-mRNA processing. *J Clin Invest* **124**, 3419–3430 (2014).
33. Kong, S. W. *et al.* Heart Failure–Associated Changes in RNA Splicing of Sarcomere Genes. *Circulation: Cardiovascular Genetics* **3**, 138–146 (2010).
34. Heinig, M. *et al.* Natural genetic variation of the cardiac transcriptome in non-diseased donors and patients with dilated cardiomyopathy. *Genome Biology* **18**, 170 (2017).
35. Ames, E., Lawson, M., Mackey, A. & Holmes, J. Sequencing of mRNA identifies re-expression of fetal splice variants in cardiac hypertrophy. *J Mol Cell Cardiol* **62**, 99–107 (2013).
36. D'Antonio, M. *et al.* In heart failure reactivation of RNA-binding proteins is associated with the expression of 1,523 fetal-specific isoforms. *PLOS Computational Biology* **18**, e1009918 (2022).
37. Gupta, S. K. *et al.* Quaking Inhibits Doxorubicin-Mediated Cardiotoxicity Through Regulation of Cardiac Circular RNA Expression. *Circulation Research* **122**, 246–254 (2018).
38. Boeckel, J.-N. *et al.* SLM2 Is A Novel Cardiac Splicing Factor Involved in Heart Failure due to Dilated Cardiomyopathy. *Genomics, Proteomics & Bioinformatics* **20**, 129–146 (2022).
39. Wei, C. *et al.* Repression of the Central Splicing Regulator RBFox2 Is Functionally Linked to Pressure Overload-Induced Heart Failure. *Cell Reports* **10**, 1521–1533 (2015).
40. Zhang, Y. *et al.* RBM20 phosphorylation and its role in nucleocytoplasmic transport and cardiac pathogenesis. *The FASEB Journal* **36**, e22302 (2022).
41. Zhang, Y. *et al.* Tyrosine phosphorylation of QKI mediates developmental signals to regulate mRNA metabolism. *The EMBO Journal* **22**, 1801–1810 (2003).
42. Martino, F. *et al.* The mechanical regulation of RNA binding protein hnRNPC in the failing heart. *Science Translational Medicine* **14**, eabo5715 (2022).
43. Zhao, Y. *et al.* Cardiomyocyte-Specific Long Noncoding RNA Regulates Alternative Splicing of the Triadin Gene in the Heart. *Circulation* **146**, 699–714 (2022).
44. Gotthardt, M. *et al.* Cardiac splicing as a diagnostic and therapeutic target. *Nat Rev Cardiol* 1–14 (2023) doi:10.1038/s41569-022-00828-0.
45. Truty, R. *et al.* Spectrum of splicing variants in disease genes and the ability of RNA analysis to reduce uncertainty in clinical interpretation. *The American Journal of Human Genetics* **108**, 696–708 (2021).
46. Groeneweg, J. A. *et al.* Functional assessment of potential splice site variants in arrhythmogenic right ventricular dysplasia/cardiomyopathy. *Heart Rhythm* **11**, 2010–2017 (2014).
47. Jaganathan, K. *et al.* Predicting Splicing from Primary Sequence with Deep Learning. *Cell* **176**, 535-548.e24 (2019).
48. Haas, J. *et al.* Atlas of the clinical genetics of human dilated cardiomyopathy. *European Heart Journal* **36**, 1123–1135 (2015).
49. Shababi, M. *et al.* Cardiac defects contribute to the pathology of spinal muscular atrophy models. *Human Molecular Genetics* **19**, 4059–4071 (2010).
50. Khayrullina, G. *et al.* SMN-deficiency disrupts SERCA2 expression and intracellular Ca2+ signaling in cardiomyocytes from SMA mice and patient-derived iPSCs. *Skeletal Muscle* **10**, 16 (2020).
51. Lotti, F. *et al.* An SMN-Dependent U12 Splicing Event Essential for Motor Circuit Function. *Cell* **151**, 440–454 (2012).
52. Reber, S. *et al.* Minor intron splicing is regulated by FUS and affected by ALS-associated FUS mutants. *EMBO J* **35**, 1504–1521 (2016).
53. Verma, B., Akinyi, M. V., Norppa, A. J. & Frilander, M. J. Minor spliceosome and disease. *Seminars in Cell & Developmental Biology* **79**, 103–112 (2018).
54. Cho, D. H. & Tapscott, S. J. Myotonic dystrophy: Emerging mechanisms for DM1 and DM2. *Biochimica et Biophysica Acta (BBA) - Molecular Basis of Disease* **1772**, 195–204 (2007).

CHAPTER 2

THE RNA-BINDING PROTEIN QKI GOVERNS A MUSCLE-SPECIFIC ALTERNATIVE SPLICING PROGRAM THAT SHAPES THE CONTRACTILE FUNCTION OF CARDIOMYOCYTES

Pablo Montañés-Agudo, Simona Aufiero, Eva N. Schepers, Ingeborg van der Made, Lucia Cócera-Ortega, Auriane C. Ernault, Stéphane Richard, Diederik W.D. Kuster, Vincent M. Christoffels, Yigal M. Pinto, Esther E. Creemers

Cardiovascular Research (2023): cvad007.

ABSTRACT

Aims

In the heart, splicing factors orchestrate the functional properties of cardiomyocytes by regulating the alternative splicing of multiple genes. Work in embryonic stem cells has shown that the splicing factor Quaking (QKI) regulates alternative splicing during cardiomyocyte differentiation. However, the relevance and function of QKI in adult cardiomyocytes remains unknown. In this study we aim to identify the *in vivo* function of QKI in the adult mouse heart.

Methods and Results

We generated mice with conditional deletion of QKI in cardiomyocytes by the Cre-Lox system. Mice with cardiomyocyte-specific deletion of QKI died during the fetal period (E14.5), without obvious anatomical abnormalities of the heart. Adult mice with tamoxifen-inducible QKI deletion rapidly developed heart failure associated with severe disruption of sarcomeres, already 7 days after knocking out QKI. RNA sequencing revealed that QKI regulates the alternative splicing of more than 1000 genes, including sarcomere and cytoskeletal components, calcium handling genes and (post)transcriptional regulators. Many of these splicing changes corresponded to the loss of muscle-specific isoforms in the heart. Forced overexpression of QKI in cultured neonatal rat ventricular myocytes directed these splicing events in the opposite direction, and enhanced contractility of cardiomyocytes.

Conclusion

Altogether, our findings show that QKI is an important regulator of the muscle-specific alternative splicing program that builds the contractile apparatus of cardiomyocytes.

Translational perspective

Alternative splicing generates protein isoforms to maintain mechanical, structural, and metabolic properties of cardiomyocytes. We are the first to show that QKI is one of the essential splicing factors in the adult heart. During heart failure, alternative splicing of numerous genes is altered, thereby affecting cardiac function. Recent observations that QKI expression is downregulated in hearts of heart failure patients indicates that loss of QKI-mediated processes contributes to decreased sarcomere organization in these patients. Modulation of QKI activity may serve as a future therapeutic strategy to adapt cardiac isoform expression and improve cardiac function in heart failure patients.

GRAPHICAL ABSTRACT

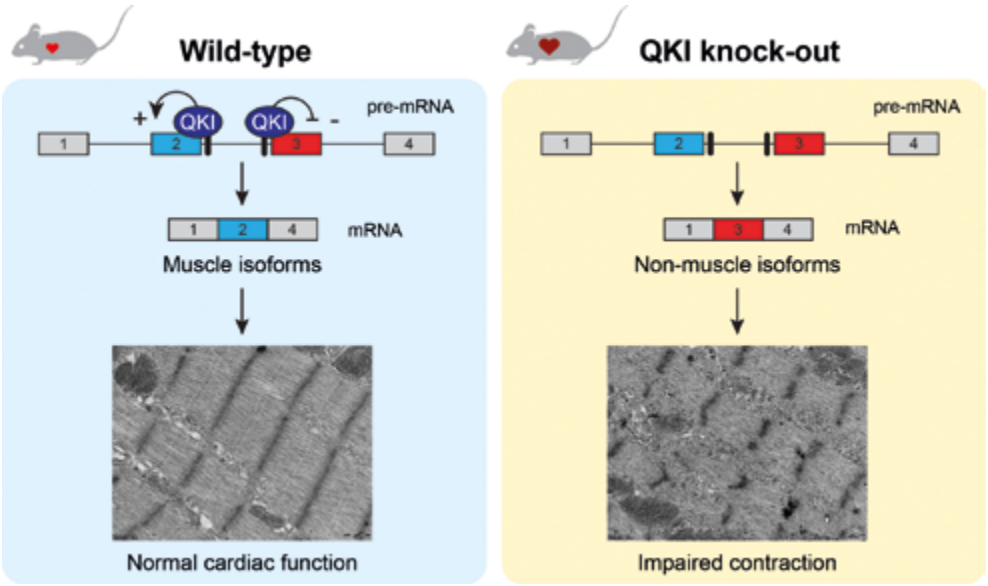

INTRODUCTION

Alternative splicing, the process by which exons from one mRNA can be spliced in different arrangements, is a crucial mechanism to expand protein diversity. It is now established that more than 95% of all human genes undergo alternative splicing to produce protein isoforms that are functionally or structurally specialized for the cell type in which they are expressed[1]. In the heart, for example, the contractile properties of the sarcomere are precisely orchestrated through alternative splicing of titin, troponin T and tropomyosin to meet the varying demands of the heart during development and disease[1,2]. One mechanism to precisely regulate alternative splicing in a tissue- and developmental stage-specific manner is via the expression of splicing factors. RBM20 is the most studied splicing factor in the heart, which has been shown to regulate networks of splicing events, particularly in sarcomere and calcium handling genes[3–5]. Mutations in *RBM20* are a frequent cause of familial dilated cardiomyopathy which highlights the functional impact of aberrant splicing in the heart[6,7]. Loss-of-function studies in mice also uncovered roles for other muscle restricted-splicing factors, namely RBM24 and RBFOX1 in the heart[8,9], but the list of RNA binding proteins controlling alternative splicing in the heart is far from complete.

The splicing factor Quaking (QKI) is a member of Signal Transduction and Activator RNA (STAR) family of RNA binding proteins, which is ubiquitously expressed with highest levels in brain and heart[10]. QKI has three main isoforms, i.e. QKI-5, QKI-6, QKI-7, that differ in the C-terminal region. QKI-5 is the predominant isoform in the heart and is the only one with a nuclear localization signal, which allows it to act as a splicing factor by binding nuclear pre-mRNAs[11]. QKI-6 and QKI-7 are cytosolic proteins, and they are mainly involved in binding mRNAs outside of the nucleus to control their stability[11,12]. The role of QKI in the nervous system has been well studied, in fact, the name 'quaking' stems from the phenotype of the 'quaking viable' mouse model that has reduced levels of myelin in its nervous system, leading to a shaking behavior, with frequent seizures[13–15]. In the heart, the function of QKI is not fully understood. Its activity in cardiomyocytes has been associated to a better outcome after ischemia/reperfusion (I/R)[16,17] and after doxorubicin toxicity[18]. Systemic loss of QKI in mice (using the *Qki*^{betaGeo} mouse line) resulted in embryonic lethality around day E9.5-E10.5, which was attributed to failure of blood circulation in the yolk sac, in which vascular remodeling was impaired[19]. Other abnormalities that were observed at this embryonic stage were open neural tubes, incomplete embryonic turning and pericardial effusion, while the hearts seemed normal[19]. In a subsequent study using the same *Qki*^{betaGeo} mouse line, several splicing changes were detected in the hearts of the KO embryos[20]. Work in human embryonic stem cell-derived cardiomyocytes (hESC-CM) indicated that QKI is required for the proper splicing of genes involved in myofibrillogenesis, such as *ACTN2*, *NEBL* and *TTN*[20]. Despite this first evidence for splicing regulation during differentiation of cardiac progenitors to early

cardiomyocytes and in the specification of cardiac mesoderm[21], the functional relevance of QKI-mediated splicing in the embryonic and adult heart remains unknown.

In this study, we investigated the function of QKI in the mouse heart by selectively deleting QKI in cardiomyocytes. To circumvent embryonic lethality due to impaired yolk sac development and to be able to ascertain a cardiomyocyte-autonomous role for QKI, we utilized the Cre-LoxP system to conditionally delete QKI from cardiomyocytes. Mice with cardiac-specific deletion of QKI died during the early fetal stages (E14.5), without obvious structural abnormalities of the heart. In the adult myocardium, loss of QKI (using the tamoxifen inducible MerCreMer) induced dilation of the ventricles and a rapid decline in cardiac function, which was associated with severe disruption of sarcomere organization. RNA-sequencing revealed splicing changes in more than a thousand genes in the adult QKI KO hearts, a large subset of which represents muscle-specific isoforms. While deletion of QKI in adult myocardium induced a rapid heart failure phenotype, we also show that forced overexpression of QKI in neonatal cardiomyocytes is able to enhance sarcomere contractility. Altogether, we are the first to show that QKI is a crucial splicing factor in the adult heart to maintain a muscle-specific splicing program.

RESULTS

Cardiomyocyte-specific removal of QKI causes embryonic lethality

To investigate the function of the splicing factor QKI in the heart, we generated a cardiomyocyte-specific QKI knockout mouse model by crossing *Qki*-floxed mice[13] with mice carrying the *Myh6-Cre* transgene[25], in which the onset of Cre expression is as early as embryonic stage E7.5[26]. In this conditional knockout allele, exon 2 of *Qki* is flanked by loxP sites. Exon 2 encodes part of the KH RNA binding domain, common to all QKI isoforms, and its deletion generates a frameshift, resulting in a null allele[13] (**Fig 1A**). We refer to the homozygous $Qki^{fl/fl}$; $Myh6\text{-}Cre^{Tg}$ as conditional QKI knock-out mice (cQKI KO), $QKI^{fl/wt}$; $Myh6\text{-}Cre^{Tg}$ as conditional QKI heterozygous mice (cQKI HET) and $Qki^{wt/wt}$;$Myh6\text{-}Cre^{Tg}$ as conditional QKI wild-type (cQKI WT) mice.

cQKI HET mice were born at the expected Mendelian ratios and were viable, but cQKI KO mice were not found at birth, indicating that QKI expression in cardiomyocytes is essential during embryonic development (**Table S3**). To pinpoint the timepoint of embryonic death, we collected embryos at different stages and found cQKI KO embryos at expected Mendelian ratios until day E14.5 (**Table S4**). From that timepoint onwards, all cQKI KO embryos were dead or reabsorbed. At E14.5, cQKI KO embryos displayed pericardial effusion and signs of necrosis (**Fig 1C**). No differences in embryo and heart size were detected between the three genotypes at E10.5 and E12.5 (**Fig S1**). Furthermore, Hematoxylin&Eosin (H&E) stainings

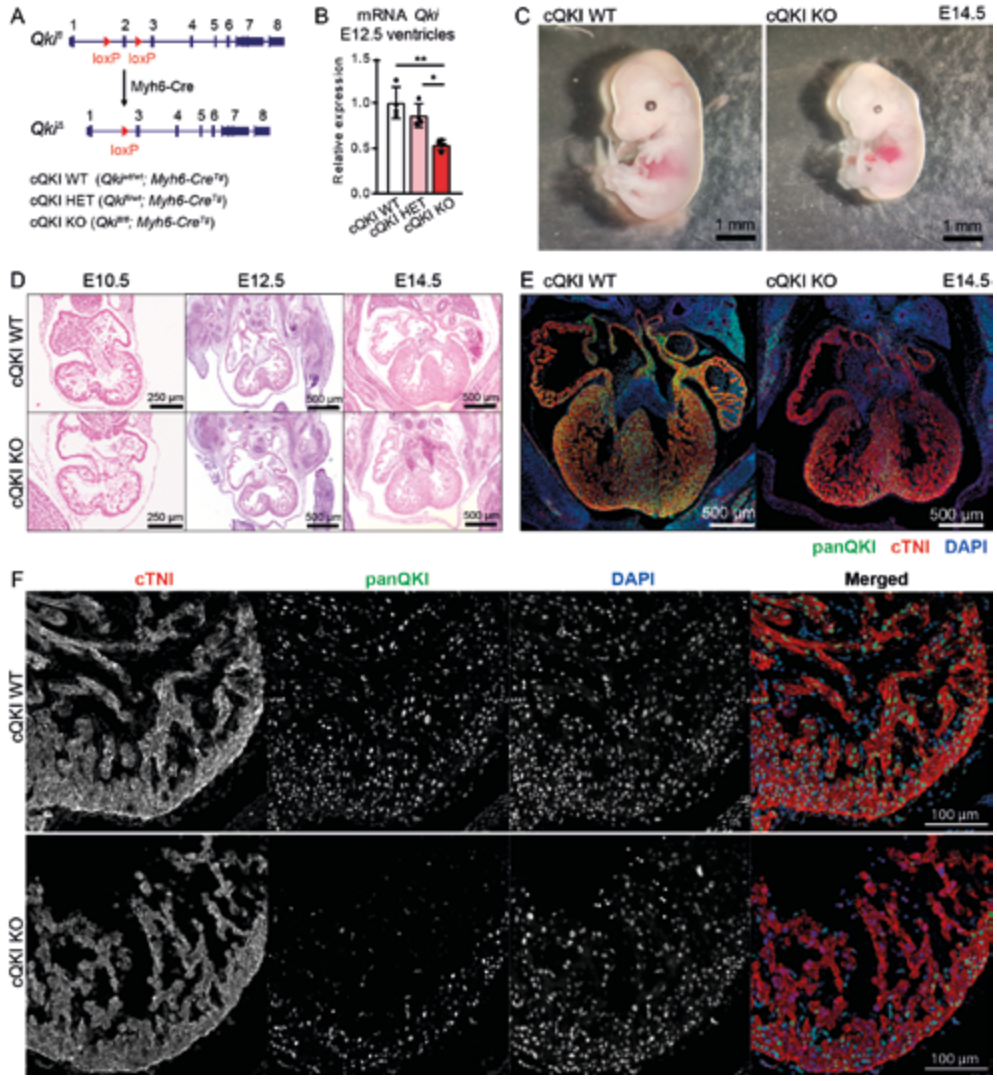

Figure 1. QKI deletion in cardiomyocytes results in early embryo lethality. (A) Schematic drawing of the floxed *Qki* allele. (B) *Qki* mRNA levels in ventricles at E12.5. n=4 embryos per group. One-way ANOVA followed by Tukey's multiple comparison test; **adjusted p<0.01; *adjusted p<0.05. (C) Representative images of mouse embryos at E14.5. Scale bar: 1 mm. (D) H&E stainings depicting four-chamber view of embryonic hearts at indicated developmental timepoints. Scale bar: 250 µm E10.5, 500 µm E12.5-14.5. (E) Four-chamber view of E14.5 hearts and (F) magnification of the LV at E12.5 immunocytochemically stained with DAPI (blue), anti-panQKI (green) and anti-cTNI (red) antibodies. Scale bar: 500 µm E14.5, 100 µm E12.5. Representative images of 3 embryos per group and per timepoint are shown.

did not reveal obvious defects in cardiac anatomy at days E10.5, E12.5 or E14.5 (**Fig 1D**), suggesting the QKI cKO hearts were functionally compromised, not anatomically.

To assess the deletion efficiency by Myh6-Cre, we performed qRT-PCR on RNA isolated from E12.5 ventricles using primers spanning exons 2 and 3 of *Qki*. This showed deletion levels of ~15% in cQKI HET and ~50% in cQKI KO hearts (**Fig 1B**). Of note, QKI is also expressed at lower levels in other cell types of the heart (e.g. vascular smooth muscle cells, fibroblasts, macrophages), which may contribute to the background expression of QKI in the knockout hearts. Next, we validated the knock-out approach by immunostainings for QKI and the cardiomyocyte marker cardiac troponin I (cTNI). In WT embryos, we could detect QKI protein in cardiomyocytes of the four chambers of the developing heart, however, QKI expression was clearly reduced in the QKI cKO embryos at day E12.5 and E14.5 (**Fig 1E-F, Fig S2**). At E14.5, residual QKI expression was observed particularly in cells of the compact myocardium and the middle axis of the heart. We do not have a clear explanation for the pattern of remaining cells, but it could be explained by cardiomyocytes not expressing the Cre recombinase or by other cell-types in that area expressing QKI.

In conclusion, the heart-specific cQKI KO mice were unable to progress beyond embryonic day E14.5. This is substantially later than the lethality caused by whole body ablation of QKI, which occurs around E9.5, and which has been attributed to abnormalities in vascular remodeling of the yolk sac[27]. Overall, this indicates that QKI regulates key processes in cardiomyocytes during development.

Cardiac-restricted removal of QKI at adulthood causes heart failure

To overcome embryonic lethality and to be able to study QKI function in the adult heart, we created a cardiac-specific tamoxifen-inducible QKI (ciQKI) knockout mouse line by crossing the *Qki*-floxed mice with mice carrying the *Myh6-mER-Cre-mER* transgene (*Myh6-MCM*^{Tg})[22]. To induce the Cre-loxP recombination, we injected tamoxifen intraperitoneally in 12- to 17-week-old WT(*Qki*$^{wt/wt}$, *Myh6-MCM*^{tg}), ciQKI HET (*Qki*$^{fl/wt}$, *Myh6-MCM*^{tg}) and ciQKI KO (*Qki*$^{fl/fl}$, *Myh6-MCM*^{tg}) mice for 4 consecutive days (**Fig 2A**). We noted that within 5 days after the last tamoxifen injection a subset of ciQKI KO mice started to become inactive, while the tamoxifen-injected WT and ciQKI HET mice appeared healthy. As low physical activity can be indicative of heart failure in the ciQKI KO group, we terminated the experiment at 7 days after the last tamoxifen injection. qRT-PCR on heart tissue revealed that *Qki* mRNA levels were reduced by 80% in the ciQKI KO and by 40% in the ciQKI HET hearts, 7 days after the last tamoxifen injection (**Fig 2B**). QKI protein levels were reduced by 80% in ciQKI KO mice, as shown by Western blotting (**Fig 2C-D**).

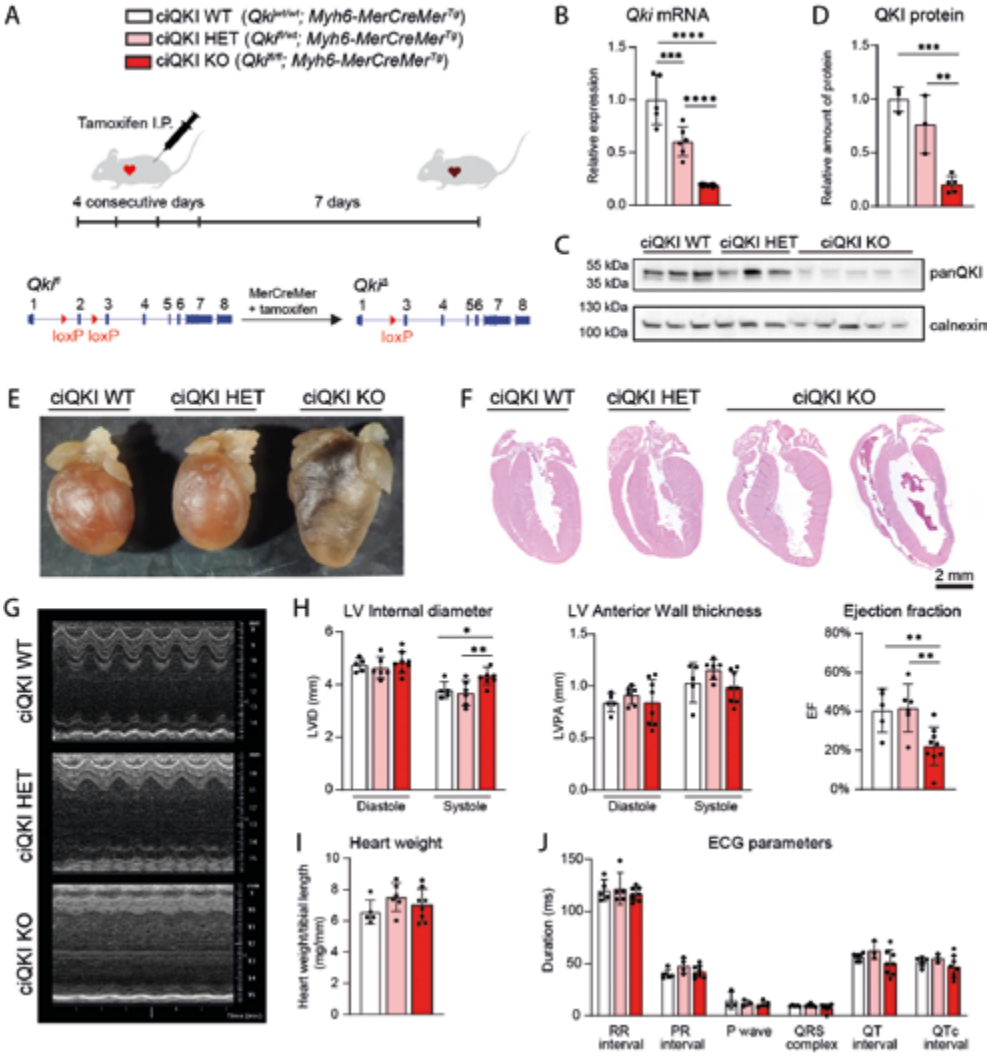

Figure 2. Deletion of QKI in adult cardiomyocytes induces heart failure. (A) Experimental approach to knock out QKI in adult cardiomyocytes by the Cre/Lox system. (B) *Qki* mRNA levels in LV tissue as measured by qPCR. (C) QKI protein levels in LV as measured by Western Blot and (D) its quantification. (E) Representative pictures of hearts after paraformaldehyde fixation. (F) H&E stainings depicting WT, HET and KO hearts. Scale bar: 2 mm (G) Representative echocardiographic M-mode traces. (H) LV internal diameter, LV anterior wall thickness and ejection fraction, measured during diastole and systole using echocardiography. (I) Normalized heart weight. (J) Electrocardiogram parameters. All data and images correspond to the same experiment, ended 7 days after the last tamoxifen injection. Number of mice per group: 5 ciQKI WT, 6 ciQKI HET, 9 ciQKI KO. Data are mean ± standard deviation. One-way ANOVA followed by uncorrected multiple comparison Fisher's least significant difference; ****p< 0.0001; ***p<0.001; **p<0.01; *p<0.05.

Inspection of global cardiac morphology and histological analysis on H&E stained sections, 7 days after the last tamoxifen injection showed enlargement and thinning of the ventricles (**Fig 2E-F**). Echocardiography confirmed a heart failure phenotype with severe systolic dysfunction in ciQKI KO mice. Specifically, ejection fraction (EF) was reduced by ~45% in ciQKI KO mice compared to the cQKI WT, and this was associated with a ~14% increase in LV internal diameter (LVID) during systole (**Fig 2G-H, Table S5**). No differences in heart weight and ECG parameters were found in ciQKI KO mice (**Fig 2I-J, Fig S3, Table S5**).

Next, we performed double immunocytochemistry for QKI and desmin (an intermediate filament connecting sarcomeric Z-disks to the cytoskeleton) on adult ciQKI WT, ciQKI HET and ciQKI KO hearts (**Fig 3A**) and evaluated them by confocal microscopy. This showed, besides a nearly complete loss of QKI protein, that the organization of the myofibrils was disrupted in the ciQKI KO hearts. Immunohistochemistry for alpha-actinin (ACTN2, which anchors actin filaments to the Z-disk) and titin (TTN, a molecular spring that connects the Z-line to the M-line in the sarcomere) yielded a comparable picture of disorganized myofilaments (**Fig S4** and **Fig S5**)**.** Of note, in the ciQKI KO hearts, we observed variation in the extent of filaments disruption, as some regions were more affected than others. No disrupted filaments were observed in the WT or ciQKI HET hearts. Ultrastructural analysis of the adult myocardium using transmission electron microscopy showed these defects in greater detail (**Fig 3B-C**). Whereas WT hearts exhibited intact sarcomeres with clearly defined Z-disks and well-organized myofibrils, ciQKI KO hearts displayed degenerated sarcomeres, and this was associated with glycogen deposits around sarcomeres (**Fig S6**)**.**

In conclusion, we show that QKI depletion in the adult myocardium leads to a dilated cardiomyopathy that rapidly progresses into heart failure and we provide evidence that disrupted sarcomeric organization underlies this contractile defect.

QKI is required for alternative splicing in cardiomyocytes

To elucidate the mechanism underlying the observed functional and ultrastructural defects, we performed RNA-sequencing in adult (5 WT and 5 ciQKI KO hearts, 7 days after tamoxifen injections) and in E12.5 embryonic hearts (4 WT and 4 cQKI KO). To be able to analyze gene expression and splice isoforms, cDNA libraries were subjected to ultra-deep sequencing, with around 250 million paired-end reads per sample.

We first performed differential gene expression analysis on the adult hearts, and we found 409 genes significantly upregulated and 444 downregulated in the ciQKI KO hearts (**Fig 4A, Online data 1**). Among the upregulated genes, there were markers of cardiac stress, such as *Acta1*, *Casq2*, *Ccn2*, *Myh7*, *Nppb*, and *Rcan1*. Among the downregulated

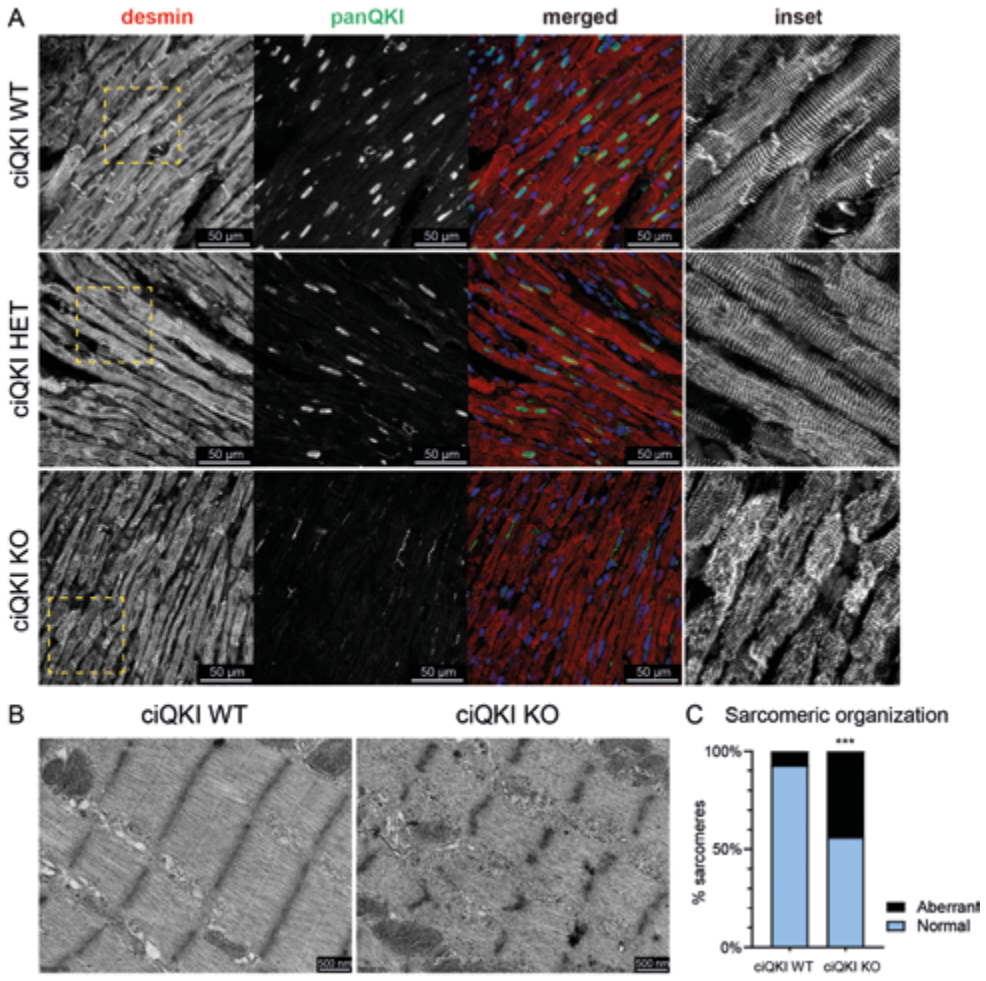

Figure 3. Loss of QKI disrupts cytoskeletal and sarcomere organization in the adult heart. (A) Immunocytochemistry showing the cytoskeletal protein desmin (red), panQKI (green) and DAPI (blue). Right panels (inset) represent magnifications of the yellow box in the desmin panels. Scale bar: 50 µm. (B) Representative transmission electron microscopy images of cardiomyocytes from ciQKI WT and ciQKI KO mice. Scale bar: 500nm. (C) Quantification of aberrant sarcomeres in LV cardiomyocytes in electron microscopy images. 3 mice per group, 4 images per mouse. χ2-test ***adjusted p<0.001.

genes, there was *Actn2*, a previously characterized target of QKI in hESC-derived cardiomyocytes[20]. Western blotting was performed to confirm the downregulation of ACTN2 and the upregulation of CAMK2D protein in the ciQKI KO hearts (**Fig S7**). To asses alternative splicing changes in the adult hearts, we detected differential

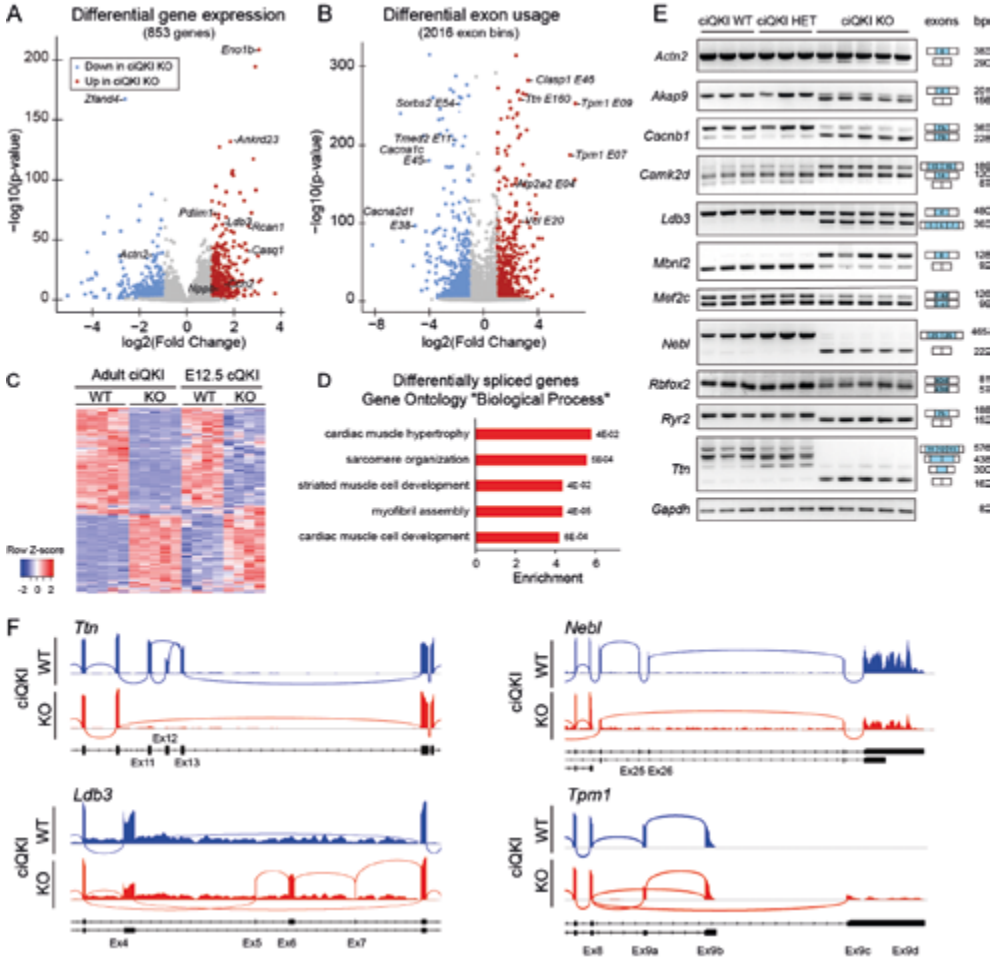

Figure 4. QKI is required for alternative splicing in cardiomyocytes of the adult heart. (A) Volcano plots showing differential gene expression and (B) differential exon usage of 5 ciQKI WT and 5 ciQKI KO hearts, 7 days after tamoxifen injections. (C) Heatmap showing differential exon usage after QKI removal in adult LV (n=5 mice per group) and in embryonic ventricles (n=4 mice per group). Z-scores were calculated in adults and embryos separately to illustrate the overlap in QKI targets between embryo and adults. (D) Pathway analysis of differentially spliced genes in the adult hearts for ''biological process'' GO terms. (E) Validation of QKI-mediated splicing events by RT-PCR in 3 ciQKI WT, 3 ciQKI HET and 5 ciQKI KO hearts (adults). (F) Representative sashimi plots of ciQKI WT and ciQKI KO hearts (adult), illustrating detailed splicing changes in *Ttn*, *Nebl*, *Ldb3* and *Tpm1*. Exon numbers and transcript isoforms are indicated below the plot.

exon usage with DEXSeq[24] and found 1023 differentially spliced genes in ciQKI KO hearts. Specifically, 927 exon bins were upregulated and 1089 exon bins were downregulated in the ciQKI KO hearts (**Fig 4B, Online data 2**). Among the mis-spliced genes, there were multiple genes directly involved in cardiac contraction, such as *Atp2a2*, *Cacna1c*, *Cacna2d2*, *Sorbs2*, *Vcl*, *Tpm1* or *Ttn*.

RNA-seq in the ventricles of E12.5 cQKI WT and cQKI KO mice also yielded differences in gene expression and splicing (**Fig S8A-B, Online data 3-4**). Principal component analysis (PCA) on exon usage and gene expression in the embryonic and adult hearts shows that splicing changes are more distinct than gene expression changes at both time-points (**Fig S8C-D**). Although there was a smaller number of differentially spliced transcripts in the E12.5 cQKI KO embryos compared to the adult ciQKI KO hearts (148 in embryos vs 1023 in adults), a substantial proportion of these mis-spliced genes (68%) did overlap with the ones observed in the adult QKI KO hearts (**Fig 4C**). A scatterplot depicting the correlation between differentially spliced exons in embryo and adult hearts also reveals that the fold changes are larger in the adult heart (**Fig S8E**). Pathway analysis of the 1023 mis-spliced genes in the adult ciQKI KO heart showed an enrichment for gene ontology "biological process" terms related to muscle biology, such as "sarcomere organization" and "striated muscle cell development" (**Fig 4D, Table S6**).

To validate the splicing changes observed by RNA-seq, we performed RT-PCR in adult heart tissue (3 ciQKI WT, 3 ciQKI HET and 5 ciQKI KO) for a panel of genes involved in muscle biology. We could confirm robust splicing changes for all genes tested. As shown in **Figure 4E**, we confirm alternative splicing changes for components of myofibrils (A*ctn2*, *Ldb3*, *Nebl* and *Ttn*), regulatory kinases (*Camk2d*, *Akap9*), calcium channels (*Cacnb1*, *Ryr2*) and transcriptional and splicing regulators (*Mbnl2*, *Mef2c, Rbfox2)*. Interestingly, ciQKI HET hearts did not show intermediate splicing changes, except for a subtle difference in *Ttn* and *Ryr2* splicing. Sashimi plots were generated to visualize splicing changes at the transcript level (**Fig 4F).** Without QKI, exon 4 of the Z-disk component *Ldb3* (/ZASP/Cypher) is partially skipped and exons 5, 6 and 7 are aberrantly included; exons 25 and 26 of the Z-disk component nebullete (Nebl) are skipped; exons coding for Z-repeats of titin (*Ttn*) are skipped (exons 11, 12 and 13)[28]; and the terminal exons of alpha-tropomyosin (*Tpm1*) are alternatively spliced[29]. In conclusion, QKI depletion in the embryonic and adult heart leads to massive splicing changes in genes crucial for muscle biology.

Intronic location of the QKI binding motifs is associated with exon skipping or inclusion

To examine the presence and location of putative QKI binding sites within the transcript, we performed an unbiased enrichment analysis of RNA-binding proteins (RBP) motifs using

ATtRACT, a database for RBPs and associated motifs[30]. We compared the presence of motifs surrounding the differentially spliced exons in adult ciQKI KO hearts with motifs surrounding an equal number of exons not differentially spliced. We limited our analysis to the proximal upstream and downstream regions, encompassing 200 nt in the flanking introns and 10 nt within the exon. As anticipated, the binding motif of QKI (ACUAAY) was the most enriched sequence in the regions flanking the mis-spliced exons **(Fig 5A, Online data 5).** Interestingly, one of the other enriched sequences was the binding motif for RBFOX1. Like QKI, RBFOX1 is a splicing regulator with enriched expression in brain and striated muscle. As multiple splicing targets are shared between RBFOX1 and QKI (e.g. *Mef2c*, *Mef2d*, *Camk2d*, *Mbnl2*)[8], it is conceivable that they cooperate in splicing networks.

Splicing factors can have opposing effects on exon usage, depending on whether they bind to their motifs up- or downstream of the exon[31]. Also for QKI it has been reported that the location of ACUAAY motifs within the transcript determines whether QKI acts as a repressor or as an activator of exon inclusion[32–35]. Therefore, we quantified and compared the presence of QKI binding sites in the proximal upstream and downstream regions of QKI-activated (exons skipped in the ciQKI KO heart), QKI-repressed (exons included in the ciQKI KO heart) and QKI-independent exons (non-differentially spliced exons)**(Fig 5B)**. We observed an increase in the number of motifs *upstream* of the QKI-repressed exons and an increase in the numbers of motifs *downstream* of QKI-activated exons, further illustrating how the positioning of QKI relative to the exon determines whether the exon is included or excluded in the final transcript. Examples of QKI-activated exons with downstream ACUAAY motifs (exon 4 of *Akap9* and exon 101 of *Dst*) are shown in **Figure 5C**. Mutually exclusive exons 3a/3b of *Slc25a3* and 10a/10b of *Rbfox2* were found to contain the motif upstream of the QKI-repressed exon *and* downstream of the QKI-activated exon.

QKI is essential for the expression of muscle-specific and developmental splice isoforms

Splice isoforms are often produced in cell-type- and/or developmental-specific manner[32], and we wondered whether this is also the case for QKI-regulated isoforms. First, we checked whether the QKI-dependent splicing events that we observed occurred exclusively in the heart or were present in other tissues as well. To do so, we performed RT-PCR on a tissue panel of adult mice, consisting of "non-muscle" tissues (cerebral cortex, kidney, lung), tissues with a high content of smooth muscle cells (colon, bladder, aorta), and striated muscle tissues (pectoralis muscle, quadriceps, atria, right ventricle and left ventricle). To be able to interrogate isoform expression across multiple tissues, we selected only those QKI targets that are expressed in a ubiquitous manner. As can be appreciated from **Figure 6A**, the picture emerges that QKI depletion prevents the expression of muscle-specific isoforms.

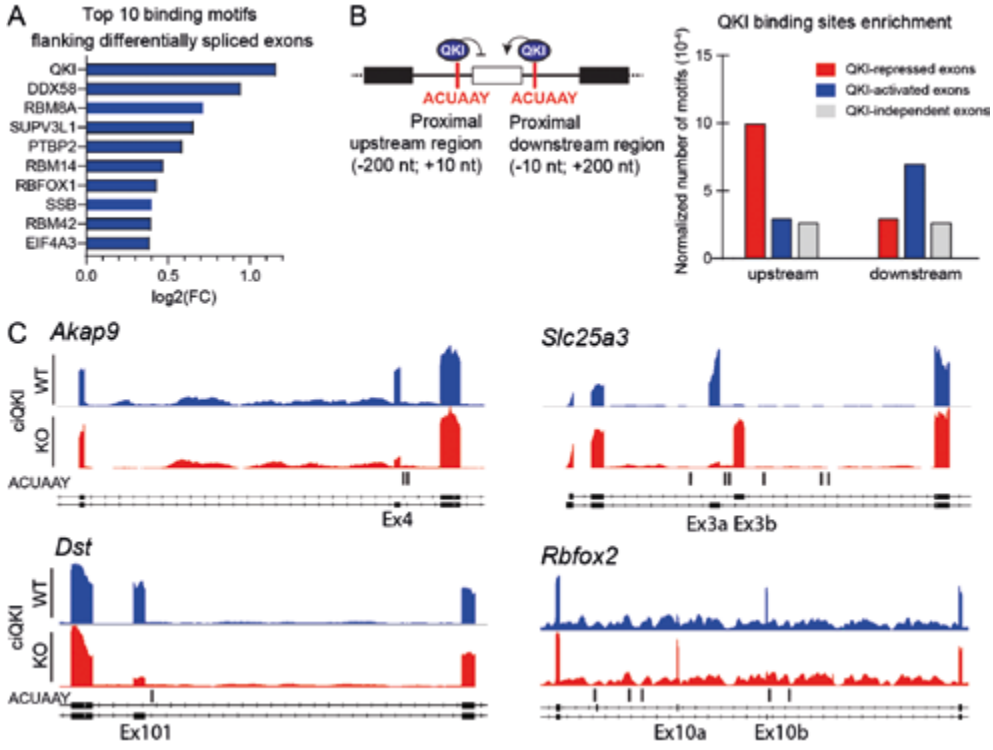

Figure 5. Location of QKI binding site determines whether QKI acts as a repressor or as an activator. (A) Enrichment of RNA binding motifs surrounding differentially spliced exons in adult ciQKI KO hearts (5 ciQKI WT vs 5 ciQKI KO). RNA binding motifs in an equal number of exons that were not differentially spliced was used as a reference. (B) Left panel: Schematic model to illustrate the positional effect of ACUAAY motifs in determining whether QKI acts as a repressor or as an activator of exon inclusion. Right panel: normalized number of ACUAAY motifs upstream and downstream of QKI-repressed, QKI-activated and a random selection of QKI-independent exons. (C) Representative bedgraphs of QKI-activated and QKI-repressed exons from RNA sequencing reads retrieved from adult ciQKI WT and KO heart (n=5/group), and the location of ACUAAY motifs indicated by vertical lines under graphs.

For instance, the isoform of *Slc25a3* containing exon 2A is highly enriched in striated muscle, but in the ciQKI KO hearts this isoform is completely lost. The same holds true for the muscle isoforms of *Tmed2, Akap9 and Nebl*. Other QKI-dependent splicing events, like *Ank3* and *Cacnb1* are not restricted to striated muscle types but are expressed in smooth muscle tissues as well. Interestingly, loss of QKI in the heart often results in the expression of isoforms that are normally present in the cerebral cortex (e.g. *Akap9*, *Ank3*, *Cacnb1*, *Fhod3*,

Slc25a3, *Tmed2*), which is remarkable since QKI is also highly expressed in the nervous system **(Fig 6A).**

Alternative splicing is a fundamental mechanism for organ development, especially in the brain and heart[35], tissues with relatively high levels of QKI. Interestingly, *Qki* mRNA levels increase in the heart throughout development, whereas in other tissues (brain, kidney, liver) *Qki* mRNA levels seem to decrease over time **(Fig 6B)**[36]. We used our RNA-seq data to investigate whether loss of QKI in the adult heart would lead to the expression of more

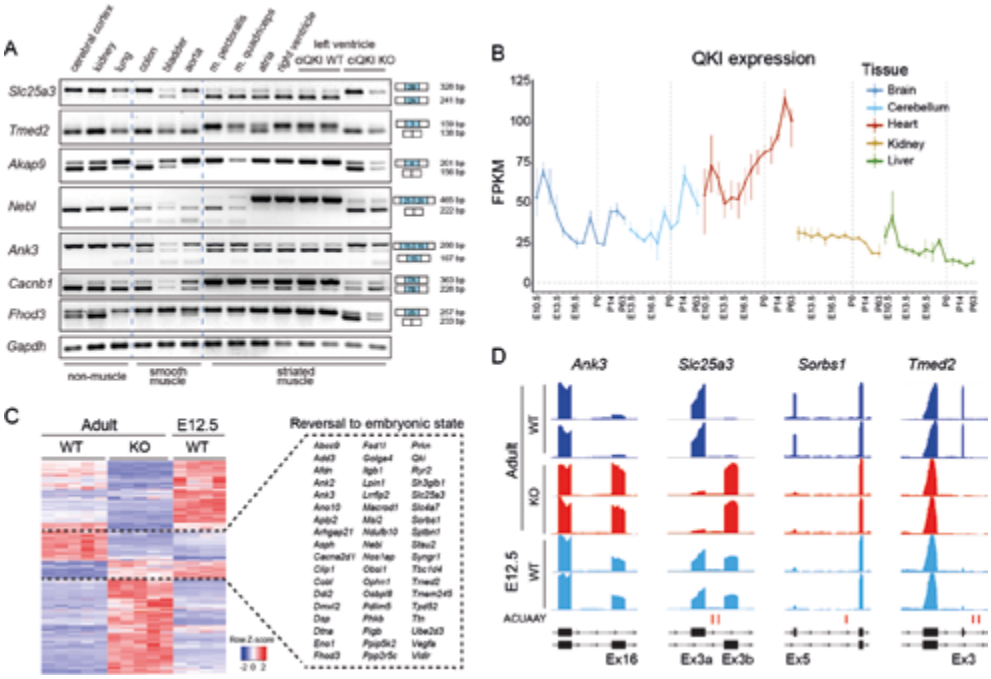

Figure 6. QKI depletion causes a loss of muscle-specific isoforms. (A) RT-PCR panel showing isoform expression across non-muscle, smooth- and striated muscle- containing tissues in adult WT mice, and in the LV from ciQKI WT and KO mice. Tissue panels of 3 different mice were analyzed with comparable results. (B) QKI expression during development across tissues in mice. Data retrieved from Cardoso-Moreira et al.[36]. (C) Heatmap showing differential exon usage in ciQKI WT and KO adult hearts (5 hearts per group) and in E12.5 WT ventricles (4 hearts). Gene names within dashed box represent splice isoforms that revert to their embryonic state after loss of QKI. (D) Representative bedgraphs showing four examples of genes that revert to the embryonic isoform in adult ciQKI KO hearts (2 mice per group shown). Predicted QKI binding sites (ACUAAY) are depicted below bedgraphs as vertical lines.

embryonic splice isoforms. As such, we compared QKI-dependent splicing events that we identified in the adult hearts with the isoforms present in wild-type E12.5 hearts. As shown in the heatmap in **Figure 6C**, there were 55 genes that switched to an embryonic isoform in the absence of QKI. Four examples of QKI-dependent genes that reverted to an embryonic isoform are illustrated in bedgraphs of **Figure 6D**. Overall, our findings illustrate that QKI controls the expression of numerous muscle- and developmental-specific splice isoforms in the heart. This puts QKI at the center of coordinated splicing networks that regulates cardiac tissue identity and cardiac development.

QKI overexpression increases cardiomyocyte contractility

Given our observation that QKI regulates a muscle-specific alternative splicing program that shapes the contractile function of cardiomyocytes, we wondered whether overexpression of QKI in neonatal rat ventricular myocytes (NRVMs) 1) would be sufficient to push the expression of adult QKI dependent splicing isoforms and 2) would affect contractility of cardiomyocytes. We limited our studies to QKI-5, since it is the predominant isoform in the heart and it is the only one with a nuclear localization signal. We made use of a bicistronic lentiviral vector to simultaneously express QKI-5 and GFP after transduction. As a control we overexpressed GFP alone. Five days after transduction, NRVMs presented QKI protein overexpression in the nucleus (**Fig 7A**) and this was associated with an increased in cell size (**Fig S9**). QKI expression was increased approximately by 2.5-fold at the protein level (**Fig 7B**) and RT-PCRs showed a shift in splicing opposite to the one observed in the ciQKI KO hearts (**Fig 7C**). This shift towards more muscle-specific isoforms consisted of increased skipping of exon 16 in *Ank3*, higher levels of the *isoform* δ-C *of Camk2d*, more inclusion of exon 4 and skipping of exons 5, 6 and 7 in *Ldb3,* and increased skipping of exon 2a in *Myocd*.

To test whether the splicing changes induced by QKI-5 overexpression affected the contractility of the NRVMs we made use of CytoCypher, a high-throughput microscopic system able to measure cardiomyocyte contraction by calculating pixel displacement over time. We performed the measurements at day 4 after transduction, before the increase in cell size occurs (**Fig S9**). Representative cell contraction transients of GFP and QKI-5 transduced NRVMs are depicted in **Figure 7D**. Interestingly, QKI-5 overexpression increased the peak height of the contraction transients, and the departure and return velocities (i.e. the maximum velocities reached on the contraction and relaxation phase of the transient) (**Fig 7E**). In summary, our *in vitro* experiments indicate that QKI-5 overexpression is sufficient to increase muscle-specific splicing and enhance the contractile properties of neonatal cardiomyocytes.

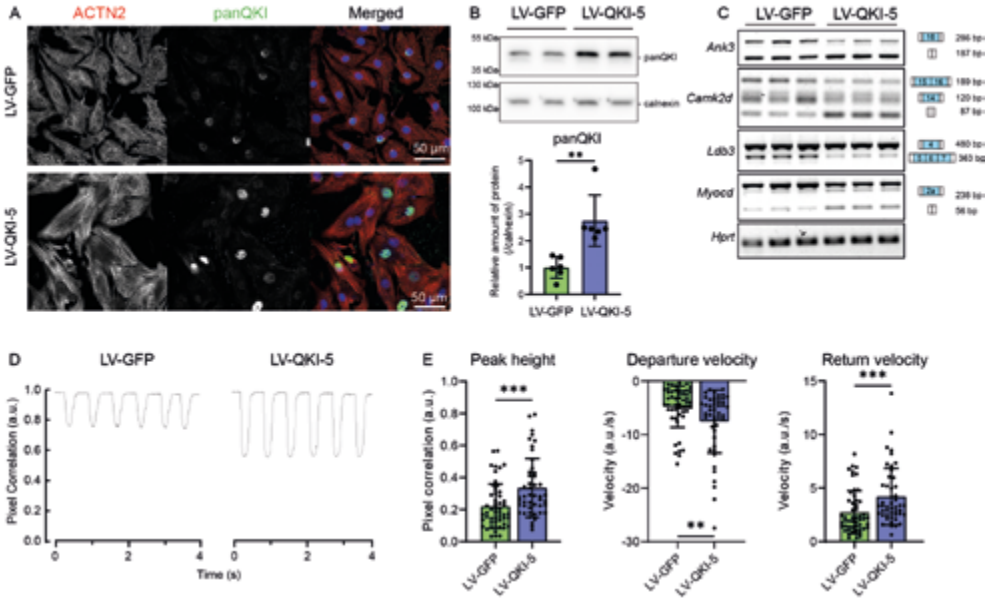

Figure 7. QKI overexpression in neonatal rat ventricular myocytes (NRVMs) increases the production of muscle isoforms and enhances contractility. (A) Representative immunocytochemistry of NRVMs 5 days after lentiviral (LV) transduction of GFP or QKI-5. ACTN2 (red), panQKI (yellow), DAPI (blue) Scale bar: 50 µm. (B) QKI protein levels as measured by Western Blot. Unpaired t-test; **p<0.01. (C) RT-PCR showing a shift in splicing in the QKI targets *Ank3*, *Camk2d*, *Ldb3* and *Myocd,* 5 days after lentiviral transduction. 3 wells per condition; representative results from 3 independent experiments are shown. (D) Representative contraction traces and (E) contraction parameters 4 days after lentiviral transduction. Departure/return velocities are the maximum velocities reached on the contraction and relaxation phase of the transient. N≥40 cells per condition. The data represents one out of four independent experiments. Data are mean ± standard deviation. Mann-Whitney test; *p<0.05; **p<0.01; ***p<0.001. All experiments were performed with a multiplicity of infection (MOI) of 1.3.

DISCUSSION

In this study, we investigated the function of QKI in the heart. We demonstrate that QKI is required in cardiomyocytes to maintain normal cardiac function during development and in the adult heart. Most strikingly, loss of QKI in adult cardiomyocytes rapidly induces heart failure, with LV dilation and severe disruption of sarcomeres, and this occurs already 7 days after deleting QKI from the heart. We show that QKI regulates the integrity and structural composition of sarcomeres, at least in part, by controlling alternative splicing of hundreds of protein-coding genes. Analysis of splicing events in ciQKI KO hearts revealed defective

splicing in numerous sarcomere genes (e.g. *Nebl*, *Ttn*, *Tpm1*, *Ldb3*, *Actn2*), cytoskeletal genes (e.g. *Ablim1*, *Ank3*, *Dst*), calcium handling genes (e.g. *Camk2d*, *Atp2a2*, *Ryr2*, *Cacna1c*) and (post)transcriptional regulators (*Mef2c*, *Myocd*, *Mbnl2*, *Rbfox1/2*). Forced overexpression of QKI-5 in cultured neonatal cardiomyocytes directed these splicing events in the opposite direction, which led to increased contractility of cardiomyocytes.

Because QKI regulates the splicing of such a large number of developmental- and disease-relevant genes, it is currently not possible to pinpoint how each defectively spliced gene contributes to the QKI KO phenotype we observe. Nevertheless, the functional relevance of a number of these splice isoforms has been reported previously. For instance, skipping of exon 8 in *Actn2*, which we observe in QKI KO hearts results in a premature stop codon, leading to degradation of the *Actn2* mRNA due to activation of the nonsense-mediated mRNA decay (NMD) pathway[20]. Within *Ttn*, exon 11-13 are skipped in the absence of QKI. These exons are located in the Z-band region of TTN and alternative splicing in this region generates a variable number of Z-repeats, presumably changing the binding sites for the scaffold protein ACTN2, and thus influencing the mechanical stability of the sarcomere[37,38]. In *Tpm1*, we observed splicing changes in the terminal exons that define TPM1 affinity for actin. Specifically, in the absence of QKI, we observed loss of the striated-muscle specific exons 9a and 9b, in favor of the exons 9c and 9d. The exons 9a and 9b encode for specific amino acid residues that are critical for the interaction of troponin with tropomyosin on the thin filaments[29,39]. For CaMKIIδ, we observed a switch from the δ-C to the δ-A isoform, resulting from inclusion of exon 15 and 16. The δ-C isoform is located in the cytoplasm, where it phosphorylates RyR2 and phospholamban, while the δ-A isoform is associated with the intercalated disc and T tubules, where Ca^{2+} channels and activated CaMKIIδ are concentrated[40,41]. The increased δA levels may lead to Ca^{2+} handling disturbances in QKI KO cardiomyocytes, but this warrants further investigation. The transcription factor MEF2C is a crucial regulator of myogenesis by controlling the expression of genes that encode a network of structural proteins. Here, we show that QKI is required for the expression of the MEF2C isoform containing the mutually exclusive α2 exon. The α2 isoform has potent myogenic activity, whereas the isoform containing α1 does not[42]. It is conceivable that mis-splicing of MEF2C in the QKI KO hearts contributes to the sarcomere phenotype by reducing the transcription of muscle genes.

Two recent studies in human stem cell already uncovered a critical role for QKI in cardiomyocyte differentiation. Chen et al. employed CRISPR/Cas9 gene editing to delete QKI from human embryonic stem cells (hESC). By differentiating these stem cells into cardiomyocytes, they revealed that QKI is essential for the formation of myofibrils during cardiomyocyte differentiation[20]. Genes involved in contractile function were found to be alternatively spliced in the absence of QKI, including *ACTN2*, *NEBL*, *ABLIM1*, *PDLIM5* and

TTN. Consistent with this work, Fagg et al. compared alternative splicing events in three cell lineages differentiated from hESCs (i.e. the endoderm, cardiac mesoderm and ectoderm cell lineages), and showed that QKI plays a critical role in the specification of cardiac mesoderm and the formation of cardiomyocytes[21]. One of the studied splicing targets in that study was Bridging Integrator1/Amphiphysin 2 (*BIN1*), a protein known for its role in cardiac development and myofibrillogenesis[43,44]. In our QKI mouse models, we did not find altered splicing or gene expression of *Bin1*, neither in the adult QKI KO hearts, nor in the embryonic QKI KO hearts. This may relate to the timing of QKI deletion using the Myh6 promoter, which starts to become active from E7.5 onwards, which is after cardiac mesoderm formation. In conclusion, these human stem cell studies uncovered a role for alternative splicing in early lineage-specific gene expression and implicate QKI as a cardiac mesoderm-enriched RNA binding protein required for differentiation of cardiomyocytes. A role for QKI in myofibril formation is however not limited to cardiomyocytes, as recent studies also provided evidence that QKI controls the formation of myofibrils of skeletal muscle in zebrafish[45] and regulates a splicing program during smooth muscle development[19,46]. In addition, QKI deficiency in muscle stem cells using a conditional QKI mouse model in combination with the Pax7-Cre driver was shown to result in loss of the myogenic progenitor cell population and muscle regeneration defects[47].

Once assembled, cardiac sarcomeres require constant maintenance as the continuous contractions of the heart are accompanied by mechanical stress, which in turn predisposes proteins to misfolding and aggregation[48]. Maintenance of sarcomeres is a complex process, in which new proteins are constantly incorporated into sarcomeres to replace old ones without compromising mechanical function. The half-lives of sarcomere proteins in the heart are estimated in the order of days to weeks[48]. Our finding that sarcomeres in the adult heart degenerate already one week after QKI depletion suggests that sarcomere maintenance is compromised by the incorporation of aberrant protein isoforms. This is particularly relevant, as there is evidence that QKI expression is lost during multiple forms of heart disease. This was shown in a mouse model of doxorubicin-mediated cardiotoxicity[18], in a rat model of ischemia/reperfusion[16], in the diabetic mouse heart[49] and in human heart failure[18]. Accordingly, reduced levels of QKI may very well contribute to the disease mechanism of sarcomere dysfunction and decreased contractility in heart failure. In this light, it has been shown that more than 1000 transcripts express aberrant isoforms in ischemic and dilated cardiomyopathies, indicating that alternative splicing is a highly regulated process and important layer of gene regulation during pathological remodelling of the heart[50,51]. It will be very interesting to see whether therapeutic upregulation of QKI using gene therapy in acquired heart disease will be able to shift splicing towards more cardioprotective isoforms and improve cardiac remodelling and function. This is strengthened by our observation that QKI overexpression

is sufficient to increase contraction and relaxation velocities of NRVMs. Moreover, Gupta et al. recently provided evidence that therapeutic overexpression of QKI is beneficial in a mouse model of doxorubicin-mediated heart failure[18]. They showed that adeno-associated virus serotype 9 (AAV9)-mediated overexpression of QKI attenuates apoptosis and atrophy of cardiomyocytes in this model. Alternative splicing of sarcomere genes was not investigated in this study, instead certain circRNA molecules were identified as mediators in the observed anti-apoptotic effect. A role for QKI in cardiomyocyte apoptosis was also reported in a study by Guo et al., who showed that QKI inhibits ischemia/reperfusion-induced cardiomyocyte apoptosis by regulating *Foxo1* mRNA stability[16]. Notably, we did not find altered expression or splicing of *Foxo1* mRNA in our QKI KO datasets.

It has become evident that alternative splicing occurs in coordinated networks, rather than in isolated events. Several splicing factors, including RBM20[3], RBM24[9], SRSF10[52], ASF/SF2[41], and RBFOX1[8] were shown to regulate alternative splicing of a large number of transcripts in the developing and/or adult heart. By comparing their splicing targets, the picture emerges that these splicing factors regulate a distinct, but overlapping set of transcripts. For instance, the switch in CaMKIIδ, from the δ-C to the δ-A isoform that we identified in QKI KO hearts, has also been found in RBM20 and ASF/SF2 KO mice[3,41]. The inclusion of the mutually exclusive exons 3a/3b of the mitochondrial phosphate carrier *Slc25a3* is regulated by QKI and RBM24[9]. Splicing of TTN is regulated by RBM20 and by QKI, however these factors control splicing of different exons. Whereas RBM20 is responsible for the inclusion of I-band exons, a region of TTN that is crucial for the elastic property of sarcomeres, QKI regulates the inclusion of Z-band exons, a region that is thought to be important for mechanical stability of the sarcomere[37]. We found that one of the most enriched sequences in the flanking introns of QKI regulated exons, is the binding motif for RBFOX1, a splicing regulator that is also enriched in brain and striated muscle. As multiple splicing targets are shared between RBFOX1 and QKI (e.g. *Mef2c*, *CamkIId*, *Mbln2*), it is conceivable that QKI and RBFOX1 engage in a complex regulatory network of alternative splicing[8]. The full extent of how QKI cooperates and competes with other splice factors is yet to be determined. Finally, our observation that QKI also regulates alternative splicing of *Rbfox1* itself, adds another layer of complexity, and warrants further exploration.

In conclusion, we are the first to show that QKI acts as a major regulator of striated muscle identity in the cardiomyocytes of the adult heart, by directing the expression of muscle-specific isoforms of numerous pre-mRNAs. This extends previous studies showing a role for QKI in cardiomyocyte differentiation during the transition from cardiac progenitors to early cardiomyocytes[20] and in the specification of cardiac mesoderm[21]. Future studies are needed to investigate whether QKI dysregulation contributes to the mechanism of contractile

dysfunction in heart disease. Specifically, the fact that QKI is downregulated in human DCM[18], and our observation that forced overexpression of QKI enhances cardiomyocyte contractility may open avenues for therapeutic strategies to adapt cardiac isoform expression and improve cardiac function in heart failure patients.

MATERIAL AND METHODS

Animal studies

Animal studies were approved by the Institutional Animal Care and Use Committee of the University of Amsterdam and carried out in compliance with the guidelines of this institution and the Directive 2010/63/EU of the European Parliament. Animal husbandry was performed by the Animal Research Institute AMC.

Cardiomyocyte-specific knock out mice of *Qki* were generated by crossing the previously generated *Qki* floxed mice[13] with the conditional *Myh6-Cre* (Jackson Laboratory stock #011038) and with the tamoxifen inducible *Myh6-MerCreMer* (Jackson Laboratory stock #005657)[22] in C57BL/6N background. In all experiments, mice had a single copy of the *Cre* or the *MerCreMer* (MCM) recombinase allele. Males and females were included in the experiments.

For inducing *MerCreMer* recombinase activity, a tamoxifen solution (2.5 mg/ml tamoxifen in 10% ethanol, 90% sunflower oil) was injected intraperitoneally for 4 consecutive days (total dose 100 mg tamoxifen/kg mouse) in 12-17 week-old mice (n per group: 5 ciQKI WT, 6 ciQKI HET, 9 ciQKI KO). Echocardiography and ECG recordings were performed as indicated in the Supplemental Methods.

RNA and protein analysis

For adult mice, total RNA was extracted from the left ventricle by using TRI reagent (Sigma, Ref T9424) following manufacturer's instructions. For E12.5 embryos, RNA from both ventricles was extracted using the kit ReliaPrep RNA Miniprep Systems (Promega, Ref Z6111). RNA quality was determined using the Agilent RNA 6000 Nano Kit and the Agilent 2100 Bioanalyser. All samples had an RNA Integrity score ≥ 8. cDNA synthesis and (q) RT-PCRs were performed as described in the Supplemental Methods. Primer sequences are found in **Table S1**.

Western blotting and histology were performed as depicted in the Supplemental Methods. Antibodies and their dilutions are listed in **Table S2.**

RNA sequencing

RNA from left ventricle samples of 5 adult ciQKI WT and 5 adult ciQKI KO mice, and 4 cQKI WT and 4 cQKI KO E12.5 ventricles was used for paired-end RNA-sequencing. Details of library preparation, RNA sequencing and data analysis are found in Supplemental Methods.

Differential gene expression and exon usage

Differential gene expression analysis was performed using the R Bioconductor package, DESeq2[23] (Bioconductor release 3.13). Transcripts Per Million (TPM) for each gene was also calculated. Genes with TPM value ≥ 0.5, an absolute log2 fold change cut-off ≥1.0 and adjusted P-value cutoff ≤0.05 were deemed significantly differentially expressed.

Differential exon usage analysis was performed using the R Bioconductor package, DEXSeq[24](Bioconductor release 3.13). Only genes with a TPM value ≥ 0.5 were considered. Exons with an absolute $\log_2$ fold change cut-off ≥ 1.0 and adjusted P-value cut-off ≤ 0.05 were deemed significantly differentially spliced.

Neonatal rat ventricular myocytes (NRVMs)

Isolation, transduction, culture and contraction measurements of NRVMs are depicted in the Supplemental Methods.

Statistics

Data was analyzed using GraphPad Prism 9 (GraphPad, San Diego, CA, USA). Data is presented as mean±standard deviation, unless differently stated. Results were analyzed with appropriate statistical tests, as indicated in the respective figure legends. A value of $p<0.05$ was considered statistically significant.

COMPETING INTERESTS

Y.M.P. is inventor on patents, holds minor shares (<5%) and serves as consultant for biotech and pharmaceutical companies that develop molecules or RNA therapies that target myocardial disease (Forbion Capital, ARMGO BV, Oxitope Pharmaceuticals, Phlox Therapeutics) and received support from Roche Diagnostics. The remaining authors have no conflicts of interest to declare.

ACKNOWLEDGMENTS

We thank Corrie de Gier-de Vries and Noelia Muñoz-Martín for experimental assistance, Eric van der Veer for providing QKI constructs and Anke Tijsen for scientific discussions.

FUNDING

This work was supported by grants from the Rembrandt Institute for Cardiovascular Science to EEC and from the Netherlands Cardiovascular Research Initiative (CVON-ARENA-PRIME), to YMP.

AUTHORS' CONTRIBUTIONS

P.M.A. and E.E.C. contributed to the experimental design, writing and editing of the manuscript. P.M.A., S.A., E.N.S., I.v.M. and E.E.C. contributed to the acquisition of data, analysis, and interpretation. L.C.O., A.C.E., S.R., D.W.D.K. and V.M.C. provided experimental resources. S.R., D.W.D.K., V.M.C, Y.M.P and E.E.C. revised the intellectual content of the manuscript. Y.M.P. and E.E.C. supervised the project. All authors read and approved the manuscript.

DATA AVAILABILITY

Raw RNA sequencing data are available at NCBI BioProject, under ID number PRJNA831665.

REFERENCES

1. Baralle, F. E. & Giudice, J. Alternative splicing as a regulator of development and tissue identity. *Nat. Rev. Mol. Cell Biol.* **18**, 437–451 (2017).
2. Weeland, C. J., Hoogenhof, M. M. van den, Beqqali, A. & Creemers, E. E. Insights into alternative splicing of sarcomeric genes in the heart. *J. Mol. Cell. Cardiol.* **81**, 107–113 (2015).
3. Guo, W. *et al.* RBM20, a gene for hereditary cardiomyopathy, regulates titin splicing. *Nat. Med.* **18**, 766–773 (2012).
4. Maatz, H. *et al.* RNA-binding protein RBM20 represses splicing to orchestrate cardiac pre-mRNA processing. *J. Clin. Invest.* **124**, 3419–3430 (2014).
5. van den Hoogenhof, M. M. G. *et al.* RBM20 Mutations Induce an Arrhythmogenic Dilated Cardiomyopathy Related to Disturbed Calcium Handling. *Circulation* **138**, 1330–1342 (2018).
6. Brauch, K. M. *et al.* Mutations in Ribonucleic Acid Binding Protein Gene Cause Familial Dilated Cardiomyopathy. *J. Am. Coll. Cardiol.* **54**, 930–941 (2009).
7. Kayvanpour, E. *et al.* Genotype-phenotype associations in dilated cardiomyopathy: meta-analysis on more than 8000 individuals. *Clin. Res. Cardiol.* **106**, 127–139 (2017).
8. Gao, C. *et al.* RBFox1-mediated RNA splicing regulates cardiac hypertrophy and heart failure. *J. Clin. Invest.* **126**, 195–206 (2016).
9. Yang, J. *et al.* RBM24 Is a Major Regulator of Muscle-Specific Alternative Splicing. *Dev. Cell* **31**, 87–99 (2014).
10. Darbelli, L. & Richard, S. Emerging functions of the Quaking RNA-binding proteins and link to human diseases. *WIREs RNA* **7**, 399–412 (2016).
11. Teplova, M. *et al.* Structure–function studies of STAR family Quaking proteins bound to their in vivo RNA target sites. *Genes Dev.* **27**, 928–940 (2013).
12. Hardy, R. J. *et al.* Neural Cell Type-Specific Expression of QKI Proteins Is Altered in quakingviable Mutant Mice. *J. Neurosci.* **16**, 7941–7949 (1996).
13. Darbelli, L., Vogel, G., Almazan, G. & Richard, S. Quaking Regulates Neurofascin 155 Expression for Myelin and Axoglial Junction Maintenance. *J. Neurosci.* **36**, 4106–4120 (2016).
14. Ebersole, T. A., Chen, Q., Justice, M. J. & Artzt, K. The quaking gene product necessary in embryogenesis and myelination combines features of RNA binding and signal transduction proteins. *Nat. Genet.* **12**, 260–265 (1996).
15. Sidman, R. L., Dickie, M. M. & Appel, S. H. Mutant Mice (Quaking and Jimpy) with Deficient Myelination in the Central Nervous System. *Science* **144**, 309–311 (1964).
16. Guo, W. *et al.* RNA Binding Protein QKI Inhibits the Ischemia/reperfusion-induced Apoptosis in Neonatal Cardiomyocytes. *Cell. Physiol. Biochem.* **28**, 593–602 (2011).
17. Wang, F., Yuan, Y., Yang, P. & Li, X. Extracellular vesicles-mediated transfer of miR-208a/b exaggerate hypoxia/reoxygenation injury in cardiomyocytes by reducing QKI expression. *Mol. Cell. Biochem.* **431**, 187–195 (2017).
18. Gupta, S. K. *et al.* Quaking Inhibits Doxorubicin-Mediated Cardiotoxicity Through Regulation of Cardiac Circular RNA Expression. *Circ. Res.* **122**, 246–254 (2018).
19. Li, Z. *et al.* Defective smooth muscle development in qkI-deficient mice. *Dev. Growth Differ.* **45**, 449–462 (2003).
20. Chen, X. *et al.* QKI is a critical pre-mRNA alternative splicing regulator of cardiac myofibrillogenesis and contractile function. *Nat. Commun.* **12**, 89 (2021).
21. Fagg, W. S. *et al.* Definition of germ layer cell lineage alternative splicing programs reveals a critical role for Quaking in specifying cardiac cell fate. *Nucleic Acids Res.* **50**, 5313–5334 (2022).
22. Sohal, D. S. *et al.* Temporally Regulated and Tissue-Specific Gene Manipulations in the Adult and Embryonic Heart Using a Tamoxifen-Inducible Cre Protein. *Circ. Res.* **89**, 20–25 (2001).
23. Love, M. I., Huber, W. & Anders, S. Moderated estimation of fold change and dispersion for RNA-seq data with DESeq2. *Genome Biol.* **15**, 550 (2014).
24. Anders, S., Reyes, A. & Huber, W. Detecting differential usage of exons from RNA-seq data. *Genome Res.* **22**, 2008–2017 (2012).

25. Agah, R. *et al.* Gene recombination in postmitotic cells. Targeted expression of Cre recombinase provokes cardiac-restricted, site-specific rearrangement in adult ventricular muscle in vivo. *J. Clin. Invest.* **100**, 169–179 (1997).

26. de Lange, F. J. *et al.* Lineage and morphogenetic analysis of the cardiac valves. *Circ. Res.* **95**, 645–654 (2004).

27. Noveroske, J. K. *et al.* Quaking is essential for blood vessel development. *genesis* **32**, 218–230 (2002).

28. Savarese, M. *et al.* The complexity of titin splicing pattern in human adult skeletal muscles. *Skelet. Muscle* **8**, 11 (2018).

29. Hammell, R. L. & Hitchcock-DeGregori, S. E. Mapping the Functional Domains within the Carboxyl Terminus of α-Tropomyosin Encoded by the Alternatively Spliced Ninth Exon (*). *J. Biol. Chem.* **271**, 4236–4242 (1996).

30. Giudice, G., Sánchez-Cabo, F., Torroja, C. & Lara-Pezzi, E. ATtRACT—a database of RNA-binding proteins and associated motifs. *Database* **2016**, baw035 (2016).

31. Fu, X.-D. & Ares, M. Context-dependent control of alternative splicing by RNA-binding proteins. *Nat. Rev. Genet.* **15**, 689–701 (2014).

32. Barash, Y. *et al.* Deciphering the splicing code. *Nature* **465**, 53–59 (2010).

33. de Bruin, R. G. *et al.* Quaking promotes monocyte differentiation into pro-atherogenic macrophages by controlling pre-mRNA splicing and gene expression. *Nat. Commun.* **7**, 10846 (2016).

34. Hall, M. P. *et al.* Quaking and PTB control overlapping splicing regulatory networks during muscle cell differentiation. *RNA* **19**, 627–638 (2013).

35. Mazin, P. V., Khaitovich, P., Cardoso-Moreira, M. & Kaessmann, H. Alternative splicing during mammalian organ development. *Nat. Genet.* **53**, 925–934 (2021).

36. Cardoso-Moreira, M. *et al.* Gene expression across mammalian organ development. *Nature* **571**, 505–509 (2019).

37. Chen, Z. *et al.* Z-band and M-band titin splicing and regulation by RNA binding motif 20 in striated muscles. *J. Cell. Biochem.* **119**, 9986–9996 (2018).

38. Gregorio, C. C. *et al.* The NH2 Terminus of Titin Spans the Z-Disc: Its Interaction with a Novel 19-kD Ligand (T-cap) Is Required for Sarcomeric Integrity. *J. Cell Biol.* **143**, 1013–1027 (1998).

39. Cao, J., Routh, A. L. & Kuyumcu-Martinez, M. N. Nanopore sequencing reveals full-length Tropomyosin 1 isoforms and their regulation by RNA-binding proteins during rat heart development. *J. Cell. Mol. Med.* **25**, 8352–8362 (2021).

40. Koval, O. M. *et al.* CaV1.2 beta-subunit coordinates CaMKII-triggered cardiomyocyte death and afterdepolarizations. *Proc. Natl. Acad. Sci. U. S. A.* **107**, 4996–5000 (2010).

41. Xu, X. *et al.* ASF/SF2-regulated CaMKIIdelta alternative splicing temporally reprograms excitation-contraction coupling in cardiac muscle. *Cell* **120**, 59–72 (2005).

42. Zhang, M., Zhu, B. & Davie, J. Alternative splicing of MEF2C pre-mRNA controls its activity in normal myogenesis and promotes tumorigenicity in rhabdomyosarcoma cells. *J. Biol. Chem.* **290**, 310–324 (2015).

43. Hong, T. *et al.* Cardiac BIN1 folds T-tubule membrane, controlling ion flux and limiting arrhythmia. *Nat. Med.* **20**, 624–632 (2014).

44. Muller, A. J. *et al.* Targeted disruption of the murine Bin1/Amphiphysin II gene does not disable endocytosis but results in embryonic cardiomyopathy with aberrant myofibril formation. *Mol. Cell. Biol.* **23**, 4295–4306 (2003).

45. Bonnet, A. *et al.* Quaking RNA-Binding Proteins Control Early Myofibril Formation by Modulating Tropomyosin. *Dev. Cell* **42**, 527-541.e4 (2017).

46. van der Veer, E. P. *et al.* Quaking, an RNA-Binding Protein, Is a Critical Regulator of Vascular Smooth Muscle Cell Phenotype. *Circ. Res.* **113**, 1065–1075 (2013).

47. Dominici, C. & Richard, S. Muscle stem cell polarity requires QKI-mediated alternative splicing of Integrin Alpha-7 (Itga7). *Life Sci. Alliance* **5**, e202101192 (2022).

48. Martin, T. G. & Kirk, J. A. Under construction: The dynamic assembly, maintenance, and degradation of the cardiac sarcomere. *J. Mol. Cell. Cardiol.* **148**, 89–102 (2020).

49. Guo, W. *et al.* QKI deficiency promotes FoxO1 mediated nitrosative stress and endoplasmic reticulum stress contributing to increased

vulnerability to ischemic injury in diabetic heart. *J. Mol. Cell. Cardiol.* **75**, 131–140 (2014).

50. Kong, S. W. *et al.* Heart Failure–Associated Changes in RNA Splicing of Sarcomere Genes. *Circ. Cardiovasc. Genet.* **3**, 138–146 (2010).
51. Lee, J.-H. *et al.* Analysis of transcriptome complexity through RNA sequencing in normal and failing murine hearts. *Circ. Res.* **109**, 1332–1341 (2011).
52. Feng, Y. *et al.* SRp38 regulates alternative splicing and is required for Ca(2+) handling in the embryonic heart. *Dev. Cell* **16**, 528–538 (2009).

SUPPLEMENTAL METHODS

Echocardiography and ECG recordings

Echocardiography and ECG recordings were performed 1 week after the last tamoxifen injection on mice sedated with 4% isoflurane and maintained in anesthesia by a mixture of O2 and 2.5% isoflurane. LV function and dimensions were measured by transthoracic two-dimensional echocardiography using a Vevo 770 Ultrasound (Visual Sonics) equipped with a 30-MHz linear array transducer. M-mode tracings in parasternal short axis view at the height of the papillary muscle were used to measure LV internal diameter at end-systole and end-diastole. For ECG acquisition, electrodes were placed at the right (R) and left (L) armpit and the left groin (F). A reference electrode was placed at the right groin. ECGs were recorded (Biosemi, Amsterdam, the Netherlands; sampling rate 2048 Hz, filtering DC 400 kHz (3 dB)) for a period of 5 min. After the recordings, sedated mice were euthanized by cervical dislocation.

cDNA synthesis and RT-PCRs

For cDNA synthesis, 500 ng of total RNA were treated with DNAse I (Invitrogen, Ref 18068-015, Waltham, MA, USA) and retrotranscribed into cDNA with random hexamers (Invitrogen, Ref N8080127) and Superscript II (Invitrogen, Ref 18064-014). qRT-PCRs were performed on a Lightcycler 480 (Roche, Mannheim, Germany) using SYBR green I Master Mix (Roche, Ref 04887352001). Data was analyzed using LinRegPCR software. RT-PCRs were performed in a 25 µL reaction containing 5 ng cDNA, 1M Betaine, 1x Buffer B2, 2.5 mM MgCl2, 200 µM dNTPs, 0.4 µM forward primer, 0.4 µM reverse primer and 0.05 U/µ HOT FIREpol® DNA polymerase (Solis Biodyne). Primer sequences are found in **Table S1.** The thermal cycling protocol included an initial denaturation at 95 °C for 15 min to activate the HOT FIREPol® DNA polymerase, followed by 35 amplification cycles of denaturation at 95 °C for 30 s, annealing at 60 °C for 30 s, extension at 72 °C for 45 s, and 5 minutes of final extension at 72°C. *Slc25a3* PCR product was digested with the restriction enzyme XbaI (Roche) to distinguish exon 2A from 2B.

Western Blotting

For protein isolation, flash-frozen tissue was homogenized by MagNA Lyser Green Beads (Roche) in RIPA buffer (50 mM Tris-HCl pH 8, 150 mM NaCl, 1% NP-40, 0.2% sodium deoxycholate, 0.1% SDS, 1 mM Na_3VO_4, 1 mM PMSF) supplemented with protease inhibitor cocktail (Roche). Protein concentration was measured by BCA assay (Pierce). Western blotting was performed following standard protocols. Proteins were separated by SDS-PAGE, transferred to PVDF membranes (Bio-Rad), block in TBST 4% milk and incubated with primary antibodies overnight at 4°C. Membranes were subsequently incubated with HRP-conjugated secondary antibodies for 1 hour at room temperature. Western blots were

developed with ECL prime western blotting detection agent (Amersham Biosciences) in ImageQuant LAS 4000 (GE 194 Healthcare Life Sciences). Western blots were quantified using Fiji (ImageJ). Antibody references are listed in **Table S2.**

Histology

Hearts and embryos were fixed in 4% paraformaldehyde and embedded in paraplast. Paraplast blocks were cut in 5 μm sections and slides were stained with hematoxylin&eosin using standard techniques. For immunohistochemistry, sections were deparaffinized, rehydrated in a series of ethanol, and boiled for 15 min in antigen unmasking solution (Vector laboratories Ref H3300, Burlingame, California, USA) in a pressure-cooker. After cell membrane permeabilization with 0.5% Triton-X-PBS and blocking with 4% BSA-PBS, samples were incubated with primary antibodies overnight at 4°C and stained with secondary antibodies and DAPI for 2 hours at room temperature. Pictures were taken on a confocal microscope (Leica SP8, Leica Microsystems, Germany). Antibodies and their dilutions are listed in **Table S2.**

Transmission electron microscopy was performed by the Cellular Imaging Facility of the Amsterdam UMC. In short, LV tissue was prefixed in 1% glutaraldehyde, 4% paraformaldehyde in 0.1M sodium cacodylate and processed for electron microscopy. Images were acquired with a FEI technai 12 transmission electron microscope. Sarcomere organization was scored manually by taking random pictures of sarcomere areas and scoring for 2 different categories - organized or aberrant (**Fig S6B**) - in 3 hearts per group (4 areas per heart) on a blinded basis.

RNA sequencing

Library preps were made with the Kapa RNA Hyperprep with RiboErase (Roche) and sequenced on a NovaSeq platform (NovaSeq S4.300; flow cell type PE150, 2 x 150nt). Quality control of FASTQ files was performed using FastQC (Babraham Bioinformatics). Trimmomatic (version 0.351) was used to remove adapters and low quality bases, using a Phred score cutoff of 30 while discarding reads with a length below 75 bases. All samples had a sequencing depth between 178-385 million reads per sample and all samples passed quality control. Paired-end reads were then aligned against the mouse genome. Gene ontology enrichment analysis was done using the online tool PANTHER[2]. Genes expressed in mouse heart with TPM > 0.5 were used as background.

RBP analysis binding sites analysis

RBP analysis was performed on the differentially spliced exons identified. Exon bins with absolute log2 fold change cut-off ≥1, adjusted P-value cutoff ≤ 0.05 and which corresponding genes are expressed with TPM value ≥ 1. Furthermore, only exon bins whose genomic

coordinates matched with the genomic coordinates of an exon reported in the genome annotation files were retained. After filtering a total of 1126 differentially expressed exons (604 upregulated exons and 522 downregulated exons) were used as foreground set. An equal number of not differentially spliced exons were used as background set. Then the table containing the collected exons was adapted to work with module 11 of the R Bioconductor package circRNAprofiler[3] to retrieve the target sequences. The following settings were used: lIntron = 200, lExon = 9, type = ie. Then the target sequences were scanned for the presence of RBP binding motifs by using module 12 with the following settings: width = 6, database = ATtRACT, rbp = TRUE, reverse = FALSE. QKI motif was included in motifs.txt (as specified by circRNAprofiler). Raw and normalized counts are reported in **Online Data 5**. Normalization was performed by dividing the number of occurrences of each motif by the total length of the target sequences. The same analysis was performed this time only for the differentially spliced exons. In detail the upregulated exons were as used as foreground set while the downregulated exons were used as background set. The QKI binding sites were then retrieved for the upstream and the downstream regions of the corresponding exons.

Lentiviral constructs

Expression plasmid pLV-QKI-5 was a gift of Dr. van der Veer (Leiden, The Netherlands). QKI-5 sequences were subcloned in a bicistronic pLV-CMV-x-IRES-GFP lentiviral vector. For lentivirus production, HEK293T cells were transfected with pLV-CMV-empty-IRES-GFP or pLV-CMV-QKI-5-IRES-GFP, in combination with the packing vectors pVSVG, pMDL and pRSV. Lentiviral particles were collected from the supernatant. Transducing units were calculated by transduction of HEK293T cells and quantification of GFP positive cells by flow cytometry.

Neonatal rat ventricular cardiomyocytes (NRVMs) isolation

NRVMs from 0–2 day old Wistar rats (Janvier Labs, Le Genest-Saint-Isle, France) were isolated as described previously[4]. In short, pups were anesthetized by isoflurane and hearts were excised after decapitation. Ventricles were cut into small pieces, which were incubated overnight in a rotating platform at 4 °C in HBSS (Gibco, Ref 14170-088, Paisley, UK) containing 1 mg/ml trypsin (USB, Ref 22720, Cleveland, OH, USA). The next day, cells were dissociated using 1 mg/ml collagenase type 2 (Worthington, Ref LS004177, Lakewood, NJ, USA) in HBSS. Cells were collected and resuspended in TUNG medium - M199 culture medium (Gibco, Ref 31150-022), 1% HEPES (Gibco, Ref 15630-080), 1% NEAA (Gibco, Ref 11140-050), 2 mg/L vitamin B12 (Sigma, Ref V2876, St. Louis, MO, USA), 3.5 g/L glucose, 1% penicillin/streptomycin (Gibco, Ref 15140-122) - supplemented with 10% FBS (Biowest, Ref S1810-500, Riverside, MO, USA). The cell suspension was pre-plated to separate myocytes from fibroblasts. After

2 hours, non-adhered myocytes were collected and counted with a LUNA-II Automated Cell Counter (Logos Biosystems, Anyang, South Korea).

NRVM transduction

NRVMs were plated on 6-well plates coated with fibronectin (Corning, Ref 356008, Bedford, MA, USA) in TUNG medium supplemented with 10% FBS containing lentiviral particles (MOI 1.3). 24h after lentiviral transduction, NRVMs were washed twice with HBBS and medium was replaced with TUNG 2% FBS supplemented with 10 nM of the cytostatic Ara-C (Sigma, ref C-6645, St Louis, MO, USA) to inhibit fibroblast proliferation.

NRVM immunohistochemistry and staining

NRVMs were seeded on fibronectin-coated glass coverslips on 24-well. Cells were fixed in 4% PFA, permeabilized with PBS 0,1% Triton X-100, blocked in 4% goat serum and incubated overnight with the primary antibodies in a wet chamber at 4°C. Secondary antibodies and DAPI (Molecular probes) were incubated for 1h at room temperature. For cell membrane staining, non-permeabilized fixed cells were incubated with WGA-488 and DAPI for 15 min at room temperature. Images were acquired with a Leica TCS SP8 X unit mounted on a Leica DMI6000 inverted microscope. Antibody references are found in **Table S2**.

Quantitative analysis of NRVM contraction

NRVMs were seeded on µ-Plate 24 Well Black ID 14 mm ibiTreat (Ibidi GmbH, Germany) coated with fibronectin (Corning, Ref 356008, Bedford, MA, USA). Cell contraction transients were recorded using the Pixel Correlation method with a CytoCypher Multicell High Throughput System (CytoCypher BV, Netherlands). During acquisition, cells were maintained in a climate control chamber (37°C, 5% CO_2, 80% humidity) and paced at 1.5 Hz. Contraction transients were analyzed with CytoCypher Cytosolver (CytoCypher BV, Netherlands).

SUPPLEMENTAL FIGURES

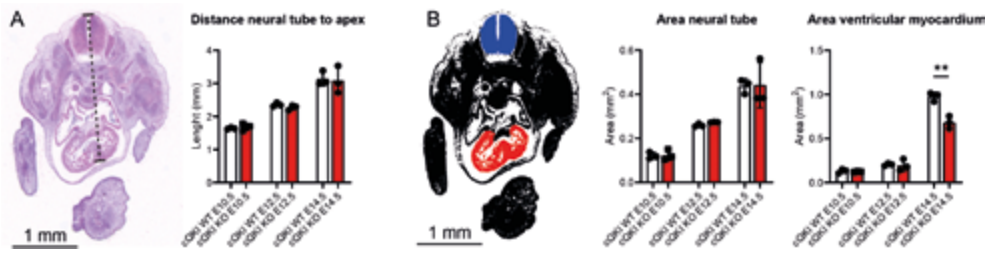

Figure S1. Embryonic measurements. (A) The length of the dorsal-ventral axis was calculated by measuring the distance between the spine and the apex of the heart using ImageJ. Scale bar: 1 mm. (B) Area of neural tube (blue) and ventricular myocardium (red) were calculated with ImageJ as shown. The sections shown in (A) and (B) are derived from a representative cQKI WT E12.5 embryo. The measurement of each embryo is the average of 3 sections. N = 3 embryos per group. Unpaired t-test; ** $p<0.01$.

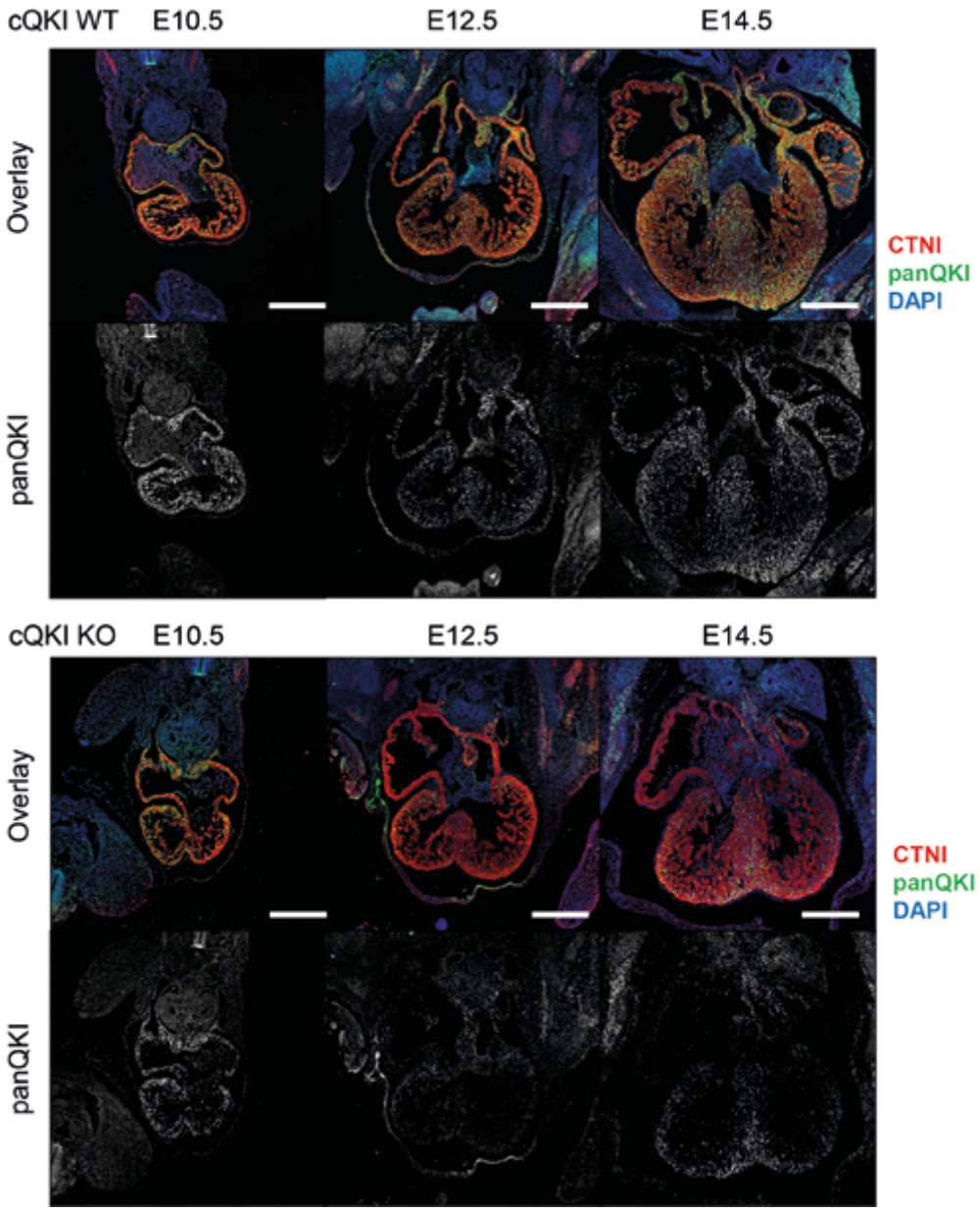

Figure S2. Representative immunocytochemistry cQKI WT and KO embryos at E10.5, E12.5 and E14.5, stained for cardiac troponin I (CTNI) and panQKI. Scale bar: 500 μm. Representative images of 3 embryos per group and per timepoint are shown.

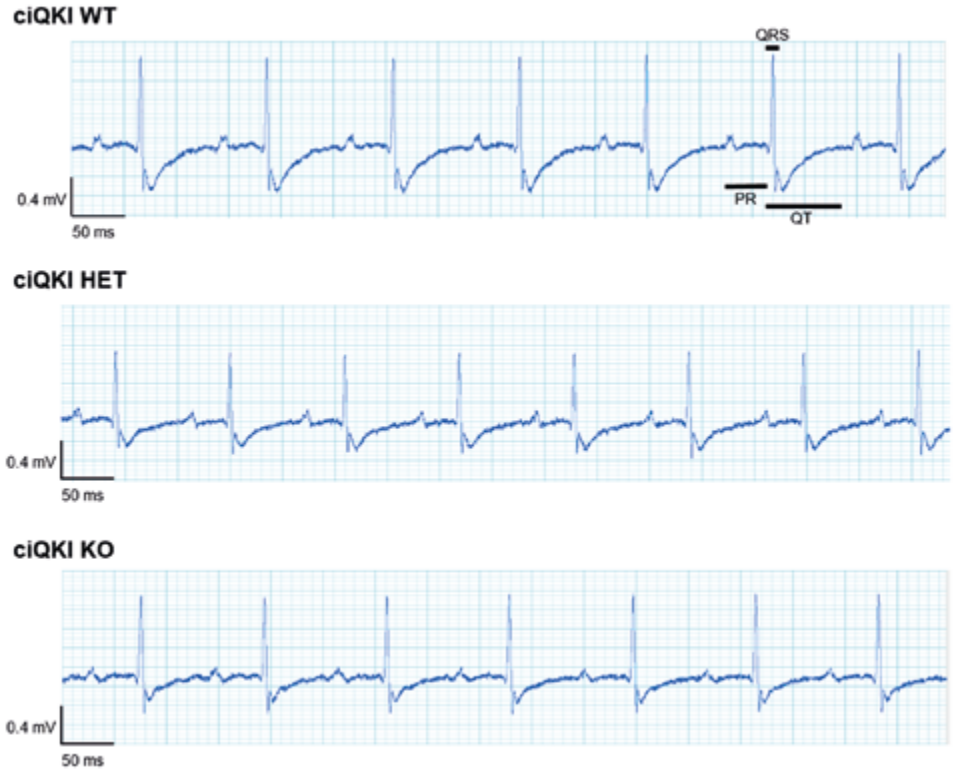

Figure S3. Representative ECG recordings of ciQKI WT, HET and KO mice, 7 days after the last tamoxifen injection does not reveal any abnormality. See **Table S5** for quantification of heart rate, PR interval, QRS interval and QTc times.

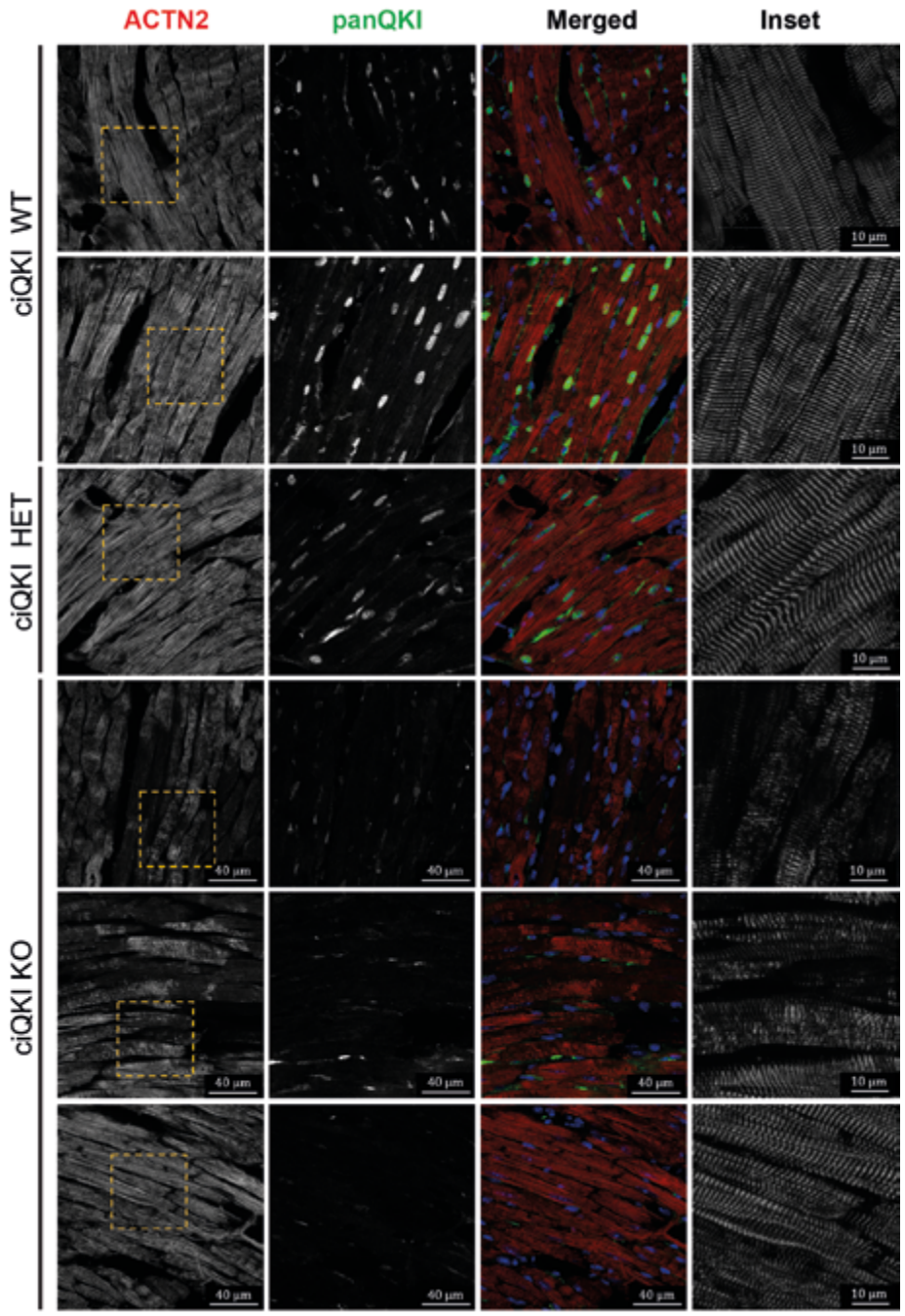

Figure S4. Knock-out of QKI induces a rapid loss of ACTN2 in cardiomyocytes. Representative immunocytochemistry for ACTN2 and panQKI in ciQKI WT, HET and KO LV tissue. Scale bar: 40 µm and 10 µm. Representative images of 3 hearts per group are shown.

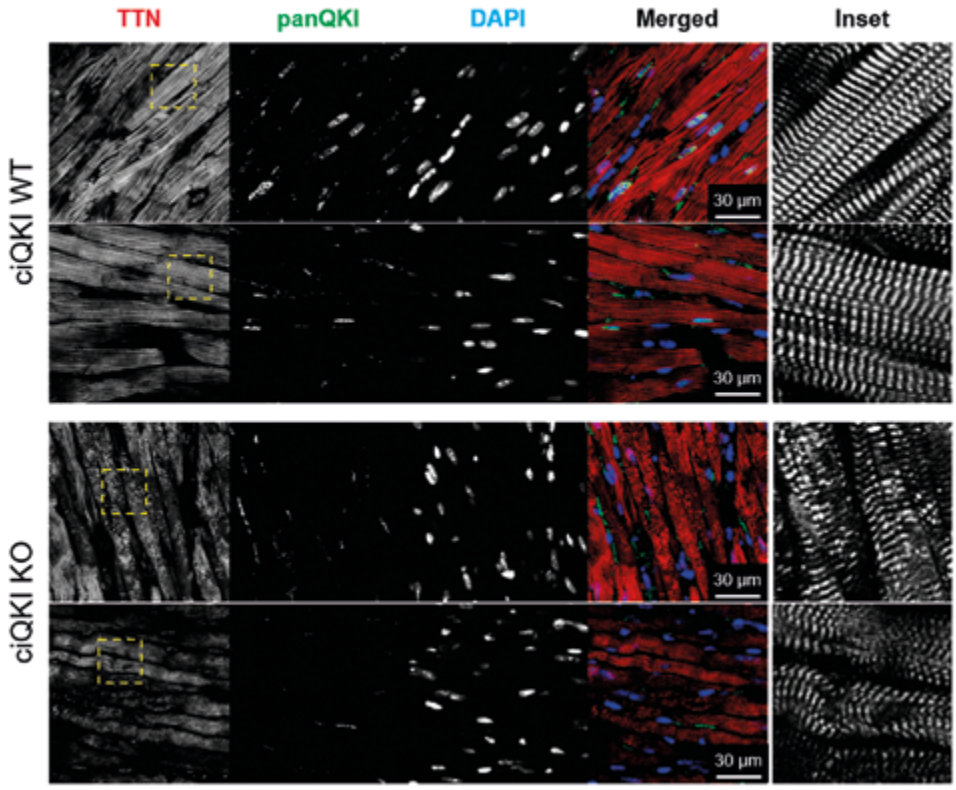

Figure S5. QKI knock-out induces loss of TTN organization in the sarcomeres. Representative immunocytochemistry for TTN and panQKI in ciQKI WT and ciQKI KO hearts. Scale bar: 30 µm.

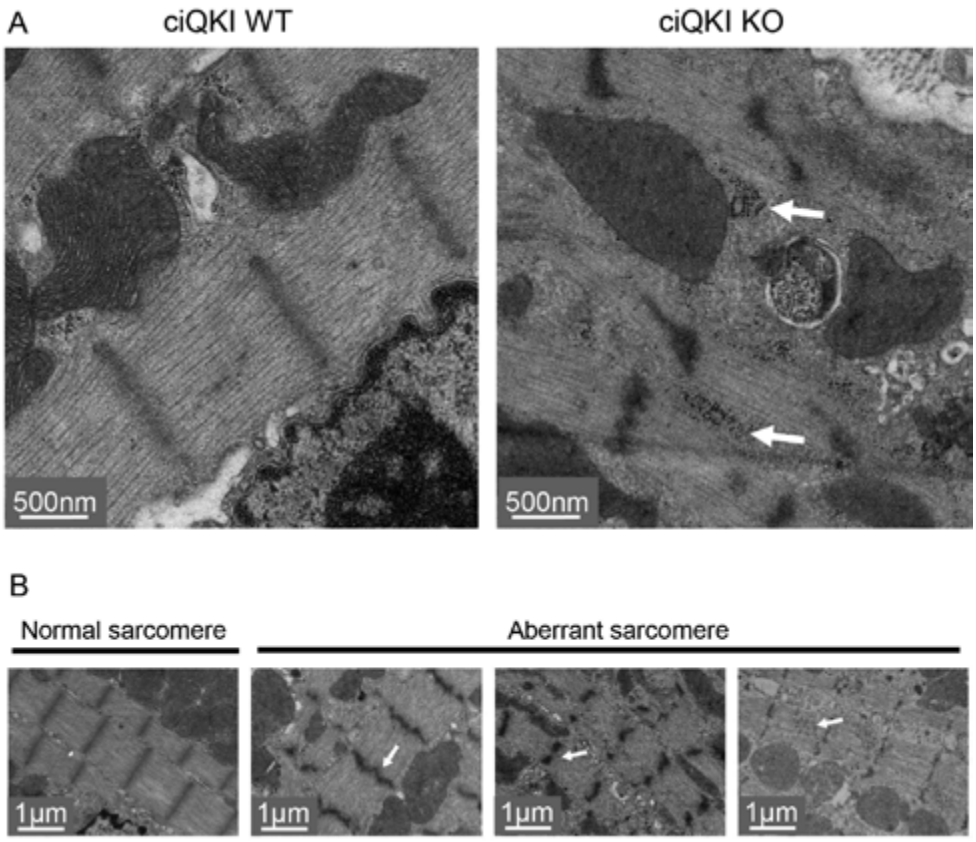

Figure S6. Transmission Electron Microscopic images of ciQKI WT and ciQKI KO myofibrils in the adult hearts. (A) Electron microscopy images of ciQKI WT and KO myofibrils illustrating glycogen deposits (white arrows) near disrupted myofibrils in ciQKI KO. Scale bar: 500 nm. (B) Example of sarcomeres scored as normal or aberrant, derived from a ciQKI WT (normal sarcomere) and a ciQKI KO (aberrant sarcomeres) respectively. Scale bar: 1 µm. Representative images of 3 hearts per group are shown.

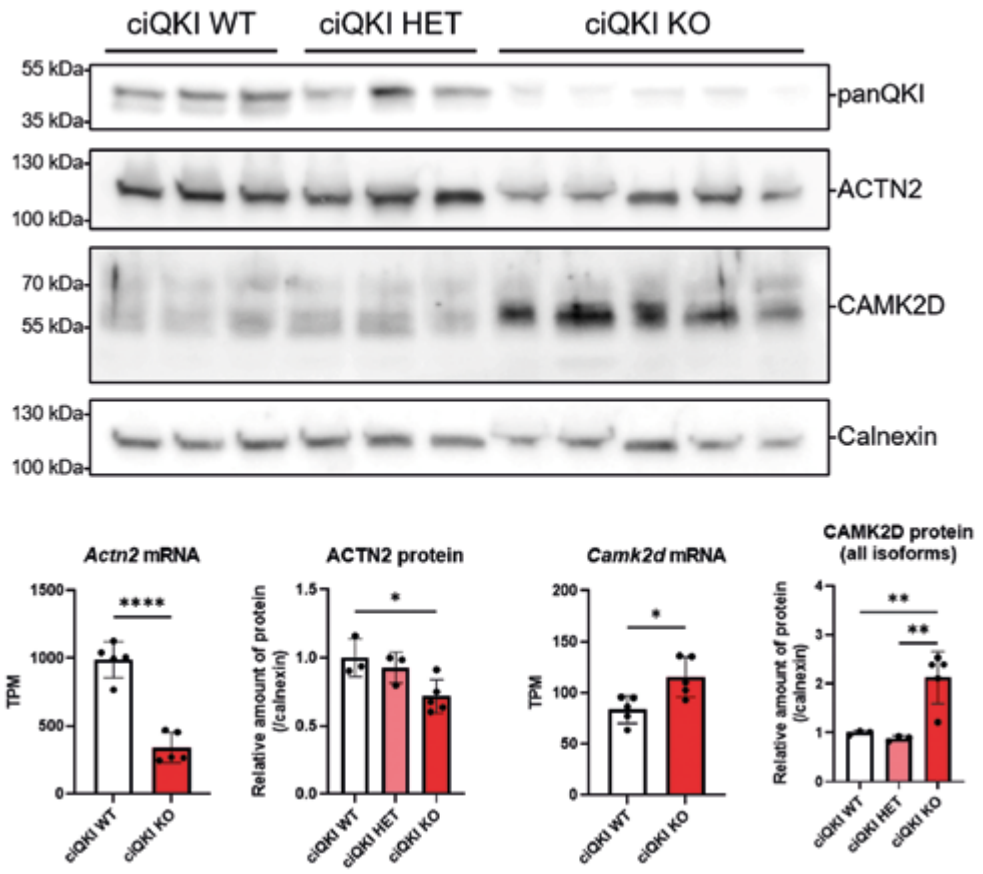

Figure S7. ciQKI KO hearts express lower levels of ACTN2 and higher levels of CAMK2D at the protein level. Western Blot showing the changes in QKI, ACTN2 and CAMK2D in left ventricles of 3 ciQKI WT, 3 ciQKI HET and 5 ciQKI KO mice, 7 days after the last tamoxifen injection. In the lower panel, protein quantifications of the blot are shown, as well mRNA levels of *Actn2* and *Camk2d* (derived from the RNA-seq). Data are mean ± standard deviation. One-way ANOVA followed by Tukey's multiple comparison test; **** adjusted p< 0.0001; ** adjusted p<0.01; * adjusted p<0.05.

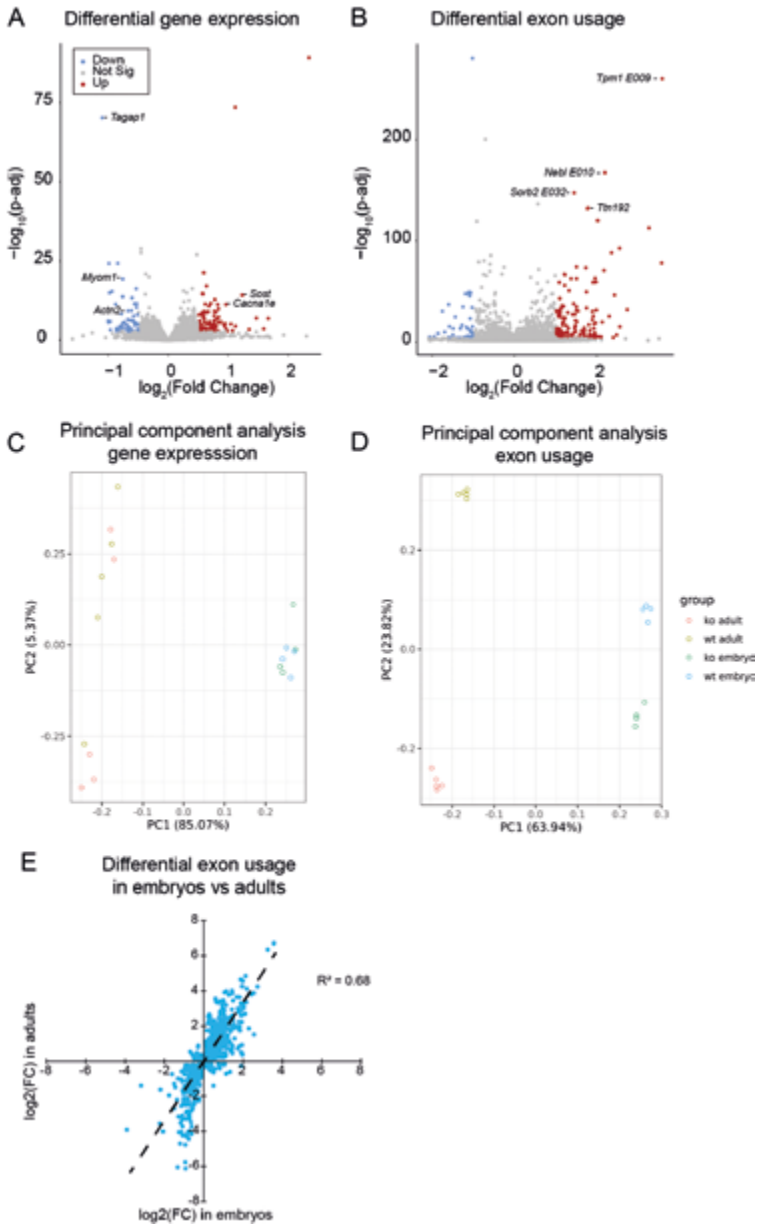

Figure S8. Gene expression and differential exon usage in embryonic hearts at E12.5 (A) Differential gene expression and (B) differential exon usage of 4 cQKI WT (*Qki*$^{wt/wt}$, *Myh6-Cre*^{tg}) and 4 cQKI KO (*Qki*$^{fl/fl}$, *Myh6-Cre*^{tg}) E12.5 hearts. (C) Principal component analysis of gene expression and (D) exon usage in embryos (E12.5, n=4 per group) and adult hearts (n=5 per group). QKI WT or KO genotypes are indicated by different colors. (E) Scatter plot showing the correlation in differential exon usage in embryos and adults. Only exon bins with adj-p ≤ 0.05 in the cQKI KO embryos were included.

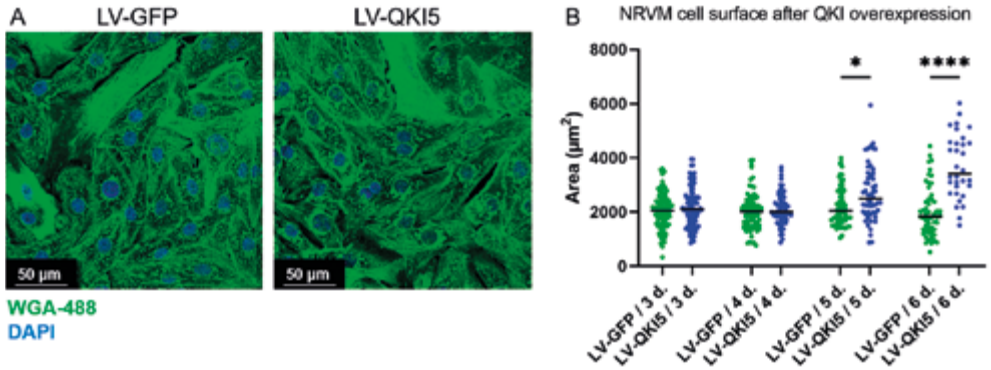

Figure S9. Cell surface measurements of NRVMs after QKI-5 overexpression. (A) Representative WGA-488 stainings, 4 days after lentiviral transduction of GFP or QKI5. Scale bar: 50 µm.(B) Cell surface measurements at different time points. Each dot represents a cell, each time point corresponds to a different isolation. n ≥ 33 cells per condition per time-point. Man-Whitney test; *** $p < 0.001$, * $p < 0.05$.

SUPPLEMENTAL TABLES

Table S1. Primer sequences

Primer	Sequence (5' – 3')	Analysis	Species
Qki 2lox Fw	ACAGAGGCTTTTCCTGACCA	Genotyping	Mouse
Qki 1lox Fw	CCTGGAATGGTGCTTTCCTA	Genotyping	Mouse
Qki 2/1lox Rv	TTCAGAACCCCCACATTACC	Genotyping	Mouse
Myh6-Cre Fw	ATGACAGACAGATCCCTCCTATCTCC	Genotyping	Mouse
Myh6-Cre Rv	CTCATCACTCGTTGCATCATCGAC	Genotyping	Mouse
Gapdh ex 7 Fw	GGTGGACCTCATGGCCTACA	qPCR	Mouse
Gapdh ex 7 Rv	CTCTCTTGCTCAGTGTCCTTGCT	qPCR	Mouse
Hprt ex 6 Fw	GCTTGCTGGTGAAAAGGACCTCTCGAAG	qPCR	Mouse
Hprt ex 8Rv	CCCTGAAGTACTCATTATAGTCAAGGGCAT	qPCR	Mouse
Tbp ex 4 Fw	TATGACCCCTATCACTCCTG	qPCR	Mouse
Tbp ex 7 Rv	TTCTTCACTCTTGGCTCCTGT	qPCR	Mouse
Qki ex 2 Fw	GGAGTGCAGAATTGCCTG	qPCR	Mouse
Qki ex 3 Rv	CTAGGTCCAAGGATTCTCC	qPCR	Mouse
Eef1e1 Fw	TCCAGTAAAGAAGACACCCAGA	qPCR	Rat
EeF1e1 Rv	GACAAAACCAGCGAGA	qPCR	Rat
Gapdh Fw	GGTGGACCTCATGGCCTAC	qPCR	Rat
Gapdh Rv	CTCTCTTGCTCTCAGTATCCTTGCT	qPCR	Rat
Hprt Fw	TGACTATAATGAGCACTTCAGGGATTT	qPCR	Rat
Hprt Rv	CGCTGTCTTTTAGGCTTTGTACTTG	qPCR	Rat
Ablim1 ex 17 Fw	GTTCCAGATCAAGGGATCAACATTTACCG	Splicing	Mouse
Ablim1 ex 19 Rv	CTTCATCAACTGTTCTTCTTGAAGCTGCC	Splicing	Mouse
Actn2 ex 7 Fw	GCCTTGGACTCTGTGCCCTCATC	Splicing	Mouse
Actn2 ex 9 Rv	CTCAGGCGTCCTGTTCTCCAGC	Splicing	Mouse
Akap9 ex 2 Fw	GCTCGGAAAGTTCTCAGAGGGTAGAC	Splicing	Mouse
Akap9 ex 4 Rv	GAAGACAGGTCTGACTGGACTGAGC	Splicing	Mouse
Ank3 ex 15 Fw	GGCATGAGGATGTAGCTGCGTTC	Splicing	Mouse, rat
Ank3 ex 18 Rv	GCGATGTGCAGTGGTGTATAGCC	Splicing	Mouse, rat
Cacnb1 ex 5 Fw	GGTCAAACTGGACAGCCTTCGTCTG	Splicing	Mouse
Cacnb1 ex 8 Rv	GACGGTCCCACCAGGATGATGG	Splicing	Mouse
Camk2d ex 14 Fw	CAGCCAAGAGTTTATTGAAGAAACCAGATGGG	Splicing	Mouse
Camk2d ex 17 Rv	CTTTCACGTCTTCATCCTCAATGGTGGTG	Splicing	Mouse
Fhod3 ex 24 Fw	CCTTATGCAATTCGAGAGGTGAACATCAAC	Splicing	Mouse
Fhod3 ex 25 Rv	GCTGCATCCTCAGCATAGCTCAG	Splicing	Mouse
Ldb3 ex 4 Fw	GCCTATTCCCATCTCCACGA	Splicing	Mouse, rat
Ldb3 ex 7 Rv	GCCTGGTACACAGGAGAGGC	Splicing	Mouse, rat
Nebl ex 24 Fw	GCTTCACTCCCGTTGTGGATGATC	Splicing	Mouse
Nebl ex 27 Rv	GCATTGACCTCATGGACGACACG	Splicing	Mouse
Mbnl2 Fw 7	CCAGCAGGCTCTGACCAGTG	Splicing	Mouse
Mbnl2 Rv 9	AGACAGTGGCGGACGTAGCG	Splicing	Mouse
Mef2c ex 6 Rv	TCTCAAAGCTGGGAGGTGGAACAG	Splicing	Mouse
Mef2c ex α1 Fw	GCCCTGAGTCTGAGGACAAGTACAG	Splicing	Mouse

Table S1. (continued)

Primer	Sequence (5' – 3')	Analysis	Species
Mef2c ex a2 Fw	CCGATCCTGACTCCTCTTATGCACTC	Splicing	Mouse
Rbfox2 ex 9 Fw	CGGACAGTGTATGGTGCAGTCC	Splicing	Mouse
Rbfox2 ex 13 Rv	GCTGTAGCCACCTCGGTACAAAC	Splicing	Mouse
Ryr2 ex 74 Fw	GACTTGCCAAACAGGACAGAAGACC	Splicing	Mouse
Ryr2 ex 76 Rv	CTCTGCTTAGAGAGTAGTTTGTGCCAC	Splicing	Mouse
Slc25a3 ex 1 Fw	GTTCTCGTCCGTAGCGCACC	Splicing	Mouse
Slc25a3 ex 3 Fw	GCCATCTTCTTTCAGTGTAATGGAGAATCC	Splicing	Mouse
Tmed2 ex 2 Fw	CACCATTGACATTGGGGAGGCTC	Splicing	Mouse
Tmed2 ex 3 Rv	CGGACTTCCATGTACTCCTGTTCGTG	Splicing	Mouse
Ttn ex 10 Fw	GCATTTGTACCAAAGGTAGTGATCTCCG	Splicing	Mouse
Ttn ex 14 Rv	CACAGCAGCTACAACTGTTGCCAC	Splicing	Mouse
Myocd ex 2 Fw	AGTTACGGCTTCAACAGAGAAGGACCCAGG	Splicing	Mouse, rat
Myocd ex 5 Rv	TTGAGCTTCATCTGAGCAGTTGGAATGG	Splicing	Mouse, rat

Table S2. Antibodies

Antibody	Dilution	Reference
Anti-α-actinin (ACTN2)	1:500 (IF)	Epitomics 2310-1
Anti-α-actinin (ACTN2)	1:10000 (WB)	Sigma A7811
Anti-calnexin	1:10000 (WB)	Milipore 208880
Anti-CaMKII	1:200 (WB)	Santa Cruz sc-9035, M-176
Anti-desmin	1:200 (IF)	ThermoFisher PA5-16705
Anti-panQKI	WB (500), 1:50 (IF)	Sigma-Aldrich MAB N147/6
Anti-titin (PEVK- IG junction)	1:100 (IF)	Myomedix TTN-5
Anti-rabbit-HRP	1:10000 (WB)	Amersham NA9340V
Anti-mouse-HRP	1:10000 (WB)	Amersham NA9310V
Donkey anti-rabbit-488	1:250 (IF)	Invitrogen A-21206
Donkey anti-mouse-647	1:250 (IF)	Invitrogen A-31571
Goat anti-rabbit-564	1:250 (IF)	Invitrogen A-11008
Goat anti-mouse-647	1:250 (IF)	Invitrogen A-21235

Table S3. Postnatal genotype distribution from *Qki* floxed *Myh6-Cre* mice (*Qki$^{fl/wt}$;Myh6-Cre^{tg} x QkiI$^{fl/wt}$; Myh6-Cre^{-}*)

Genotypes	**Qki$^{wt/wt}$ Myh6-Cre^{-}**	**Qki$^{fl/wt}$ Myh6-Cre^{-}**	**Qki$^{fl/fl}$ Myh6-Cre^{-}**	**Qki$^{wt/wt}$ Myh6-Cre^{tg}**	**Qki$^{fl/wt}$ Myh6-Cre^{tg}**	**Qki$^{fl/fl}$ Myh6-Cre^{tg}**
% observed (n)	20% (23)	34% (40)	13% (15)	9% (10)	25% (30)	0% (0)
% expected	12.5%	25%	12.5%	12.5%	25%	12.5%

Chi-squared test ($\chi 2$) was used to calculate the statistical difference between observed and expected genotypes in the offspring. p-val $\chi 2$ = 1,63E-04.

Table S4. Genotype distribution in E10.5-E14.5 embryos of the *Qki* floxed *Myh6-Cre* line (*Qki$^{fl/wt}$;Myh6-Cre^{tg} x Qki$^{fl/wt}$; Myh6-Cre^{-}*)

Genotypes	**Qki$^{wt/wt}$ Myh6-Cre^{-}**	**Qki$^{fl/wt}$ Myh6-Cre^{-}**	**Qki$^{fl/fl}$ Myh6-Cre^{-}**	**Qki$^{wt/wt}$ Myh6-Cre^{tg}**	**Qki$^{fl/wt}$ Myh6-Cre^{tg}**	**Qki$^{fl/fl}$ Myh6-Cre^{tg}**
% observed (n)	15.5 % (15)	25.8 (25)	9.3% (9)	11.3 % (11)	26.8% (26)	11.3% (11)
% expected (n)	12.5% (12)	25.0% (24)	12.5% (12)	12.5% (12)	25.0% (24)	12.5% (12)

Chi-squared test ($\chi 2$) was used to calculate the statistical difference between observed and expected genotypes in the offspring. p-val = 0,81.

Table S5. Cardiac parameters of ciQKI WT, HET and KO mice 7 days after the last tamoxifen injection.

	ciQKI WT (n=5)	**ciQKI HET (n=6)**	**ciQKI KO (n=9)**	**ANOVA p-value**
BW (g)	23.24 ± 2.37	24.62 ± 4.48	21.36 ± 3.48	0.25
HW (mg)	109.6 ± 13.89	126.8 ± 17.37	105.8 ± 37.42	0.37
HW/TL (mg/mm)	6.56 ± 0.78	7.52 ± 0.91	7.01 ± 1.04	0.27
HW/BW (mg/g)	4.72 ± 0.41	5.23 ± 0.79	5.42 ± 0.61	0.18
LW/TL(mg/mm)	7.21 ± 1.11	8.08 ± 2.04	7.74 ± 1.65	0.70
LVID; d (mm)	4.75 ± 0.25	4.64 ± 0.41	4.85 ± 0.41	0.61
LVID; s (mm)	3.79 ± 0.32	3.68 ± 0.47	4.33 ± 0.34*#	0.01
LVPW;d (mm)	0.59 ± 0.14	0.63 ± 0.08	0.56 ± 0.14	0.61
LVPW;s (mm)	0.69 ± 0.12	0.74 ± 0.09	0.68 ± 0.14	0.66
FS (%)	19.94 ± 6.24	20.69 ± 6.96	10.27 ± 4.81*#	0.005
EF(%)	40.39 ± 11.20	41.67 ± 12.27	22.12 ± 9.83*#	0.005
Heart Rate (BPM)	501.26 ± 39.94	497.50 ± 50.03	515.86 ± 28.61	0.69
PR Interval (ms)	39.93 ± 4.60	46.41 ± 7.24	42.42 ± 5.65	0.24
QRS Interval (ms)	9.55 ± 0.64	10.02 ± 1.58	9.02 ± 1.01	0.31
QTc (ms)	52.26 ± 4.53	53.67 ± 4.38	47.09 ± 10.61	0.36

Data are presented as mean ± standard deviation. Statistical significance was calculated with one-way ANOVA test followed by multiple comparison Fisher's LSD test. * p-val < 0.05 against ciQKI WT; # p-val < 0.05 against ciQKI HET. BW, body weight; HW, heart weight; TL, tibia length; LW, lung weight; LVID, left ventricular internal diameter; d, diastolic; s, systolic; LVPW, left ventricular posterior wall thickness; FS, fractional shortening; EF, ejection fraction.; QTc, heart-rate corrected QT interval.

Table S6. Gene Ontology Enrichment analysis of the mis-spliced genes in the conditional inducible QKI KO hearts.

GO term "biological process"	# background	# dataset	# expected	Fold Enrichment	P value
cardiac muscle hypertrophy	32	13	2.26	5.76	3.30E-02
sarcomere organization	36	14	2.54	5.52	2.13E-02
myofibril assembly	56	17	3.95	4.31	3.06E-02
striated muscle cell development	56	17	3.95	4.31	3.06E-02
cardiac muscle cell development	65	19	4.58	4.15	1.33E-02
cardiac cell development	71	19	5	3.8	3.98E-02
GO term "cellular component"	**# background**	**# dataset**	**# expected**	**Fold Enrichment**	**P value**
cell cortex region	36	13	2.54	5.12	1.58E-02
A band	34	12	2.40	5.01	4.12E-02
Z disc	108	38	7.61	4.99	1.49E-10
I band	118	40	8.32	4.81	9.05E-11
calcium channel complex	40	13	2.82	4.61	3.96E-02
sarcomere	169	51	11.91	4.28	1.59E-12
GO term "molecular function"	**# background**	**# dataset**	**# expected**	**Fold Enrichment**	**P value**
calmodulin binding	146	33	10.29	3.21	1.49E-04
actin filament binding	186	35	13.11	2.67	3.39E-03
actin binding	376	70	26.50	2.64	2.07E-08
cytoskeletal protein binding	854	143	60.18	2.38	3.85E-16
protein binding	7009	566	493.95	1.15	1.49E-02
DNA binding	1729	77	121.85	0.63	2.38E-02

Gene ontology enrichment analysis was performed with the online tool PANTHER[2] comparing the mis-spliced genes in ciQKI KO samples (expression ≥ 0.5 TPM; exon bins with absolute log2FC > 1, p-adj < 0.05) against all genes expressed in the ciQKI WT (≥ 0.5 TPM). #, number of genes. Fisher's Exact with Bonferroni correction for multiple testing.

SUPPLEMENTAL REFERENCES

1. Bolger, A. M., Lohse, M. & Usadel, B. Trimmomatic: a flexible trimmer for Illumina sequence data. *Bioinformatics* **30**, 2114–2120 (2014).
2. Mi, H. *et al.* PANTHER version 16: a revised family classification, tree-based classification tool, enhancer regions and extensive API. *Nucleic Acids Res.* **49**, D394–D403 (2021).
3. Aufiero, S. *circRNAprofiler: circRNAprofiler: An R-Based Computational Framework for the Downstream Analysis of Circular RNAs*. (Bioconductor version: Development (3.11), 2020). doi:10.18129/B9.bioc.circRNAprofiler.
4. Haan, A. D. den *et al.* Organ Explant Culture of Neonatal Rat Ventricles: A New Model to Study Gene and Cell Therapy. *PLOS ONE* **8**, e59290 (2013).

CHAPTER 3

QUAKING REGULATES CIRCULAR RNA PRODUCTION IN CARDIOMYOCYTES

Pablo Montañés-Agudo, Ingeborg van der Made, Simona Aufiero,
Anke J. Tijsen, Yigal M. Pinto, Esther E. Creemers

Submitted

ABSTRACT

Circular RNAs (circRNAs) are a class of non-coding RNA molecules that are gaining increasing attention for their roles in various pathophysiological processes. Quaking (QKI) is an RNA-binding protein and splicing factor, and has been identified as a major regulator of circRNA formation during epithelial-to-mesenchymal transition. In this study, we aimed to investigate the role of QKI in the formation of circRNAs in the heart. We performed RNA-sequencing on hearts of QKI knock out mice and show that 17% of the circRNAs in the adult mouse heart are differently expressed after loss of QKI. We also uncovered a relation between back-splicing and linear splicing by QKI, as the majority of the QKI-regulated circRNAs (58%) were derived from mRNAs that underwent QKI-dependent alternative splicing. RBM20, another major splicing factor expressed in the heart, has recently been identified as a crucial regulator of circRNA formation from the Ttn gene. We compared the differentially expressed circRNAs in the QKI KO model with those in an RBM20 KO model and found that QKI and RBM20 regulate the formation of a distinct, but partially overlapping set of circRNAs. Strikingly, virtually all Ttn-derived circRNAs that are controlled by QKI and by RBM20, are regulated in an opposite manner. Our findings provide new insights into the role of QKI in the regulation of circRNAs in the heart, and suggest that QKI is important in cardiac physiology not only by regulating alternative splicing of specific exons, but also by regulating the formation of circRNAs.

INTRODUCTION

Circular RNAs (circRNAs) are a class of non-coding RNA molecules that are increasingly being recognized for their regulatory roles in critical biological pathways. While the function of most circRNAs is currently unknown, it has been shown that some circRNAs exert a regulatory function by acting as miRNA sponges, as protein-scaffolding molecules, or as transcription or splicing regulators[1]. Some circRNAs have even been shown to possess protein-coding potential[2–4]. In the human heart, thousands of different circRNA molecules are expressed, with the highest numbers produced from the *TTN* and *RYR2* transcripts[1,5,6]. Multiple circRNAs have been linked to pathological processes. For instance, *circFOXO3*, which is increasingly expressed in aging hearts, was shown to be involved in senescence and doxorubicin-induced cardiomyopathy in the mouse heart, by interacting with anti-senescent protein ID1 and the transcription factor E2F1[7]. The highly conserved *circRNA-INSR*, derived from the host gene encoding the insulin receptor, was shown to have protective effects in doxorubicin-induced cardiomyopathy. Interestingly, *circRNA-INSR* interacts with single-stranded DNA-binding protein 1 (SSBP1) to preserve mitochondrial DNA stability and prevent cardiomyocyte apoptosis, after doxorubicin treatment in mice[8]. In human induced pluripotent stem cell-derived cardiomyocytes (hiPSC-CMs), evidence was provided that circRNAs derived from the *TTN* transcript are involved in alternative splicing by affecting the function of the splicing factors SRSF10 and RBM20[9].

As our knowledge of circRNAs in the heart keeps growing, so does the need to understand the factors that control its formation. CircRNAs are generated by a non-canonical form of RNA splicing known as back-splicing, where the splice donor site of one exon is ligated to the splice acceptor site of an upstream exon. This back-splicing event creates a covalently-closed single-stranded circular RNA structure consisting of one or multiple exons, and in some cases also introns. Due to the unusual disposition of the exons within this circle, a new sequence called the back-spliced junction (BSJ) is formed. The BSJ is not present in the linear transcripts and is used to identify the circRNAs from RNA-sequencing reads. Mechanistically, the back-splicing reaction is executed by the spliceosome, and it requires that the two introns flanking the back-spliced exons are brought into close proximity of each other. This can be achieved by looping of the pre-mRNA, mediated by base-pairing of cis-acting elements (e.g. by complementary Alu repeats flanking the back-spliced exons) or by dimerization of trans-acting elements, such as splicing factors[1]. One of the splicing factors that has been shown to regulate back-splicing is the RNA-binding protein Quaking (QKI)[10].

Our lab has recently generated a mouse model with a conditional deletion of QKI in cardiomyocytes to study the function of QKI in the heart[11]. Removal of QKI in the adult heart induced dilation of the ventricles and a rapid decline in cardiac function, and this was

associated with severe disruption of sarcomere organization. Numerous changes in alternative splicing were identified, mostly in sarcomeric, cytoskeletal and calcium-handling genes. We thus concluded that QKI is a major regulator of striated muscle identity by governing a muscle-specific alternative splicing program in cardiomyocytes[11]. This extended earlier studies, in which an essential role for QKI was demonstrated in cardiomyocyte differentiation of cardiac progenitors and in the specification of cardiac mesoderm[12,13].

However, as a splicing factor, QKI has not only been shown to regulate alternative splicing, but also back-splicing. In an elegant study, Conn et al.[10] developed a minigene-based reporter system to screen for RNA-binding proteins that control circRNA formation during human epithelial-to-mesenchymal transition (EMT). They showed that the production of over one-third of abundant circRNAs is dynamically regulated by QKI. Three lines of evidence subsequently revealed that QKI plays a direct role in circRNA production: 1) they found an enrichment of QKI binding motifs in introns flanking QKI-regulated circRNAs, 2) QKI was shown to bind to sites flanking circRNA-forming exons, and 3) insertion of synthetic QKI binding motifs into linear RNA was sufficient to induce exon circularization[10].

Given the essential role of QKI in the alternative splicing program of cardiomyocytes[11], and the identification of QKI as a major regulator of circRNA formation during EMT[10], we hypothesized that QKI is also crucial for the formation of circRNAs in the heart. In this study, we explored QKI-dependent circRNA formation in the heart by using our previously characterized cardiomyocyte-specific QKI knock-out (KO) mouse model. By performing ultra-deep RNA-sequencing and *de novo* circRNA prediction, we show that 17% of the circRNAs that are present in the adult heart are differentially expressed after loss of QKI. We uncovered a relation between back-splicing and linear splicing by QKI, as the majority of the QKI-regulated circRNAs (58%) were derived from mRNAs that underwent QKI-dependent alternative splicing as well. Finally, we compared the differentially expressed circRNAs in the QKI KO model with those in an RBM20 KO model and found that QKI and RBM20 regulate the formation of a distinct, but overlapping set of circRNAs. Strikingly, the TTN-derived circRNAs that are regulated by QKI and by RBM20, are mostly regulated in an opposite manner.

RESULTS

QKI regulates formation of circRNAs in adult cardiomyocytes

To study QKI-dependent circRNA formation in the heart, we used the cardiomyocyte-specific QKI knock-out (KO) mouse line that we previously developed. This mouse line was generated by crossing the QKI-floxed mice[14] with the tamoxifen-inducible Myh6-MerCreMer (Myh6-MCM^{Tg}) line[15]. Deletion of QKI in adult cardiomyocytes resulted in

a heart failure phenotype that developed already within one week after tamoxifen injections. Cardiac dysfunction was attributed to splicing defects in important cardiac genes such as *Ttn*, *Camk2d* and *Tpm1*[11].

To investigate whether QKI regulates circRNA formation in cardiomyocytes, we analyzed RNA-sequencing data of the QKI KO model for the expression of circRNAs (NCBI bioproject: PRJNA831665). This dataset was generated from ribosomal–depleted total RNA libraries, which contain a wide variety of RNA species, including circRNAs. RNA-seq was performed on left ventricles of 5 conditional inducible QKI knock-out hearts (QKI KO = $Qki^{fl/fl}$; *Myh6-MCM*^{Tg}) and 5 wild-type hearts (QKI WT = $Qki^{wt/wt}$; *Myh6-MCM*^{Tg}), one week after tamoxifen injections. CircRNA detection was performed with the bioinformatics tool MapSplice2[16], which identifies circRNAs based on reads covering back-spliced junctions (BSJ) (**Figure 1A, 1B).** A total of 4190 unique circRNAs were detected in any of the 10 samples. We filtered out the lowly and inconsistently expressed circRNAs and continued our analysis with 494 detected circRNAs that had at least three normalized read counts in all samples of one condition. Among the most highly expressed circRNAs in the QKI WT heart, we found several circRNAs previously described in the mouse and human heart, such as *circTtn*$^{121\text{-}88}$, *circTtn*$^{121\text{-}87}$ *and circSlc8a1*$^{2\text{-}2}$ (annotation used: *circGene*$^{back\text{-}spliced\ exons}$) (**Online Data 1**).

Next, we performed differential expression analysis of circRNAs between the adult QKI KO and WT samples with the bioinformatics tool circRNAprofiler[17]. Interestingly, 17% of the detected circRNAs were differentially expressed in the adult heart after loss of QKI (i.e. 86 of the 494 detected circRNAs, absolute $\log_2$(fold change) ($\log_2$FC) ≥ 1.0, adj. p-val ≤ 0.05), with 25 circRNAs being downregulated and 61 upregulated (**Figure 1C**, **Table S1**). Remarkably, 1 circRNA was completely absent (*circSlmap*$^{23\text{-}13}$) and 13 circRNAs were uniquely expressed in the QKI KO mice (arising from *Plekha5*, *Qki*, *Mlip*, *Ehbp1*, *Slmap*, *Pde4dip*, *Strn3*, *Ppp1r12b*, *Obscn*, *Cnksr3* and *Agtpbp1*). We also noted that many genes give rise to more than 1 dysregulated circRNA, with *Ttn* being the gene with the highest number of dysregulated circRNAs (**Figure 1D**). These finding indicate that QKI is involved in the biogenesis of a large proportion of circRNAs in the adult heart.

Differential gene expression analysis was performed to compare the expression levels of circRNAs with the expression levels of their corresponding cognate host genes. QKI KO hearts presented 647 differentially expressed genes (absolute $\log_2$FC ≥ 1.0, adj. p-val ≤ 0.05, TPM ≥ 0.5), but there was no significant correlation with the expression of circRNAs arising from these genes. This indicates that the differences observed in circRNA formation are not dependent on changes in transcription (**Figure S1**).

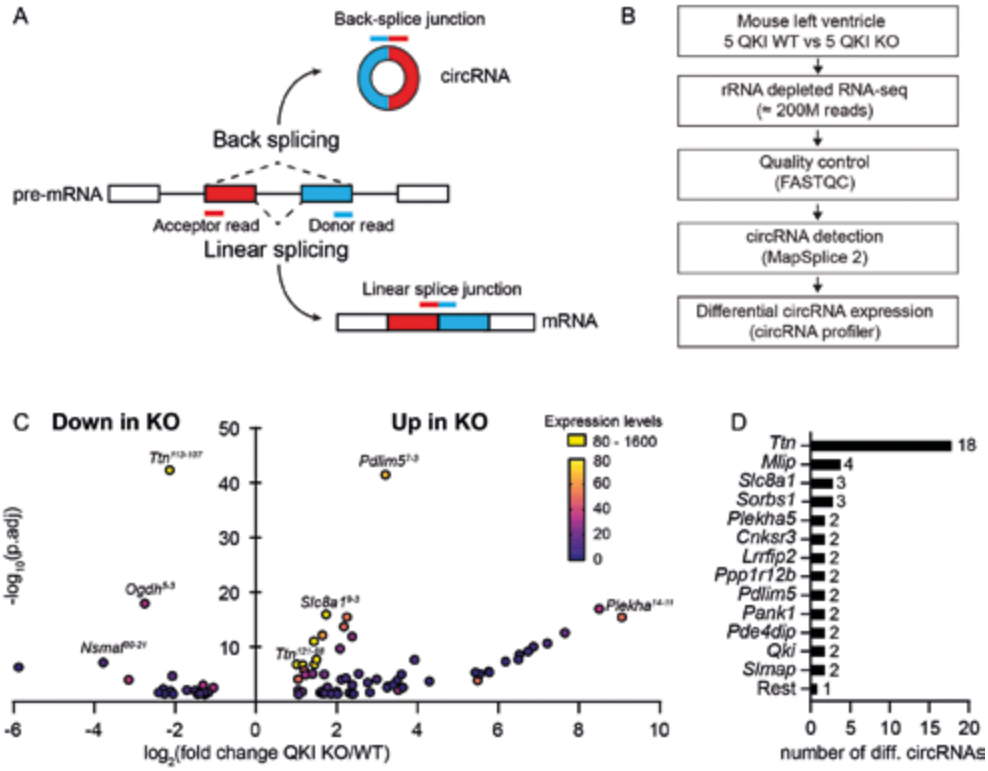

Figure 1. QKI regulates circRNA production in the adult mouse heart. (A) Diagram depicting the detection strategy to distinguish between linear splicing and back splicing. (B) Flow chart for the detection and quantification of circRNAs in QKI WT and KO hearts. (C) Volcano plot showing the differentially expressed circRNAs in the QKI KO hearts. The color code of each dot represents the expression level of each circRNA (average of the normalized counts in 5 WT and 5 KO samples). (D) Number of differentially expressed circRNAs per gene in the QKI KO hearts.

We asked whether the large differences in circRNA expression that we observed in the QKI KO hearts (i.e. 17% of the expressed circRNAs) could in part be explained by more generic changes induced during the development of the cardiomyopathy. To dissect the changes that are specific for loss of QKI, we quantified circRNA expression in hearts where cardiac dysfunction was induced by transverse aortic constriction (TAC) as compared to sham surgery (n = 4 sham vs 4 TAC). Three weeks after TAC surgery, hearts became hypertrophic and displayed reduced ejection fraction (**Figure S2A-B**). CircRNAs were detected in RNA sequencing reads using the same bioinformatics pipeline as the QKI KO study. Interestingly, in this model only 3% of the circRNAs (4 out of 129 circRNAs) were differently expressed in TAC hearts compared to the sham operated control hearts (**Figure S2C**). In addition, only *circTtn*$^{121\text{-}87}$ was also

changed in the QKI KO hearts, but the change was in the opposite direction. While the disease mechanisms after TAC and loss of QKI differ, these findings suggest that more general cardiac remodeling and dysfunction by itself does not lead to robust changes in circRNA expression. In conclusion, these findings indicate that changes in circRNA formation in the QKI KO heart are not secondary consequences of the diseased heart.

Experimental validation of the QKI-dependent circRNAs

To test whether the QKI-dependent circRNAs identified by RNA-sequencing, were bona fide circRNAs we selected 10 circRNAs for validation by RT-PCR. The selection of these 10 circRNAs (i.e., *circOgdh*$^{5\text{-}3}$, *circTtn*$^{113\text{-}107}$, *circPdlim5*$^{9\text{-}3}$, *circPdlim5*$^{9\text{-}4}$, *circArhgap32*$^{18\text{-}14}$, *circMyzap*$^{12\text{-}6}$, *circPde4dip* $^{8\text{-}5}$, *circTtn*$^{121\text{-}87}$ and *circTtn*$^{121\text{-}88}$, *circPlekha5*$^{14\text{-}11}$) was based on expression levels and statistical significance in the QKI WT vs QKI KO comparison. In order to exclusively amplify the circRNA molecules and not the linear transcripts, divergent primers were designed flanking the back-splice junction, with the forward primer annealing to the downstream exon and the reverse primer to the upstream exon. As shown in **Figure 2A,** we could confirm the presence of all tested circRNAs in adult mouse hearts by RT-PCR. Of note, *circPlekha5*$^{14\text{-}11}$ was validated in QKI KO samples, since this circRNA was only detected in the KO and not in the WT hearts (**Figure 2B**). We also tested their expected resistance to exoribonucleases RNAse R digestion. Whereas the linear *Hprt* transcript was clearly sensitive to RNAse R digestion, the 10 circRNAs were all resistant to RNAse R digestion. Finally, Sanger sequencing was performed and confirmed the presence of the back-spliced junction in the amplicons of the 10 tested circRNAs **(Figure S3).** Together, these experiments demonstrate that the back-splice junctions identified by MapSplice2 represent bona fide circRNAs.

Next, we verified the changes in circRNA expression between the QKI genotypes by RT-PCR (**Figure 2C**). Here, we included QKI heterozygous (HET) hearts to check whether they presented an intermediate circRNA expression level. We confirmed the reduction in *circOgdh*$^{5\text{-}3}$ and *circTtn*$^{113\text{-}107}$ in the QKI KO*;* and the increase in *circPdlim5* $^{9\text{-}3}$, *circPdlim5* $^{9\text{-}4}$, *circPlekha5*$^{14\text{-}11}$, *circArhgap32*$^{18\text{-}14}$, *circMyzap*$^{12\text{-}6}$, *circPde4dip*$^{8\text{-}5}$, *circTtn*$^{121\text{-}87}$ and *circTtn*$^{121\text{-}88}$ **(Figure S4).** Heterozygous mice did not show intermediate levels of expression for most of the circRNAs, except for *circMyzap*$^{12\text{-}6}$. This is in line with the absence of a cardiac phenotype and the lack of strong splicing changes in the heterozygous KO mice[11].

Regulation of linear splicing and back-splicing by QKI

Since QKI activity is essential for proper splicing of multiple cardiac genes, we investigated whether changes in circRNA formation were associated with changes in alternative splicing. To do so, we compared the 86 differentially expressed circRNAs in the QKI KO mice with

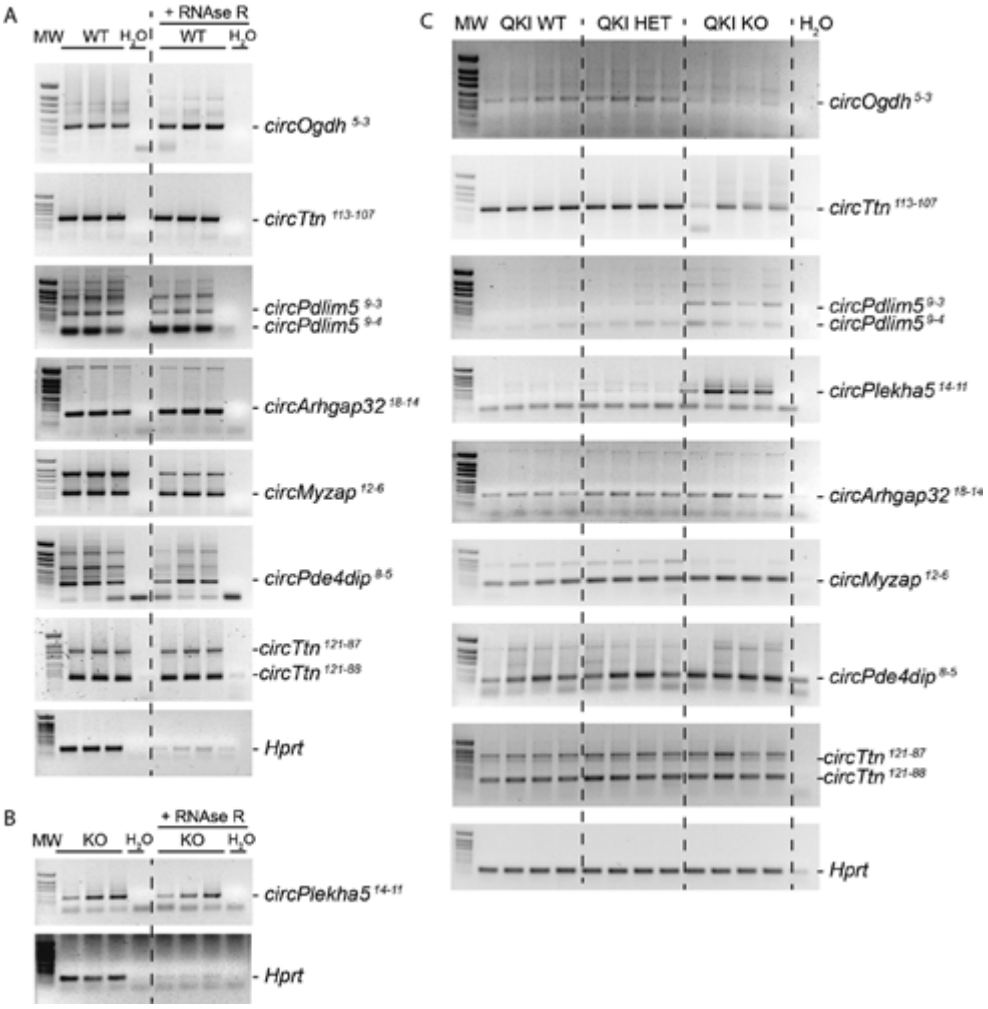

Figure 2. Experimental validation of detected circRNAs. (A) RT-PCR verification of a selection of the detected circRNAs in left ventricle samples with and without RNA R treatment of 3 wildtype and (B) 3 QKI KO. (C) RT-PCRs showing differentially expressed circRNAs in 4 QKI WT, 4 QKI HET and 4 QKI KO adult mice. Molecular ladder sizes are 712, 481, 404, 363, 242, 190, 147, 118 and 110 bp.

the alternatively spliced exons of the corresponding host genes as identified by DEXSeq[11]. We found that 50 of the 86 differently expressed circRNAs (58%) displayed at least one alternatively spliced exon in the host gene (**Figure 3A**).

In order to assess where the QKI-mediated alternative splicing changes were occurring in these 50 circRNAs, we focused on the regions were circRNAs were arising and we divided it in five

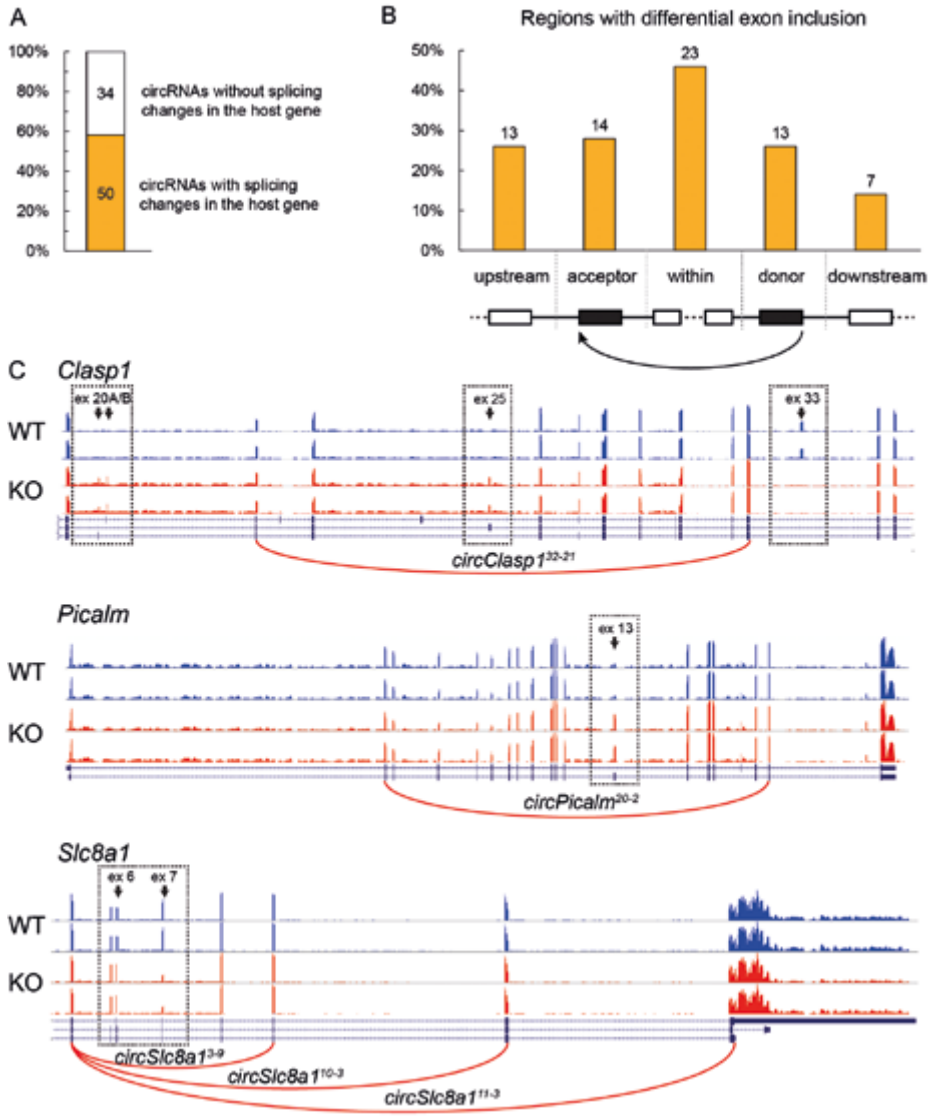

Figure 3. A majority of the QKI-dependent circRNAs is linked to alternative splicing. (A) Number of QKI-dependent circRNAs that are associated with changes in exon usage of the corresponding host gene in the QKI KO mice. (B) Number of QKI-dependent circRNAs arising from regions that also underwent alternative splicing changes in the QKI KO hearts. The back-spliced region was divided in five parts: acceptor and donor back-spliced exons, exons between the back-spliced exons, and exons immediately upstream and downstream of the back-spliced exons. (C) Representative examples of QKI-regulated circRNAs with differentially spliced exons in their back-spliced regions. Bed graphs show exon coverage of 2 mice per genotype. Black arrows indicate the significantly different exons. Red arcs indicate the significantly differently expressed circRNAs in QKI KO hearts.

parts: 1) acceptor back-spliced exon and 2) donor back-spliced exon, 3) exons located between the back-spliced exons, 4) exons immediately upstream and 5) immediately downstream of the back-spliced exons (**Figure 3B**). We counted the number of circRNAs with alternative splicing changes (i.e. differential exon usage) in each location and found alternative splicing changes most frequently taking place in exons within the back-spliced exons (23/50). 22 of the 50 circRNAs revealed alternative splicing changes of the exons used for circularization (acceptor exon: n=14, donor exon: n=13). 19 circRNAs were associated with splicing changes upstream and/or downstream of the back-spliced exons (upstream: n = 13, downstream: n= 7). **Figure 3C** depicts three examples of genes in which alternative splicing events are associated with circRNA expression upon QKI loss (i.e. *circClasp1*$^{32\text{-}21}$, *circPicalm*$^{20\text{-}2}$, *circSlc8a1*$^{9\text{-}3}$, *circSlc8a1*$^{10\text{-}3}$, *and circSlc8a1*$^{11\text{-}3}$). All five circRNAs shown contain alternatively spliced exons between the back-spliced exons. *circClasp1*$^{32\text{-}21}$ is an interesting circRNA, as it shows, besides alternative splicing changes in an exon located between the back-spliced exons, also alternative splicing changes in two exons immediately upstream and immediately downstream the back-spliced exons. In conclusion, our findings reveal that regions with QKI-dependent back-splicing are often associated with QKI-dependent linear splicing.

QKI and RBM20 regulate back-splicing of a distinct, but overlapping set of circRNAs

Aside from QKI, there is one other splicing factor known thus far to regulate circRNA formation in the heart. This is the RNA-binding motif protein 20 (RBM20)[9,18], a well-studied heart and muscle-specific splicing factor in which mutations can cause inherited dilated cardiomyopathy[19]. Our group has previously generated RBM20 KO mice to investigate the role of RBM20 in the heart, also in circRNA formation[18,20]. In these RBM20 KO hearts, we identified 41 differentially expressed circRNAs, of which 12 were produced from the *Ttn* gene[20]. We compared the QKI-dependent and RBM20-dependent circRNAs to look for commonalities in their regulation. The Venn Diagram in **Figure 4A** depicts a distinct, but overlapping set of circRNAs regulated by QKI and RBM20. A total of 15 circRNAs, arising from 8 different genes, were regulated by QKI *and* RBM20 (absolute $\log_2$FC ≥ 0.58, p-value ≤ 0.05). The scatterplot in **Figure 4B** shows the fold-changes of these 15 circRNAs in both KO models. We did not find a common direction of regulation for the overlapping circRNAs. Whereas the expression of for instance *circFan*$^{8\text{-}3}$ and *circPde4dip*$^{8\text{-}5}$ changed in the same direction in both KO models; *circSorbs1*$^{20\text{-}10}$ and *circArghap26*$^{11\text{-}7}$ expression changed in the opposite direction (**Figure 4C**).

CircRNAs derived from TTN are oppositely regulated by QKI and RBM20

Since multiple circRNAs arising from *Ttn* were differentially expressed in both the QKI KO (24 circRNAs) and the RBM20 KO hearts (12 circRNAs), we took a closer look at the location of

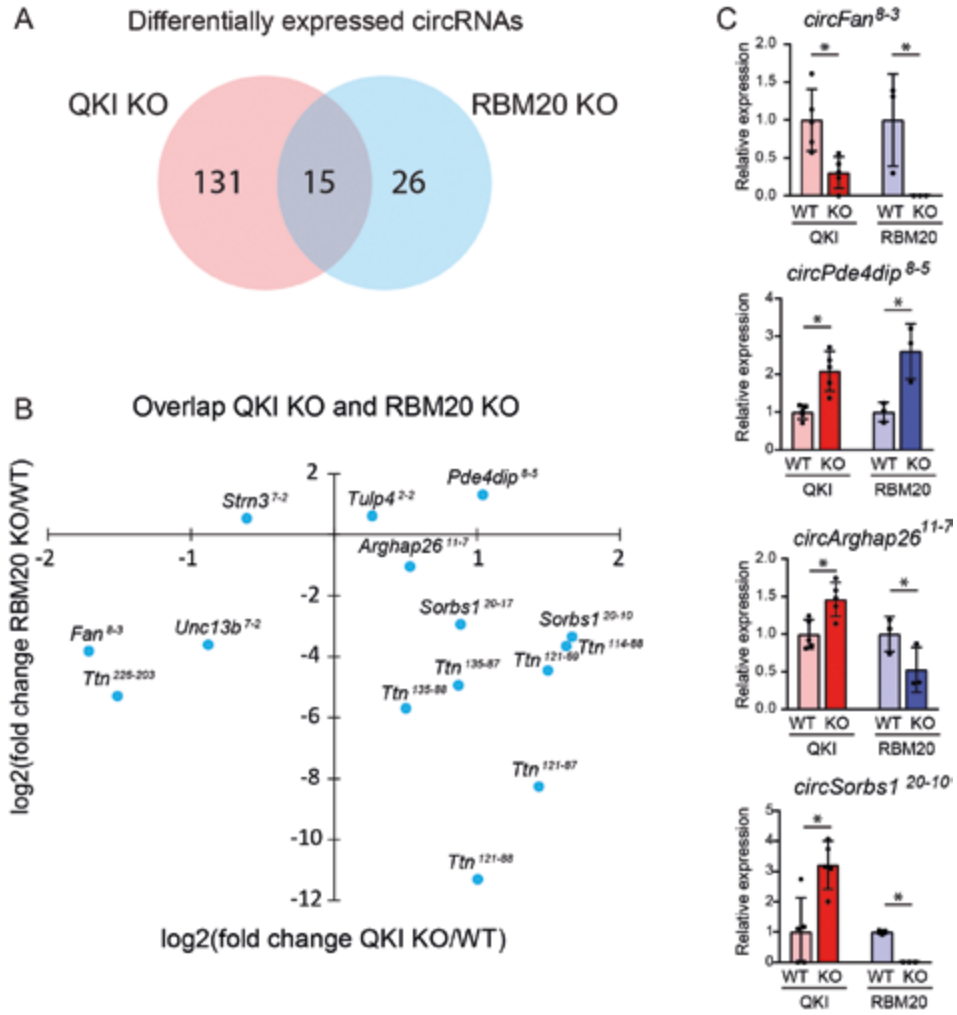

Figure 4. QKI and RBM20 regulate back-splicing in distinct ways. (A) Venn diagram showing the overlap between the differentially expressed circRNAs in the QKI KO and RBM20 KO hearts. CircRNAs with absolute $log_2FC \geq 0.58$ and p-value ≤ 0.05 were deemed differentially expressed. (B) Scatter plot showing expression changes (log_2FC) of the differentially expressed circRNAs in the QKI and RBM20 KO hearts. (C) Relative expression of *circFan*$^{8\text{-}3}$, *circPde4dip*$^{8\text{-}5}$, *circArghap26*$^{11\text{-}7}$ and *circSorbs1*$^{20\text{-}10}$ in QKI and RBM20 WT and KO mice. Relative expression is the normalized BSJ counts relative to the average of the corresponding WT. * p-val ≤ 0.05.

the back-spliced exons of the *Ttn*-derived circRNAs. First, we visualized the genomic location of the back-spliced exons of all 33 *Ttn* circRNAs detected in wild-type hearts (**Figure S5**). Most circRNAs originated by back-splicing of exons located in the middle I-band (i.e. exons

47 to 143). This region includes the two most highly expressed circRNAs: *circTtn*$^{121\text{-}88}$ and *circTtn*$^{121\text{-}87}$. A smaller subset of circRNAs arise from the distal I-band, but their expression levels are lower. Strikingly, when comparing the upregulated and downregulated circRNAs in the QKI KO and the RBM20 KO hearts, an opposite regulation was observed: the circRNAs in the middle I-band are increased in the QKI KO, but reduced (or even absent) in the RBM20 KO hearts (**Figure 5A, 5B**). In conclusion, QKI and RBM20 regulate the formation of a distinct, but overlapping set of circRNAs in an opposite manner.

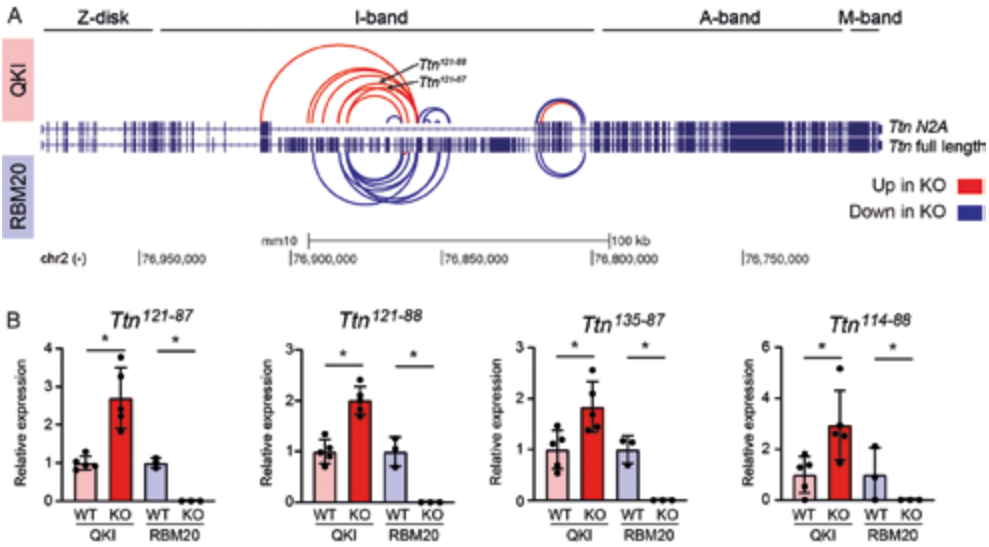

Figure 5. Circular RNAs arising from *Ttn* are regulated by QKI and RBM20. (A) Differentially expressed circRNAs arising from the *Ttn* gene in QKI and RBM20 KO hearts. The full lenght isoform of *Ttn* and the *Ttn* isoform N2A are shown. Each arc represents a differentially expressed circRNA, with downregulated circRNAs depicted in blue and upregulated circRNAs in red. (B) Expression of *circTtn*'s follows an opposite direction in QKI KO and RBM20 KO hearts. Relative expression is the normalized BSJ counts relative to the average of the corresponding WT. * p-val ≤ 0.05.

DISCUSSION

In this work, we have shown that the splicing factor QKI is crucial for circRNA formation in the heart. We found that ~17% of the circRNAs present in the adult mouse heart are differentially spliced in the absence of QKI. Interestingly, we found circRNAs being down- and upregulated in the QKI KO, which indicates that QKI can act either as a positive or as a negative regulator of circRNA formation. We also found that changes in circRNA formation after loss of QKI are often associated with alternative splicing changes of the host transcript. These splicing changes were not only occurring in the back-spliced exons, but also between them or in close proximity.

Conn et al. were the first to postulate that QKI promotes the formation of circRNAs[10]. They observed that QKI knockdown in immortalized human mammary epithelial cells led to a strong decrease in circRNA abundance. Specifically, of the 300 abundantly expressed circRNAs, 105 were decreased more than-2 fold by QKI knockdown, whereas only 7 were increased[10]. They proposed a mechanism in which QKI binds to intronic QKI-binding motifs flanking the exons to be back-spliced[10]. Since QKI exerts its function in a dimer fashion[21], the homodimerization of two QKI proteins surrounding these exons would bring the donor and acceptor splice sites in close proximity, thus favoring the back-splicing reaction[10]. This molecular mechanism may explain the 25 downregulated circRNAs that we observed in the QKI KO hearts, but not the 61 upregulated circRNAs. This fact, in combination with the extensive alternative splicing events occurring in the back-spliced region, point to a more complex regulation of splicing by QKI in the heart. Further research is necessary to uncover the mode of action of QKI in circRNA formation and alternative splicing. Experimentally assessing the precise location where QKI binds to the mRNA using cross-linking immunoprecipitation assays (RNA CLIP) and identification of splicing factors that QKI interacts with, will provide insights in (back) splicing regulation by QKI in the heart.

Comparison of the QKI and RBM20 knockout models revealed surprising little overlap between QKI- and RBM20-dependent circRNAs, except for circRNAs derived from the *Ttn* gene. Interestingly, *Ttn*-derived circRNAs were mostly regulated in an opposite manner by QKI and RBM20. The intricate pattern of splicing and back-splicing in the *Ttn* transcript is noteworthy for the following two reasons. First, the *Ttn* gene generates the largest number of circRNAs, which are highly expressed and mainly produced from the middle I-band region[18,22]. This region is also known for extensive alternative splicing to generate diverse TTN isoforms with varying length and mechanical properties[23–25]. Second, multiple circRNAs from the middle I-band are regulated by QKI and RBM20 in opposite ways, with an increase in QKI KO and virtually complete loss in RBM20 KO hearts. Interestingly, alternative splicing changes in TTN's I-band region do not point to an opposite regulation

by QKI and RBM20, as I-band exons are more included in both KO models. However, there are differences. In the RBM20 KO hearts all exons of the I-band are included (exons 49 to 202), while in the QKI KO only a smaller region is included (exons 88 to 121)[11]. This smaller region controlled by QKI produces the most highly expressed circRNAs: *circTtn*$^{121\text{-}88}$ and *circTtn*$^{121\text{-}87}$. Studies indicate that the RBM20-dependent skipped exons of the I-band are the source of circRNAs[18], as observed in RBM20 KO mice and in patients carrying RBM20 mutations, where the loss of function leads to the inclusion of all exons and complete loss of circRNAs. These differences may be caused by the different ways QKI and RBM20 regulate splicing. RBM20 functions as a splicing repressor[24], while QKI can act as a positive or negative regulator of splicing, dependent on the position where QKI binds relative to the spliced exon[26]. The mechanism behind this behavior is not well understood, but it may involve QKI dimerizing and controlling splicing through looping of the pre-mRNA of the middle I-band[10]. Adding another layer of complexity, Tijsen et al.[9] have shown that the human *circTTN*$^{145\text{-}79}$ (not conserved in mouse) controls the splicing activity of RBM20 and SRSF10. This finding suggests that circRNAs derived from *Ttn* may work as a positive feedback loop to maintain proper splicing of *Ttn* itself.

We are not the first to study QKI-dependent circRNAs in the heart. Gupta et al. previously identified three QKI-dependent circRNAs (*circTtn*$^{113\text{-}107}$, *circFhod3*$^{13\text{-}11}$ and *circStrn3*$^{7\text{-}2}$) when investigating the cardioprotective function of QKI against doxorubicin toxicity[27]. In our QKI KO mouse model we confirmed the QKI-dependent regulation of two of those circRNAs (i.e. *circTtn*$^{113\text{-}107}$ and *circStrn3*$^{7\text{-}2}$), but *circFhod3*$^{13\text{-}11}$, which was expressed in our dataset, did not appear a target of QKI, at least in cardiomyocytes. Some of the QKI-dependent circRNAs that we identified were previously reported to be implicated in cardiomyocyte function. For example, decreased expression of *circTtn*$^{113\text{-}107}$ was shown to increase doxorubicin-induced apoptosis in mouse HL-1 myocytes[27]. Although overexpressing some of these cardioprotective circRNAs could be an interesting therapeutic approach, this is complicated due to the large size of some of these circRNAs and the difficulties to promote their circularization. An alternative strategy could be to upregulate the expression of circRNAs through modulating QKI activity. This is also interesting in light of the recent observation that cardiac QKI expression is downregulated in patients with heart failure[27]. Our previous work has already shown that QKI overexpression can enhance contractility in neonatal rat ventricular myocytes presumably by enhancing alternative splicing towards the expression of muscle-specific isoforms[11]. The current study suggests that changes in circRNA formation may have contributed to the increased contractile properties upon QKI overexpression as well.

Taken together, our study shows that the splicing factor QKI regulates circRNA biogenesis in adult cardiomyocytes *in vivo*. We propose that QKI is important in cardiac physiology not

only by regulating alternative splicing of specific exons, but also by regulating the formation of circRNAs. Functional follow-up studies on QKI-regulated circRNAs are required to shed light on the relevance of these circRNAs in the healthy and diseased heart.

MATERIALS AND METHODS

Knockout mouse models

Animal studies were approved by the Institutional Animal Care and Use Committee of the University of Amsterdam and carried out in compliance with the guidelines of this institution and the Directive 2010/63/EU of the European Parliament. Animal husbandry was performed by the Animal Research Institute AMC.

Generation of the cardiomyocyte-specific QKI KO and inducible cardiomyocyte-specific QKI KO mice was described previously[11]. In brief, mice were generated by crossing the QKI-floxed line[14] with the tamoxifen-inducible Myh6-MerCreMer (Myh6-MCM) (Jackson Laboratory stock #005657)[15] line in C57BL/6N background. For inducing MCM recombinase activity, a tamoxifen solution (2.5 mg/ml tamoxifen in 10% ethanol, 90% sunflower oil) was injected intraperitoneally for 4 consecutive days (total dose 100 mg tamoxifen/kg mouse) in 12-17 week-old mice (n per group: 5 QKI WT, 6 QKI HET, 9 QKI KO). The MCM recombinase allele was present in one copy in all the mice. Both males and females were included in the experiments. RBM20 KO mice were previously generated and characterized[18].

Transverse aorta constriction

Transverse aorta constriction (TAC) was performed in 8 week old male mice (mixed background (F2) of C57BL/6 and FVB) as previously described[28]. 3 weeks after TAC or sham surgery echocardiography was performed as previously described[11] and mice were sacrificed while being sedated.

RNA sequencing

Total RNA from left ventricle tissue of adult mice (5 WT and 5 QKI KO) was extracted by using TRI reagent (Sigma, Ref T9424). RNA quality was determined using the Agilent RNA 6000 Nano Kit and the Agilent 2100 Bioanalyser. All samples had an RNA Integrity score ≥ 8. Library preps were made with the Kapa RNA Hyperprep with RiboErase (Roche) and sequenced on a NovaSeq platform (NovaSeq S4.300; flow cell type PE150, 2 x 150nt, sequencing depth ~108.5 – 225.5 million reads per sample). Quality control of FASTQ files was performed using FASTQC[29]. Trimmomatic (version 0.351)[30] was used to remove adapters and low quality bases, using a Phred score cutoff of 30 while discarding reads with a length below 75 bases. The paired-end RNA-seq reads passing the quality controls from the five QKI KO mice and five wild-type mice were then aligned against the mouse

genome, Gencode annotation release vM25 (GRCm38/mm10), using MapSplice2 (version 2.2.0). For circRNAs detection we set the following options: --min-fusion-distance 200 (as suggested by the authors), --filtering 1, and --min-map-len 50. FASTQ files are available in the NCBI Sequence Read Archive [NCBI bioprojects PRJNA831665 (QKI KO).

Differential gene expression analysis was performed using the R Bioconductor package, DESeq2[31] (Bioconductor release 3.13). Transcripts Per Million (TPM) for each gene were also calculated. Genes with TPM value ≥ 0.5, an absolute $\log_2$FC ≥ 1.0 and adjusted P-value ≤ 0.05 were deemed significantly differentially expressed[11].

Differential exon usage analysis was performed using the R Bioconductor package, DEXSeq[32] (Bioconductor release 3.13). Only genes expressed with TPM value ≥ 0.5 were considered. Exon bins with absolute $\log_2$FC ≥ 1.0 and adjusted P-value ≤ 0.05 were deemed differentially spliced[11].

Differential circRNA expression analysis was performed using the R Bioconductor package circRNAprofiler[17] (Bioconductor release 3.13). CircRNAs with an absolute $\log_2$FC change ≥ 1.0 and adjusted p-value ≤ 0.05 were deemed significantly differentially expressed in the QKI KO hearts (**Table S1**).

RNA sequencing of the 3 week TAC mice (4 sham, 4 TAC) was performed at QIAGEN Benelux B.V. (The Netherlands) (NextSeq platform 2 x 100 bp, sequencing depth 88 – 113 million reads per sample). Bioinformatic analysis was performed using the same bioinformatics pipeline as for the QKI KO mice.

RNA sequencing of the RBM20 KO mice (3 WT, 3 KO) was performed previously by Khan et al[18]. Bioinformatic analysis was performed using the same pipeline as in the QKI KO mice, but in the mouse genome annotation GRCm39/mm39. In order to compare the differentially expressed circRNAs in the RBM20 KO with the QKI-dependent circRNAs, coordinates of the back-spliced exons were converted to the GRCm38/mm10 annotation with the LiftOver tool from the UCSC genome browser[33]. For comparison of QKI-dependent and RBM20-dependent circRNAs, we used the following cut-offs: $\log_2$FC ≥ 0.58 and P-value ≤ 0.05. FASTQ files are available in the NCBI Sequence Read Archive [NCBI bioprojects PRJNA417769 (RBM20 KO)].

RNAse R digestion and RT-PCRs

To validate circularity of circRNAs, an RNase R digestion step was performed on 3 QKI WT and 3 QKI KO samples. Specifically, 2.5 μg of RNA were incubated in 1x RNase R buffer

with or without 5 units of RNase R (Epicentre) at 37°C for 10 minutes followed by heat inactivation at 95°C for 3 minutes.

For cDNA synthesis, 500 ng of total RNA were treated with DNAse I (Invitrogen, Ref 18068-015, Waltham, MA, USA) and retrotranscribed into cDNA with random hexamers (Invitrogen, Ref N8080127) and Superscript II (Invitrogen, Ref 18064-014).

RT-PCRs were performed in a 25 µL reaction containing 5 ng cDNA, 1M Betaine, 1x Buffer B2, 2.5 mM MgCl2, 200 µM dNTPs, 0.4 µM forward primer, 0.4 µM reverse primer and 0.05 U/µ HOT FIREpol® DNA polymerase (Solis Biodyne). The thermal cycling protocol included an initial denaturation at 95 °C for 15 min to activate the HOT FIREPol® DNA polymerase, followed by 25-35 amplification cycles of denaturation at 95°C for 30 s, annealing at 59-62°C for 30 s, extension at 72 °C for 45 s, and 5 minutes of final extension at 72°C. Primer sequences are found in **Table S2.**

Visualization of circRNAs

circRNAs were visualized on the UCSC genome browser[33] by creating a custom track with the back-spliced exons. CircRNAs were drawn manually.

FUNDING

This work was supported by grants from the Rembrandt Institute for Cardiovascular Sciences (2017) to E.E.C. and from the Netherlands Cardiovascular Research Initiative CVON (CVON-ARENA-PRIME) to Y.M.P.

CONFLICT OF INTEREST

Y.M.P. is an inventor on patents, holds minor shares (<5%), and serves as a consultant for biotech and pharmaceutical companies that develop molecules or RNA therapies that target myocardial disease (Forbion Capital, ARMGO BV, Oxitope Pharmaceuticals, Phlox Therapeutics) and received support from Roche Diagnostics. The remaining authors have no conflicts of interest to declare.

REFERENCES

1. Aufiero, S., Reckman, Y. J., Pinto, Y. M. & Creemers, E. E. Circular RNAs open a new chapter in cardiovascular biology. *Nat. Rev. Cardiol.* **16**, 503–514 (2019).
2. Pamudurti, N. R. *et al.* Translation of CircRNAs. *Mol. Cell* **66**, 9-21.e7 (2017).
3. Yang, Y. *et al.* Extensive translation of circular RNAs driven by N6-methyladenosine. *Cell Res.* **27**, 626–641 (2017).
4. Legnini, I. *et al.* Circ-ZNF609 Is a Circular RNA that Can Be Translated and Functions in Myogenesis. *Mol. Cell* **66**, 22-37.e9 (2017).
5. Chen, X. *et al.* circRNADb: A comprehensive database for human circular RNAs with protein-coding annotations. *Sci. Rep.* **6**, 34985 (2016).
6. Tan, W. L. W. *et al.* A landscape of circular RNA expression in the human heart. *Cardiovasc. Res.* **113**, 298–309 (2017).
7. Du, W. W. *et al.* Foxo3 circular RNA promotes cardiac senescence by modulating multiple factors associated with stress and senescence responses. *Eur. Heart J.* **38**, 1402–1412 (2017).
8. Lu, D. *et al.* A circular RNA derived from the insulin receptor locus protects against doxorubicin-induced cardiotoxicity. *Eur. Heart J.* **43**, 4496–4511 (2022).
9. Tijsen, A. J. *et al.* Titin Circular RNAs Create a Back-Splice Motif Essential for SRSF10 Splicing. *Circulation* **143**, 1502–1512 (2021).
10. Conn, S. J. *et al.* The RNA Binding Protein Quaking Regulates Formation of circRNAs. *Cell* **160**, 1125–1134 (2015).
11. Montañés-Agudo, P. *et al.* The RNA-binding protein QKI governs a muscle-specific alternative splicing program that shapes the contractile function of cardiomyocytes. *Cardiovasc. Res.* cvad007 (2023) doi:10.1093/cvr/cvad007.
12. Chen, X. *et al.* QKI is a critical pre-mRNA alternative splicing regulator of cardiac myofibrillogenesis and contractile function. *Nat. Commun.* **12**, 89 (2021).
13. Fagg, W. S. *et al.* Definition of germ layer cell lineage alternative splicing programs reveals a critical role for Quaking in specifying cardiac cell fate. *Nucleic Acids Res.* **50**, 5313–5334 (2022).
14. Darbelli, L., Vogel, G., Almazan, G. & Richard, S. Quaking Regulates Neurofascin 155 Expression for Myelin and Axoglial Junction Maintenance. *J. Neurosci.* **36**, 4106–4120 (2016).
15. Sohal, D. S. *et al.* Temporally Regulated and Tissue-Specific Gene Manipulations in the Adult and Embryonic Heart Using a Tamoxifen-Inducible Cre Protein. *Circ. Res.* **89**, 20–25 (2001).
16. Wang, K. *et al.* MapSplice: Accurate mapping of RNA-seq reads for splice junction discovery. *Nucleic Acids Res.* **38**, e178 (2010).
17. Aufiero, S. *circRNAprofiler: circRNAprofiler: An R-Based Computational Framework for the Downstream Analysis of Circular RNAs*. (Bioconductor version: Development (3.11), 2020). doi:10.18129/B9.bioc.circRNAprofiler.
18. Khan, M. A. F. *et al.* RBM20 Regulates Circular RNA Production From the Titin Gene. *Circ. Res.* **119**, 996–1003 (2016).
19. Guo, W. *et al.* RBM20, a gene for hereditary cardiomyopathy, regulates titin splicing. *Nat. Med.* **18**, 766–773 (2012).
20. Aufiero, S. *et al.* Cardiac circRNAs arise mainly from constitutive exons rather than alternatively spliced exons. *RNA* **24**, 815–827 (2018).
21. Beuck, C., Qu, S., Fagg, W. S., Ares, M. & Williamson, J. R. Structural analysis of the quaking homodimerization interface. *J. Mol. Biol.* **423**, 766–781 (2012).
22. Djebali, S. *et al.* Landscape of transcription in human cells. *Nature* **489**, 101–108 (2012).
23. Loescher, C. M., Hobbach, A. J. & Linke, W. A. Titin (TTN): from molecule to modifications, mechanics, and medical significance. *Cardiovasc. Res.* **118**, 2903–2918 (2022).
24. Maatz, H. *et al.* RNA-binding protein RBM20 represses splicing to orchestrate cardiac pre-mRNA processing. *J. Clin. Invest.* **124**, 3419–3430 (2014).
25. Li, S., Guo, W., Dewey, C. N. & Greaser, M. L. Rbm20 regulates titin alternative splicing as a splicing repressor. *Nucleic Acids Res.* **41**, 2659–2672 (2013).
26. Neumann, D. P., Goodall, G. J. & Gregory, P. A. The Quaking RNA-binding proteins as regulators of cell differentiation. *WIREs RNA* **13**, e1724 (2022).

27. Gupta, S. K. *et al.* Quaking Inhibits Doxorubicin-Mediated Cardiotoxicity Through Regulation of Cardiac Circular RNA Expression. *Circ. Res.* **122**, 246–254 (2018).

28. Tijsen, A. J. *et al.* The microRNA-15 family inhibits the TGFβ-pathway in the heart. *Cardiovasc. Res.* **104**, 61–71 (2014).

29. Babraham Bioinformatics - FastQC A Quality Control tool for High Throughput Sequence Data. https://www.bioinformatics.babraham.ac.uk/projects/fastqc/.

30. Bolger, A. M., Lohse, M. & Usadel, B. Trimmomatic: a flexible trimmer for Illumina sequence data. *Bioinforma. Oxf. Engl.* **30**, 2114–2120 (2014).

31. Love, M. I., Huber, W. & Anders, S. Moderated estimation of fold change and dispersion for RNA-seq data with DESeq2. *Genome Biol.* **15**, 550 (2014).

32. Anders, S., Reyes, A. & Huber, W. Detecting differential usage of exons from RNA-seq data. *Genome Res.* **22**, 2008–2017 (2012).

33. Kent, W. J. *et al.* The Human Genome Browser at UCSC. *Genome Res.* **12**, 996–1006 (2002).

SUPPLEMENTAL FIGURES

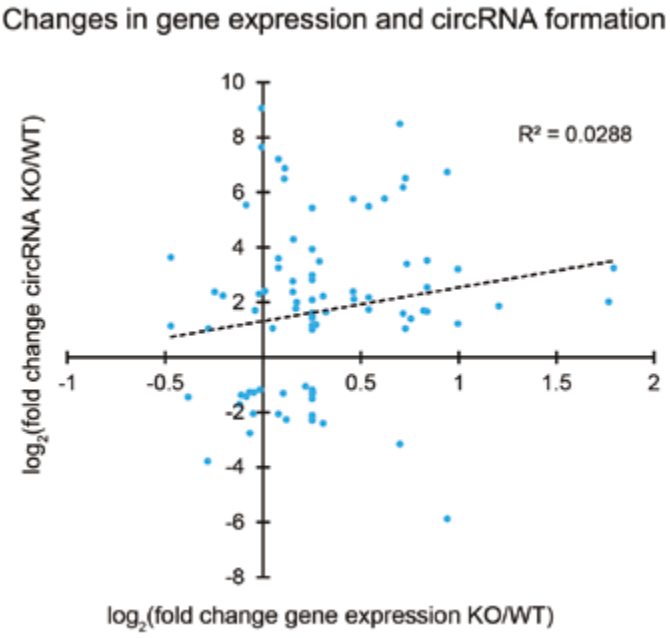

Figure S1. There is no correlation between gene expression and circRNA formation. Scatter plot depicting the changes in circRNA expression against the changes in expression of the host gene in the QKI KO mice. Each dot is a circRNA. Only circRNAs with adj. p-val ≤ 0.05 are shown.

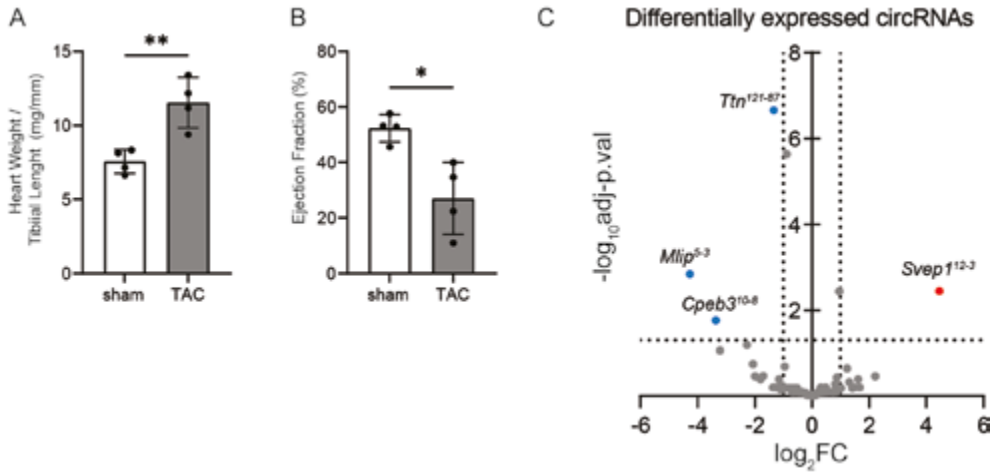

Figure S2. Differentially expressed circRNAs in the mouse heart 3 weeks after transverse aortic constriction (TAC). (A) Normalized heart weight. (B) Ejection fraction. Data are mean ± standard deviation. Unpaired t-test, * $p < 0.05$, ** $p < 0.01$. (C) Volcano plot depicting differentially circRNA expression. n = 4 per group.

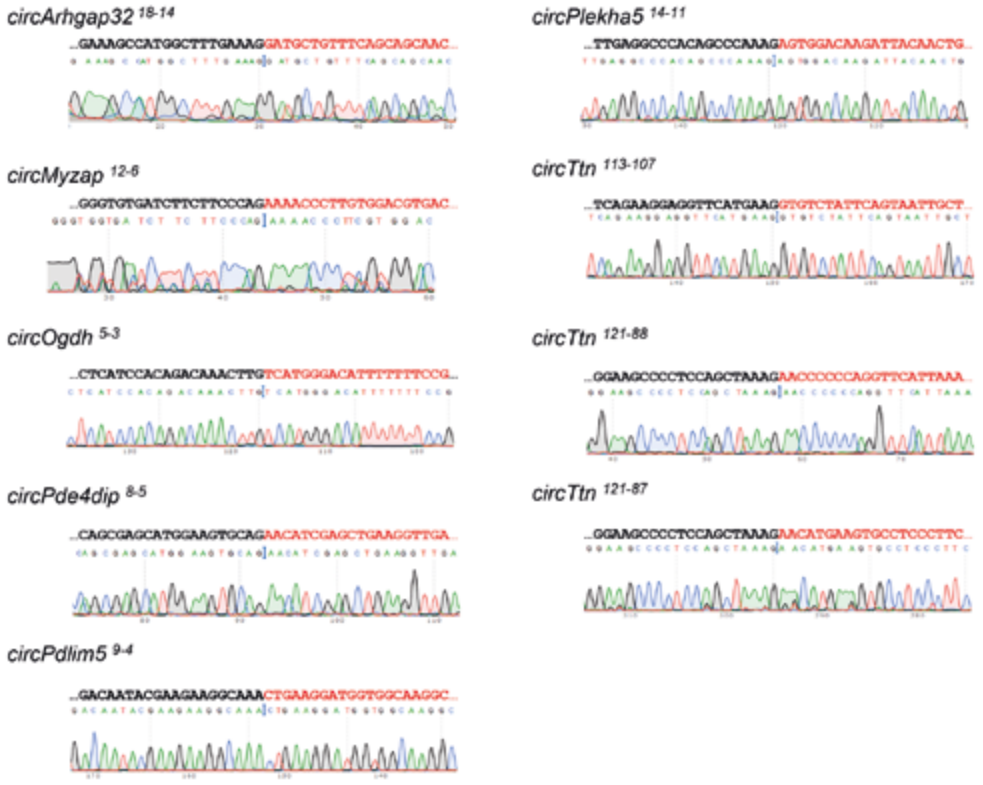

Figure S3. Sanger sequencing verification of selected circRNAs. For each circRNA, the expected back-spliced junction sequence is indicated with the corresponding donor exon in black and acceptor in red. Chromatogram with the sequencing results is shown below.

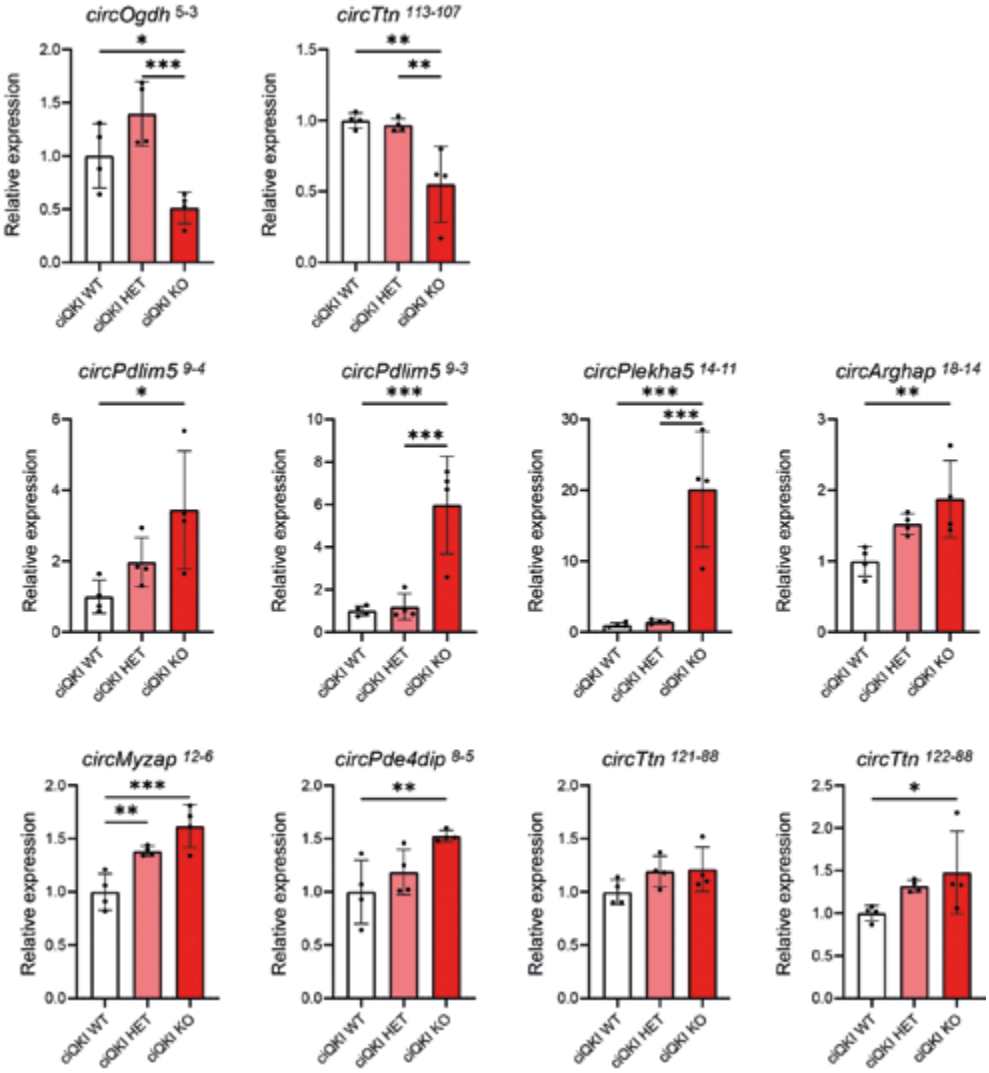

Figure S4. Quantification of RT-PCRs shown in Figure 3C. Relative expression is the ratio between the intensity of the amplicon band of the circRNA against *Hprt*. Ordinary one-way ANOVA, followed by Uncorrected Fisher's Least Significant Difference test; **** p< 0.0001; *** p<0.001; ** p<0.01; * p<0.05.

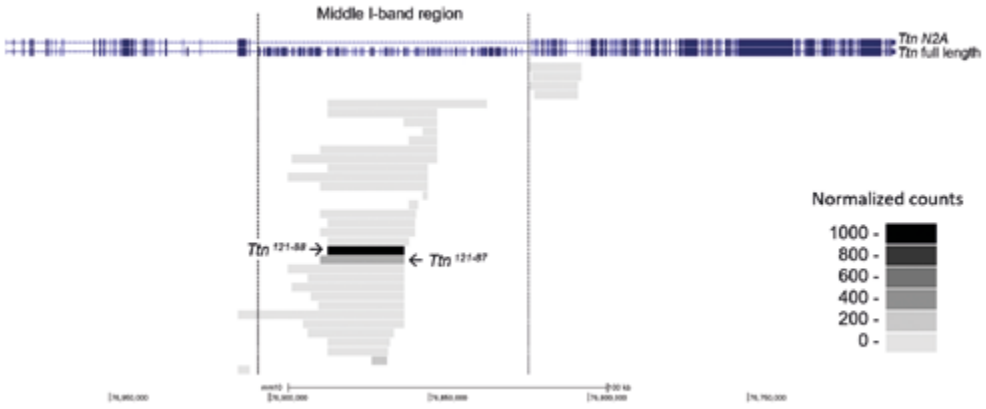

Figure S5. Most circular RNAs arising from *Ttn* are generated from exons within the middle I-band region. View of the *Ttn* gene (full length isoform and N2A isoform) and all the *circTtn*'s detected in QKI WT hearts. Each bar connects the back spliced exons of each circRNA. Grey scale represents the level of expression of each circRNA (normalized counts of 5 QKI WT hearts).

SUPPLEMENTAL TABLES

Table S1. List of differentially expressed circRNAs in adult QKI knock-out hearts

		Average normalized counts			
Gene	**circRNA id (mm10)**	**QKI WT**	**QKI KO**	**log2FC**	**adj p-val**
Slmap	chr14:26428316-26416203	9,8	0,0	-5,9	5,0E-07
Nsmaf	chr4:6417207-6398319	22,7	1,6	-3,8	7,4E-08
Qki	chr17:10282981-10238893	67,5	7,6	-3,2	1,0E-04
Ogdh	chr11:6313788-6317080	57,7	8,5	-2,8	1,2E-18
St6galnac3	chr3:153411871-153411462	8,4	1,5	-2,4	2,2E-02
Ttn	chr2:76856366-76847388	14,1	2,7	-2,3	5,0E-03
Ttn	chr2:76856366-76853605	78,9	16,4	-2,3	3,5E-02
Arl8b	chr6:108813627-108818613	10,7	2,3	-2,3	4,1E-02
Ttn	chr2:76868085-76863274	201,4	45,7	-2,1	4,9E-43
Ttn	chr2:76852137-76850570	21,9	4,9	-2,1	1,1E-02
Mlip	chr9:77217048-77173959	25,1	6,0	-2,1	2,1E-05
Lamp2	chrX:38442140-38424267	9,3	2,1	-2,1	4,2E-02
Fan1	chr7:64371659-64361940	20,8	6,4	-1,7	7,4E-03
Ttn	chr2:76818816-76802231	18,9	6,8	-1,5	9,2E-03
Vav3	chr3:109562743-109578364	17,1	6,4	-1,4	4,4E-02
Nsd3	chr8:25640577-25649703	21,2	7,8	-1,4	1,3E-02
S100pbp	chr4:129183717-129178241	15,2	5,7	-1,4	3,5E-02
Ttn	chr2:76818816-76803293	18,3	7,2	-1,3	2,1E-02
Arhgap21	chr2:20860036-20855354	47,3	18,6	-1,3	9,8E-04
Ube3a	chr7:59240967-59247217	15,9	6,4	-1,3	2,2E-02
Tent4a	chr13:69515903-69512890	20,4	8,6	-1,3	2,2E-02
Psd3	chr8:67908889-67882981	19,0	8,0	-1,3	4,9E-02
Amotl1	chr9:14575439-14571623	21,3	9,7	-1,2	2,1E-02
Ttn	chr2:76857987-76847388	37,7	16,4	-1,2	2,2E-02
Spopl	chr2:23545579-23537328	44,2	21,4	-1,1	2,7E-03
Ttn	chr2:76881839-76857904	1063,3	2134,1	1,0	1,5E-07
Pde4dip	chr3:97796808-97792739	32,5	67,6	1,0	7,9E-05
Oxr1	chr15:41797474-41826052	13,3	27,1	1,0	8,3E-03
Map4k4	chr1:40003757-40010677	10,0	20,9	1,1	4,8E-02
Pank1	chr19:34841109-34812278	12,1	26,4	1,1	1,5E-02
Ttn	chr2:76888087-76857904	50,3	113,5	1,2	1,9E-07
Picalm	chr7:90160448-90197020	27,6	64,6	1,2	1,8E-06
Pdlim5	chr3:142314448-142303943	19,1	44,7	1,2	1,2E-05
Corin	chr5:72454506-72422025	14,1	35,7	1,4	8,0E-06
Ttn	chr2:76884197-76857904	342,8	925,4	1,4	9,4E-12
Ttn	chr2:76894423-76857904	56,0	154,7	1,4	1,5E-07
Ttn	chr2:76893177-76857904	43,3	122,0	1,5	1,9E-08
Ppp1r12b	chr1:134842733-134834435	8,7	25,5	1,6	2,4E-02
Ttn	chr2:76881839-76862800	8,3	24,5	1,6	1,3E-02

Table S1. (continued)

Gene	circRNA id (mm10)	Average normalized counts		log2FC	adj p-val
		QKI WT	QKI KO		
Arhgap32	chr9:32246447-32250787	29,2	92,6	1,6	7,6E-13
Sorbs1	chr19:40365166-40336986	5,2	16,8	1,7	3,5E-02
Slc35f5	chr1:125568547-125579327	11,4	35,3	1,7	1,0E-05
Rere	chr4:150500003-150510038	4,5	15,0	1,7	3,0E-02
Slc8a1	chr17:81445593-81428182	47,5	155,7	1,7	1,1E-16
Akap6	chr12:53139381-53142768	7,2	26,4	1,8	2,4E-03
Alpk2	chr18:65350708-65349028	3,7	12,2	1,9	4,1E-02
Zfp644	chr5:106638635-106635610	4,3	15,8	2,0	1,3E-02
Enah	chr1:181961919-181905469	2,8	12,2	2,0	4,1E-02
Ttn	chr2:76884633-76857904	9,8	41,0	2,1	2,0E-10
Asph	chr4:9639347-9630773	5,8	24,6	2,1	9,4E-05
Slc8a1	chr17:81445593-81408067	18,1	81,0	2,2	2,0E-14
Myo9a	chr9:59801914-59843138	4,3	21,1	2,2	5,4E-05
Agl	chr3:116782643-116778619	18,6	85,1	2,2	3,5E-16
Erc1	chr6:119825819-119824386	2,0	8,7	2,3	2,6E-02
Rbm41	chrX:139968599-139954907	1,0	5,9	2,4	4,2E-02
Lrrfip2	chr9:111188762-111205847	9,4	47,8	2,4	1,3E-12
Cnksr3	chr10:7154485-7152864	3,2	17,4	2,4	9,0E-04
Fkbp15	chr4:62336547-62329348	0,8	5,2	2,4	4,1E-02
Sorbs1	chr19:40377016-40340685	3,4	22,3	2,5	7,8E-06
Lrrfip2	chr9:111182819-111205847	2,6	18,0	2,8	3,1E-04
Ttn	chr2:76888087-76861097	2,0	11,0	2,8	2,1E-02
Ttn	chr2:76817075-76803293	3,1	23,2	3,0	8,1E-05
Pdlim5	chr3:142352885-142303943	13,3	121,0	3,2	3,5E-42
Mapk4	chr18:73971276-73969891	1,2	12,8	3,2	2,6E-03
Mlip	chr9:77243727-77229485	1,2	13,0	3,3	1,7E-03
Raph1	chr1:60527489-60518980	1,0	12,0	3,4	8,9E-04
Mllt10	chr2:18101458-18146872	1,5	18,9	3,5	1,4E-04
Sorbs1	chr19:40344439-40321793	4,8	56,4	3,5	7,4E-03
Mlip	chr9:77230955-77229485	1,4	17,3	3,6	1,0E-05
Pank1	chr19:34827373-34812278	0,7	9,7	3,6	2,6E-03
Ttn	chr2:76909953-76857904	1,4	23,9	3,9	2,3E-08
Clasp1	chr1:118521827-118552156	0,5	11,7	4,3	1,8E-04
Ttn	chr2:76889591-76857904	0,0	8,2	5,4	4,8E-06
Slc8a1	chr17:81445593-81388810	2,1	98,6	5,5	1,3E-04
Agtpbp1	chr13:59482604-59475660	0,0	9,0	5,5	8,3E-06
Cnksr3	chr10:7154485-7134522	0,0	10,5	5,8	3,3E-06
Obscn	chr11:59016373-59015436	0,0	10,5	5,8	4,2E-06
Ppp1r12b	chr1:134865960-134834435	0,0	13,9	6,2	4,7E-08
Strn3	chr12:51661713-51643104	0,0	17,3	6,5	1,9E-08
Pde4dip	chr3:97710444-97706872	0,0	17,6	6,5	2,5E-09

Table S1. (continued)

		Average normalized counts			
Gene	**circRNA id (mm10)**	**QKI WT**	**QKI KO**	**log2FC**	**adj p-val**
Slmap	chr14:26428316-26422421	0,0	20,4	6,7	7,0E-10
Ehbp1	chr11:22151892-22137838	0,0	22,5	6,9	9,0E-11
Mlip	chr9:77231029-77229485	0,0	28,6	7,2	2,3E-11
Plekha5	chr6:140543720-140568881	0,0	38,7	7,6	2,6E-13
Qki	chr17:10274063-10238893	0,0	69,6	8,5	1,1E-17
Plekha5	chr6:140543720-140556070	0,0	102,4	9,1	3,8E-16

Table S2. Primer sequences

Primer	**Sequence 5' - 3'**	**Annealing on exon**
circArhgap32 Rv	GAGTTGCTGGATGACATCATGG	14
circArhgap32 Fw	CGCAAGTTGCAGCGTAATGAAAG	18
circMyzap Rv	TCTAACTGCCTCTGCTTCTCCCG	6
circMyzap Fw	GACAGAAACCCAGCCCAAGACTG	12
circNsmaf Rv	TCAAGTCTACACCACCTTCATAGGTCAG	20
circNsmaf Fw	AAGTCGGTCTGGTGAGCTGC	31
circOgdh Rv	TCGACGTTAGGTTGTGCTTCCACC	3
circOgdh Fw	TGATCTGGACTCCTCCGTGCC	5
circPde4dip Rv	TGTCCTGGAGTTCTCGTTTCAGGC	5
circPde4dip Fw	CTGAGGCAGAGCTTGGCTGC	8
circPdlim5 Rv	CACTCTTGGCTGCAGCTGAA	4
circPdlim5 Fw	GAATCTGAAAATGACAATACGAAGAAGGC	9
circPlekha5 Rv	CCGTATCTTTCAGCTTCTAAGGC	11
circPlekha5 Fw	ACACCTTAGCACAGCTCATG	14
circSorbs1 Rv	CGGTCTCCCAAACTCCAATTCCG	16
circSorbs1 Fw	CCAGACATTACGTCAGAGCCTCCTG	20
circSorbs1 Rv	TGTAGACACATCGCTCAGGTCCTG	8
circSorbs1 Fw	CCAGACATTACGTCAGAGCCTCCTG	20
circTtn Rv	TGGTTGTTAAGTACAGTTCCGCTG	107
circTtn Fw	GACTATGAAGAGATCAAGGTGGAAGC	113
circTtn Fw	CAGAGGCTCCAAAGAAACCTGCTC	121
circTtn Rv	CTGCTTCACGATCCGTGATTGGTC	88
Hprt Fw	CCTAAGATGAGCGCAAGTTGAA	9
Hprt Rv	CCACAGGACTAGAACACCTGCTAA	9
Qki Fw	GGAGTGCAGAATTGCCTG	2
Qki Rv	CTAGGTCCAAGGATTCTCC	3

CHAPTER 4

INSIGHTS INTO ALTERNATIVE SPLICING IN THE HEART FROM KNOCKOUT MOUSE MODELS

Pablo Montañés-Agudo, Yigal M. Pinto and Esther E. Creemers

Article in press:
Montañés-Agudo, Pablo, Yigal M. Pinto, and Esther E. Creemers.
"Splicing factors in the heart: Uncovering shared and unique targets."
Journal of Molecular and Cellular Cardiology (2023)

ABSTRACT

Alternative splicing generates specialized protein isoforms to allow the heart to adapt during development and disease. To gain insight in how alternative splicing is regulated in the heart, we re-analyzed original RNA-sequencing data from eight published mouse models, in which splicing factors have been genetically deleted (HNRNPU, MBNL1/2, QKI, RBM20, RBM24, RBPMS, SRSF3, SRSF4). We show that key splicing events in *Camk2d*, *Ryr2*, *Tpm1*, *Tpm2* and *Pdlim5* require the combined action of the majority of these splicing factors. The largest overlap was found between the splicing networks of MBNL, QKI and RBM24. Next, we re-analyzed a RNA-sequencing study on hearts of 128 heart failure patients. Here, we observed that MBNL1, QKI and RBM24 expression varied greatly. This variation in expression correlated with differential splicing of their downstream targets as found in mice, suggesting that aberrant splicing by MBNL1, QKI and RBM24 might contribute to the disease mechanism in heart failure.

INTRODUCTION

Over 95% of the human genes undergo alternative pre-mRNA splicing (AS), a mechanism to produce different isoforms of a protein from a single gene[1]. In the heart, AS coordinates the expression of protein isoforms to adapt cardiac function to changing demands during embryonic and postnatal development. For instance, increased passive stiffness of the myocardium during the course of development is mediated by the expression of shorter, less elastic titin (TTN) isoforms[2,3]. Besides splicing regulation of sarcomeric proteins, numerous ion channels (e.g. RyR2, L-type calcium channel) undergo AS in order to change their physiological properties[4,5].

Each AS event is carried out by the spliceosome, and regulated by a combination of sequence-specific RNA-binding proteins, or splicing factors. These splicing factors determine which exons are included in the mature mRNA transcript by facilitating or impeding spliceosome assembly on certain pre-mRNA locations. Splicing factors are often expressed in a cell type-specific manner, allowing the generation of cell type-specific mRNA isoforms[6,7]. The most well-studied splicing factor in the heart is RNA-binding motif protein 20 (RBM20). RBM20 has been shown to regulate a network of splicing events in genes related to sarcomere structure and calcium handling[8,9]. The discovery in 2009 that mutations in RBM20 cause severe forms of familial dilated cardiomyopathy (DCM) has sparked great interest in splicing regulation in the cardiac field. Since then, many knockout (KO) mouse models have be generated to delete single splicing factors and investigate the molecular basis of AS regulation in the heart (i.e. SRSF1-SRSF5, SRSF10, hnRNPA1, hnRNPU, MBNL1-MBNL3, RBM20, RBM24, RBM38, CELF1, PCBP2, QKI, RBFOX1, RBFOX2, and RBPMS)[9–34]. Interestingly, almost all of these splicing factor KO models develop signs of cardiac dysfunction, either during development, early postnatal stages or at adulthood. At the molecular level, these cardiac phenotypes are often attributed to sarcomeric and cytoskeletal defects and to abnormalities in calcium handling. Splicing analyses in these KO models revealed a certain overlap in the regulated splicing events. For instance, the inclusion of *Camk2d* exons 14, 15 and 16 is controlled by splicing factors HNRNPU, QKI, RBM20, as well as SRSF1; and the switch of the mutually exclusive exons 3A/3B of the mitochondrial phosphate carrier *Slc25a3* requires both RBM24 and QKI. Despite the intriguing observation that multiple splicing factors control AS of the same exons, the extent of this overlap between different splicing factors is currently unknown.

It is estimated that around 300-400 splicing regulators exist in the human genome[35,36], when considering core components of the spliceosome and splicing factors. The expression of such a large number of splicing regulators raises the question what their specific functions are, and more specific, which AS events they control. Understanding the molecular basis of AS

is crucial, even more because the expression of certain splicing factors (e.g. QKI, RBM20) is dysregulated in heart disease[37,38]. Moreover, aberrant splicing patterns of sarcomeric and ion channel genes have also been observed in cardiac pathologies including hypertrophy and heart failure[38–41]. Since AS regulation is extremely complex, systematic approaches are needed to identify the precise role of each splicing regulator and how they interact with their targets. Unraveling this complexity will eventually lead to the identification of the 'splicing code', i.e. the genomic sequence that defines the posttranscriptional fate of exons. Moreover, fundamental knowledge about isoform selection will lead to a better understanding of the processes that go awry in disease, and ultimately will enable researchers to shift splicing towards desired changes in cardioprotective protein isoforms to reduce pathological effects.

To gain insights in the molecular basis of AS in the heart, we first re-analyzed original RNA-sequencing data from 8 published mouse models, in which splicing factors have been genetically deleted (i.e. HNRPU, MBNL1+2, QKI, RBM20, RBM24, RBPMS, SRSF3 and SRSF4). We systematically analyzed and compared changes in gene expression and splicing and found AS events unique to each model, but also many commonalities. The largest overlap was observed between the splicing networks of MBNL, QKI and RBM24, with as much as ~30-40% of the AS events shared between at least 2 out of 3 models. We found that splicing events in crucial regulators of contraction, such as *Camk2d*, *Ryr2*, *Tpm1*, *Tpm2* and *Pdlim5*, require the concerted action of five splicing regulators: RBM20, RBM24, MBNL1+2, QKI and RBPMS. Finally, we performed an analysis of a large-scale RNA-sequencing study in hearts of 128 patients with dilated cardiomyopathy (DCM). Here, we observed a substantial amount of variation in the expression of the splicing factors MBNL1, QKI and RBM24. This expression variation correlated well with AS of their down-stream targets, further implicating aberrant AS by MBNL1, QKI and RBM24 as a contributing disease mechanism in heart failure.

RESULTS

Reported splicing factor knock-out models and their phenotypes

Based on an extensive literature search, we assembled a list of splicing factors, of which the function has been investigated in the heart. We limited the search to genetic loss-of-function studies in mice, since these models provide robust insights into cardiac development, contractile function and arrhythmias. As such, we did not include studies using human iPS-derived cardiomyocytes with mutations in splicing factors. This led to the identification of 29 splicing factor KO models (including constitutive, conditional and inducible loss-of-function models) corresponding to 20 genes[9–34]. These included six SR factors (SRSF1, SRSF2, SRSF3, SRSF4, SRSF5, SRSF10), two hnRNPs (hnRNPA1, hnRNPU), three Muscleblind-like Splicing Regulators (MBNL1, MBNL2, MBNL3) and nine other splicing factors (RBM20, RBM24, RBM38, CELF1, PCBP2, QKI, RBFOX1, RBFOX2, and RBPMS).

Table 1 summarizes the phenotypes of the 29 splicing factor KO models. Of the 29 KO models reported, 9 display embryonic lethality with signs of cardiac dysfunction (i.e. hnRNPA1, MBNL1+2, PCBP2, QKI (2 models), RBM24, SRSF3 (2 models), SRSF10), 7 display lethality at early postnatal stages (i.e. CELF1, hnRNPU (2 models), MBNL1, RBM24, RBPMS, SRSF5), 10 KO models develop dysfunction of the adult heart (i.e. MBNL1, MBNL3, QKI, RBFOX1, RBFOX2, RBM20, SRSF1, SRSF2, SRSF3, SRSF4), and in 2 models there was no cardiac phenotype observed (i.e. MBNL2, RBM38). For our analysis, we focused on the splicing factors with a role in the postnatal and adult heart. Most of these KO models developed cardiac dilatation and contractile dysfunction. At the molecular level, these phenotypes were mostly attributed to sarcomere and cytoskeletal defects and abnormalities in calcium handling (**Table 1**).

RNA-sequencing reveals hundreds of differentially expressed and differently spliced genes

To gain insight in the coordinated regulation of AS in the heart, we reanalyzed and compared original RNA-sequencing data from mouse models in which splicing factors were genetically deleted. From the 29 models reviewed in **Table 1**, raw sequencing reads of 8 different KO models and their corresponding wild-type controls were publicly available in the GEO database: HNRPU KO[12], MBNL1+2 Double KO (DKO)[15], QKI KO[21], RBM20 KO[9], RBM24 KO[26], RBPMS KO[28], SRSF3 KO[31] and SRSF4 KO[32]. **Table S1** summarizes the genotypes and characteristics of samples used for analyses.

To enable comparison of AS events between models, reads were mapped to Ensembl reference transcriptome GRCm38 (version M25, Ensembl genebuild 100) and a bioinformatics pipeline was implemented for expression (DESeq2) and splicing analysis (DEXSeq)[42,43].

First, we examined differential gene expression in the 8 KO models (**Figure 1A, Table S2**). Significant gene expression changes were found in every KO model, but the SRSF3 and HNRNPU KO mice stood out with a remarkable large number of deregulated genes (>8000). Gene ontology pathway analysis on the differentially expressed genes (**Figure 1B**) roughly divided the KO models in two groups: 1. Splicing factors that affect striated muscle cell processes and/or ion transport (i.e MBNL, QKI, RBM20, RBM24, RBPMS and SRSF4) and 2. splicing factors not involved in these processes (i.e. SRSF3 and HNRNPU). Extracellular matrix/fibrosis terms were enriched in MBNL, RBM20 and RBM24 KO models, which matches the fibrosis observed in the hearts of these mice[9,15,25]. Immune and inflammatory terms were enriched in MBNL, QKI, RBM20, RBM24 and SRSF4 KO models, suggesting that an underlying immune response was triggered by the splicing factor deficiency.

Table 1. List of splicing factors knock-out mouse models with a cardiac phenotype

Gene name	Knock-out model	Phenotype	Ref.
CELF1 (/CUGBP1)	Constitutive *Celf1 –/–*	Reduced viability, retarded growth, altered electrophysiological and contractile functions at early postnatal stages.	10
HNRNPA1	Constitutive *hnRNPA1 –/–*	Embryonic lethality (E18.5). Hypoplastic and dilated heart.	11
HNRNPU	Conditional *Hnrnpu$^{fl/fl}$; Ckmm-Cre^{tg}*	Postnatal lethality (14 days). Dilated heart.	12
	Conditional *Hnrnpu$^{fl/fl}$; Myh6-Cre^{tg}*	Postnatal lethality (10 days). Dilated heart.	12
MBNL1+2	*Compound Mbnl1 –/–; Mbnl2 +/–*	Postnatal lethality (5 weeks). Cardiac conduction defects, atrial dilatation and left ventricular hypertrophy.	13
	Double knockout *Mbnl 1–/–; Mbnl2 –/–*	Embryonically lethal.	14
	Double knockout *Mbnl1–/–; Mbnl2$^{fl/fl}$; Myh6-Cre^{tg}*	Postnatal lethality (8-45 weeks). DCM, conduction block, SCD.	15
MBNL1	Constitutive *Mbnl1 –/–*	Adult lethality (2 months). Cardiac conduction defects, sinus node dysfunction, cardiac hypertrophy, myocardial fibrosis, necrosis and calcification, sudden cardiac death.	16
MBNL2	Constitutive *Mbnl2–/–*	No cardiac phenotype reported. No changes in cardiac splicing reported.	17
MBNL3	Constitutive *Mbnl3 –/–*	Systolic defects, ventricular hypertrophy.	18
PCBP2	Constitutive *Pcbp2 –/–*	Embryonic lethality (E14.5). Global edema and pericardial effusion.	19
QKI	Constitutive *Qki –/–*	Embryonic lethality (E10.5).	20
	Conditional *Qki$^{fl/fl}$; Myh6-Cre^{tg}*	Embryonic lethality (E14.5).	21
	Conditional inducible *Qki$^{fl/fl}$; Myh6-MCM^{tg}*	Lethal 1 week after tamoxifen injections. DCM, heart failure.	21
RBFOX1 (/A2BP1)	Conditional *Rbfox1$^{fl/fl}$; Nkx2.5-Cre^{tg}*	Exacerbation of cardiac hypertrophy and HF upon TAC.	22
RBFOX2	Conditional *Rbfox2$^{fl/fl}$; Nkx2.5-Cre^{tg}*	Embryonically lethal (E11.5). Underdeveloped hearts with a thin and hypoplastic outflow tract.	23
	Conditional *Rbfox2$^{fl/fl}$; Mlc2v-Cre^{tg}*	Adult lethality (8-56 weeks). DCM, HF, systolic disfunction. Defective EC Coupling.	24
RBM20	Constitutive *Rbm20 –/–*	Arrhytmogenic DCM.	9

Table 1. (continued)

Gene name	Knock-out model	Phenotype	Ref.
RBM24	Constitutive *Rbm24 –/–*	Embryonic lethality (E12.5-14.5).	25
	Conditional *Rbm24$^{fl/fl}$; Myh6-Cre^{tg}*	DCM, postnatal lethality (11 days – 2 months).	26
RBM38	Constitutive *Rbm38 –/–*	No cardiac phenotype.	27
RBPMS	Constitutive *Rbpms –/–*	Perinatal lethality (1-4 days). Premature cardiomyocyte binucleation, noncompaction of myocardium.	28
SRSF1 (/ASF/SF2)	Conditional *Srsf1$^{fl/fl}$; Mlc2v-Cre^{tg}*	Adult lethality (6-10 weeks). DCM, AV block sarcomeres, Ca^{2+} leaks.	29
SRSF2 (/SC35)	Conditional *Srsf2$^{fl/fl}$; Mlc2v-Cre^{tg}*	Non-lethal DCM, defective excitation-contraction coupling.	30
SRSF3	Conditional *Srsf3$^{fl/fl;}$ Nkx2.5-Cre^{tg}*	Embryonic lethality.	31
	Conditional *Srsf3$^{fl/fl}$; Myh6-Cre^{tg}*	Embryonic lethality. Reduced cardiomyocyte proliferation.	31
	Conditional inducible *Srsf3$^{fl/fl}$; Myh6-MCM^{tg}*	Lethality 1 week after induction. Systolic dysfunction.	31
SRSF4	Conditional *Srsf4$^{fl/fl;}$ Nkx2.5-Cre^{tg}*	Cardiac hypertrophy, diastolic dysfunction, abnormal repolarization.	32
SRSF5	Constitutive *Srsf5 –/–*	Perinatal lethality (1 day). Cardiac dysfunction with noncompaction of the ventricular myocardium.	33
SRSF10 (Srp38)	Constitutive *Srsf10 –/–*	Embryonic lethality (E15.5), atrial and ventricular septal defects; hypoplastic myocardium, calcium handling defects.	34

Mouse models used for RNAseq analysis in this manuscript are underscored. DCM, dilated cardiomyopathy; HF, Heart Failure; TAC, transaortic constriction.

We next inferred AS in the 8 KO models by testing for differential exon usage in the RNA-seq data using DEXseq[43] (**Table S3**). **Figure 1C** shows the number of up- and downregulated exon bins (i.e. one exon or part of an exon) per model. While most KO models have hundreds of differentially spliced exon bins, SRSF3 and HNRNPU KO models present thousands. Pathway analysis on the alternatively spliced genes categorized the KO models in the same two groups as the gene expression analysis (**Figure 1D**). Group 1 contained KO models in which mis-spliced genes were enriched for terms related to contraction and/or electrophysiology (i.e. MBNL, QKI, RBM20, RBM24, RBPMS and SRSF4), and group 2, containing SRSF3 and HNRNPU, showed enrichment of alternatively spliced genes in terms related to RNA processing ("mRNA 3'-end processing"; "RNA splicing").

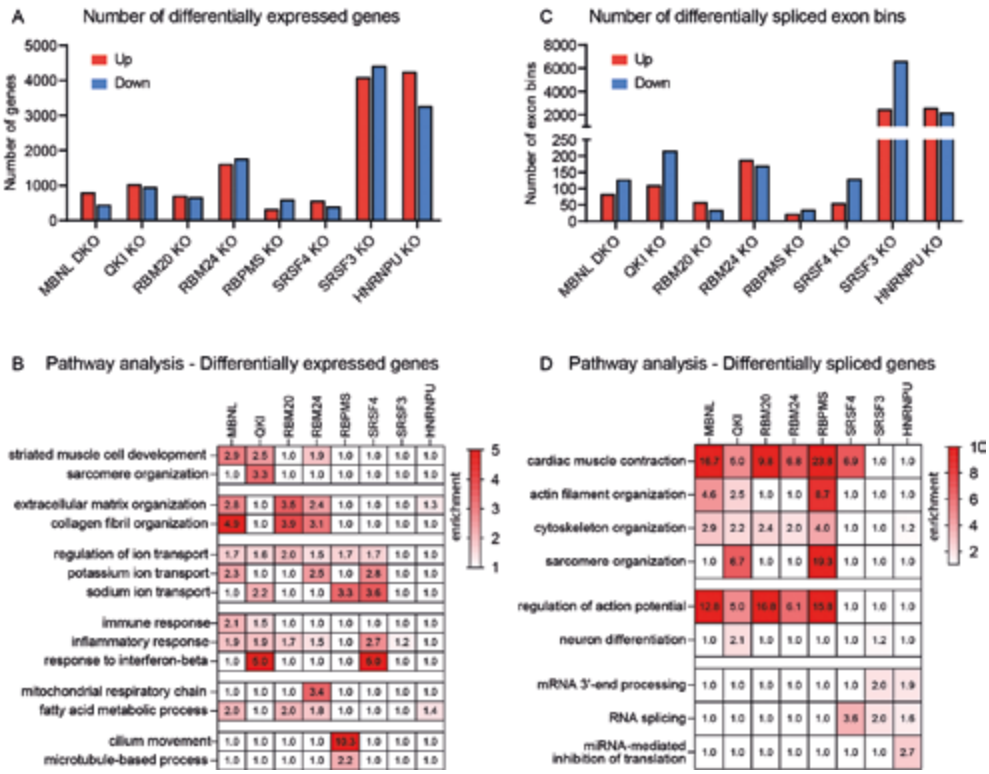

Figure 1. Gene expression and splicing analysis in eight splicing factor mouse KO models. (A) Number of differentially expressed genes in each KO model (base mean expression ≥ 1, absolute log2FC ≥ 0.58 and p-adj. ≤ 0.05). (B) Pathway analysis for gene ontology "Biological process" on differentially expressed genes. (C) Number of differentially spliced exons bins per model (normalized counts ≥ 10, absolute log2FC ≥ 1, and p-adj. ≤ 0,05). (D) Pathway analysis for gene ontology "Biological process" on mis-spliced genes. Mis-spliced genes were defined as genes with at least with one differentially spliced exon bin.

In conclusion, RNA-seq analysis of these 8 KO models revealed numerous changes in gene expression and AS. Six of these KO models (i.e. MBNL, QKI, RBM20, RBM24, RPBMS, SRSF4) showed splicing defects in genes related to muscle contraction, cytoskeletal organization and excitation. This is largely in line with the reported phenotypes in these models. HNRNPU and SRSF3 KOs displayed the largest changes in gene expression and splicing, but did not show enrichment for muscle specific terms. Therefore, we excluded these two splicing factor models from further analysis and focus on the other six splicing factors that regulate splicing events related to muscle contraction.

Similar splicing events are controlled by multiple splicing factors

We next compared the 6 splicing factor KO models with splicing changes in genes related to muscle contraction and excitation (**Figure 2**). Of the 709 genes that were alternatively spliced in at least one of the models, 132 genes were shared by at least 2 models. **Figure 2A** visualizes the intersection of the shared splicing changes by means of an UpSet plot. The largest overlap in mis-spliced genes was found between MBNL, QKI and RBM24 KO mice, with 62 commonly mis-spliced genes in QKI and RBM24 KO, 44 in QKI and MBNL DKO and 38 in MBNL and RBM24 KO. Strikingly, five crucial regulators of heart muscle contraction and conduction were mis-spliced in five out of six models: *Camk2d, Pdlim5, Ryr2, Tpm1 and Tpm2.*

Figure 2B shows exon inclusion changes in *Camk2d* (Calcium/Calmodulin Dependent Protein Kinase II Delta, CaMK2δ). As a multifunctional Ser/Thr protein kinase and key regulator of excitation-contraction coupling, splicing changes in CaMK2δ are relevant for cardiomyocyte biology[44]. AS in the mutually skipped exons 14, 15 and 16 result in four isoforms with different functional properties: CaMKIIδ-A (exons 15 and 16), CaMKIIδ-B (exon 14), CaMKIIδ-C (none) and CaMKIIδ-9 (exon 16)[45]. Exon 14 harbors a functional nuclear localization signal, and targets CaMKIIδ-B to the nucleus where it can associate with histone deacetylases to regulate transcription[46]. Skipping of exon 14 occurs in MBNL, QKI, RBM20 and RBM24 KO hearts, indicating that reduced nuclear CaMKIIδ levels may participate in the phenotype in these mice. Changes in exon 15 inclusion lead to altered expression of CaMKIIδ-A, an isoform known to associate with the intercalated disc and T-tubules[29], and can be appreciated in QKI and RBM20 KO hearts. Of note, the RNA-seq tracks of the RBPMs KO mice were not included in the bedgraphs, since this RNA-seq was derived from neonatal hearts (1 day after birth), while all other datasets were retrieved from adult (i.e. MBNL, QKI, RBM20) or 23-day old (i.e. RBM24) hearts. Consequently, the wild-type mice of the RBPMS KO model expressed a fetal isoform of *Camk2d*, and did not compare well with the other wild-types. **Figure 2C** shows AS of Tropomyosin 2 (*Tpm2*) in the five KO models. *Tpm2* has two isoforms: the skeletal muscle isoform with exons 6B and 9A and the smooth muscle isoform with exons 6A and 9D[47]. In control hearts, the smooth muscle isoform is predominantly expressed, whereas in the MBNL, QKI, RBM20 and RBM24 KO, there are shifts from exon 6A to 6B, and from 9D to 9A, indicative of increased expression of the skeletal *Tpm2* isoform. **Figure S1** shows AS changes between the short and long isoform of *Pdlim5* in the five mouse models.

Splicing of titin is mainly driven by RBM20 and QKI

Titin (*Ttn*) is one of the most well-studied spliced genes in the heart partly due to its role in the RBM20 cardiomyopathy[8,37]. Through AS, *Ttn* can be processed into multiple isoforms

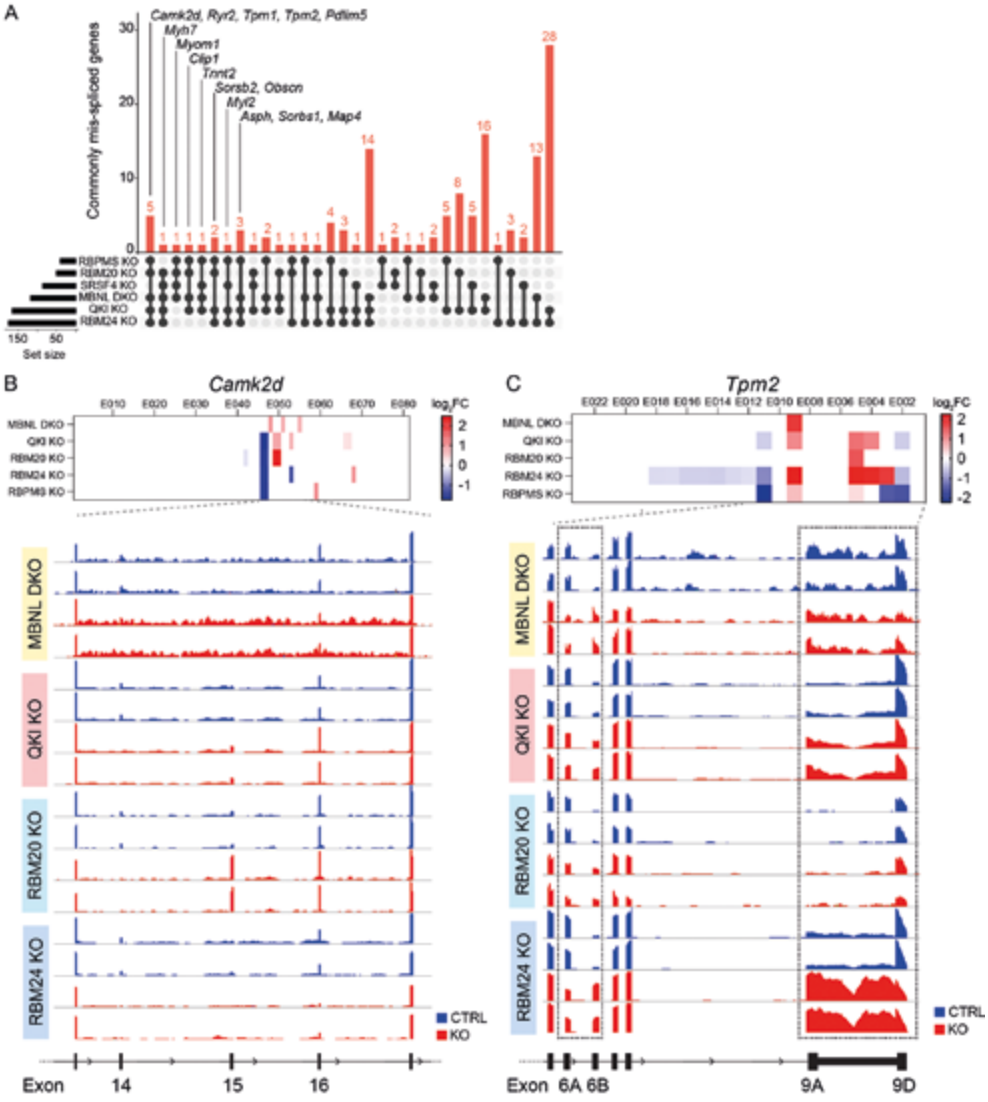

Figure 2. Shared splicing targets in different splicing factor KO models. (A) Overlap of mis-spliced genes in MBNL DKO, QKI KO, RBM20 KO, RBM24 KO, RBPMS KO and SRSF4 KO hearts. (B) Heatmap showing significant changes (p-adj. ≤ 0.05) in exon usage and representative bed graphs showing the read coverage of the spliced exons in *Camk2d* and (C) in *Tpm2* in the individual KO models (n=2/group shown). Transcript and exon numbers are shown below bedgraphs.

with unique mechanical properties (**Figure 3A**)[2,3]. We used our analysis to examine whether splicing of *Ttn* is altered in any other model than the RBM20 KO. **Figure 3B** shows the statistical significance of differential exon usage of all 363 exons of *Ttn* in the 8 KO models. The most

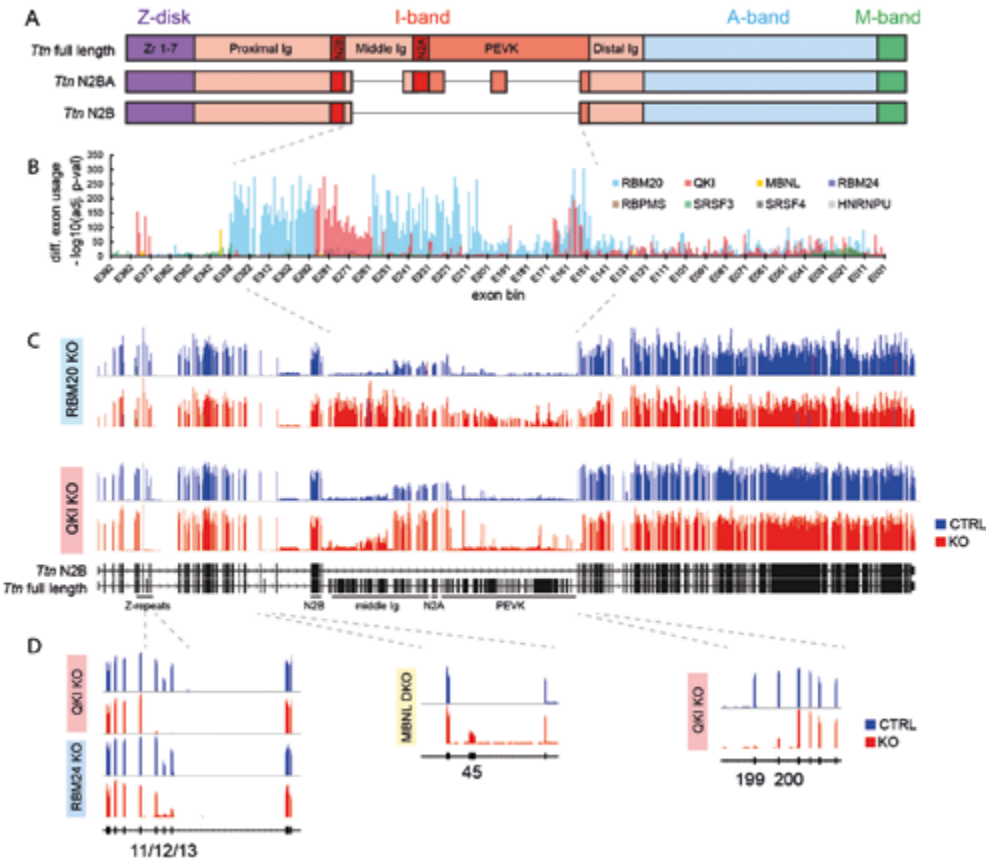

Figure 3. Multiple splicing factors participate in the splicing of titin. (A) Diagram of the main splice isoforms of titin (*Ttn)*. (B) Statistical significance (Adj. P-value) of differential exon inclusion of all the *Ttn* exons in the eight analyzed models. (C) Representative bedgraphs illustrating the splicing changes in the entire *Ttn* gene in RBM20 KO and QKI KO. (D) Bedgraphs showing specific splicing changes in the QKI KO, RBM24 KO and MBNL DKO models.

significant splicing changes are observed in the I-band region and occur in the RBM20 and in the QKI KO hearts. The read coverage of the entire *Ttn* gene in RBM20 and QKI KO hearts is depicted in **Figure 3C**. In the RBM20 KO there is a shift towards full length titin due to the inclusion of the middle I-band exons. In the QKI KO, *Ttn* shifts towards the N2BA isoform due to inclusion of several middle immunoglobin domains, the N2A and the PEVK regions. In addition to splicing changes in TTN's I-band region, there were also other regions affected in the KO models (**Figure 3D**). For instance, exons 11, 12 and 13 (encoding one of the Z-repeats that anchor TTN to the Z-disk) are skipped in the QKI KO. Interestingly, in RBM24 KO hearts, exons 12 and 13 are lost, but not 11. In MBNL DKO, there is increased inclusion of

exon 45, which corresponds to the rare I-band segment Novex-1, whose function is not well understood[3,48]. The I-band exons 199 and 200 (which are located directly after the RBM20-dependent region) are lost exclusively in the QKI KO. In conclusion, splicing of *Ttn* is complex, and aside from RBM20, also QKI, MBNL and RBM24 are involved in *Ttn* splicing. Further research is needed to determine the functional relevance of these splicing events.

Overlap between splicing targets of QKI, MBNL and RBM24

As the largest overlap in alternatively spliced exons between the KO models was found between MBNL, QKI and RBM24 KO mice (**Figure 2A**), we further focused our comparative analysis on these three splicing factors. We found that about 30-40% of the alternatively spliced exons were shared between at least two of these three KO models. A total of 30 exons belonging to 14 genes (i.e. *Asph, Eno1, Itgb1, Lrrfip2, Map4, Mef2d, Mff, Nebl, Pdlim5, Stau2, Tpm1, Tpm2, Trak1, Ube2d3)* were commonly mis-spliced in all three KO models (**Figure 4A**). Most of these exons followed the same direction of effect in terms of gain- or loss of exon inclusion (**Figure 4B**) and examples are shown for the genes *Eno1*, *Itgb1* and *Ube2d3* (**Figure 4C**). However, some transcripts were differently spliced in these three KO models. For instance, inclusion of exon 2 of *Sorbs2* occurred only in MBNL and QKI KO hearts and not in the RBM24 KO; while skipping of exon 5 occurred in QKI and RBM24 KO, but not in the MBNL DKO. Interestingly, we found several examples in which loss of QKI seemed to have an opposite effect on splicing when compared to loss of MBNL and RBM24 (e.g. *Lmo7, Mff* and *Mef2d)* (**Figure 4D**). In conclusion, this analysis demonstrates that the expression of specific splice isoforms in the heart does not depend on the expression of one specific splicing factor but requires the function of multiple splicing factors.

Splicing in the human heart correlates with MBNL1, QKI and RBM24 expression

Based on the results of the MBNL1, QKI and RBM24 KO mouse models, we hypothesized that changes in the expression of these splicing factors in the human heart would affect AS of its target genes. To address this we made use of RNA-seq dataset from left ventricular myocardium of a cohort of 128 patients with end-stage heart failure, reported by Heinig M. et al[40]. After assessing gene expression of the splicing factors in every sample, we selected 10 samples with the highest and 10 samples with the lowest expression of MBNL1, QKI or RBM24, and performed differential exon usage analysis between the corresponding extremes (**Figure S2**). We selected several of the robustly spliced exons from the mouse models, and compared them to the orthologous exons in the human heart. Interestingly, we found that several transcripts were indeed differentially spliced in human hearts with aberrant MBNL1, QKI or RBM24 expression. Representative bedgraphs of *Eno1*, *Tmed2* and *Tpm2* of the mouse models and of patients with high and low expression of MBNL1, QKI and RBM24 are shown in **Figure 5**. The shifts from exon 4A to 4B in *Eno1* and exon 6A to 6B in *Tpm2*

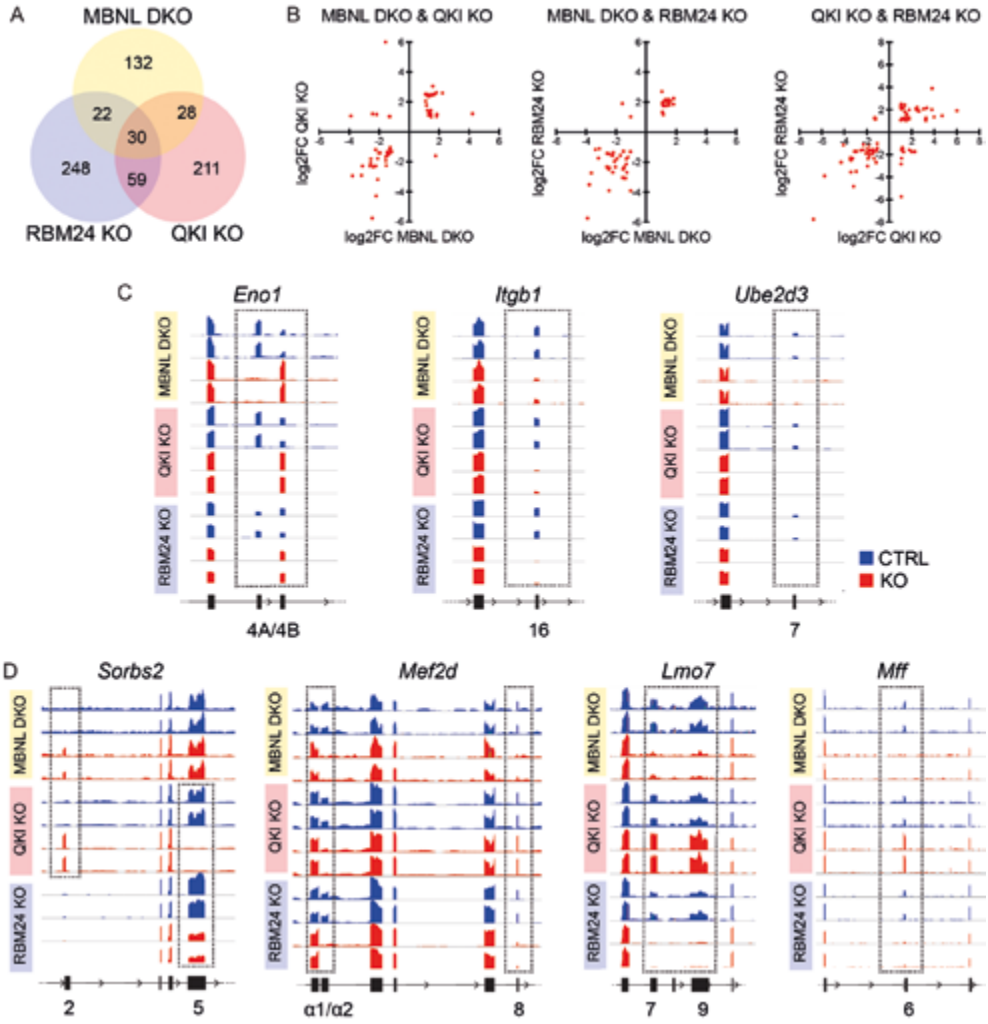

Figure 4. Overlap in splicing targets between QKI, MBNL1/2 and RBM24. (A) Venn diagram depicting the number of shared mis-spliced exons in the QKI KO, MBNL DKO and RBM20 KO model. (B) Scatter plot of the common mis-spliced exons reveal the same direction of effect for most exons. (C) Bedgraphs showing commonly (*Eno1*, *Itgb1*, *Ube2d3*) and (D) differently regulated exons (*Sorbs2*, *Mef2d*, *Lmo7*, *Mff*) in the 3 models (n=2/group shown). Transcript and exon numbers are indicated below the bedgraph. Dashed boxes highlight splicing changes in the transcript.

occurring in the three mouse KO models are also observed, albeit to a lesser extent, when comparing patients with high and low MBNL1, QKI or RBM24 mRNA expression. Reduced inclusion of the mini exon 3 in *Tmed2* is also observed in human samples with low expression of the splicing factors.

In conclusion, there is a substantial amount of variation in splicing factor expression in failing human hearts between patients. We provide evidence that the expression variation of MBNL, QKI and RBM24 correlates with splicing of several of their target genes. Further research is required to demonstrate causality and to understand the implication of these splicing alterations in the pathophysiology of heart failure.

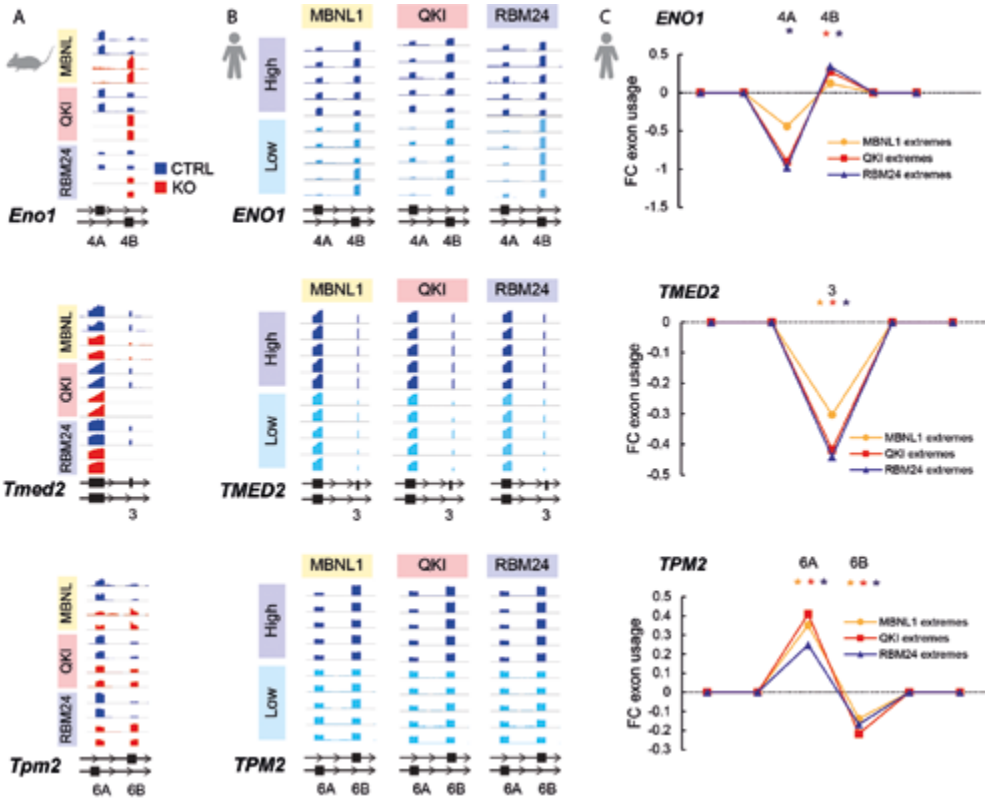

Figure 5. Variation in the expression of MBNL1, QKI and RBM24 correlates with alternative splicing events in their down-stream targets. (A) Representative bedgraphs showing splicing changes in *Eno1*, *Tmed2* and *Tpm2* in the hearts of the mouse models MBNL DKO, QKI KO and RBM24 KO. (B) Representative bedgraphs showing splicing changes in *ENO1*, *TMED2* and *TPM2* in left ventricle tissue of human end-stage heart failure patients with high or low expression levels of the splicing factors MBNL1, QKI and RBM24. For selection of patient numbers based on splicing factor expression levels we refer to Figure S2. (C) Quantification of the changes in exon usage of the exon depicted in B. Exon numbers are indicated above the graph. * LRT p-value ≤ 0.05 (* color indicates the addressed comparison).

DISCUSSION

In this study, we investigated alternative splicing in the heart by re-analyzing a total of eight previously reported mouse models that each had one single splicing factor knocked out. In addition, we analyzed a large-scale human RNA sequencing study of 128 failing hearts. The main observations of our *de novo* analyses are: (1) The eight splicing factors are clustered in two functional groups based on pathway analysis of their targets that are mis-spliced in the respective mouse hearts. One group shows enrichment of mis-spliced exons in genes related to contraction and/or electrophysiology (i.e. MBNL, QKI, RBM20, RBM24, RBPMS and SRSF4). The second group, contains SRSF3 and HNRNPU, shows enrichment of mis-spliced genes related to RNA processing. (2) Well-known splicing events that affect regulators of cardiac muscle contraction (i.e. *Camk2d*, *Ryr2*, *Tpm1*, *Tpm2* and *Pdlim5*) are regulated by the majority of the eight splicing factors. (3) Most overlap between the splicing networks occurred between MBNL, QKI and RBM24. (4) In human DCM samples, mRNA expression of the splicing factors MBNL1, QKI and RBM24 varied strongly. This expression variation correlated well with AS in some of their down-stream targets.

It is known that each AS event requires the combined activity of multiple splicing factors and *cis*-acting binding sites in conjunction with the core splicing machinery[49]. Within this complex interplay, splicing factors can act synergistically or antagonistically, depending on the location of the binding site relative to the regulated exon, but also on the expression of auxiliary proteins in a given cell type[49]. This implies that AS events identified in loss-of-function studies are likely to reflect not only loss of the splicing factor under study but also the effect of perturbations of its cooperating factors. Here, we identified a total of 30 jointly regulated exons by MBNL, QKI and RBM24, indicating the concerted action of these splicing factors in cardiomyocytes. While the majority of these 30 splicing events showed identical regulation in the 3 models, few AS events showed opposite regulation by QKI compared to MBNL and RBM24 (e.g. *Mef2d*, *Lmo7*, *Mff*). Interestingly, Hall et al. documented overlapping splicing networks of QKI and the splicing regulator PTB during myogenesis[50]. In that study, 172 jointly regulated exons were found, with ~50% of the exons being regulated in the same direction and ~50% in the opposite direction. Along the course of myogenic differentiation, QKI expression increases while PTB decreases, thus driving the upregulation of QKI-activated exons and the downregulation of PTB-repressed exons. In conclusion, studying individual splicing factors is crucial to understand the basis of cardiac splicing, but it is the combined action of all the splicing factors in a given cell type that creates the cell-type specific splicing profile.

AS is thought to play an important role in the etiology of cardiac disease including hypertrophy and heart failure[38–41]. Heinig et al. identified 1,212 exons that were differently spliced in hearts

of 97 DCM patients compared to 108 non-diseased controls[40]. We reanalyzed the DCM dataset from that study and found that endogenous expression of MBNL1, QKI and RBM24 correlated with representative splicing events identified in the KO mouse models (i.e. *ENO1*, *TMED2*, *TPM2*). Similar observations have been made for RBM20 expression and RBM20-dependent splicing events in the same patient cohort[37]. The variation in expression of splicing factors between patients is interesting, and may underlie, or reflect the heterogeneous nature of heart failure mechanisms. For a complete understanding of AS and its regulation in cardiac diseases there are several questions remaining. First, how much of the AS variation observed at the mRNA levels is also represented at the protein level? How much of the AS events result in the production of a truly different functional protein? Can splicing factors be used therapeutically, for instance to shift splicing networks towards increased expression of cardio-protective protein isoforms to reduce pathological effects?

The design of our study has a few limitations. First, there is variability between the samples from the different mouse studies, including RNA and library preparation methods (poly-A vs rRNA-depleted total RNA), age of the mice (ranging from 1 day old to 6 months old), and KO technology used (i.e constitutive vs cardiomyocyte-specific KO). Variation in age, but also in disease end-point complicates comparisons, because AS is dynamically regulated during development and the course of disease[6]. This became particularly clear in the RBPMS model, in which RNA-seq was performed on neonates of 1 day old. At this age, several splice-isoforms were clearly different in the controls of the RBPMS KO compared to the other models. However, this limitation does not undermine the results of this study, it merely indicates that the group of commonly regulated AS events is likely underestimated. Second, we are unable to discriminate between direct versus indirect splicing targets in the KO models. In order to confirm that splicing events are direct targets of a splicing factor, it is required to validate the interaction by means of RIP-seq or CLIP-seq. Unfortunately, these data are not available for the 8 splicing factors we investigated.

In conclusion, we have shown that key cardiac splicing events require the concerted action of multiple splicing factors. In fact, we identified a substantial amount of overlap in the targets of several well-studied splicing factors in the heart. The observation that the expression of QKI, RBM24 and MBNL1 is dysregulated in a subset of patients with end-stage heart failure may represent a starting point for future studies to elucidate their role and mechanism in the failing heart.

MATERIAL AND METHODS

Mapping and analysis of RNA-seq data

Bioinformatics analysis was performed using the web-based computational workbench Galaxy (https://galaxyproject.org)[1]. FASTQ files from the 8 knockout models were downloaded from NCBI Sequence Read Archive (SRA). Characteristics of downloaded SRR samples are listed in **Table S1**. The sequencing depth ranged from $16x10^6$ in MBNL1+2 DKO model to $355x10^6$ in the QKI KO model. Quality control of FASTQ files was performed using FASTQC (https://www.bioinformatics.babraham.ac.uk/projects/fastqc/). Paired-end reads of the selected mice were aligned against the mouse Ensembl reference transcriptome GRCm38 (version M25, Ensembl genebuild 100), using STAR aligner (Galaxy Version 2.7.8a) with default settings[2]. Differential gene expression was performed using the DESeq2[3]. To interrogate different exon usage for all exon bins in the mapped sequences we used the Bioconductor package DEXSeq (version 1.28.1)[4].

The FASTQ files of left ventricular tissue samples from 128 patients with end-stage dilated cardiomyopathy (DCM) are available from the European Genome-phenome Archive (EGAS00001002454). These tissue samples were retrieved during left ventricular device implantation or/and cardiac transplantation as described[5]. They were snap-frozen and stored in liquid nitrogen, until RNA was extracted checked on quality using the bioanalyzer[5]. Non-stranded, poly(A)-selected RNA libraries were prepared for sequencing on HiSeq 2000 (Illumina) using paired-end chemistry[5]. We retrieved the FASTQ files and aligned them against the human genome assembly GRCh38 (version 38, Ensembl genebuild 104) using STAR aligner (Galaxy Version 2.7.8a) with default settings[2]. Differential gene expression was performed using the DESeq2[3]. To interrogate different exon usage for all exon bins in the mapped sequences we used the Bioconductor package DEXSeq (version 1.28.1)[4].

Data visualization

GOrilla (cbl-gorilla.cs.technion.ac.il)[6] was used to find enriched gene ontology (GO) terms in differentially expressed genes and the genes with alternatively spliced exons.

IGV (Integrative Genomics Viewer)[7] was used to generate BedGraphs in order to visualize read coverage and alternative splicing events in the different KO models.

The online tool Intervene[8] was used to create the UpSet plot to visualize the overlap between datasets

Statistical analysis

Genes with base mean expression ≥ 1, absolute $\log_2$(fold change) ≥ 0.58 and and adjusted p-value ≤ 0.05 were deemed significantly differentially expressed.

Exon bins with a base mean count ≥ 5, absolute $\log_2$(fold change) ≥ 1 and adjusted p-value ≤ 0.05 were considered differentially spliced.

REFERENCES

1. Pan Q, Shai O, Lee LJ, Frey BJ, Blencowe BJ. Deep surveying of alternative splicing complexity in the human transcriptome by high-throughput sequencing. *Nat Genet*. 2008;40:1413–1415.
2. Gigli M, Begay RL, Morea G, Graw SL, Sinagra G, Taylor MRG, Granzier H, Mestroni L. A Review of the Giant Protein Titin in Clinical Molecular Diagnostics of Cardiomyopathies. *Front Cardiovasc Med*. 2016;3:21.
3. Bang M-L, Centner T, Fornoff F, Geach AJ, Gotthardt M, McNabb M, Witt CC, Labeit D, Gregorio CC, Granzier H, Labeit S. The Complete Gene Sequence of Titin, Expression of an Unusual ≈700-kDa Titin Isoform, and Its Interaction With Obscurin Identify a Novel Z-Line to I-Band Linking System. *Circ Res*. 2001;89:1065–1072.
4. George CH, Rogers SA, Bertrand BMA, Tunwell REA, Thomas NL, Steele DS, Cox EV, Pepper C, Hazeel CJ, Claycomb WC, Lai FA. Alternative Splicing of Ryanodine Receptors Modulates Cardiomyocyte Ca2+ Signaling and Susceptibility to Apoptosis. *Circ Res*. 2007;100:874–883.
5. Hu Z, Liang MC, Soong TW. Alternative Splicing of L-type CaV1.2 Calcium Channels: Implications in Cardiovascular Diseases. *Genes*. 2017;8:344.
6. Mazin PV, Khaitovich P, Cardoso-Moreira M, Kaessmann H. Alternative splicing during mammalian organ development. *Nat Genet*. 2021;53:925–934.
7. Rodriguez JM, Pozo F, Domenico T di, Vazquez J, Tress ML. An analysis of tissue-specific alternative splicing at the protein level. *PLOS Comput Biol*. 2020;16:e1008287.
8. Guo W, Schafer S, Greaser ML, Radke MH, Liss M, Govindarajan T, Maatz H, Schulz H, Li S, Parrish AM, Dauksaite V, Vakeel P, Klaassen S, Gerull B, Thierfelder L, Regitz-Zagrosek V, Hacker TA, Saupe KW, Dec GW, Ellinor PT, MacRae CA, Spallek B, Fischer R, Perrot A, Özcelik C, Saar K, Hubner N, Gotthardt M. RBM20, a gene for hereditary cardiomyopathy, regulates titin splicing. *Nat Med*. 2012;18:766–773.
9. van den Hoogenhof MMG, Beqqali A, Amin AS, van der Made I, Aufiero S, Khan MAF, Schumacher CA, Jansweijer JA, van Spaendonck-Zwarts KY, Remme CA, Backs J, Verkerk AO, Baartscheer A, Pinto YM, Creemers EE. RBM20 Mutations Induce an Arrhythmogenic Dilated Cardiomyopathy Related to Disturbed Calcium Handling. *Circulation*. 2018;138:1330–1342.
10. Giudice J, Xia Z, Li W, Cooper TA. Neonatal cardiac dysfunction and transcriptome changes caused by the absence of Celf1. *Sci Rep*. 2016;6:35550.
11. Liu T-Y, Chen Y-C, Jong Y-J, Tsai H-J, Lee C-C, Chang Y-S, Chang J-G, Chang Y-F. Muscle developmental defects in heterogeneous nuclear Ribonucleoprotein A1 knockout mice. *Open Biol*. 7:160303.
12. Ye J, Beetz N, O'Keeffe S, Tapia JC, Macpherson L, Chen WV, Bassel-Duby R, Olson EN, Maniatis T. hnRNP U protein is required for normal pre-mRNA splicing and postnatal heart development and function. *Proc Natl Acad Sci*. 2015;112:E3020–E3029.
13. Lee K-Y, Li M, Manchanda M, Batra R, Charizanis K, Mohan A, Warren SA, Chamberlain CM, Finn D, Hong H, Ashraf H, Kasahara H, Ranum LPW, Swanson MS. Compound loss of muscleblind-like function in myotonic dystrophy. *EMBO Mol Med*. 2013;5:1887–1900.
14. Sta Maria NS, Zhou C, Lee SJ, Valiulahi P, Li X, Choi J, Liu X, Jacobs R, Comai L, Reddy S. Mbnl1 and Mbnl2 regulate brain structural integrity in mice. *Commun Biol*. 2021;4:1342.
15. Lee K-Y, Seah C, Li C, Chen Y-F, Chen C-Y, Wu C-I, Liao P-C, Shyu Y-C, Olafson HR, McKee KK, Wang ET, Yeh C-H, Wang C-H. Mice lacking MBNL1 and MBNL2 exhibit sudden cardiac death and molecular signatures recapitulating myotonic dystrophy. *Hum Mol Genet*. 2022;31:3144–3160.
16. Dixon DM, Choi J, El-Ghazali A, Park SY, Roos KP, Jordan MC, Fishbein MC, Comai L, Reddy S. Loss of muscleblind-like 1 results in cardiac pathology and persistence of embryonic splice isoforms. *Sci Rep*. 2015;5:9042.
17. Charizanis K, Lee K-Y, Batra R, Goodwin M, Zhang C, Yuan Y, Shiue L, Cline M, Scotti MM, Xia G, Kumar A, Ashizawa T, Clark HB, Kimura T, Takahashi MP, Fujimura H, Jinnai K, Yoshikawa H, Gomes-Pereira M, Gourdon G,

Sakai N, Nishino S, Foster TC, Ares M, Darnell RB, Swanson MS. Muscleblind-Like 2 Mediated Alternative Splicing in the Developing Brain and Dysregulation in Myotonic Dystrophy. *Neuron*. 2012;75:437–450.

18. Choi J, Dixon DM, Dansithong W, Abdallah WF, Roos KP, Jordan MC, Trac B, Lee HS, Comai L, Reddy S. Muscleblind-like 3 deficit results in a spectrum of age-associated pathologies observed in myotonic dystrophy. *Sci Rep*. 2016;6:30999.

19. Ghanem LR, Kromer A, Silverman IM, Chatterji P, Traxler E, Penzo-Mendez A, Weiss MJ, Stanger BZ, Liebhaber SA. The Poly(C) Binding Protein Pcbp2 and Its Retrotransposed Derivative Pcbp1 Are Independently Essential to Mouse Development. *Mol Cell Biol*. 2016;36:304–319.

20. Li Z, Takakura N, Oike Y, Imanaka T, Araki K, Suda T, Kaname T, Kondo T, Abe K, Yamamura K. Defective smooth muscle development in qkI-deficient mice. *Dev Growth Differ*. 2003;45:449–462.

21. Pablo Montañés-Agudo, Simona Aufiero, Eva N. Schepers, Ingeborg van der Made, Lucia Cócera-Ortega, Auriane C. Ernault, Stéphane Richard, Diederik W.D. Kuster, Vincent M. Christoffels, Yigal M. Pinto, Esther E. Creemers. The RNA-binding protein QKI governs a muscle-specific alternative splicing program that shapes the contractile function of cardiomyocytes. *Cardiovasc Res*. In press.

22. Gao C, Ren S, Lee J-H, Qiu J, Chapski DJ, Rau CD, Zhou Y, Abdellatif M, Nakano A, Vondriska TM, Xiao X, Fu X-D, Chen J-N, Wang Y. RBFox1-mediated RNA splicing regulates cardiac hypertrophy and heart failure. *J Clin Invest*. 2016;126:195–206.

23. Verma SK, Deshmukh V, Thatcher K, Belanger KK, Rhyner AM, Meng S, Holcomb RJ, Bressan M, Martin JF, Cooke JP, Wythe JD, Widen SG, Lincoln J, Kuyumcu-Martinez MN. RBFOX2 is required for establishing RNA regulatory networks essential for heart development. *Nucleic Acids Res*. 2022;50:2270–2286.

24. Wei C, Qiu J, Zhou Y, Xue Y, Hu J, Ouyang K, Banerjee I, Zhang C, Chen B, Li H, Chen J, Song L-S, Fu X-D. Repression of the Central Splicing Regulator RBFox2 Is Functionally Linked to Pressure Overload-Induced Heart Failure. *Cell Rep*. 2015;10:1521–1533.

25. Yang J, Hung L-H, Licht T, Kostin S, Looso M, Khrameeva E, Bindereif A, Schneider A, Braun T. RBM24 Is a Major Regulator of Muscle-Specific Alternative Splicing. *Dev Cell*. 2014;31:87–99.

26. Liu J, Kong X, Zhang M, Yang X, Xu X. RNA binding protein 24 deletion disrupts global alternative splicing and causes dilated cardiomyopathy. *Protein Cell*. 2019;10:405–416.

27. van den Hoogenhof MMG, van der Made I, Beqqali A, de Groot NE, Damanafshan A, van Oort RJ, Pinto YM, Creemers EE. The RNA-binding protein Rbm38 is dispensable during pressure overload-induced cardiac remodeling in mice. *PLoS ONE*. 2017;12:e0184093.

28. Gan P, Wang Z, Morales MG, Zhang Y, Bassel-Duby R, Liu N, Olson EN. RBPMS is an RNA-binding protein that mediates cardiomyocyte binucleation and cardiovascular development. *Dev Cell*. 2022;57:959-973.e7.

29. Xu X, Yang D, Ding J-H, Wang W, Chu P-H, Dalton ND, Wang H-Y, Bermingham JR, Ye Z, Liu F, Rosenfeld MG, Manley JL, Ross J, Chen J, Xiao R-P, Cheng H, Fu X-D. ASF/SF2-regulated CaMKIIdelta alternative splicing temporally reprograms excitation-contraction coupling in cardiac muscle. *Cell*. 2005;120:59–72.

30. Ding J-H, Xu X, Yang D, Chu P-H, Dalton ND, Ye Z, Yeakley JM, Cheng H, Xiao R-P, Ross Jr J, Chen J, Fu X-D. Dilated cardiomyopathy caused by tissue-specific ablation of SC35 in the heart. *EMBO J*. 2004;23:885–896.

31. Ortiz-Sánchez P, Villalba-Orero M, López-Olañeta MM, Larrasa-Alonso J, Sánchez-Cabo F, Martí-Gómez C, Camafeita E, Gómez-Salinero JM, Ramos-Hernández L, Nielsen PJ, Vázquez J, Müller-McNicoll M, García-Pavía P, Lara-Pezzi E. Loss of SRSF3 in Cardiomyocytes Leads to Decapping of Contraction-Related mRNAs and Severe Systolic Dysfunction. *Circ Res*. 2019;125:170–183.

32. Larrasa-Alonso J, Villalba-Orero M, Martí-Gómez C, Ortiz-Sánchez P, López-Olañeta MM, Rey-Martín MA, Sánchez-Cabo F, McNicoll F, Müller-McNicoll M, García-Pavía P, Lara-Pezzi E. The SRSF4–GAS5-Glucocorticoid Receptor Axis Regulates Ventricular Hypertrophy. *Circ Res*. 2021;129:669–683.

33. Zhang X, Wang Z, Xu Q, Chen Y, Liu W, Zhong T, Li H, Quan C, Zhang L, Cui C-P. Splicing

factor Srsf5 deletion disrupts alternative splicing and causes noncompaction of ventricular myocardium. *iScience*. 2021;24:103097.

34. Feng Y, Valley MT, Lazar J, Yang AL, Bronson RT, Firestein S, Coetzee WA, Manley JL. SRp38 regulates alternative splicing and is required for Ca(2+) handling in the embryonic heart. *Dev Cell*. 2009;16:528–538.

35. Seiler M, Peng S, Agrawal AA, Palacino J, Teng T, Zhu P, Smith PG, Caesar-Johnson SJ, Demchok JA, Felau I, Kasapi M, Ferguson ML, Hutter CM, Sofia HJ, Tarnuzzer R, Wang Z, Yang L, Zenklusen JC, Zhang J (Julia), Chudamani S, Liu J, Lolla L, Naresh R, Pihl T, Sun Q, Wan Y, Wu Y, Cho J, DeFreitas T, Frazer S, Gehlenborg N, Getz G, Heiman DI, Kim J, Lawrence MS, Lin P, Meier S, Noble MS, Saksena G, Voet D, Zhang H, Bernard B, Chambwe N, Dhankani V, Knijnenburg T, Kramer R, Leinonen K, Liu Y, Miller M, Reynolds S, Shmulevich I, Thorsson V, Zhang W, Akbani R, Broom BM, Hegde AM, Ju Z, Kanchi RS, Korkut A, Li J, Liang H, Ling S, Liu W, Lu Y, Mills GB, Ng K-S, Rao A, Ryan M, Wang J, Weinstein JN, Zhang J, Abeshouse A, Armenia J, Chakravarty D, Chatila WK, Bruijn I de, Gao J, Gross BE, Heins ZJ, Kundra R, La K, Ladanyi M, Luna A, Nissan MG, Ochoa A, Phillips SM, Reznik E, Sanchez-Vega F, Sander C, Schultz N, Sheridan R, Sumer SO, Sun Y, Taylor BS, Wang J, Zhang H, Anur P, Peto M, et al. Somatic Mutational Landscape of Splicing Factor Genes and Their Functional Consequences across 33 Cancer Types. *Cell Rep*. 2018;23:282-296.e4.

36. Fisher E, Feng J. RNA splicing regulators play critical roles in neurogenesis. *WIREs RNA*. 2022;13:e1728.

37. Maatz H, Jens M, Liss M, Schafer S, Heinig M, Kirchner M, Adami E, Rintisch C, Dauksaite V, Radke MH, Selbach M, Barton PJR, Cook SA, Rajewsky N, Gotthardt M, Landthaler M, Hubner N. RNA-binding protein RBM20 represses splicing to orchestrate cardiac pre-mRNA processing. *J Clin Invest*. 2014;124:3419–3430.

38. D'Antonio M, Nguyen JP, Arthur TD, Matsui H, Donovan MKR, D'Antonio-Chronowska A, Frazer KA. In heart failure reactivation of RNA-binding proteins is associated with the expression of 1,523 fetal-specific isoforms. *PLOS Comput Biol*. 2022;18:e1009918.

39. Kong SW, Hu YW, Ho JWK, Ikeda S, Polster S, John R, Hall JL, Bisping E, Pieske B, dos Remedios CG, Pu WT. Heart Failure–Associated Changes in RNA Splicing of Sarcomere Genes. *Circ Cardiovasc Genet*. 2010;3:138–146.

40. Heinig M, Adriaens ME, Schafer S, van Deutekom HWM, Lodder EM, Ware JS, Schneider V, Felkin LE, Creemers EE, Meder B, Katus HA, Rühle F, Stoll M, Cambien F, Villard E, Charron P, Varro A, Bishopric NH, George AL, dos Remedios C, Moreno-Moral A, Pesce F, Bauerfeind A, Rüschendorf F, Rintisch C, Petretto E, Barton PJ, Cook SA, Pinto YM, Bezzina CR, Hubner N. Natural genetic variation of the cardiac transcriptome in non-diseased donors and patients with dilated cardiomyopathy. *Genome Biol*. 2017;18:170.

41. Ames E, Lawson M, Mackey A, Holmes J. Sequencing of mRNA identifies re-expression of fetal splice variants in cardiac hypertrophy. *J Mol Cell Cardiol*. 2013;62:99–107.

42. Love MI, Huber W, Anders S. Moderated estimation of fold change and dispersion for RNA-seq data with DESeq2. *Genome Biol*. 2014;15:550.

43. Anders S, Reyes A, Huber W. Detecting differential usage of exons from RNA-seq data. *Genome Res*. 2012;22:2008–2017.

44. Gray C, Heller Brown J. CaMKIIdelta subtypes: localization and function. *Front Pharmacol*. 2014;5.

45. Duran J, Nickel L, Estrada M, Backs J, van den Hoogenhof MMG. CaMKIIδ Splice Variants in the Healthy and Diseased Heart. *Front Cell Dev Biol*. 2021;9.

46. Srinivasan M, Edman CF, Schulman H. Alternative splicing introduces a nuclear localization signal that targets multifunctional CaM kinase to the nucleus. *J Cell Biol*. 1994;126:839–852.

47. Wang C-LA, Coluccio LM. Chapter 3 - New Insights into the Regulation of the Actin Cytoskeleton by Tropomyosin. In: Jeon KW, editor. International Review of Cell and Molecular Biology. Academic Press; 2010. p. 91–128.

48. Chen Z, Song J, Chen L, Zhu C, Cai H, Sun M, Stern A, Mozdziak P, Ge Y, Means WJ, Guo W. Characterization of TTN Novex Splicing Variants

across Species and the Role of RBM20 in Novex-Specific Exon Splicing. *Genes*. 2018;9:86.

49. Fu X-D, Ares M. Context-dependent control of alternative splicing by RNA-binding proteins. *Nat Rev Genet*. 2014;15:689–701.

50. Hall MP, Nagel RJ, Fagg WS, Shiue L, Cline MS, Perriman RJ, Donohue JP, Ares M. Quaking and PTB control overlapping splicing regulatory networks during muscle cell differentiation. *RNA N Y N*. 2013;19:627–638.

SUPPLEMENTAL TABLES

Table S1. Characteristics of the analyzed RNA-sequencing data

Knock-out model	Genotype	N per group	Sex	Age at sequencing	RNA and library	Platform	Depth (millions)	NCBI project	Ref.
HNRNPU KO	Conditional *Hnrnpu*$^{fl/fl}$; *Ckmm-Cre*^{tg}	2	Male, female	14 days	Nextera library	Illumina HiSeq 2500	148.1-167.6	PRJNA281957	9
MBNL1/2 DKO	Double knockout *Mbnl1*$^{-/-}$; *Mbnl2*$^{fl/fl}$; *Myh6-Cre*^{tg}	3	Not stated	3-6 months	Poly-(A)	Illumina NextSeq 500 v2	16.3 - 34.2	GSE184574	10
QKI KO	Conditional inducible *Qki*$^{fl/fl}$; *Myh6-MCM*^{tg}	3	Male, female	12-17 weeks	rRNA-depleted RNA	Novaseq	355.2 - 477.8	PRJNA831665	11
RBM20 KO	Constitutive *Rbm20*$^{-/-}$	3	Male	25 weeks	rRNA-depleted RNA	Illumina Nextseq 500	154.2 - 192.1	PRJNA417769	12
RBM24 KO	Conditional *Rbm24*$^{fl/fl}$; *Myh6-Cre*^{tg}	2	Not stated	23 days	rRNA-depleted	Illumina HiSeq PE150	52.2 - 59.6	PRJNA415257	13
RBPMS KO	Constitutive *Rbpms*$^{-/-}$	3	Male, female	1 day	KAPPA mRNA hyperprep kit	Illumina Nextseq 500	50.7-59.3	PRJNA758402	14
SRSF3 KO	Conditional inducible *Srsf3*$^{fl/fl}$; *Myh6-MCM*^{tg}	3	Male	2-3 months	Not stated	Illumina-HiSeq 2500 platform	178 - 268	GSE123002	15
SRSF4 KO	Conditional *Srsf4*$^{fl/fl}$; *NKx2.5-Cre*^{tg}	3	Male	2 months	polyA	Illumina HiSeq 2000	190.5 -264.8	GSE131145	16

SUPPLEMENTAL FIGURES

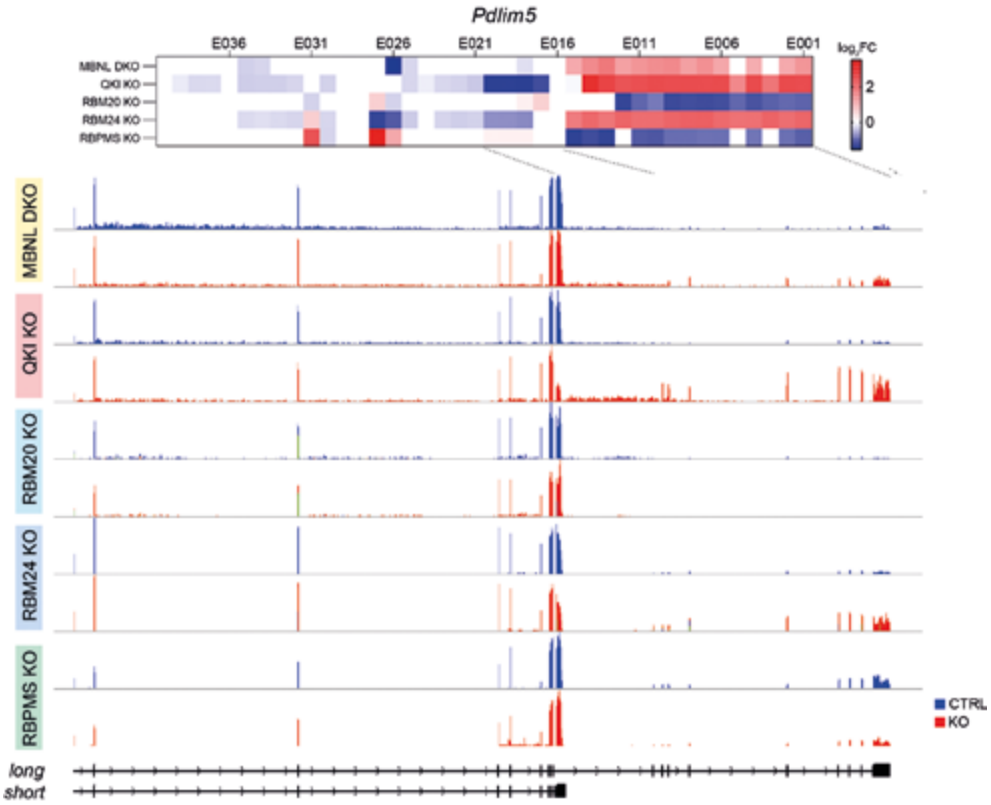

Figure S1. Splicing changes in the sarcomere scaffolding protein PDLIM5 in MBNL DKO, QKI KO, RBM20 KO, RBM24 KO and RBPMS KO. Heat map showing changes in exon usage per exon bin (log_2(Fold Change WT/KO)) and representative bed graphs showing the splicing changes in *Camk2d,* Heat map showing *Pdlim5* exhibits 2 isoforms: long-*Pdlim5* (present in immature proliferating cardiomyocytes) and short-*Pdlim5* (present in mature cardiomyocytes)[14]. MBNL, QKI and RBM24 KO hearts shows a shift from the short to the long isoform. RBM20 KO displays a modest reduction of the residual long-*Pdlim5* isoform. Contrary to the rest of controls, RBPMS CTRL hearts present the long isoform due to their young age (postnatal day 1). RBPMS KO present a reduction in the long isoform.

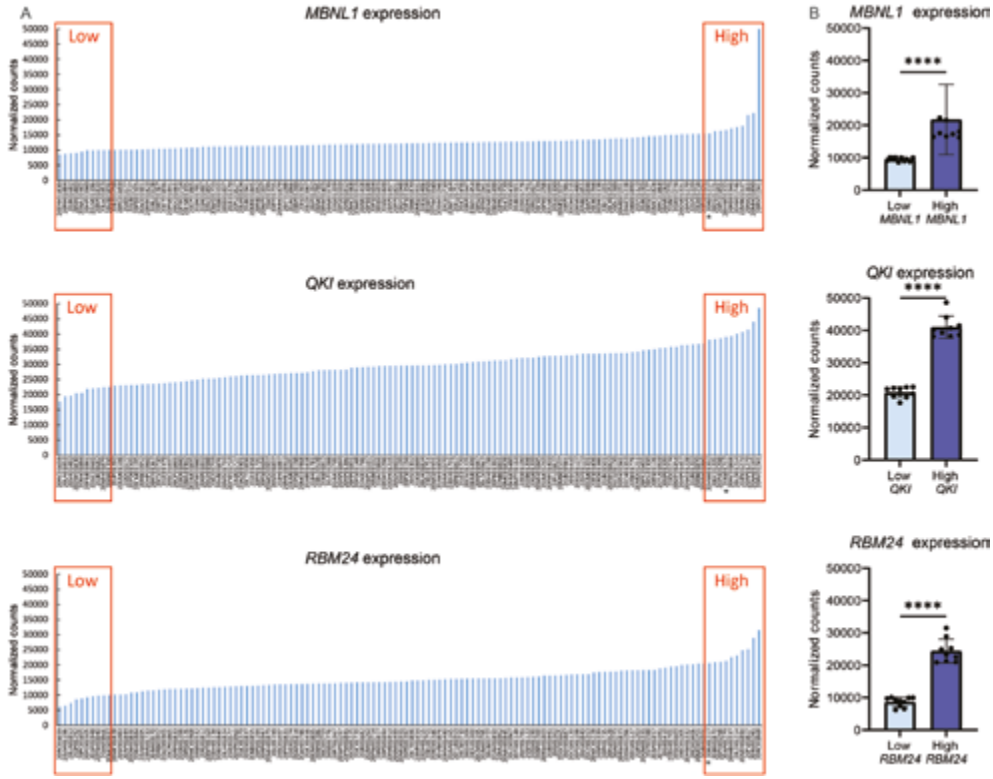

Figure S2. Expression of MBNL1, QKI and RBM24 in human heart tissue. (A) Normalized counts for the expression of the splicing factors *MBNL1*, *QKI* and *RBM24* in a cohort of 128 human failing heart samples. The red boxes indicates the 10 samples with the highest and the lowest expression for each splicing factor. Sample 20RJ01217 (*) was excluded from further analysis due to the presence of a pathological RBM20 mutation (RBM20 E913K). (B) Gene expression of the low and high *MBNL1*, *QKI* and *RBM24* groups. Mann-Whitney test; **** $p < 0.0001$.

SUPPLEMENTAL REFERENCES

1. Afgan E, Baker D, Batut B, van den Beek M, Bouvier D, Čech M, Chilton J, Clements D, Coraor N, Grüning BA, Guerler A, Hillman-Jackson J, Hiltemann S, Jalili V, Rasche H, Soranzo N, Goecks J, Taylor J, Nekrutenko A, Blankenberg D. The Galaxy platform for accessible, reproducible and collaborative biomedical analyses: 2018 update. *Nucleic Acids Res*. 2018;46:W537–W544.
2. Dobin A, Davis CA, Schlesinger F, Drenkow J, Zaleski C, Jha S, Batut P, Chaisson M, Gingeras TR. STAR: ultrafast universal RNA-seq aligner. *Bioinformatics*. 2013;29:15–21.
3. Love MI, Huber W, Anders S. Moderated estimation of fold change and dispersion for RNA-seq data with DESeq2. *Genome Biol*. 2014;15:550.
4. Anders S, Reyes A, Huber W. Detecting differential usage of exons from RNA-seq data. *Genome Res*. 2012;22:2008–2017.
5. Heinig M, Adriaens ME, Schafer S, van Deutekom HWM, Lodder EM, Ware JS, Schneider V, Felkin LE, Creemers EE, Meder B, Katus HA, Rühle F, Stoll M, Cambien F, Villard E, Charron P, Varro A, Bishopric NH, George AL, dos Remedios C, Moreno-Moral A, Pesce F, Bauerfeind A, Rüschendorf F, Rintisch C, Petretto E, Barton PJ, Cook SA, Pinto YM, Bezzina CR, Hubner N. Natural genetic variation of the cardiac transcriptome in non-diseased donors and patients with dilated cardiomyopathy. *Genome Biol*. 2017;18:170.
6. Eden E, Navon R, Steinfeld I, Lipson D, Yakhini Z. GOrilla: a tool for discovery and visualization of enriched GO terms in ranked gene lists. *BMC Bioinformatics*. 2009;10:48.
7. Robinson JT, Thorvaldsdóttir H, Winckler W, Guttman M, Lander ES, Getz G, Mesirov JP. Integrative genomics viewer. *Nat Biotechnol*. 2011;29:24–26.
8. Khan A, Mathelier A. Intervene: a tool for intersection and visualization of multiple gene or genomic region sets. *BMC Bioinformatics*. 2017;18:287.
9. Ye J, Beetz N, O'Keeffe S, Tapia JC, Macpherson L, Chen WV, Bassel-Duby R, Olson EN, Maniatis T. hnRNP U protein is required for normal pre-mRNA splicing and postnatal heart development and function. *Proc Natl Acad Sci*. 2015;112:E3020–E3029.
10. Lee K-Y, Seah C, Li C, Chen Y-F, Chen C-Y, Wu C-I, Liao P-C, Shyu Y-C, Olafson HR, McKee KK, Wang ET, Yeh C-H, Wang C-H. Mice lacking MBNL1 and MBNL2 exhibit sudden cardiac death and molecular signatures recapitulating myotonic dystrophy. *Hum Mol Genet*. 2022;31:3144–3160.
11. Pablo Montañés-Agudo, Simona Aufiero, Eva N. Schepers, Ingeborg van der Made, Lucia Cócera-Ortega, Auriane C. Ernault, Stéphane Richard, Diederik W.D. Kuster, Vincent M. Christoffels, Yigal M. Pinto, Esther E. Creemers. The RNA-binding protein QKI governs a muscle-specific alternative splicing program that shapes the contractile function of cardiomyocytes. *Cardiovasc Res*. In press.
12. van den Hoogenhof MMG, Beqqali A, Amin AS, van der Made I, Aufiero S, Khan MAF, Schumacher CA, Jansweijer JA, van Spaendonck-Zwarts KY, Remme CA, Backs J, Verkerk AO, Baartscheer A, Pinto YM, Creemers EE. RBM20 Mutations Induce an Arrhythmogenic Dilated Cardiomyopathy Related to Disturbed Calcium Handling. *Circulation*. 2018;138:1330–1342.
13. Liu J, Kong X, Zhang M, Yang X, Xu X. RNA binding protein 24 deletion disrupts global alternative splicing and causes dilated cardiomyopathy. *Protein Cell*. 2019;10:405–416.
14. Gan P, Wang Z, Morales MG, Zhang Y, Bassel-Duby R, Liu N, Olson EN. RBPMS is an RNA-binding protein that mediates cardiomyocyte binucleation and cardiovascular development. *Dev Cell*. 2022;57:959-973.e7.
15. Ortiz-Sánchez P, Villalba-Orero M, López-Olañeta MM, Larrasa-Alonso J, Sánchez-Cabo F, Martí-Gómez C, Camafeita E, Gómez-Salinero JM, Ramos-Hernández L, Nielsen PJ, Vázquez J, Müller-McNicoll M, García-Pavía P, Lara-Pezzi E. Loss of SRSF3 in Cardiomyocytes Leads to Decapping of Contraction-Related mRNAs and Severe Systolic Dysfunction. *Circ Res*. 2019;125:170–183.
16. Larrasa-Alonso J, Villalba-Orero M, Martí-Gómez C, Ortiz-Sánchez P, López-Olañeta MM, Rey-Martín MA, Sánchez-Cabo F, McNicoll F, Müller-McNicoll M, García-Pavía P, Lara-Pezzi E. The SRSF4–GAS5-Glucocorticoid Receptor Axis Regulates Ventricular Hypertrophy. *Circ Res*. 2021;129:669–683.

CHAPTER 5

INHIBITION OF MINOR INTRON SPLICING REDUCES NA^+ AND CA^{2+} CHANNEL EXPRESSION AND FUNCTION IN CARDIOMYOCYTES

Pablo Montañés-Agudo, Simona Casini, Simona Aufiero, Auriane C. Ernault, Ingeborg van der Made, Yigal M. Pinto, Carol Ann Remme, Esther E. Creemers

Journal of Cell Science 135, no. 1 (2022): jcs259191.

ABSTRACT

Eukaryotic genomes contain a tiny subset of 'minor class' introns with unique sequence elements that require their own splicing machinery. These minor introns are present in certain gene families with specific functions, such as voltage-gated sodium and voltage-gated calcium channels. Removal of minor introns by the minor spliceosome has been proposed as a post-transcriptional regulatory layer, which remains unexplored in the heart. Here, we investigate whether the minor spliceosome regulates electrophysiological properties of cardiomyocytes by knocking-down the essential minor spliceosome component *U6atac* in neonatal rat ventricular myocytes. Loss of *U6atac* led to robust minor intron retention within *Scn5a* and *Cacna1c*, resulting in reduced protein levels of $Na_v1.5$ and $Ca_v1.2$. Functional consequences were studied through patch-clamp analysis, and revealed reduced sodium and L-type calcium currents after loss of *U6atac*. In conclusion, minor intron splicing modulates voltage-dependent ion channel expression and function in cardiomyocytes. This may be of particular relevance in situations in which minor splicing activity changes, such as in genetic diseases affecting minor spliceosome components, or in acquired diseases in which minor spliceosome components are dysregulated, such as heart failure.

INTRODUCTION

The accurate removal of introns by pre-mRNA splicing is a fundamental step in eukaryotic gene expression. Two types of introns coexist in eukaryotes: major introns and minor introns, which diverge in their consensus sequences at the 5' splice site, branch point sequence and 3' splice site[1]. The vast majority of introns are major introns (>99%), whereas a small minority (<1%) represents minor introns. Specifically, 722 minor introns are found in only 699 human genes[2], and thus, most minor intron-containing gene (MIGs) contain a single minor intron, flanked by 'normal' major introns. The existence of major and minor introns, with different splicing consensus sequences, requires not one, but two different splicing machineries: the so-called major 'U2-dependent' and minor 'U12-dependent' spliceosomes, each containing their own unique core components.

Minor introns and the minor spliceosome are highly conserved; in fact, the position of minor introns within genes is more conserved than that of major introns[3]. Minor introns, which trace back to the last eukaryotic common ancestor, are enriched in numerous gene families, some of which are crucial for cardiomyocyte function, such as voltage-gated sodium and calcium channels, and mitogen activated-protein kinases (MAPK)[4]. Although the exact function of minor introns has remained an enigma, the fact that they have endured in modern genomes indicates that they confer an evolutionary advantage, despite the increased metabolic load on the cell of maintaining two parallel splicing machineries[4]. Recent studies have uncovered a crucial functional difference between minor and major splicing: minor introns generally splice at a slower rate than major introns[5]. As a consequence, minor introns are on average 2-fold more retained than their neighbouring major introns[6,7]. It has been proposed that unspliced transcripts are either trapped in the nucleus, or degraded by the exosome or via nonsense-mediated decay (NMD)[5]. This suggests that minor introns act as regulatory switches to control the expression of sets of MIGs, which can be accomplished by altering the levels of minor spliceosome components. Indeed, Younis et al. recently demonstrated that *U6atac*, one of the minor spliceosome's specific snRNAs, has a short half-life and can be rate limiting for minor intron splicing in HeLa cells. They showed that *U6atac* can be stabilized by activated p38 MAPK, which is produced in response to cellular stress. This resulted in enhanced splicing of minor introns and increased expression of numerous genes that contain them. It was concluded that the minor spliceosome enables proteins to be produced rapidly in response to stress, bypassing the need for a new round of transcription[7].

Mutations in core components of the minor spliceosome are responsible for several complex syndromes. To date five minor spliceosome congenital human diseases have been described: Isolated Growth Hormone Deficiency (IGHD), Microcephalic Osteodysplastic Primordial Dwarfism type I/Taybi-Linder Syndrome (MOPD1/TALS), Roifman syndrome (RFMN),

Lowry Wood Syndrome (LWS) and Early Onset Cerebellar Ataxia (EOCA)[8]. These pathologies show diverse and pleiotropic symptoms, but all share a neurological component with varying degrees of severity. While these diseases mostly underscore the importance of the minor spliceosome in neurons, its function in the cardiovascular system has, to the best of our knowledge, not yet been explored. Nevertheless, the fact that numerous MIGs are known to encode protein families essential for cardiomyocyte biology (e.g. sodium and calcium channels, MAPKs, and calpains), raises the intriguing possibility that minor spliceosome regulation is critical for cardiac (electro-)physiology.

Here, we investigated whether minor intron splicing may constitute a regulatory mechanism to control gene expression in the heart. By knocking down the minor spliceosome component *U6atac* in neonatal rat ventricular myocytes (NRVMs), we demonstrate robust effects on minor intron retention in the sodium channel *Scn5a*/$Na_v1.5$ and the L-type calcium channel *Cacna1c*/$Ca_v1.2$, and show the functional consequences through patch-clamp analysis.

Altogether, our study provides the first evidence that alterations in minor splicing activity modulate cardiac electrophysiology, which may be of vital importance in genetic diseases affecting minor spliceosome components and in acquired diseases in which minor spliceosome components are dysregulated, including heart failure.

RESULTS

Minor-intron containing genes (MIGs) are expressed in the heart

To explore the potential relevance of minor intron splicing in cardiac physiology, we first examined the expression of minor-intron containing genes (MIGs) in published RNA sequencing data of 100 human non-diseased hearts (left ventricular tissue)[9]. Of the 699 previously identified MIGs[2], we found a total of 582 expressed in these hearts (**Supplemental Data 1**). The average expression of MIGs was significantly higher than the expression of genes without minor introns (**Fig 1A**), indicating that MIGs constitute an actively expressed subset of genes in the heart.

As an initial characterization of MIGs in the heart, we performed gene ontology enrichment analysis using the GOrilla bioinformatic tool[10]. As shown in **Fig 1B**, MIGs expressed in the heart are enriched in ´biological process´ terms related to electrophysiology and to protein palmitoylation. Analysis of the ´cellular component´ terms revealed an enrichment in the categories of "voltage gated sodium channel complex" and "voltage gated calcium channel complex" (**Fig 1C**), which includes the gene families encoding the alpha subunit of voltage-gated sodium channels (e.g. *SCN5A, SCN10A*) and numerous subunits of the voltage-gated calcium channels (e.g. *CACNA1C, CACNA1G*).

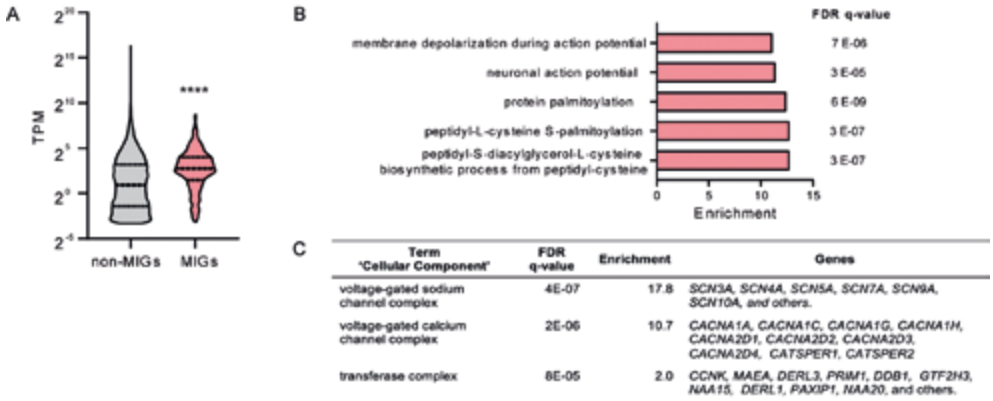

Term 'Cellular Component'	FDR q-value	Enrichment	Genes
voltage-gated sodium channel complex	4E-07	17.8	*SCN3A, SCN4A, SCN5A, SCN7A, SCN9A, SCN10A, and others.*
voltage-gated calcium channel complex	2E-06	10.7	*CACNA1A, CACNA1C, CACNA1G, CACNA1H, CACNA2D1, CACNA2D2, CACNA2D3, CACNA2D4, CATSPER1, CATSPER2*
transferase complex	8E-05	2.0	*CCNK, MAEA, DERL3, PRIM1, DDB1, GTF2H3, NAA15, DERL1, PAX3P1, NAA20, and others.*

Figure 1. Minor-intron containing genes (MIGs) expressed in the heart. (A) Expression of MIGs and genes without minor introns in non-diseased hearts. n = 100. Mann-Whitney test, **** $p < 0.0001$. TPM: transcripts per million. (B) ´Biological process´ and (C) 'cellular component´ terms enriched in the subset of MIGs expressed in the human heart according to gene ontology enrichment analysis (GOrilla). FDR q-value is the adjusted p-value for multiple testing using the Benjamini and Hochberg method. Enrichment is the percentage of genes in a specific gene ontology term in the input (MIGs) divided by the percentage in the background (all genes).

Knock-down of U6atac results in minor intron retention in NRVMs

Given our observation that numerous MIGs are expressed in the heart and that minor introns are enriched in e.g. voltage-gated sodium and calcium channels, we next investigated the impact of minor splicing on MIG expression in cardiomyocytes. To this end, we performed a gapmeR-mediated knockdown of the non-coding small nuclear RNA *U6atac* in NRVMs (**Fig 2A**). We chose to knockdown *U6atac* because it is an essential component of the minor spliceosome that is known to be a limiting factor in minor splicing[7]. We transfected 6-well plates with NRVMs with either an anti-*U6atac* or a non-targeting negative control gapmeR. The anti-*U6atac* gapmeR successfully knocked down *U6atac* up to 60%, 48h after transfection (**Fig 2A**).

To quantify minor retention in these transfected cells, we designed 4 sets of qPCR primers surrounding the minor and one of the major introns for a panel of 5 highly expressed MIGs in cardiomyocytes: the sodium channel *Scn5a*, the calcium channel *Cacna1c*, the calcium-activated protease *Capn2*, the phosphatase *Pten* and the splicing factor *Srsf10*. As depicted in **Fig 2B**, the qPCR analysis included a primer set detecting the retained minor intron (primer 1 and 2), a primer set that detects the correctly spliced exons surrounding the minor intron (primer 1 and 3), a primer set that detects intron retention of an unrelated major intron

of the same gene (primer 4 and 5) and a primer set that detects the transcript in which that major intron is spliced out (primer 4 and 6). The latter primer set also provides an indication of the expression level of the transcript. Overall, with this strategy, we were able to discriminate between the fully spliced transcripts and the transcripts that still contained the retained intron. The major introns were included to confirm that major intron retention was not affected by our approach (**Fig 2B**).

Knockdown of *U6atac* led to a strong increase in retention of all the minor introns tested: intron 3 of *Scn5a*, intron 13 of *Cacna1c*, intron 14 of *Capn2*, intron 1 of *Pten* and intron 2 of *Srsf10* (**Fig 2C**). Accordingly, levels of the corresponding minor intron-flanking exons spliced together decreased (**Fig 2D**), which, as expected, shows that minor intron retention occurs at the expense of proper splicing. Interestingly, a 60% reduction in *U6atac* produced a similar reduction (i.e.~50-80%) in minor intron splicing. This »1:1 reduction ratio in *U6atac* and properly spliced transcripts underscores that *U6atac* is an essential component of the minor

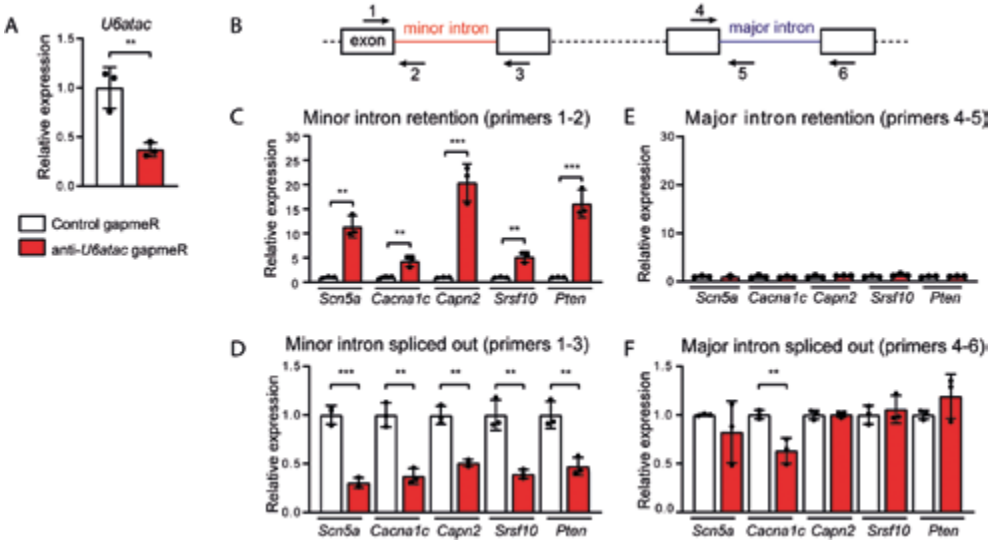

Figure 2. Effect of *U6atac* knockdown on minor intron retention in neonatal rat ventricular myocytes (NRVMs). (A) Relative expression of the minor splicing component *U6atac* 48h after gapmeR mediated knockdown in NRVMs. (B) Schematic illustration of the primer design for qPCR analysis. (C) Relative expression of minor introns, (D) minor intron-flanking exons, (E) major introns and (F) major intron-flanking exons as detected by qPCR using primers depicted in (B). Relative expression was calculated using as reference the geometric mean of *Gapdh*, *Hprt1* and *Eef1e1*. 3 wells per condition. Data are presented as mean ± s.d. Unpaired Student's t-test; * $p < 0.05$; ** $p < 0.01$; *** $p < 0.001$.

spliceosome. We did not observe an increase in major intron retention, which further validates that the knockdown of *U6atac* affects only minor and not major splicing (**Fig 2E**). mRNA expression levels of MIG was generally unaltered after *U6atac* knockdown (**Fig 2F**), with the exception of *Cacna1c* which was downregulated.

To validate the specificity of our approach, we repeated the experiment with a different anti-*U6atac* gapmeR (**Fig S1A-C**) and with gapmeRs against the minor spliceosome component *U4atac* (**Fig S1D-E**). With the four different gapmeRs we were able to induce minor intron retention, which indicates that the levels of both *U4atac* and *U6atac* are essential for proper minor splicing activity.

Nonsense mediated decay (NMD) may eliminate transcripts in which the minor intron is retained. To test whether this is indeed the case after *U6atac* knockdown, we inhibited the NMD pathway 24h after gapmeR transfection by incubating the NRVMs with the translation inhibitors cycloheximide or emetine for 3h. As shown in **Fig S2**, cycloheximide or emetine did not further increase minor intron retention in *Scn5a* or *Cacna1c* or mRNA levels, indicating that these transcripts with minor introns retained are not targeted by NMD. We included *Myh7b* – a bone fide target of the NMD pathway in cardiomyocytes – as a positive control for NMD inactivation[11].

Impact of minor splicing knock-down on cardiomyocyte morphology

To get a global impression of the morphology and condition of the cells after disrupting the minor spliceosome, we performed immunostainings 48 hours after anti-*U6atac* and control gapmeR transfections. Immunocytochemistry with alpha-actinin after *U6atac* knockdown did not reveal obvious differences in the sarcomere structure of NRVMs, nor did we observe evident changes in the morphology or numbers of residual fibroblasts as was detected by the vimentin staining (**Fig 3A**). Using automated image acquisition (Incucyte), we performed live cell analysis at three time points (24h, 48h and 72h) after transfection of the gapmeRs. As shown in **Fig 3C,** there was no difference in cell confluence over time between anti-*U6atac* and control gapmeRs. To analyze cell death, we employed a fluorescent probe based on Annexin V (Annexin V-ATTO-488) to measure phosphatidylserine exposure during apoptosis and the DNA dye YOYO-3 to measure permeabilized dead cells. The fluorescent areas of the Annexin-V probe and YOYO-3 in each image was analyzed to calculate the ratio of apoptotic and dead cells relative to the total cell area. Cell death remained rather constant over time, with a slight, but significant increase in the anti-*U6atac* condition at 48h and 72 hours after transfections (**Fig 3D**). Apoptosis was significantly increased at the 24h time point after *U6atac* knockdown, but not at later timepoints (**Fig 3E**). Since cell confluence

was not decreased in the *U6atac* knockdown groups over time, we conclude that inhibition of minor intron splicing does not affect cell viability or lead to evident damage of the cells.

We examined the hypertrophic response of the NRVMs after *U6atac* knock-down by culturing them in serum free medium or in 2% fetal bovine serum (FBS) for 48h (**Fig 3F, G**). We quantified cell surfaces after staining the cell membrane with WGA-488, as a measure of hypertrophy. Without serum (0% FBS), we did not observe a difference in cell size after *U6atac* knockdown. Serum stimulation (2% FBS) induced hypertrophy in both gapmeR groups, however the hypertrophic response was blunted in the anti-*U6atac* group. These results indicate that *U6atac* knockdown also affects cardiomyocyte hypertrophy, which may be mediated by PTEN, a key regulator in the PI3K/AKT signalling, or other MIGs that participate in the hypertrophic response.

Minor intron retention of Scn5a decreases $Na_v1.5$ expression and sodium current density

Since our pathway analysis revealed that cardiac MIGs are enriched for ion channels, this points to a potential link between minor intron splicing and electrophysiological properties of the cardiomyocyte. With minor introns being enriched in both voltage-gated calcium and sodium channels genes, we hypothesized that the expression of these ion channels proteins critically depends on the activity of the minor spliceosome. We specifically focused on the predominant voltage-dependent sodium and calcium α-subunits expressed in the heart: *Scn5a* (encoding $Na_v1.5$), and *Cacna1c* (encoding $Ca_v1.2$).

Consistent with the experiment shown in **Fig 2C**, *U6atac* knockdown in NRVMs resulted in strong retention of the minor intron of *Scn5a* (**Fig 4A-B**). In turn, this decreased the levels of the $Na_v1.5$ protein, as shown by Western blotting (**Fig 4C-D**), while leaving the mRNA levels unaffected (**Fig 2F**). To assess the functional consequences of these molecular alterations, we studied the sodium current (I_{Na}) characteristics in anti-*U6atac* and control treated NRVMs using conventional patch-clamp. A fluorescently labeled gapmeR was co-transfected along with the anti-*U6atac* and control gapmeRs to measure transfected cells only. Fig 4D illustrates representative I_{Na} traces induced by depolarizing steps from a holding potential of –100 mV 48h after transfection with the gapmeRs. The I_{Na}-voltage relationship (**Fig 4F**) showed a strong and significant decrease in the I_{Na} density after *U6atac* knock down, reaching a ~59% reduction at -25 mV (-82.3±18.5 pA/pF in *U6atac* versus -198.8±36.4 pA/pF in control cells; $p<0.05$; **Table S4**). Comparison of activation and inactivation parameters (the half-voltage of (in)activation $V_{1/2}$ and the slope factor k) revealed a significant shift of $V_{1/2}$ of activation towards more positive potential (+4.4 mV) and a decrease in the activation curve steepness (increased k) after *U6atac* knockdown (**Table S4**). These changes in kinetic properties can

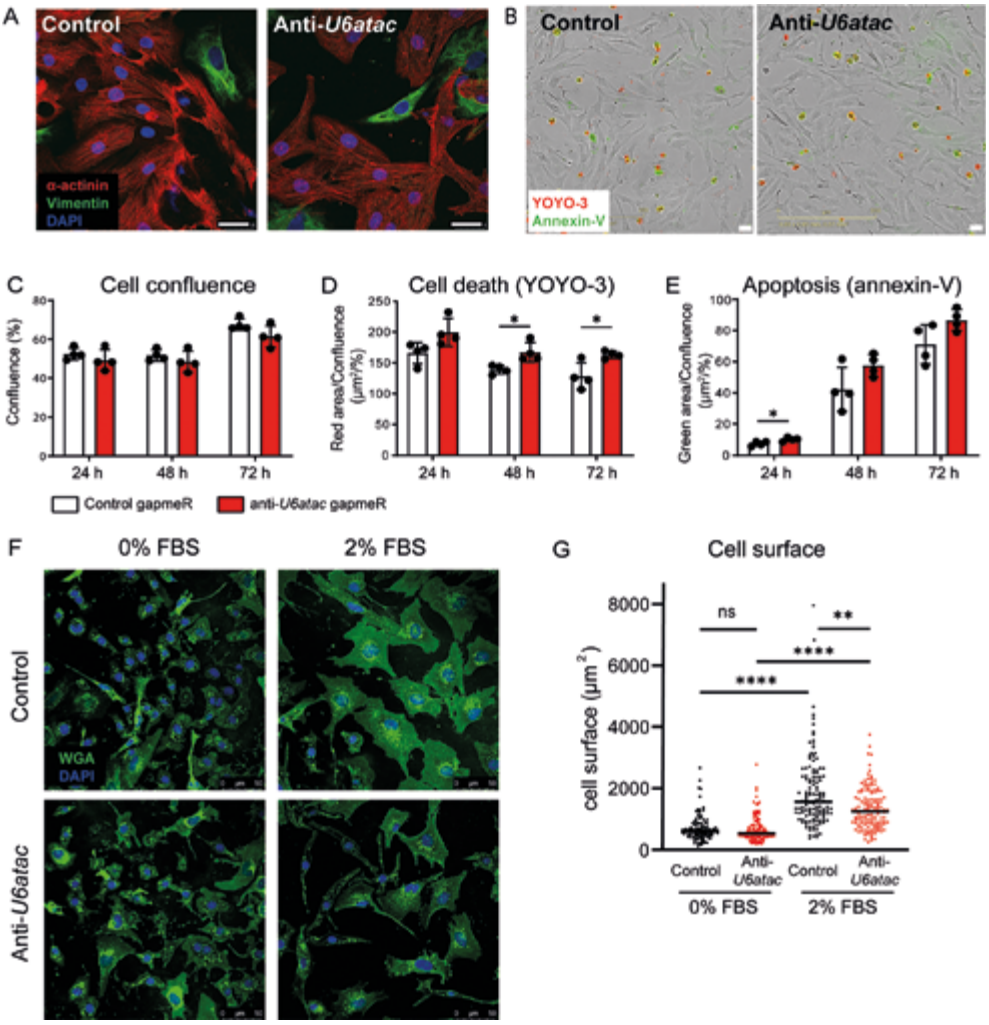

Figure 3. Impact of minor splicing knock-down on cardiomyocyte growth, survival and size (A) Representative immunocytochemistry of neonatal rat ventricular myocytes (NRVMs) 48h after transfection with control or anti-U6atac gapmeRs. In red alpha-actinin (cardiomyocyte marker), in green vimentin (fibroblast marker), in blue DAPI. (B) Representative phase-contrast images of NRVMs and quantification of (C) cell confluence, (D) cell death and (E) apoptosis. 4 wells per condition. Data are presented as mean ± s.d. Unpaired Student's t-test;* $p < 0.05$. Scale bars = 25 mm. (F) Representative images of transfected NRVMs after 48h incubation in medium with 0% FBS or 2% FBS and (G) quantification. In green WGA (membrane marker), in blue DAPI. n > 100 cells per condition. One-way ANOVA on ranks (Kruskal-Wallis test), followed by Dunn's test for post hoc analyses; ** $p < 0.01$; **** $p < 0.0001$.

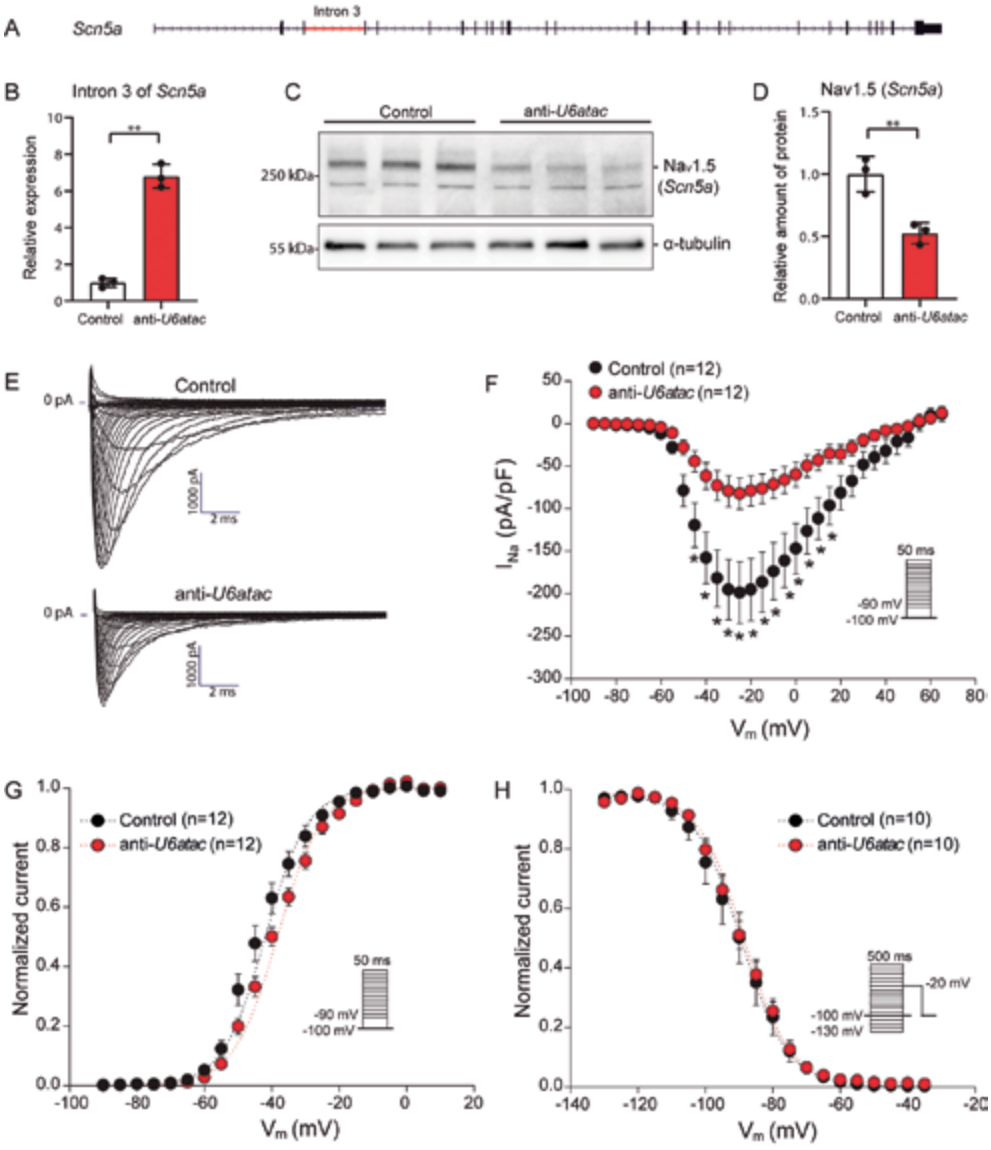

Figure 4. Minor intron retention of *Scn5a* reduces translation into $Na_v1.5$ and sodium current (I_{Na}) density. (A) Gene structure of *Scn5a* with its minor intron indicated in red (B) Minor intron retention in *Scn5a* 48h after *U6atac* knockdown measured by qRT-PCR. (C) $Na_v1.5$ (*Scn5a*) detection by western blot and (D) its quantification. 3 wells per condition. (E) Representative I_{Na} traces recorded from NRVMs transfected with control or anti-*U6atac* gapmeR. (F) Average I_{Na}-voltage relationships, (G) I_{Na}-voltage dependence of activation and (H) inactivation. Insets: voltage protocols. Patch-clamp data are presented as mean ± S.E.M. n indicates number of cardiomyocytes. Two-way repeated measures ANOVA followed by Holm-Sidak test for post hoc analyses; * $p < 0.05$.

lead to a decrease in I_{Na} in response to channel voltage activation. In contrast, I_{Na} inactivation parameters remained unaltered (**Fig 3H, Table S4**). Hence, a decrease in minor spliceosome activity can affect $Na_v1.5$ protein levels and consequently reduce I_{Na} density in cardiomyocytes.

Minor intron retention of *Cacna1c* decreases Cav1.2 expression and L-type calcium current

Cacna1c, which encodes the L-type calcium channel $Ca_v1.2$ contains 44 introns, 2 of which are minor introns: intron 2 and 13 (**Fig 5A, S3**). Minor intron retention of *Cacna1c* after U6atac knockdown resulted in a significant decrease of $Ca_v1.2$ protein levels (~30%) as assessed by Western Blotting (**Fig 5C-D**). In addition to this decrease, a new band of smaller molecular weight (» 100 kDa) appeared upon *U6atac* knockdown (**Fig 5C**). Interestingly, this smaller band does not correspond to the size of the predicted alternative open reading frame that arises when the minor intron is retained in *Cacna1c* (**Fig S3**). It is therefore not clear whether the 100 kDa band resulted from an aberrantly spliced isoform or whether it represents a degraded or cleaved product.

To assess the functional consequence of the decreased $Ca_v1.2$ expression, we performed patch clamp analysis to investigate L-type calcium current (I_{CaL}). Representative I_{CaL} traces recorded from NRVMs transfected with the control or anti-*U6atac* gapmeR are depicted in figure 5E. The current-voltage (I-V) relationship (**Fig 5F**) showed a robust and significant decrease in the I_{CaL} density after *U6atac* knockdown, reaching a ~36% reduction at -0 mV (control -16.0±1.7 pA/pF vs anti-*U6atac* -10.3±1.0 pA/pF, $p < 0.05$; **Table S5**). Finally, I_{CaL} voltage dependence of activation and inactivation parameters ($V_{1/2}$ and k) were similar in both groups (**Fig 5G-H, Table S5**). Together these data demonstrate that a decrease in minor spliceosome activity leads to a reduction in $Ca_v1.2$ protein levels and consequently to a reduced I_{CaL} in cardiomyocytes.

Dysregulation of minor spliceosome components in human heart disease

The minor spliceosome is comprised of five snRNAs (*U11, U12, U4atac, U5, U6atac*) and seven associated proteins (*ZMAT5*/20K, *SNRNP25*/25K, *ZCRB1*/31K, *SNRNP35*/35K, *SNRNP48*/48K, *PDCD7*/59K, and *RNPC3*/65K) (**Fig 6A**). These components are exclusive to the minor spliceosome and are not found in the major spliceosome, except for the snRNA *U5* that is common to both spliceosomes[12]. To investigate whether human heart disease may be associated with perturbations in the activity of the minor spliceosome, we compared the expression of these components in the 100 non-diseased hearts with that of 128 dilated cardiomyopathy (DCM) hearts[9]. Interestingly, we found that a number of these minor spliceosome components were differentially expressed in DCM (**Fig 6B, S4**). As shown in **Fig 6B**, some components were significantly downregulated (i.e. *RNU4ATAC*, *SNRNP25*,

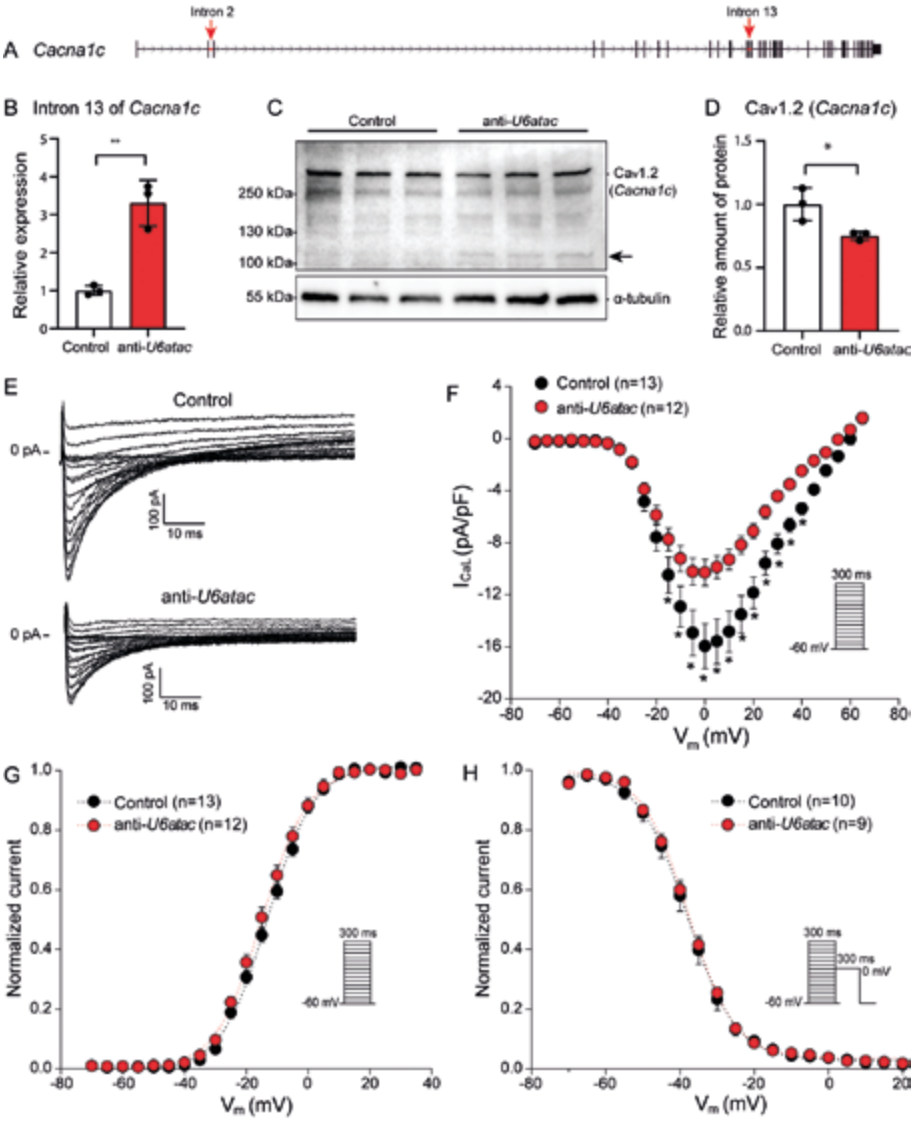

Figure 5. Minor intron retention of *Cacna1c* hampers translation into $Ca_v1.2$ and reduces L-type calcium current (I_{CaL}) density. (A) Gene structure of *Cacna1c* with minor introns indicated with red arrows. (B) Minor intron retention in *Cacna1c* after *U6atac* knockdown measured by qRT-PCR. (C) $Ca_v1.2$ (*Cacna1c*) detection by western blot and (D) its quantification. Black arrow indicates a potential truncated isoform of $Ca_v1.2$. 3 wells per condition. (E) Representative I_{CaL} traces recorded from NRVMs co-transfected with control or anti-*U6atac* gapmeR. (F) Average I_{CaL}-voltage relationships, (G) I_{CaL}-voltage dependence of activation and (H) inactivation. Insets: voltage protocols. Patch-clamp data are presented as mean ± S.E.M. n indicates number of cardiomyocytes. Two-way repeated measures ANOVA followed by Holm-Sidak test for post hoc analyses; * $p < 0.05$.

A

Minor spliceosome components	Official gene symbol	Name
Small nuclear RNAs	*RNU4ATAC*	U4atac
	RNU6ATAC	U6atac
	RNU11	U11
	RNU12	U12
	RNU5	U5
Proteins	*ZMAT5*	20K
	SNRNP25	25K
	ZCRB1	31K
	SNRNP35	35K
	SNRNP48	48K
	PDCD7	99K
	RNPC3	65K

B

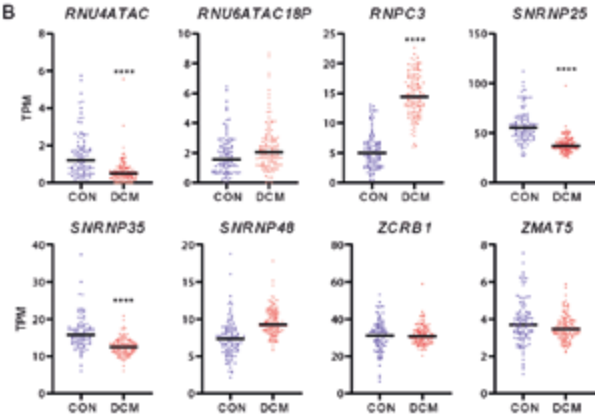

Figure 6. Minor spliceosome components expressed in the human failing heart. (A) Minor U12-dependent spliceosome components and (B) its expression in 100 non-diseased (CON) and 128 dilated cardiomyopathy (DCM) hearts. **** adjusted $p < 0.0001$; *** adjusted $p < 0.001$.

SNRNP35) whereas others were upregulated (i.e. *RNPC3*). In addition, we also plotted the expression of major spliceosome components in this dataset (**Fig S4**). This shows that some major spliceosome components are dysregulated in DCM as well. This is in line with previous studies reporting decreased splicing efficiency in heart failure[13], but it also indicates that dysregulation of minor spliceosome components is not a unique feature in DCM.

Transcriptional dysregulation of minor spliceosome components did not lead to overt and systematic changes in mRNA levels of MIG in this dataset, although some MIGs were found to be differentially expressed in DCM hearts (e.g. *STX10*, *RABGGTA*, *C2CD3*) (**Fig S5**). Nevertheless, it is conceivable that perturbations in minor spliceosome activity may have affected protein levels of MIGs through intron retention, without decreasing mRNA levels.

DISCUSSION

In this study we show that a large proportion (582/699) of minor intron-containing genes (MIGs) is expressed in the human heart and that a substantial number of these genes is directly involved in cardiac electrophysiology (e.g. *SCN5A* and *CACNA1C*). To explore a potential role of the minor spliceosome in the electrical activity of cardiomyocytes, we knocked-down the minor spliceosome-specific component *U6atac* in NRVM, and observed that loss of *U6atac* hampered splicing of the minor introns of *Scn5a* and *Cacna1c* and reduced their protein levels. Consequently, reduced levels of these voltage-gated ion channels decreased I_{Na} and I_{CaL}, as demonstrated by patch-clamp analysis. Together our findings

identify a novel mechanism by which I_{Na} and I_{CaL} may be modulated in cardiac pathologies in which the expression of components of the minor spliceosome is dysregulated.

Sodium channels play an essential role in the initiation and propagation of the cardiac action potential, by allowing the Na^+ influx during the depolarizing phase of the action potential[14]. The α-subunit of the sodium channel contains essential elements for its function, including the ion-conducting pore. Nine different α-subunits of the sodium channel (encoded by *SCN1A* through *SCN11A*) are expressed throughout the body and each and every one of these α-subunits contains a minor intron[4,15,16]. $Na_v1.5$, encoded by the *SCN5A* gene, is the predominant α-subunit in the heart. Alterations in $Na_v1.5$ and reduced sodium current density have been reported in common pathophysiological conditions such as ischemia and heart failure[17]. Sodium current reduction slows cardiac conduction, and as such may contribute to the increased arrhythmic risk in the setting of these disorders[14]. The underlying molecular mechanism(s) may relate to regulation at the (post)transcriptional level, trafficking of $Na_v1.5$ to the cell membrane and/or post-translational modifications of $Na_v1.5$ (e.g. phosphorylation, glycosylation, ubiquitination, etc.). An example of regulation at the post-transcriptional level is the abnormal C-terminal splicing of *SCN5A* that occurs in heart failure, which produces truncated and non-functional $Na_v1.5$ channels[18]. In our current study, we raise the intriguing possibility that changes in minor spliceosome activity may also contribute to changes at the post-transcriptional level, resulting in minor intron retention and reduced sodium current density in heart failure. In a large RNA seq database of 100 non-diseased and 128 failing hearts (i.e. DCM), we found that several minor spliceosome components are differentially expressed. Since some components were significantly downregulated (i.e. *RNU4ATAC*, *SNRNP25*, *SNRNP35*), whereas others were upregulated (i.e. *RNPC3*) in DCM, it is difficult to predict whether the downstream effects would either represent an increase or decrease in minor intron retention. In this same RNA-seq dataset, we did not detect clear and global differences in the mRNA expression of MIGs. However, this is not unexpected, as it is conceivable that protein expression of MIGs was affected without reducing mRNA levels. In fact, for 4 out of 5 MIGs tested after U6atac knockdown, we indeed observed an increase in minor intron retention without reducing mRNA levels (**Fig 2F**). Furthermore, inhibition of minor spliceosome activity by *U6atac* did show a reduction in $Na_v1.5$ protein on Western blot with a concomitant decrease in sodium current density, whereas it left *Scn5a* mRNA levels unaffected. Future studies investigating the relation between minor spliceosome activity and sodium channel function in the hearts of knockout mice or human patients with specific minor spliceosome mutations will be awaited with great interest.

Minor introns are also present in voltage-gated calcium channels. These channels open at depolarizing membrane potentials leading to an influx of Ca^{2+} into the cell. The entry of

Ca^{2+} constitutes an intracellular signal that triggers a wide spectrum of calcium-sensitive mechanisms, such as the calcium-induced calcium release and the sarcomere contraction in cardiomyocytes[19]. Calcium channels are composed of 5 different subunits: α1, α2, δ , β and γ. The α1 subunit is the core component of the channel containing the conduction pore, the voltage-sensing domain and the gating apparatus. The other 4 auxiliary subunits have regulating functions[19]. The heart expresses two types of calcium channels that differ in their α1 subunit: L-type channels which open at high voltages are mostly expressed in ventricular cardiomyocytes, and T-type channels that open at low voltages, are only present in pacemaker, atrial, and Purkinje cells. There is at least one minor intron in all 10 homologous genes encoding α1 subunits (*CACNA1A* to *CACNA1S*) and in the 4 different α2δ genes encoding the α2 and δ subunits genes (*CACNA2D1* to *CACNA2D4*)[4,16]. Our current findings demonstrate that a decrease in minor spliceosome activity induced by *U6atac* knockdown resulted in a reduction of *Cacna1c* mRNA, $Ca_v1.2$ protein and I_{CaL}. Interestingly, *U6atac* knockdown also yielded a truncated isoform of the $Ca_v1.2$ protein of approximately 100 kDa. Whether this truncated variant represents an alternative splice isoform of *Cacna1c*, triggered by activation of cryptic splice sites when the minor intron is retained is currently unknown. It is also not known if this truncated $Ca_v1.2$ variant is expressed in (patho)physiological conditions of the heart, which exons it comprises and whether it has functional relevance. That splice variants in *Cacna1c* are able to affect calcium currents is illustrated by the exclusion of alternative exon 33 in *Cacna1c* leads to greater I_{CaL} density. A mouse model in which exon 33 was deleted revealed a proarrhythmogenic phenotype, including premature ventricular contractions, tachycardia and lengthened QT interval[20,21]. Complementary to such alternative exon usage, our findings point to an independent means by which intron retention regulates levels of the encoded proteins.

In our studies, we made use of immature NRVM instead of adult cardiomyocytes because they are suitable for transfections and for prolonged culturing. There are differences between neonatal and adult cardiomyocytes in terms of electrophysiology, but we expect that inhibition of minor splicing also affects sodium and L-type calcium currents in fully mature cardiomyocytes. During cardiomyocyte maturation, alternative splicing of exon 6 of *Scn5a*[22] and exons 21, 31, 32 and 33 of *Cacna1c*[23–25] is known to occur, associated with differences in sodium and L-type calcium current properties. However, these alternative splice events occur downstream of the minor introns of *Scn5a* and *Cacna1c* and should be present in fetal and mature isoforms of both genes.

So far, no cardiac disease has been linked directly to minor intron splicing. Mutations causing loss-of-function of the minor spliceosome are responsible for rare and complex syndromes, mainly affecting growth and the nervous system[8,26–28]. Yet, some MOPD1/TALS

and Roifman syndrome patients (caused by mutations in *RNU4ATAC*) present with cardiac defects, including coarctation of aorta, Tetralogy of Fallot, atrial septal defect, ventricular septal defect and non-compaction of the heart. This suggests that a deficiency in minor splicing is detrimental for cardiac development[28,29]. It is currently unknown whether patients with loss-of-function mutations of the minor spliceosome also present with electrical disorders or arrhythmias.

In mice, constitutive deletion of the minor spliceosome components *Rnu11* or *Rnpc3* results in early embryonic lethality[27,30]. Using conditional knockout mouse models, Baumgartner et al. were recently able to show that deletion of *Rnu11* specifically in the embryonic mouse cortex resulted in microcephaly due to increase abnormal intron retention of MIGs involved in cell cycle, DNA damage control and apoptosis[30]. Furthermore, constitutive deletion of *Rnpc3* in adult mice resulted in reduced levels of lymphocytes, monocytes, erythrocytes and thrombocytes, decreased thymus size and degeneration of lining of the gastrointestinal tract within one week after deleting *Rnpc3*[27]. These conditional knockout models indicate that proper MIG expression is required for the survival of rapidly dividing cell population and that differentiated cells are less vulnerable to minor spliceosome inactivation[4]. Unfortunately, the hearts of *Rnpc3* and *Rnu11* knockout mice have not been subjected to careful functional and biochemical analyses. Our study indicates that it is likely that the hearts of these mice are compromised on the (electro)physiological level, due to the reduced expression and function of e.g. *Scn5a* and *Cacna1c*.

There is evidence that some accessory splicing factors regulating minor splicing are important for a normal function of the heart. For example, SMN1 has recently been identified as a splicing factor involved in minor splicing[31–33]. SMN1 is required for the survival of motor neurons, and mutations in this gene are responsible of spinal muscular atrophy. Spinal muscular atrophy patients also present with a cardiac phenotype, which includes bradycardia and premature heart failure; symptoms that were initially thought to originate from innervation problems. However, cell models have shown that SMN1 is also important for proper cardiomyocyte function[34]. Another potential minor splicing regulator in the heart is the ubiquitously expressed RNA-binding protein FUS. Mutations in FUS are responsible for amyotrophic lateral sclerosis (ALS). The same mutations causing ALS also affect minor intron retention, and may contribute to the arrhythmias and sudden cardiac death observed in ALS patients[35].

More research is needed to address a possible contribution of aberrant minor intron splicing in human cardiac disease and to evaluate cardiac function in minor spliceosome diseases. We interrogated the expression of MIGs and minor spliceosome components in the hearts of DCM patients, however we were not able to investigate minor intron retention levels, as this

requires ultra-deep high throughput RNA sequencing coupled with advanced bioinformatic algorithms, which requires experiments beyond the scope of this study. Besides DCM and heart failure, it will be interesting to investigate a possible contributing role for minor intron retention in (inherited) cardiac disorders in which the electrical activity of the heart is affected, such as for instance Brugada syndrome (which is associated with mutations in *SCN5A* and *CACNA1C*), and arrhythmogenic cardiomyopathy, disorders with an increasingly recognized complex genetic basis[36].

In conclusion, we here provide the first evidence that alterations in minor splicing can affect cardiac electrophysiology by modulating the expression and function of voltage-gated ion channels in cardiomyocytes. This novel insight may be of vital importance in genetic disorders affecting minor spliceosome components and in acquired diseases in which minor spliceosome components are dysregulated, including heart failure.

MATERIALS AND METHODS

RNAseq data and differential gene expression analysis

The paired-end reads from 100 human non-diseased and 128 dilated cardiomyopathy (DCM) hearts (left ventricle tissue) previously generated[9] were aligned against the human genome reference hg38 using STAR2[37] (Version 2.7) and the Ensemble GRCh38 release 100 annotation file. Differential gene expression analysis was performed using the R Bioconductor package, DESeq2[38] (Bioconductor release 3.12). Genes with TPM (transcripts per million) ≥ 0.1, absolute log2 fold change ≥ 0.58 and adjusted p-value cutoff ≤0.05 were deemed significantly differentially expressed.

Intron location and pathway analysis

Minor intron coordinates were obtained from Minor Intron Database (MIDB, https://midb.pnb.uconn.edu/)[2]. Minor introns in rat were selected by homology with the human sequences. Gene ontology enrichment analysis was performed using the online tool Gorilla[10]. Enrichment analysis was performed on MIGs with mean TPM value ≥ 0.1 against all the genes expressed above the same threshold in human non-diseased hearts. GO terms with FDR q-value ≤ 0.001 were considered significant.

Neonatal rat ventricular myocytes (NRVMs) isolation and gapmeR transfection

Animal studies were approved by the Institutional Animal Care and Use Committee of the University of Amsterdam and carried out in compliance with the guidelines of this institution and the Directive 2010/63/EU of the European Parliament.

NRVMs from 0–2 day old Wistar rats (Janvier Labs, Le Genest-Saint-Isle, France) were isolated as described previously[39]. In short, pups were anesthetized by isoflurane and hearts were excised after decapitation. Ventricles were cut into small pieces, which were incubated overnight in a rotating platform at 4 °C in HBSS (Gibco, Ref 14170-088, Paisley, UK) containing 1 mg/ml trypsin (USB, Ref 22720, Cleveland, OH, USA). The next day, cells were dissociated using 1 mg/ml collagenase type 2 (Worthington, Ref LS004177, Lakewood, NJ, USA) in HBSS. Cells were collected and resuspended in TUNG medium - M199 culture medium (Gibco, Ref 31150-022), 1% HEPES (Gibco, Ref 15630-080), 1% NEAA (Gibco, Ref 11140-050), 2 mg/L vitamin B12 (Sigma, Ref V2876, St. Louis, MO, USA), 3.5 g/L glucose, 1% penicillin/streptomycin (Gibco, Ref 15140-122) - supplemented with 10% FBS (Biowest, Ref S1810-500, Riverside, MO, USA). The cell suspension was pre-plated to separate myocytes from fibroblasts. After 2 hours, non-adhered myocytes were collected and counted with a LUNA™ Automated Cell Counter (Logos Biosystems, Anyang, South Korea).

1 x 10^6 NRVMs were plated on 6-well plates coated with fibronectin (Corning, Ref 356008, Bedford, MA, USA). 4-20h after seeding, NRVMs were transfected with 25 nM control or anti-*U6atac* gapmeRs (Qiagen, Ref 339511, Germantown, MD, USA) by lipofectamine 2000 (Thermo Fisher Scientific, Ref 11668-019, Carlsbad, CA, USA) in TUNG medium without FBS. After 6h of incubation, medium was replaced by TUNG with 2% FBS. Cells were harvested or analyzed 48h after transfection. Experiments were repeated at least in 3 different isolations, plating 3 wells per condition each time. GapmeR sequences are found in **Table S1**.

For NMD inhibition, NRVMs were incubated with the translation inhibitors cycloheximide (300 μg/μl; Sigma, Ref 01810) or emetine (150 μg/μl; Sigma, Ref E2375) for 3h, 24h after gapmeR transfection.

For patch clamp experiments, 1 x 10^5 NRVM were seeded over fibronectin-coated glass coverslips on 24-well plate and co-transfected with 25 nM gapmeRs and 25 nm FAM-labeled control (Qiagen, Ref 339515) by lipofectamine 2000. 48h after transfection, sodium and calcium current recordings were performed in fluorescent cardiomyocytes with the use of the patch-clamp technique.

RNA isolation and qRT-PCR

RNA was extracted using TRI reagent (Sigma, Ref T9424) following manufacturer's instructions. 500 ng of total RNA was treated with DNAse I (Invitrogen, Ref 18068-015, Waltham, MA, USA) and retrotranscribed into cDNA with random hexamers (Invitrogen, Ref N8080127) and Superscript II (Invitrogen, Ref 18064-014).

qRT-PCR was performed on a Lightcycler 480 (Roche, Mannheim, Germany) using SYBR green I Master (Roche, Ref 04887352001). Data was analyzed using LinRegPCR software. Primer sequences are found in **Table S2**. We designed our primers to generate a single amplicon per PCR reaction. We verified the specificity of our qPCR primers by performing melting curve analysis, agarose electrophoresis separation and sequencing the amplicons. This confirmed that all qPCR products represented only one amplicon with the correct sequence.

Live-cell analysis: confluence, cell death and apoptosis

1 x 10^5 NRVMs were plated on 24-well plates coated with fibronectin. 24h after transfection, medium was replaced by medium containing 0.25 µg/ml recombinant Annexin V-ATTO-488 (Adipogen Life Sciences) and 300 nM YOYO3-612/631 (Invitrogen). Cell confluence was quantified over time by phase contrast. Immediately after treatment, cells were incubated in an IncuCyte ZOOM System (Essen Bioscience, Ann Arbor, MI, USA) as previously described[40]. Experiment was conducted over 72h with a scan every 24h to avoid photobleaching of fluorescent reporters. Using the x20 objective, 16 images per well were taken with data from phase contrast, green channel (Excitation: 440/480 nm; Emission: 504/544 nm), and red channel (Ex: 565/605 nm; Em: 625/705 nm) were collected. Fluorescent events were processed and analyzed using the IncuCyte ZOOM. Processing definitions for Annexin-V(488) and YOYO3(612/631) labelled cells were defined as follows: Channel: Green; Top-Hat; Radius: 100 µM, Threshold: 2.0 RCU; Edge Sensitivity: 0; Pixel Adjust: 0; Area: >9 µm; Eccentricity: undefined; Mean Intensity: undefined; Integrated Intensity: undefined. Channel: Red; Top-Hat; Radius: 100 µM, Threshold: 2.0 RCU; Edge Sensitivity: 0; Pixel Adjust: 0; Area: >11 µm; Eccentricity: undefined; Mean Intensity: undefined; Integrated Intensity: undefined. The total fluorescent areas of Annexin V and YOYO-3 in each image were analyzed to determine the apoptotic and dead cells relative to the whole image area. Those results were normalized to cell confluence in order to minimize the differences in cell density after plating.

Immunostaining

1 x 10^5 NRVM were seeded over fibronectin-coated glass coverslips on 24-well plate. 48h after transfection, cells were fixed in 4% PFA, permeabilized with PBS 0.1% Triton X-100, block in 4% goat serum and incubated overnight with the primary antibodies in a wet chamber at 4°C. Secondary antibodies were incubated for 1h at room temperature, followed by 1h of DAPI staining. Cell membranes were stained with Wheat Germ Agglutinin, Alexa Fluor™ 488 Conjugate (Invitrogen, Ref W11261) following manufacturer's protocol. Images were acquired with a Leica TCS SP8 X unit mounted on a Leica DMI6000 inverted microscope. Cell surface was quantified with the software Leica Application Suite X (LAS X). Antibodies and dyes references are found in **Table S3**.

Protein isolation and western blot

For protein isolation, cells were scraped and homogenized by sonication in RIPA buffer (50mM Tris-HCl pH8, 150mM NaCl, 1% NP-40, 0.2% sodium deoxycholate, 0.1% SDS, 1 mM Na_3VO_4, 1 mM PMSF) supplemented with protease inhibitor cocktail (Roche, Ref 11836170001). Protein concentration was measured by BCA assay (Pierce, Ref 23227, Rockford, IL, USA). Western blotting was performed following standard protocols. Proteins were separated by SDS-PAGE, transferred to PVDF membranes (Bio-Rad, Ref 17001917, Hercules, CA, USA), block in TBST 4% milk and incubated with primary antibodies overnight at 4°C. Membranes were subsequently incubated with HRP-conjugated secondary antibodies for 1 hour at room temperature. Western blots were developed with ECL prime western blotting detection agent (Amersham Biosciences, Ref RPN2232, Buckinghamshire, UK) in ImageQuant LAS 4000 (GE Healthcare Life Sciences). Western blots were quantified using Fiji (ImageJ). Antibody references are listed in **Table S3**.

Electrophysiology data acquisition and analysis

Sodium current (I_{Na}) and L-type calcium current (I_{CaL}) were measured with the ruptured patch-clamp technique, using an Axopatch 200B amplifier (Molecular Devices, San Jose, CA, USA). Voltage control, data acquisition, and analysis of currents were performed with pClamp10.6/Clampfit (Molecular Devices, San Jose, CA, USA). Borosilicate glass patch pipettes (Harvard Apparatus, Holliston, MA, USA) with a tip resistance of 2-2.5 MΩ were used. Series resistance (Rs) and cell membrane capacitance (Cm) were compensated for 80%. Current densities were calculated by dividing current amplitude by Cm. Cm was determined by dividing the decay time constant of the capacitive transient in response to 5 mV hyperpolarizing steps from -40 mV, by the Rs. I_{Na} and I_{CaL} were filtered at 5 kHz and 2 kHz, respectively. I_{Na} was digitized at 40 kHz, while I_{CaL} was digitized at 20 kHz.

Sodium current measurements

I_{Na} was measured in single cells using a pipette solution containing (in mM): 3.0 NaCl, 133 CsCl, 2.0 $MgCl_2$, 2.0 Na_2ATP, 2.0 TEACl, 10 EGTA, 5.0 HEPES; pH 7.3 (CsOH). Cells were superfused with a bath solution containing (in mM): 130 NaCl, 20 CsCl, 1.8 $CaCl_2$, 1.2 $MgCl_2$, 11.0 glucose, 5.0 HEPES, 0.005 nifedipine; pH 7.4 (CsOH). I_{Na} was measured at room temperature in response to depolarizing voltage steps from a holding potential of -100 mV (cycle length of 5 seconds). I_{Na} was defined as the difference between peak and steady state current (at 50 ms). Voltage dependence of activation and inactivation curves were fitted with Boltzmann function ($y=[1+\exp\{(V-V_{1/2})/k\}]^{-1}$), where $V_{1/2}$ is the half-maximal voltage of (in)activation and k, the slope factor. Potentials were not corrected for the estimated change in liquid junction potential.

L-type calcium current measurements

I_{CaL} was measured in single cells at 36°C. The pipette solution contained (in mM): 140 CsCl, 5 K_2-ATP, 10 HEPES, 10 EGTA; pH 7.2 (CsOH). The external solution contained (in mM): 145 TEACl, 5.4 CsCl, 1.8 $CaCl_{2,}$ 1 $MgCl_2$, 5.5 glucose, 0.2 4,4'-Diisothiocyano-2,2'-stilbenedisulfonic acid (DIDS), 5 HEPES; pH 7.4 (CsOH). I_{CaL} was measured in response to depolarizing voltage steps from a holding potential of -60 mV (cycle length of 5 seconds) and it was defined as the difference between peak and steady state current (at 300 ms). Voltage dependence of activation and inactivation curves were fitted with Boltzmann function ($y=[1+\exp\{(V-V_{1/2})/k\}]^{-1}$), where $V_{1/2}$ is the half-maximal voltage of (in)activation and k, the slope factor. Potentials were corrected for the estimated change in liquid junction potential (11 mV).

Statistical analysis

Data was analyzed using GraphdPad Prism 9 (GraphPad, San Diego, CA, USA). Data is presented as mean ± standard deviation, unless differently stated. Results were analyzed with appropriate statistical tests, as indicated in the respective figure legends. A value of $p < 0.05$ was considered statistically significant.

COMPETING INTERESTS

The authors declare no competing or financial interests.

FUNDING

This work was supported by grants from the Rembrandt Institute of Cardiovascular Science [to E.E.C.], the Netherlands Research Initiative [CVON ARENA PRIME, to Y.M.P.; CVON2018-30 PREDICT2 and CVON2015-12 e-Detect to C.A.R.] and Fondation pour la Recherche Médicale [PBR201810007613 to A.C.E.]. Open access funding provided by University of Amsterdam. Deposited in PMC for immediate release.

REFERENCES

1. Turunen, J. J., Niemelä, E. H., Verma, B. & Frilander, M. J. The significant other: splicing by the minor spliceosome. *WIREs RNA* **4**, 61–76 (2013).
2. Olthof, A. M., Hyatt, K. C. & Kanadia, R. N. Minor intron splicing revisited: identification of new minor intron-containing genes and tissue-dependent retention and alternative splicing of minor introns. *BMC Genomics* **20**, 686 (2019).
3. Basu, M. K., Makalowski, W., Rogozin, I. B. & Koonin, E. V. U12 intron positions are more strongly conserved between animals and plants than U2 intron positions. *Biology Direct* **3**, 19 (2008).
4. Baumgartner, M., Drake, K. & Kanadia, R. N. An Integrated Model of Minor Intron Emergence and Conservation. *Frontiers in Genetics* **10**, 1113 (2019).
5. Patel, A. A., McCarthy, M. & Steitz, J. A. The splicing of U12-type introns can be a rate-limiting step in gene expression. *The EMBO Journal* **21**, 3804–3815 (2002).
6. Niemelä, E. H. *et al.* Global analysis of the nuclear processing of transcripts with unspliced U12-type introns by the exosome. *Nucleic Acids Research* **42**, 7358–7369 (2014).
7. Younis, I. *et al.* Minor introns are embedded molecular switches regulated by highly unstable U6atac snRNA. *eLife* **2013**, (2013).
8. Verma, B., Akinyi, M. V., Norppa, A. J. & Frilander, M. J. Minor spliceosome and disease. *Seminars in Cell & Developmental Biology* **79**, 103–112 (2018).
9. Heinig, M. *et al.* Natural genetic variation of the cardiac transcriptome in non-diseased donors and patients with dilated cardiomyopathy. *Genome Biology* **18**, 170 (2017).
10. Eden, E., Navon, R., Steinfeld, I., Lipson, D. & Yakhini, Z. GOrilla: a tool for discovery and visualization of enriched GO terms in ranked gene lists. *BMC Bioinformatics* **10**, 48 (2009).
11. Bell, M. L., Buvoli, M. & Leinwand, L. A. Uncoupling of Expression of an Intronic MicroRNA and Its Myosin Host Gene by Exon Skipping. *Mol Cell Biol* **30**, 1937–1945 (2010).
12. Will, C. L. *et al.* The human 18S U11/U12 snRNP contains a set of novel proteins not found in the U2-dependent spliceosome. *RNA* **10**, 929–941 (2004).
13. Kong, S. W. *et al.* Heart Failure–Associated Changes in RNA Splicing of Sarcomere Genes. *Circulation: Cardiovascular Genetics* **3**, 138–146 (2010).
14. Remme, C. A. & Wilde, A. A. Targeting sodium channels in cardiac arrhythmia. *Current Opinion in Pharmacology* **15**, 53–60 (2014).
15. Patel, A. A. & Steitz, J. A. Splicing double: insights from the second spliceosome. *Nat Rev Mol Cell Biol* **4**, 960–970 (2003).
16. Wu, Q. & Krainer, A. R. AT-AC Pre-mRNA Splicing Mechanisms and Conservation of Minor Introns in Voltage-Gated Ion Channel Genes. *Molecular and Cellular Biology* **19**, 3225–3236 (1999).
17. Rook, M. B., Evers, M. M., Vos, M. A. & Bierhuizen, M. F. A. Biology of cardiac sodium channel Nav1.5 expression. *Cardiovascular Research* **93**, 12–23 (2012).
18. Shang Lijuan L. *et al.* Human Heart Failure Is Associated With Abnormal C-Terminal Splicing Variants in the Cardiac Sodium Channel. *Circulation Research* **101**, 1146–1154 (2007).
19. Bodi, I., Mikala, G., Koch, S. E., Akhter, S. A. & Schwartz, A. The L-type calcium channel in the heart: the beat goes on. *J Clin Invest* **115**, 3306–3317 (2005).
20. Li, G. *et al.* Exclusion of alternative exon 33 of CaV1.2 calcium channels in heart is proarrhythmogenic. *PNAS* **114**, E4288–E4295 (2017).
21. Liao, P. *et al.* Molecular alteration of Cav1.2 calcium channel in chronic myocardial infarction. *Pflugers Arch - Eur J Physiol* **458**, 701–711 (2009).
22. Onkal, R. *et al.* Alternative splicing of Nav1.5: An electrophysiological comparison of 'neonatal' and 'adult' isoforms and critical involvement of a lysine residue. *Journal of Cellular Physiology* **216**, 716–726 (2008).
23. Diebold, R. J. *et al.* Mutually exclusive exon splicing of the cardiac calcium channel alpha 1 subunit gene generates developmentally regulated isoforms in the rat heart. *PNAS* **89**, 1497–1501 (1992).
24. Hu, Z. *et al.* Aberrant Splicing Promotes Proteasomal Degradation of L-type CaV1.2

Calcium Channels by Competitive Binding for CaVβ Subunits in Cardiac Hypertrophy. *Sci Rep* **6**, 35247 (2016).

25. Liao, P. *et al.* Alternative Splicing Generates a Novel Truncated Cav1.2 Channel in Neonatal Rat Heart *. *Journal of Biological Chemistry* **290**, 9262–9272 (2015).
26. Benoit-Pilven, C. *et al.* Clinical interpretation of variants identified in RNU4ATAC, a non-coding spliceosomal gene. *PLOS ONE* **15**, e0235655 (2020).
27. Doggett, K. *et al.* Early developmental arrest and impaired gastrointestinal homeostasis in U12-dependent splicing-defective Rnpc3-deficient mice. *RNA* **24**, 1856–1870 (2018).
28. Merico, D. *et al.* Compound heterozygous mutations in the noncoding RNU4ATAC cause Roifman Syndrome by disrupting minor intron splicing. *Nature Communications* **6**, 8718 (2015).
29. Edery, P. *et al.* Association of TALS Developmental Disorder with Defect in Minor Splicing Component U4atac snRNA. *Science* **332**, 240–243 (2011).
30. Baumgartner, M. *et al.* Minor spliceosome inactivation causes microcephaly, owing to cell cycle defects and death of self-amplifying radial glial cells. *Development (Cambridge)* **145**, (2018).
31. Lotti, F. *et al.* A SMN-Dependent U12 Splicing Event Essential for Motor Circuit Function. *Cell* **151**, 440–454 (2012).
32. Boulisfane, N. *et al.* Impaired minor tri-snRNP assembly generates differential splicing defects of U12-type introns in lymphoblasts derived from a type I SMA patient. *Human Molecular Genetics* **20**, 641–648 (2011).
33. Li, L. *et al.* Defective minor spliceosomes induce SMA-associated phenotypes through sensitive intron-containing neural genes in Drosophila. *Nature Communications* **11**, 5608 (2020).
34. Khayrullina, G. *et al.* SMN-deficiency disrupts SERCA2 expression and intracellular Ca2+ signaling in cardiomyocytes from SMA mice and patient-derived iPSCs. *Skeletal Muscle* **10**, 16 (2020).
35. Reber, S. *et al.* Minor intron splicing is regulated by FUS and affected by ALS-associated FUS mutants. *EMBO J* **35**, 1504–1521 (2016).
36. Cerrone Marina, Remme Carol Ann, Tadros Rafik, Bezzina Connie R., & Delmar Mario. Beyond the One Gene–One Disease Paradigm. *Circulation* **140**, 595–610 (2019).
37. Dobin, A. *et al.* STAR: ultrafast universal RNA-seq aligner. *Bioinformatics* **29**, 15–21 (2013).
38. Love, M. I., Huber, W. & Anders, S. Moderated estimation of fold change and dispersion for RNA-seq data with DESeq2. *Genome Biology* **15**, 550 (2014).
39. Haan, A. D. den *et al.* Organ Explant Culture of Neonatal Rat Ventricles: A New Model to Study Gene and Cell Therapy. *PLOS ONE* **8**, e59290 (2013).
40. Gelles, J. D. & Chipuk, J. E. Robust high-throughput kinetic analysis of apoptosis with real-time high-content live-cell imaging. *Cell Death and Disease* **7**, e2493–e2493 (2016).

SUPPLEMENTAL FIGURES

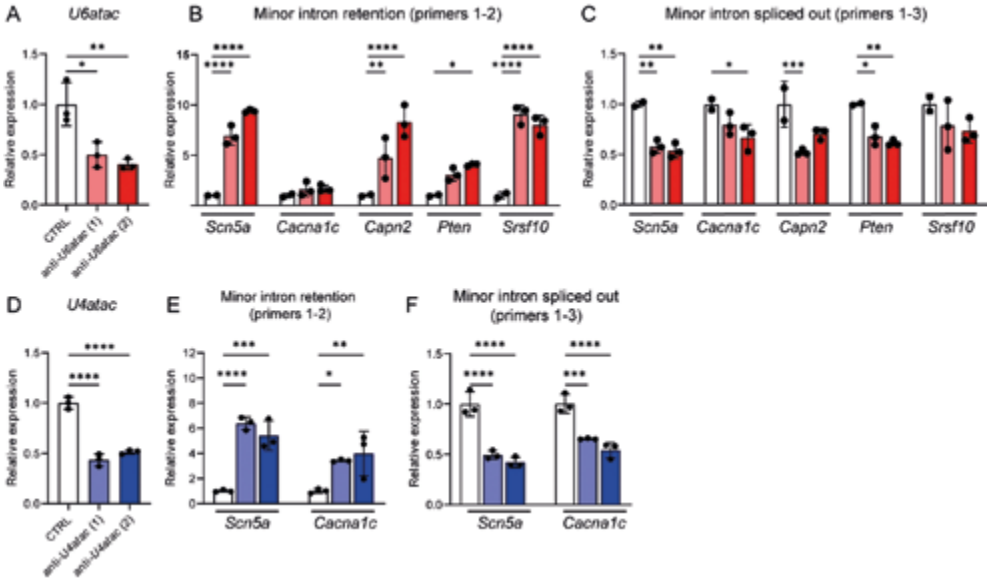

Figure S1. Specificity of anti-*U6atac* and anti-*U4atac* gapmeRs. (A) Relative expression of the minor splicing component *U6atac*, (B) minor introns and (C) minor intron-flanking exons 24h after transfection with either a non-targeting control or 2 different anti-*U6atac* gapmeRs. (D) Relative expression of the minor splicing component *U4atac*, (E) minor introns and (F) minor intron-flanking exons 24h after transfection NRVMs with either a non-targeting control or 2 different anti-*U4atac* gapmeRs. Reference gene: *Hprt1*. Data are presented as mean ± s.d. Unpaired Student's t-test; * $p < 0.05$; ** $p < 0.01$; *** $p < 0.001$, **** $p < 0.0001$.

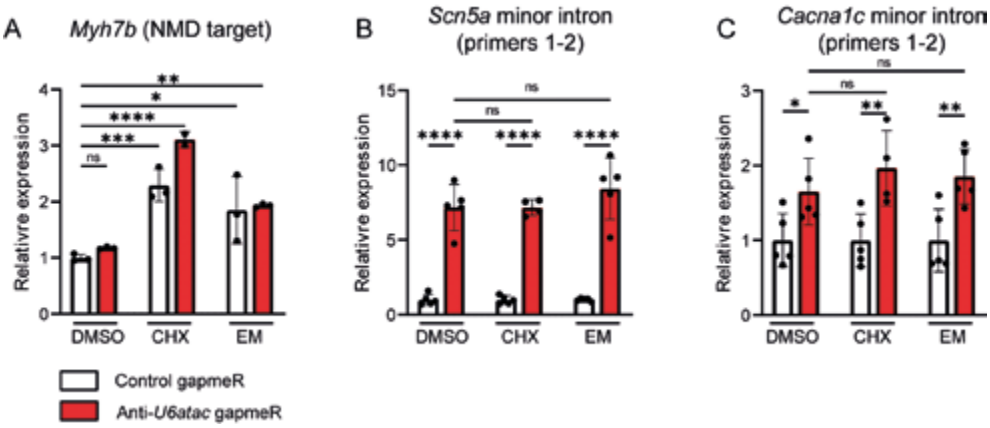

Figure S2. NMD inhibition do not rescue the effect of minor intron retention. (A) Relative expression of the NMD-target *Myh7b*, (B) minor intron of *Scn5a and* (C) minor intron of *Cacna1c*. Cells were incubated for 3h with DMSO (control), 300 µg/µl cycloheximide (CHX) or 150 µg/µl emetine (EM) 24h after transfection with gapmeRs. Reference gene: *Hprt1*. Data are mean ± s.d. One-way ANOVA, followed by Holm-Sidak test for post hoc analyses; * $p < 0.05$; ** $p < 0.01$; *** $p < 0.001$, **** $p < 0.0001$.

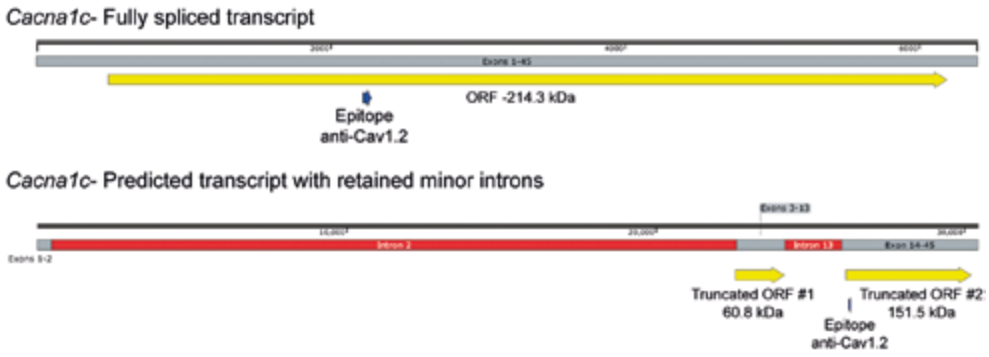

Figure S3. Predicted size of the transcript and open reading frames of *Cacna1c* after minor intron retention.

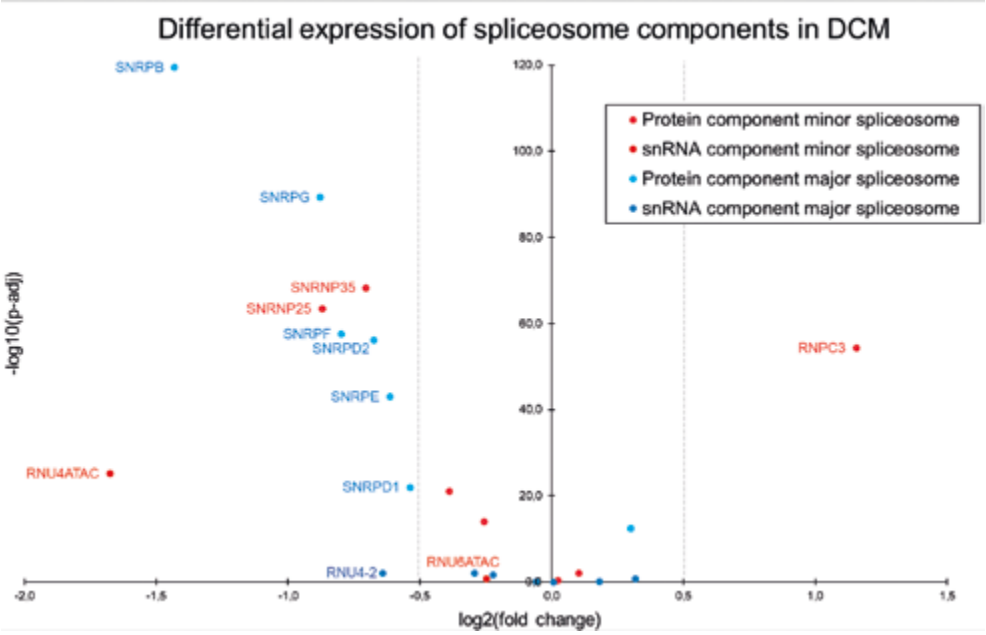

Figure S4. Volcano plot showing differential expression of the protein and snRNA components of the minor and the major spliceosome in 100 non-diseased (CON) and 128 dilated cardiomyopathy (DCM) hearts. Only genes with TPM ≥ 0.1 were considered. Genes with absolute log2 fold change ≥ 0.58 (dashed lines) and adjusted p-value ≤ 0.05 were considered significantly differentially expressed.

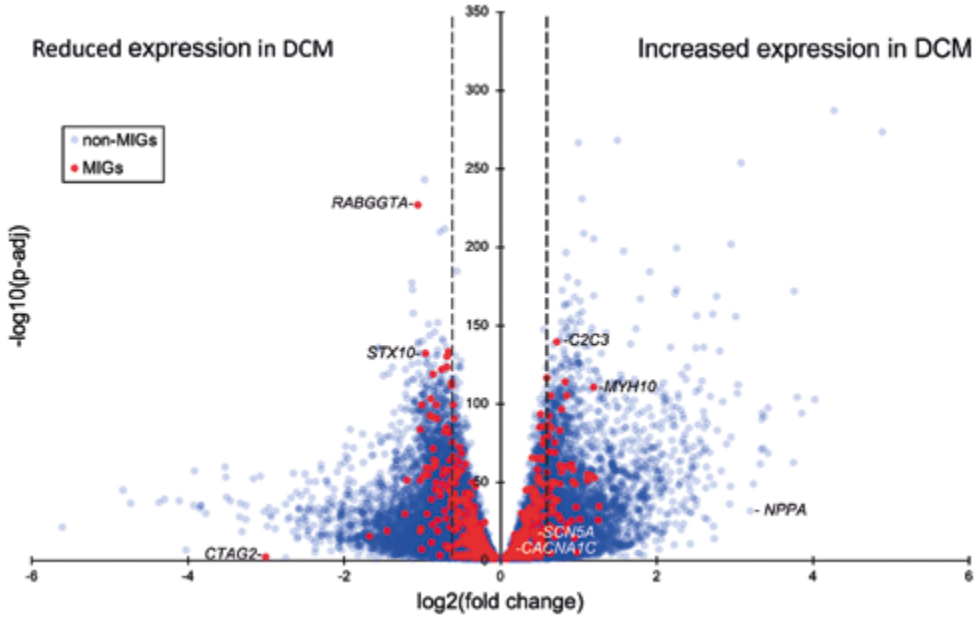

Figure S5. Volcano plot showing differential expression of minor-intron containing genes (MIGs) and genes non-containing minor introns (non-MIGs) in 100 non-diseased (CON) and 128 dilated cardiomyopathy (DCM) hearts. Only genes with TPM ≥ 0.1 were considered. Genes with absolute log2 fold change ≥ 0.58 (dashed lines) and adjusted p-value ≤ 0.05 were considered significantly differentially expressed.

SUPPLEMENTAL TABLES

Table S1. Antisense LNA GapmeR sequences

GapmeR	Sequence 5' -3'
Non-targeting negative control	AACACGTCTATACGC
Anti-*U6atac* (1)	CAATGCCTTAACCGTA
Anti-*U6atac* (2)	TGCCTTAACCGTATG
Anti-*U4atac* (1)	GTAGCGCAACCCCAAG
Anti-*U4atac* (2)	TAACCGATGCAGGTGT
FAM-labeled control	/56-FAM/AACACGTCTATACGC

Table S2. Primer sequences

Primer	Sequence	Annealing on exon/intron (total number)
GAPDH Fw	GGTGGACCTCATGGCCTACA	
GAPDH Rv	CTCTCTTGCTCTCAGTATCCTTGCT	
HPRT1 Fw	TGACTATAATGAGCACTTCAGGGATTT	
HPRT1 Rv	CGCTGTCTTTTAGGCTTTGTACTTG	
EEF1E1 Fw	TCCAGTAAAGAAGACACCCAGA	
EEF1E1 Rv	GACAAAACCAGCGAGACACA	
U6ATAC Fw	GGTTAGCACTCCCCTTGACA	
U6ATAC Rv	AAGTAGGTGGCAATGCCTTAACC	
SCN5A 1 Fw	TCTTCCGGTTCAGTGCCACC	Exon 3 (28)
SCN5A 2 Rv	CAGGACAGATGCGGATTAAGAGC	Intron 3 (27)
SCN5A 3 Rv	GGATGGTGCACATGATGAGCATG	Exon 4 (28)
SCN5A 4 Rv	AGGATGACGATGATGCTGTCG	Exon 15 (28)
SCN5A 5 Fw	ACCGACTCCTTCTCTCTTCTTC	Intron 14 (27)
SCN5A 6 Fw	GAGGAGATGCTGCAGGTCGG	Exon 14 (28)
CACNA1C 1 Fw	TGGGATCATGGCTTATGGCGGC	Exon 13 (45)
CACNA1C 2 Rv	GGCAGCATCAGCACCAAAGG	Intron 13 (44)
CACNA1C 3 Rv	ATCAGCCAGGTTGTCCACCG	Exon 14 (45)
CACNA1C 4 Fw	GAAGTTGTGTCCTCACCGTG	Exon 35 (45)
CACNA1C 5 Rv	TCACAAAGGCAAACAGGTAGC	Intron 35 (44)
CACNA1C 6 Rv	GGCAAACAGTGTAGCATTGAAC	Exon 36 (45)
CAPN2 1 Fw	GGCTTCAGCATCGAGACCTG	Exon 14 (21)
CAPN2 2 Rv	CAGGCTGCCTGTCCACA	Intron 14 (20)
CAPN2 3 Rv	CGTCCAGAGGATGTAGAACTCC	Exon 15 (21)
CAPN2 4 Fw	ATTGGAGATGGATTCAGAAGGC	Exon 16 (21)
CAPN2 5 Rv	GCTAAGGGTCTGAGCGAC	Intron 16 (20)
CAPN2 6 Rv	CTAGAACTCTTCTCAAGATGGTCTG	Exon 17 (21)
PTEN 1 Fw	TCAGCCACAGGCTCCCAGAC	Exon 1 (9)

Table S2. (continued)

Primer	Sequence	Annealing on exon/intron (total number)
PTEN 2 Rv	TTCGCATCCGTCTACTCCCACG	Intron 1 (8)
PTEN 3 Rv	ACACCTTCAAGTCTTTCTGCAGG	Exon 2 (9)
PTEN 4 Fw	GTGTGTGGTGACATCAAAGTAG	Exon 7 (9)
PTEN 5 Rv	ACTAATCTCCTAACCAAAGGCAC	Intron 7 (8)
PTEN 6 Rv	TCCTCTGGTCCTGGTATGAAG	Exon 8 (9)
SRSF10 1 Rv	GCGTCTTCAGCATCACGAACATC	Exon 3 (5)
SRSF10 2 Fw	GAGTTGTTTCAGACTTCACAAGCC	Intron 2 (4)
SRSF10 3 Fw	AGATTTACGTCGGGAATTTGGTCG	Exon 2 (5)
SRSF10 4 Rv	TACGCCGTGGTCTTCCAG	Exon 5 (5)
SRSF10 5 Fw	TGTGTATCTTGGATGCTTCATTAAGG	Intron 4 (4)
SRSF10 6 Fw	GGAGGAGATCAAGGAGTCGG	Exon 4 (5)

Table S3. List of antibodies used

Antibody	Use	Dilution	Reference
Anti-tubulin	WB	1:5000	GeneTex Cat No. GTX628802-01
Anti-$Na_v1.5$(SCN5A)	WB	1:200	Sigma S0819
Anti-$Ca_v1.2$ (CACNA1C)	WB	1:200	Alomone Cat No. ACC-003
Anti-rabbit-HRP	WB	1:10000	Amersham NA9340V
Anti-mouse-HRP	WB	1:10000	Amersham NA9310V
Anti-Vimentin	IF	1:1000	Abcam AB92537
Anti-alpha-actinin	IF	1:750	Sigma A781
Goat anti-rabbit-488	IF	1:250	Invitrogen A-11008
Goat anti-mouse-647	IF	1:250	Invitrogen A-21235

Table S4. Sodium current properties in neonatal rat ventricular myocytes (NRVMs) 48h after transfection with control or anti-U6atac gapmeR.

	Control	n	Anti-U6atac	n
Current density				
$\mathbf{I_{Na}}$ **(pA/pF)**	-198.8±36.4	12	-82.3±18.5*	12
Activation				
$\mathbf{V_{1/2}}$ **(mV)**	-43.7±1.6	12	-39.3±1.1*	12
k **(mV)**	6.5±0.3		7.5±0.2*	12
Inactivation				
$\mathbf{V_{1/2}}$ **(mV)**	-90±2.7	10	-89.1±1.4	10
k **(mV)**	-5.9±0.3	10	-6.9±0.5	10

INa, sodium current density at -25 mV; V1/2 of (in)activation, half-voltage of (in)activation; k, slope of the (in) activation curve; n, number of cells. * $p < 0.05$ vs control; unpaired Student's t-test or Mann-Whitney U test when data were not normally distributed.

Table S5. L-type calcium current properties in neonatal rat ventricular myocytes (NRVMs) 48h after transfection with control or anti-U6atac gapmeR.

	Control	n	Anti-U6atac	n
Current density				
$\mathbf{I_{CaL}}$ **(pA/pF)**	-16.0±1.7	13	-10.3±1.0*	12
Activation				
$\mathbf{V_{1/2}}$ **(mV)**	-13.0±0.8	13	-14.6±1.1	12
k **(mV)**	7.3±0.2	13	7.3±0.3	13
Inactivation				
$\mathbf{V_{1/2}}$ **(mV)**	-38.3±1.3	10	-37.7±0.7	9
k **(mV)**	-6.0±0.3	10	-6.1±0.2	9

ICaL, L-type calcium current density at 0 mV; V1/2 of (in)activation, half-voltage of (in)activation; k, slope of the (in)activation curve; n, number of cells. * $p < 0.05$ vs control; unpaired Student's t-test.

CHAPTER 6

TRIADIN-ANTISENSE: A lncRNA IN THE BACKSTAGE OF CARDIAC ALTERNATIVE SPLICING

Pablo Montañés-Agudo, Yigal M. Pinto

Circulation 146, no. 9 (2022): 715-717.

We increasingly recognize that non-coding RNAs provide a vast and multifaceted regulatory landscape in the heart. Herein, long non-coding RNAs (lncRNAs) represent a sizable proportion of larger non-coding RNAs with versatile functions. lncRNAs are quite heterogeneous. As a class, they share the requirement of at least 200 nucleotides, and they do not have apparent protein-coding potential[1]. However, some lncRNAs have lately been found to be able to translate into peptides, making their functions even more versatile[2]. We still do not know the function of most lncRNAs, but we do know that they are as abundant as coding mRNAs: the last release of the human genome consortium GENCODE (v40)[3] counts 18805 annotated lncRNA genes versus 19988 protein-coding genes. Functionally, lncRNAs can regulate important processes within the cell. For instance, they regulate gene expression by directly interacting with transcription factors, by creating discrete compartments within the nucleus, or by guiding chromatin modification[4]. Alternative splicing is another process controlled by lncRNAs[5].

Malat1/Neat2, one of the first characterized lncRNAs, participates in alternative splicing by controlling the phosphorylation of serine-/arginine-rich (SR) proteins, a well-characterized family of splicing factors[6]. In the heart, other lncRNAs such as circular RNAs derived from the titin gene, enable the splicing factors RBM20 (RNA-binding protein motif 20) and SRSF10 serine/arginine-rich splicing factor 10) to properly splice important cardiac genes including *Casq2* or *Camk2d*[7].

In this issue of Circulation, Zhao et al.[8] uncover the function of the cardiomyocyte-specific lncRNA triadin-antisense (*Trdn-as)*. *Trdn-as* is encoded within the triadin (*Trdn*) gene. Triadin is a well-known molecular component of the calcium release unit of the cardiomyocyte. It interacts with the ryanodine receptor (RYR2) and with calsequestrin to enhance the sarcoplasmic reticulum (SR) Ca^{2+} release that couples cell excitation with contraction (**Figure 1**). Triadin is composed of 41 exons, which can be alternatively spliced to four distinct isoforms that vary between cardiac and skeletal muscle cells. Triadin-1 is the shortest isoform, and it is the predominant one in cardiomyocytes[9,10].

Zhao and colleagues generated *Trdn-as* knockout (KO) mice that developed reduced ejection fraction, reduced exercise capacity, and died prematurely. At the cellular level, isolated adult ventricular cardiomyocytes exhibited increased SR Ca^{2+} content and reduced Ca^{2+} transients upon isoproterenol treatment. Moreover, *Trdn-as* KO mice were prone to premature ventricular contractions and ventricular tachycardia upon adrenergic stimulation with isoproterenol, a phenotype reminiscent of catecholaminergic polymorphic ventricular tachycardia (CPVT). Globally, the phenotype of *Trdn-as* KO mice resembles the calcium-handling defects observed in *Trdn* KO mice[11] and also in patients with the triadin knockout

syndrome[12]. Interestingly, the cardiac isoform of triadin triadin-1 was greatly reduced in *Trdn-as* KO mice. Triadin-1 over-expression was sufficient to rescue the Ca^{2+}-handling defects. Based on this, Zhao et al. propose that the function of *Trdn-as* is to facilitate the splicing of *Trdn* pre-mRNA to the cardiac triadin-1 isoform (**Figure 1**). Forced over-expression of *Trdn-as* increases triadin-1 expression in their model, and it can do so even in C2C12 cells, a skeletal muscle cell line that does not express *Trdn-as*. Mechanistically, they demonstrated that *Trdn-as* interacts with the *Trdn* pre-mRNA and with the SR splicing factors SRSF1 and SRSF10. Moreover, the interaction of SRSF1 with *Trdn* pre-mRNA as measured by RNA-immunoprecipitation was significantly decreased in the absence of *Trdn-as*, thereby suggesting that *Trdn-as* is required to correctly splice the cardiac triadin-1 isoform.

Previous studies examined the function of the *Trdn-as* lncRNA. Zhang et al.[13] already observed a correlation between the expression of *Trdn-as* and cardiac triadin-1 in the heart. Over-expression of *Trdn-as* in HL-1 cells induced a small increase in the ratio of cardiac triadin-1 over skeletal triadin-4 (*Trdn95*). Based on these findings, Zhang et al. proposed a model in which *Trdn-as* blocks the formation of the long skeletal triadin-4 in favor of the short cardiac triadin-1 isoform, but these experimental results could very well fit with Zhao's model.

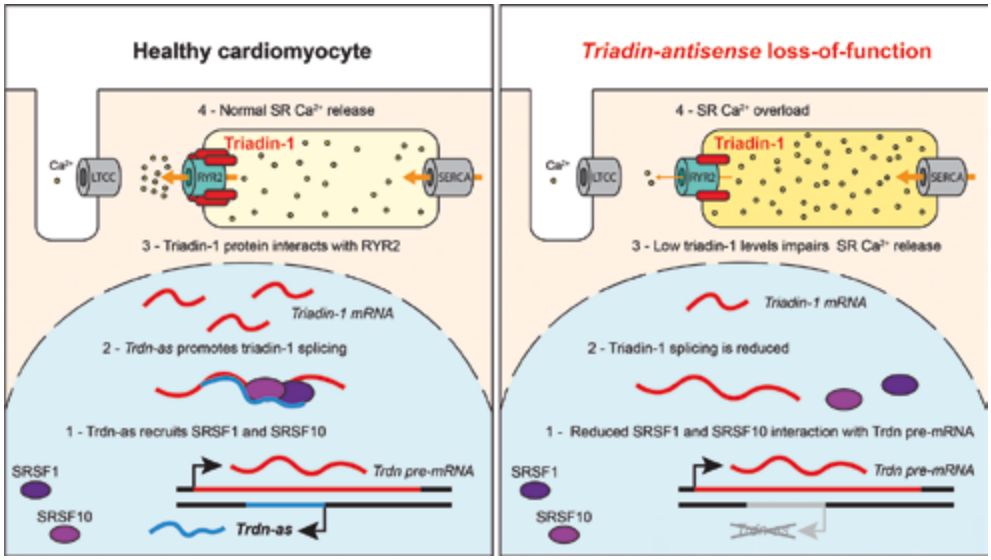

Figure 1. Function of the lncRNA *triadin-antisense* (*Trdn-as*) proposed by Zhao et al.[8]. LTCC, L-type *calcium* channel; RYR2, ryanodine receptor 2; SERCA, sarco/endoplasmic reticulum Ca^{2+}-ATPase; SR, sarcoplasmic reticulum; SRSF1/10; serine/arginine-rich splicing factor 1/10; *Trdn*, triadin; *Trdn-as*, triadin-antisense.

Interestingly, van Heesch et al.[2] were able to detect a translated short open reading frame in the human *Trdn-as*, which could be translated *in vitro* to a ~7 kDa microprotein. However, they only detected this microprotein in 2 out of 5 human hearts, and not in mice. Zhao and colleagues also tried to detect these microproteins, but they found no evidence for them. Thus, existence of a small protein encoded within *Trdn-as* remains elusive.

From a gene-regulatory point of view, *Trdn-as* is an example of how a cell-specific lncRNA can control ubiquitously expressed splicing factors to elicit a cell-specific effect. In this case, cardiomyocyte-specific *Trdn-as* recruits more ubiquitous splicing factors to orchestrate the formation of triadin-1 selectively in cardiomyocytes. Skeletal muscle cells also express *Trdn*, *Srsf1* and *Srsf10*; but since they do not express *Trdn-as*, the cardiac triadin-1 isoform is not produced. From a therapeutic perspective, this finding highlights potential new tools to modulate Ca^{2+}-cycling in heart disease. Both *Trdn-as* lncRNA and cardiac triadin isoform-1 are reduced in heart failure and ventricular arrhythmias[8,13]. Speculatively, a therapeutic strategy to target *Trdn-as* to rescue triadin function and SR Ca^{2+} release in these patients, thereby improving systolic function and reducing the pro-arrhythmogenic spontaneous depolarizations caused by spontaneous Ca^{2+} release events, could be envisioned.

Many other lncRNAs have been shown to be altered in cardiovascular diseases, such as heart failure and cardiac hypertrophy. So far, research has focused on the contribution of these lncRNAs to disease. However, how the expression of these lncRNAs is regulated remains poorly understood in most cases. As in the regulation of coding mRNAs, lncRNAs can be controlled at the transcriptional and post-transcriptional level by transcription factors, epigenetic modifications, microRNAs, and by many other mechanisms. The lncRNA *Myheart* (*Mhrt*) is one of the few examples whose regulation has been examined in the heart[14]. *Mhrt* stands for *Myh-associated RNA transcripts* and refers to several antisense transcripts encoded within the *Myh7* loci. *Mhrt* is highly expressed in the adult heart, and it inhibits the pro-hypertrophic chromatin-remodeling factor BRG1. Upon pressure overload, activation of the stress-induced complex BRG1–HDAC–PARP represses the *Mhrt* promoter and reduces its expression. Thus, *Mhrt* governs negative feedback with BRG1 that prevents cardiac hypertrophy until there is a pathological stressor. Little is known about other mechanisms that regulate lncRNAs in the heart, including *Trdn-as.* Further research is required to understand whether these lncRNAs are just contributing to disease or whether they are part of a compensatory response.

The regulation of *Trdn* by *Trdn-as* raises the question whether other cardiac antisense lncRNAs regulate splicing. To address this at the whole-transcriptome level, it would be of great value to develop a global picture of all the intermolecular RNA interactions occurring in the heart *in vivo*. It is already possible to capture and measure RNA-RNA interactions with

high-throughput technologies such as RNA in situ conformation sequencing (RIC-seq)[15]. RIC-seq captures RNA-RNA interactions by crosslinking RNA molecules that are in physical proximity to each other. After several steps, chimeric RNA fragments can be sequenced to identify how RNAs interact with each other at single-nucleotide resolution. Mapping the lncRNA interactome will guide us in the study of uncharacterized lncRNAs, and it will tell us whether the control of splicing by antisense lncRNAs constitutes a general biological principle that applies to other cardiac genes.

In conclusion, lncRNAs are recently recognized players in the regulation of alternative splicing in the heart. The field is just starting to characterize some of them, but a great deal of additional research is needed to develop a more comprehensive view of all their functions. Unravelling new lncRNAs, such as *Trdn-as* , will foster a much deeper understanding of gene regulation in the heart, and it will provide new targets to expand therapeutic options in cardiovascular disease.

CONFLICT OF INTEREST DISCLOSURES

YMP serves as consultant for biotech and pharmaceutical companies that develop molecules that target myocardial disease, including CPVT. YMP is inventor on patents related to cardiomyopathy and holds minor shares (< 5%) in a spin-off aimed at developing therapies for heart disease.

REFERENCES

1. Statello, L., Guo, C.-J., Chen, L.-L. & Huarte, M. Gene regulation by long non-coding RNAs and its biological functions. *Nat. Rev. Mol. Cell Biol.* **22**, 96–118 (2021).
2. Heesch, S. van *et al.* The Translational Landscape of the Human Heart. *Cell* **178**, 242-260.e29 (2019).
3. Frankish, A. *et al.* GENCODE reference annotation for the human and mouse genomes. *Nucleic Acids Res.* **47**, D766–D773 (2019).
4. Papait, R., Kunderfranco, P., Stirparo, G. G., Latronico, M. V. G. & Condorelli, G. Long Noncoding RNA: a New Player of Heart Failure? *J Cardiovasc. Transl. Res.* **6**, 876–883 (2013).
5. Pisignano, G. & Ladomery, M. Epigenetic Regulation of Alternative Splicing: How LncRNAs Tailor the Message. *Non-Coding RNA* **7**, 21 (2021).
6. Tripathi, V. *et al.* The Nuclear-Retained Noncoding RNA MALAT1 Regulates Alternative Splicing by Modulating SR Splicing Factor Phosphorylation. *Mol. Cell* **39**, 925–938 (2010).
7. Tijsen, A. J. *et al.* Titin Circular RNAs Create a Back-Splice Motif Essential for SRSF10 Splicing. *Circulation* **143**, 1502–1512 (2021).
8. Yuanbiao Zhao *et al.* A cardiomyocyte-specific long noncoding RNA regulates alternative splicing of the Triadin gene in the heart. *Circulation* (2022).
9. Chopra, N. & Knollmann, B. C. Triadin regulates cardiac muscle couplon structure and microdomain Ca2+ signalling: a path towards ventricular arrhythmias. *Cardiovasc. Res.* **98**, 187–191 (2013).
10. Marty, I. *et al.* Triadin: what possible function 20 years later? *J. Physiol.* **587**, 3117–3121 (2009).
11. Chopra, N. *et al.* Ablation of triadin causes loss of cardiac Ca2+ release units, impaired excitation–contraction coupling, and cardiac arrhythmias. *Proc. Natl. Acad. Sci.* **106**, 7636–7641 (2009).
12. Hancox, J. C., James, A. F., Walsh, M. A. & Stuart, A. G. Triadin mutations - a cause of ventricular arrhythmias in children and young adults. *J. Congenit. Cardiol.* **1**, 9 (2017).
13. Zhang, L., Salgado-Somoza, A., Vausort, M., Leszek, P. & Devaux, Y. A heart-enriched antisense long non-coding RNA regulates the balance between cardiac and skeletal muscle triadin. *Biochim. Biophys. Acta BBA - Mol. Cell Res.* **1865**, 247–258 (2018).
14. Han, P. *et al.* A long noncoding RNA protects the heart from pathological hypertrophy. *Nature* **514**, 102–106 (2014).
15. Cai, Z. *et al.* RIC-seq for global in situ profiling of RNA–RNA spatial interactions. *Nature* **582**, 432–437 (2020).

CHAPTER 7

GENERAL DISCUSSION AND FUTURE PERSPECTIVES

GENERAL DISCUSSION AND FUTURE PERSPECTIVES

As many groundbreaking scientific advances, the discovery of RNA splicing was a serendipitous finding. Back in 1977, the groups of Richard J. Roberts and Phillip A. Sharp were simultaneously investigating the genome organization of the adenovirus Ad2[1–3]. Their goal was to map the genes of Ad2 by hybridizing the RNAs produced by the virus to its DNA. RNA:DNA hybrids can be observed under the electron microscope to determine the genome region from which the RNAs have been transcribed. This technique was commonly used to map prokaryotic genomes, but when used to analyze Ad2, they found something unexpected. Some fragments of DNA were free in loops, not hybridizing to the RNA. This meant that the RNAs of Ad2 were not continuously covering the DNA sequence. Later they found out that after transcription some parts of the RNA are removed (introns), while the remaining fragments are spliced together (exons)[1–3]. The discovery of splicing granted the Nobel Prize in Physiology or Medicine jointly to Richard J. Roberts and Phillip A. Sharp in 1993.

Since then, the field of RNA splicing has greatly advanced. Today we acknowledge the vital importance of alternative splicing during gene expression and its role in expanding the coding potential of the human genome. Many of the molecular mechanisms governing alternative splicing and their connection to human disorders have been described. In the heart, alternative splicing has been proven essential to generate the highly specialized proteome of cardiomyocytes and to adapt it to different stages of development and disease. Studies in this thesis have focused on the mechanisms that regulate alternative splicing in the heart. By understanding the regulation of alternative splicing in the heart, we can obtain new insights into the underlying causes of cardiac disease and thus develop effective treatments in the future.

QKI is an essential regulator of cardiac splicing

A great deal of the work in this thesis has focused on the splicing factor Quaking (QKI). Our studies have uncovered a crucial role for QKI in regulating the muscle-specific splicing program of cardiomyocytes *in vivo* (chapter 2). We found that QKI is required to maintain normal cardiac function during development and in the adult heart by controlling alternative splicing of hundreds of protein-coding genes. Our work adds to previous studies which showed the importance of QKI in splicing for the lineage specification of the cardiac mesoderm[4] and for myofibrillogenesis during cardiomyocyte differentiation[5]. The role of QKI in splicing of muscle-related genes is not only important for cardiomyocytes. The orthologues of QKI in other species have been demonstrated essential for myofibril formation during muscle development, as evidenced in zebrafish[6,7] and *Drosophila* larvae[8]. QKI also participates in the transition from fibroblasts toward myofibroblasts occurring in heart failure[9], in the transition from myoblast to myotubes[10], and in the differentiation and

function of vascular smooth muscle cells (VSMC)[11,12]. Intriguingly, QKI has been also shown important for the differentiation and maturation of other cell types[13], such as neural stem cells[14], astrocytes[15], oligodendrocytes[16] and monocytes[17]. It is currently unknown how QKI can participate in the differentiation and function of such a diverse number of cell types. It may be due to the expression of different QKI isoforms in each cell type, to interactions with other splicing factors, or to splicing of downstream targets that are specific to certain cell types. Additional research is required to address this.

Besides a role for QKI in alternative splicing, we also demonstrated that QKI is required for back-splicing, and thus the formation of circRNAs in the heart (chapter 3). circRNAs are a class of non-coding RNA that are emerging as regulators of cardiac function. Our work revealed that ~17% of the circRNAs present in the adult mouse heart are differentially expressed in the absence of QKI. Interestingly, we found that QKI can act either as a positive or as a negative regulator of circRNA formation and that changes in circRNA expression are often associated with alterations in the linear splicing of the host gene. Hence, our research suggests that QKI governs both linear and back-splicing in an interdependent manner. This is in line with a previous report that revealed that QKI controls back-splicing[18] during epithelial-to-mesenchymal transition *in vitro*. In the heart, Gupta et al. reported that QKI overexpression can reduce doxorubicin-induced toxicity in the heart, and this was associated with reduced expression of three circRNAs (derived from *Ttn*, *Fhod3* and *Strn3*)[19]. We propose that QKI is important in cardiac physiology not only by regulating linear splicing, but also by the formation of circRNAs. Follow-up studies to characterize the QKI-regulated circRNAs are required to shed light on the relevance of these QKI-dependent circRNAs in the healthy and diseased heart

Changes in cardiac splicing during disease

The field of alternative splicing was initiated by noticing disparities in the splicing profile of the different tissues within the body. These different profiles are due to cell-type specific splicing programs, that create specific isoforms in each cell type within the body even though they share the same genome[20,21]. The field of alternative splicing is now exploring the splicing changes that occur during disease and during compensatory responses to pathological stimuli.

Changes in the splicing program of the heart have been observed upon pressure overload and during several cardiomyopathies. For instance, in mice, pressure overload induced by transverse aorta constriction (TAC) reverses splice isoforms to a so-called "fetal" splicing program[22]. In humans, this "fetal" splicing pattern is also observed during heart failure, and interestingly, is reversed after left ventricular assist device (LVID) implantation[23]. This suggests that splicing may act as a compensatory mechanism to the changing mechanical

forces that the heart faces. Recent studies are starting to delve into this by exploring how splicing changes upon challenging the heart. For example, upon TAC and myocardial infarction, there is an increase in PTBP1 expression and a high proportion of differentially spliced exons containing the PTBP1 binding sequence. Indeed, PTBP1 transduction alone induces pathological cardiac hypertrophy and diastolic dysfunction[24]. The heterogeneous nuclear ribonucleoprotein C (hnRNPC) has been shown to respond to mechanical stress by relocating to the sarcomeric Z-disc, thus modifying its function as a splicing factor and impacting many splicing targets[25]. This indicates that splicing factors play a critical role in regulating cellular responses in the heart. We speculate that the regulation of QKI activity may be involved in this type of response.

Regulation of QKI activity

As we described in chapter 2, the expression levels of QKI increase during heart development, which coincides with the occurrence of certain splicing events that are mediated by QKI[21]. Additionally, we showed that overexpression of QKI-5 in cultured neonatal cardiomyocytes increases the production of muscle-specific isoforms, the contractility of these cells, and their size. Thus, an increase in QKI activity may contribute to the hypertrophic growth of cardiomyocytes during cardiac development. In this thesis, we also observed a correlation between the expression levels of QKI, RBM24, and MBNL1 and some of the splicing events that they regulate in human heart failure samples (chapter 4). This suggests that variations in splicing factor expression can underlie alterations in the expression of protein isoforms during disease. We speculate that variations in QKI expression might contribute to disease, especially since its expression has been observed to decrease in cases of human heart failure[19]. Gene therapy approaches using the overexpression or activation of QKI or other splicing factors may be effective in regulating the expression of beneficial protein isoforms in the heart. These studies are awaited with great interest.

Splicing represents an additional mode of regulating QKI activity. The *QKI* gene itself is subjected to alternative splicing, resulting in three different isoforms: QKI-5, QKI-6 and QKI-7[26]. These three isoforms differ in the regulatory C-terminal domain. QKI-5 presents a nuclear localization signal, allowing it to enter the nucleus and function as a splicing factor. QKI-6 and QKI-7 are the predominant isoforms in the cytoplasm, and they regulate the stabilization of transcripts by binding to 3' UTRs[26]. Since our lab is interested in splicing regulation in the heart, we focused our studies on QKI-5, which is also the main isoform in cardiomyocytes. However, low levels of QKI-6 and QKI-7 are detected in the heart. Whether they have a function in cardiomyocytes is currently unknown. Our understanding of the regulation of QKI splicing is also limited, aside from knowing that QKI undergoes a complex self-regulation feedback, in which QKI-5 promotes the splicing of the QKI

pre-mRNA into QKI-5, and QKI-6 promotes the translation of QKI-6[27]. Alterations in the ratios of these three QKI isoforms may be relevant to control QKI-dependent activity throughout cardiac development and disease.

In addition to the three primary splicing isoforms, QKI has a tandem acceptor splice site in exon 6[28]. This alternative splice site leads to the removal of 24 nucleotides that encode an 8-amino acid sequence (ALAFSLAA). Since the 8 amino acid deletion occurs at the beginning of the regulatory C-terminal domain, this splicing event may control QKI activity and may change the interactions with other splicing regulators. Interestingly, this splicing event has only been detected in the heart and in skeletal muscle, which are tissues in which QKI sustains muscle-specific splicing[29,30]. Thus, the muscle-specific QKI$^{\Delta ALAFSLAA}$ isoform may explain the differential function of QKI in (cardio-)myocytes versus other cell types. Further research is required to assess the differences between the canonical QKI isoforms and the muscle-specific QKI$^{\Delta ALAFSLAA}$ isoforms.

Post-translational modifications are also known to regulate QKI activity. In fact, QKI belongs to the conserved protein family of "signal transduction activators of RNA" (STARs), which are RNA-binding proteins that connects RNA metabolism to signaling pathways through post-translational modifications[31]. In the nervous system, QKI has been shown to be phosphorylated by Src protein tyrosine kinases at a tyrosine cluster in a proline-rich PXXP motif within its regulatory C-terminal region. This modification has been studied in the context of myelinization, and has been shown to hamper the interaction between QKI and the target mRNA *Myelin Basic Protein* (*MBP*)[32]. In the human and mouse heart, nothing is known about the phosphorylation status of QKI. However, in *Drosophila melanogaster*, the QKI orthologue HOW (="Held Out Wings") undergoes phosphorylation in embryonic somatic muscles and heart cardioblasts[8]. This phosphorylation is carried out by MAPK/ERK map kinases and promotes the dimerization of HOW to enhance its binding to mRNA targets. Most remarkably, this phosphorylation regulates the interaction between HOW and *sallimus* (sls), which is the fly orthologue of the mammalian titin. Therefore, it is likely that the phosphorylation of QKI affects the splicing of mRNA targets in the human heart during development and disease.

Numerous regulators govern cardiac splicing

300 to 400 different splicing regulators are estimated to exist in humans[33,34]. This includes core components of the spliceosome, essential splicing factors (e.g. families of hnRPC and SR splicing factors) and tissue-specific splicing factors (e.g. RBM20). When studying QKI-dependent splicing, we noticed a considerable overlap with the targets of other splicing factors. For instance, we found that both QKI and RBM20[35] regulate the same exons in *Ttn*,

Camk2d, and *Ldb3*. This led us to consider that splicing factors act cooperatively, and that a more integrated approach is needed to gain a deeper understanding of the molecular basis of alternative splicing in the heart. Therefore, in chapter 4, we explored the connection between the splicing programs of different splicing factors in the heart. To achieve this, we compared splicing changes in previously published KO models of splicing factors. The majority of these KO models exhibited cardiac dysfunction at different developmental or adult stages. The defects at the molecular level were largely affecting sarcomere and cytoskeletal organization, as well as calcium handling. By re-analyzing the original RNA-sequencing data from 8 published mouse models, we confirmed a large overlap among the splicing networks of these splicing factors. In the case of MBNL, QKI and RBM24, as much as ~30-40% of the alternative splicing events were shared between at least 2 out of 3 models. Some crucial genes, such as *Camk2d*, *Tpm2* or *Pdlim5*, required the combined action of several splicing factors. Our conclusion is that studying individual splicing factors one at a time is crucial, but future research will need to address alternative splicing regulation from an integrative perspective and consider all the distinct splicing regulators simultaneously.

In addition to the traditional splicing regulators, long non-coding RNAs (lncRNAs) have recently emerged as regulators of splicing. In chapter 6 we commented on how triadin-antisense controls splicing by recruiting splicing factors to the triadin pre-mRNA. Other lncRNAs have been described to have similar functions, such as Malat1/Neat2 controlling the phosphorylation of serine/arginine-rich (SR) splicing factors[36] or circRNAs derived from titin controlling SRSF10 and RBM20[37] function. In the upcoming years, as the functions of new lncRNAs are uncovered, we will realize that they are a critical elements controlling splicing.

Intron retention: the ignored alternative splicing modality

Introns are typically considered as silent sequences of DNA that simply facilitate alternative splicing. Nevertheless, introns serve crucial roles, such as hosting regulatory elements (e.g. enhancers, microRNAs or lncRNAs) and controlling gene expression through intron retention. Intron retention controls gene expression because transcripts that are not completely spliced cannot be translated. Transcripts with a retained intron are either confined to the nucleus, or removed by RNA degradation pathways, such as the nonsense-mediated decay (NMD)[38]. As a modality of alternative splicing, intron retention is also regulated in a tissue- and developmental-specific manner[39]. Indeed, intron retention is the most common modality of alternative splicing in the heart, with higher levels of retention occurring in the fetal versus the adult heart[40]. Besides, retention of specific introns in sarcomere genes (i.e. *TNNT2, TNNI3, MYH7, MYBPC3)* has been observed in left ventricle samples from ischemic cardiomyopathy patients[41]. This implies that intron retention, similar to other forms of alternative splicing, may play a role in both heart development and disease. However, intron

retention is generally overlooked because RNA-seq generally does not provide sufficient intron read coverage.

In this thesis (chapter 5), we studied intron retention of a very particular class of introns, named minor or U12-dependent introns. We focused on minor introns because they appear to be enriched in genes crucial for cardiomyocyte function (i.e. calcium channels). Our study revealed that reduced expression of the minor spliceosome components U6atac and U4atac leads to minor intron retention in sodium and calcium channel genes. In turn, this hampered the expression and function of these channels. This is an important finding, because minor intron splicing has been postulated as a bottleneck in RNA processing, and the minor spliceosome component U6atac has been suggested as the main limiting factor in minor splicing[42]. In addition, we found that the expression of several minor spliceosome components is altered in the human failing heart. Thus, it is conceivable that during development or disease, minor splicing activity controls the expression of minor-intron containing genes. Further research involving ultra-deep RNA sequencing is required to assess whether retention of major and minor introns is a significant mechanism of gene expression regulation in the heart.

Technical limitations to study RNA splicing

Currently, the most widely used technique to study RNA splicing is RNA-sequencing (RNA-seq). RNA-seq provides information of the entire transcriptome of the sample, which is essential to understand splicing. But it has some limitations that are worth considering.

(1) Short- versus long-read RNA-seq. Short-read RNA-seq is the most widely used assay to study the transcriptome. It is based on quantifying 75-150 bp reads covering the exome to calculate gene expression and differential splicing. However, short-reads cannot directly determine the full-length sequence of an entire transcript, and computational steps are required to infer the exon composition. The challenge becomes greater when assessing genes with a large number of exons susceptible to be alternatively spliced, such as titin. New long-read sequencing technologies, such as Nanopore sequencing[43], can solve this problem by performing ultra-long reads covering the entire transcript. Nanopore sequencing has been able to detect the full-length transcript of the multiple isoforms of tropomyosins (*Tpm1*, *Tpm2*, *Tpm3* and *Tpm4*) during rat heart development with ultra-long reads of 100 kb to 882 kb[44]. This technology confirmed that alternative splicing of exon 6A in *Tpm1* is controlled by the splicing factors RBFOX2 and PTBP1 in an opposite way. Nanopore sequencing can also be used to study circRNAs and determine their full-length sequence[45]. Short-reads enable the quantification of back-splice junctions, but the full composition of circRNAs cannot be directly determined. Analysis of circRNAs performed on long-read RNA-seq data can

be advantageous in simultaneously quantifying circRNA expression and determining their exonic and intronic composition.

(2) Poly-A RNA-seq. Before performing RNA-seq, it is necessary to eliminate unwanted RNAs in order to prevent the system from becoming saturated with irrelevant reads. This is particularly important for eliminating ribosomal RNAs, which account for 80-90% of the RNAs within the sample[47]. Typically this step involves selection of polyadenylated (poly(A)) transcripts using oligo(dT) primers or depletion of ribosomal RNAs. PolyA-enrichment is the most common practice because it focuses on protein-coding genes and it requires less sequencing depth. Samples depleted of ribosomal RNAs require a deeper sequencing, but they provide information on non-polyA transcripts, such as circRNAs or pre-mature mRNAs that are in the process of being spliced. Of the splicing factor KO mouse models that we examined in chapter 3 and chapter 4, only the QKI KO and RBM20 KO were analyzed from ribosomal RNA-depleted RNA. Thus, only QKI-dependent and RBM20-dependent circRNAs could be assessed. We expect that other splicing factors also regulate circRNA formation in the heart.

(3) Bulk versus single-cell RNA-seq. Bulk RNA-seq analyzes all RNAs present in a complex sample composed of different cell populations. This is a common practice to analyze the expression of splice isoforms. Unfortunately, it is not feasible to determine the specific cellular population in which a transcript is expressed using bulk RNA-seq. Bulk RNA-seq may be problematic when comparing samples with different cellular composition. For instance, samples with a higher proportion of cardiomyocytes would present a higher expression levels of cardiomyocyte-specific genes, but also of cardiomyocyte-specific isoforms. The way forward is to apply single-cell RNA sequencing to study splicing patterns in individual cells, but the sequencing coverage is at the moment still too low for this purpose. In the near future, new technologies based on single-cell sequencing, such as VASA-seq (Vast Transcriptome Analysis of Single Cells by dA-tailing)[48], will offer a more rigorous approach to analyze splicing.

Modulation of splicing as a therapeutic approach

In this thesis, we have shown that splicing defects can cause severe cardiomyopathies. However, the regulation of alternative splicing is also a subject of intense research for the treatment of diseases. In this regard, it is possible to modulate splicing with splice-switching antisense oligonucleotides (SSOs). SSOs are synthetic nucleic acids, 15-30 nucleotides in length, that modulate splicing by binding to pre-mRNAs via complementary Watson–Crick base pairing[49,50]. SSOs can be used to mask splice sites or intronic splicing enhancers to promote exon skipping, or to block intronic splicing silencers to promote exon

inclusion. SSOs are particularly useful to modify splicing of mutated genes causing disease. SSOs can be used to block cryptic splice sites surged by mutation, such as a cryptic splice site in lamin (*LMNA*^{G609G}) that results in the formation of progerin[51]. In the mouse heart, SSOs have been successfully applied to skip exon 326 of *TTN* carrying a DCM-causing frame shift mutation[52]; and to correct the splicing defects in *MYPBC3* caused by a mutated exon 6 resulting in HCM[53]. Some SSO-based drugs are already approved by regulatory agencies for its use to prevent the production of disease-causing mutated proteins in patients. For instance, SSOs inducing exon skipping in the cytoskeletal protein dystrophin (*DMD*) have been approved by the United States Food and Drug Administration (FDA) to alleviate the symptoms of Duchenne muscular dystrophy (i.e. casimersen)[54]. SSOs can also be used to modify gene expression. The technology coined as "Targeted Augmentation of Nuclear Gene Output" (TANGO), uses SSOs to increase the endogenous expression of protein by shifting from non-productive alternative spliced transcripts to productive ones[55]. The use of TANGO can result in a 2-3 fold change increase in gene expression. However it is limited to genes that present considerable endogenous expression of a non-productive transcript.

Modifying the expression of splicing factors can also be used to modulate splicing. In mice, antisense oligonucleotides (ASOs) targeting RBM20 have been used to reduce its expression and induce a shift in titin splicing from the adult and stiff isoforms towards the long and complaint one (fetal). This change in TTN splicing alters the mechanical properties of the heart, leading to an improvement in ventricular filling[56]. Viral delivery of splicing factors may represent another therapeutic approach to treat cardiac disease. Transduction of mice with QKI-5 by AAV9 (adeno-associated virus serotype 9) has been used to alleviate doxorubicin-induced cardiotoxicity[19]. Our observation that QKI overexpression in cultured neonatal cardiomyocytes enhances contractility suggests this may represent an approaches to improve cardiomyocyte function in the compromised heart. Further research into the therapeutic potential of QKI would be an intriguing avenue of research.

REFERENCES

1. Berget, S. M., Moore, C. & Sharp, P. A. Spliced segments at the 5′ terminus of adenovirus 2 late mRNA*. *Proceedings of the National Academy of Sciences* **74**, 3171–3175 (1977).
2. Chow, L. T., Gelinas, R. E., Broker, T. R. & Roberts, R. J. An amazing sequence arrangement at the 5′ ends of adenovirus 2 messenger RNA. *Cell* **12**, 1–8 (1977).
3. Suran, M. Finding the tail end: The discovery of RNA splicing. *Proceedings of the National Academy of Sciences* **117**, 1829–1832 (2020).
4. Fagg, W. S. *et al.* Definition of germ layer cell lineage alternative splicing programs reveals a critical role for Quaking in specifying cardiac cell fate. *Nucleic Acids Res* **50**, 5313–5334 (2022).
5. Chen, X. *et al.* QKI is a critical pre-mRNA alternative splicing regulator of cardiac myofibrillogenesis and contractile function. *Nat Commun* **12**, 89 (2021).
6. Bonnet, A. *et al.* Quaking RNA-Binding Proteins Control Early Myofibril Formation by Modulating Tropomyosin. *Developmental Cell* **42**, 527-541.e4 (2017).
7. Lobbardi, R. *et al.* Fine-tuning of Hh signaling by the RNA-binding protein Quaking to control muscle development. *Development* **138**, 1783–1794 (2011).
8. Nir, R., Grossman, R., Paroush, Z. & Volk, T. Phosphorylation of the Drosophila melanogaster RNA–Binding Protein HOW by MAPK/ERK Enhances Its Dimerization and Activity. *PLOS Genetics* **8**, e1002632 (2012).
9. Chothani, S. *et al.* Widespread Translational Control of Fibrosis in the Human Heart by RNA-Binding Proteins. *Circulation* **140**, 937–951 (2019).
10. Hall, M. P. *et al.* Quaking and PTB control overlapping splicing regulatory networks during muscle cell differentiation. *RNA* **19**, 627–638 (2013).
11. Caines, R. *et al.* The RNA-binding protein QKI controls alternative splicing in vascular cells, producing an effective model for therapy. *Journal of Cell Science* **132**, jcs230276 (2019).
12. van der Veer, E. P. *et al.* Quaking, an RNA-Binding Protein, Is a Critical Regulator of Vascular Smooth Muscle Cell Phenotype. *Circulation Research* **113**, 1065–1075 (2013).
13. Neumann, D. P., Goodall, G. J. & Gregory, P. A. The Quaking RNA-binding proteins as regulators of cell differentiation. *WIREs RNA* **13**, e1724 (2022).
14. Hayakawa-Yano, Y. *et al.* An RNA-binding protein, Qki5, regulates embryonic neural stem cells through pre-mRNA processing in cell adhesion signaling. *Genes Dev.* **31**, 1910–1925 (2017).
15. Sakers, K. *et al.* Loss of Quaking RNA binding protein disrupts the expression of genes associated with astrocyte maturation in mouse brain. *Nat Commun* **12**, 1537 (2021).
16. Darbelli, L., Choquet, K., Richard, S. & Kleinman, C. L. Transcriptome profiling of mouse brains with qkI-deficient oligodendrocytes reveals major alternative splicing defects including self-splicing. *Sci Rep* **7**, 7554 (2017).
17. de Bruin, R. G. *et al.* Quaking promotes monocyte differentiation into pro-atherogenic macrophages by controlling pre-mRNA splicing and gene expression. *Nat Commun* **7**, 10846 (2016).
18. Conn, S. J. *et al.* The RNA Binding Protein Quaking Regulates Formation of circRNAs. *Cell* **160**, 1125–1134 (2015).
19. Gupta, S. K. *et al.* Quaking Inhibits Doxorubicin-Mediated Cardiotoxicity Through Regulation of Cardiac Circular RNA Expression. *Circulation Research* **122**, 246–254 (2018).
20. Baralle, F. E. & Giudice, J. Alternative splicing as a regulator of development and tissue identity. *Nat Rev Mol Cell Biol* **18**, 437–451 (2017).
21. Mazin, P. V., Khaitovich, P., Cardoso-Moreira, M. & Kaessmann, H. Alternative splicing during mammalian organ development. *Nat Genet* **53**, 925–934 (2021).
22. Ames, E., Lawson, M., Mackey, A. & Holmes, J. Sequencing of mRNA identifies re-expression of fetal splice variants in cardiac hypertrophy. *J Mol Cell Cardiol* **62**, 99–107 (2013).
23. D'Antonio, M. *et al.* In heart failure reactivation of RNA-binding proteins is associated with the expression of 1,523 fetal-specific isoforms. *PLOS Computational Biology* **18**, e1009918 (2022).
24. Martí-Gómez, C. *et al.* Functional Impact and Regulation of Alternative Splicing in Mouse

Heart Development and Disease. *J. of Cardiovasc. Trans. Res.* **15**, 1239–1255 (2022).

25. Martino, F. *et al.* The mechanical regulation of RNA binding protein hnRNPC in the failing heart. *Science Translational Medicine* **14**, eabo5715 (2022).
26. Chen, X. *et al.* The Emerging Roles of the RNA Binding Protein QKI in Cardiovascular Development and Function. *Frontiers in Cell and Developmental Biology* **9**, 1411 (2021).
27. Fagg, W. S. *et al.* Autogenous cross-regulation of Quaking mRNA processing and translation balances Quaking functions in splicing and translation. *Genes Dev.* **31**, 1894–1909 (2017).
28. Mironov, A., Denisov, S., Gress, A., Kalinina, O. V. & Pervouchine, D. D. An extended catalogue of tandem alternative splice sites in human tissue transcriptomes. *PLOS Computational Biology* **17**, e1008329 (2021).
29. Montañés-Agudo, P. *et al.* The RNA-binding protein QKI governs a muscle-specific alternative splicing program that shapes the contractile function of cardiomyocytes. *Cardiovascular Research* cvad007 (2023) doi:10.1093/cvr/cvad007.
30. Dominici, C. & Richard, S. Muscle stem cell polarity requires QKI-mediated alternative splicing of Integrin Alpha-7 (Itga7). *Life Sci Alliance* **5**, e202101192 (2022).
31. Vernet, C. & Artzt, K. STAR, a gene family involved in signal transduction and activation of RNA. *Trends in Genetics* **13**, 479–484 (1997).
32. Zhang, Y. *et al.* Tyrosine phosphorylation of QKI mediates developmental signals to regulate mRNA metabolism. *The EMBO Journal* **22**, 1801–1810 (2003).
33. Seiler, M. *et al.* Somatic Mutational Landscape of Splicing Factor Genes and Their Functional Consequences across 33 Cancer Types. *Cell Reports* **23**, 282-296.e4 (2018).
34. Fisher, E. & Feng, J. RNA splicing regulators play critical roles in neurogenesis. *WIREs RNA* **13**, e1728 (2022).
35. van den Hoogenhof, M. M. G. *et al.* RBM20 Mutations Induce an Arrhythmogenic Dilated Cardiomyopathy Related to Disturbed Calcium Handling. *Circulation* **138**, 1330–1342 (2018).
36. Tripathi, V. *et al.* The Nuclear-Retained Noncoding RNA MALAT1 Regulates Alternative Splicing by Modulating SR Splicing Factor Phosphorylation. *Molecular Cell* **39**, 925–938 (2010).
37. Tijsen, A. J. *et al.* Titin Circular RNAs Create a Back-Splice Motif Essential for SRSF10 Splicing. *Circulation* **143**, 1502–1512 (2021).
38. Patel, A. A., McCarthy, M. & Steitz, J. A. The splicing of U12-type introns can be a rate-limiting step in gene expression. *The EMBO Journal* **21**, 3804–3815 (2002).
39. Mansilla, A. *et al.* Developmental regulation of a proinsulin messenger RNA generated by intron retention. *EMBO Rep* **6**, 1182–1187 (2005).
40. Wang, H. *et al.* Genome-wide analysis of alternative splicing during human heart development. *Sci Rep* **6**, 35520 (2016).
41. Kong, S. W. *et al.* Heart Failure–Associated Changes in RNA Splicing of Sarcomere Genes. *Circulation: Cardiovascular Genetics* **3**, 138–146 (2010).
42. Younis, I. *et al.* Minor introns are embedded molecular switches regulated by highly unstable U6atac snRNA. *eLife* **2013**, (2013).
43. Jain, M. *et al.* Nanopore sequencing and assembly of a human genome with ultra-long reads. *Nat Biotechnol* **36**, 338–345 (2018).
44. Cao, J., Routh, A. L. & Kuyumcu-Martinez, M. N. Nanopore sequencing reveals full-length Tropomyosin 1 isoforms and their regulation by RNA-binding proteins during rat heart development. *J Cell Mol Med* **25**, 8352–8362 (2021).
45. Rahimi, K., Venø, M. T., Dupont, D. M. & Kjems, J. Nanopore sequencing of brain-derived full-length circRNAs reveals circRNA-specific exon usage, intron retention and microexons. *Nat Commun* **12**, 4825 (2021).
46. David, J. K., Maden, S. K., Wood, M. A., Thompson, R. F. & Nellore, A. Retained introns in long RNA-seq reads are not reliably detected in sample-matched short reads. *Genome Biol* **23**, 240 (2022).
47. Zhao, S., Zhang, Y., Gamini, R., Zhang, B. & von Schack, D. Evaluation of two main RNA-seq approaches for gene quantification in clinical RNA sequencing: polyA+ selection versus rRNA depletion. *Sci Rep* **8**, 4781 (2018).

48. Salmen, F. *et al.* High-throughput total RNA sequencing in single cells using VASA-seq. *Nat Biotechnol* 1–14 (2022) doi:10.1038/s41587-022-01361-8.

49. Havens, M. A. & Hastings, M. L. Splice-switching antisense oligonucleotides as therapeutic drugs. *Nucleic Acids Res* **44**, 6549–6563 (2016).

50. Roberts, T. C., Langer, R. & Wood, M. J. A. Advances in oligonucleotide drug delivery. *Nat Rev Drug Discov* **19**, 673–694 (2020).

51. Osorio, F. G. *et al.* Splicing-Directed Therapy in a New Mouse Model of Human Accelerated Aging. *Science Translational Medicine* **3**, 106ra107-106ra107 (2011).

52. Gramlich, M. *et al.* Antisense-mediated exon skipping: a therapeutic strategy for titin-based dilated cardiomyopathy. *EMBO Molecular Medicine* **7**, 562–576 (2015).

53. Gedicke-Hornung, C. *et al.* Rescue of cardiomyopathy through U7snRNA-mediated exon skipping in Mybpc3-targeted knock-in mice. *EMBO Molecular Medicine* **5**, 1128–1145 (2013).

54. Zakeri, S. E. *et al.* Casimersen for the treatment of Duchenne muscular dystrophy. *Trends in Pharmacological Sciences* **43**, 607–608 (2022).

55. Lim, K. H. *et al.* Antisense oligonucleotide modulation of non-productive alternative splicing upregulates gene expression. *Nat Commun* **11**, 3501 (2020).

56. Lisakowski, V. B. *et al.* RBM20 ASOs improve ventricular filling in a mouse model with increased titin-based stiffness. *Biophysical Journal* **121**, 396a (2022).

57. Barash, Y. *et al.* Deciphering the splicing code. *Nature* **465**, 53–59 (2010).

58. Liao, S. E. & Regev, O. Splicing at the phase-separated nuclear speckle interface: a model. *Nucleic Acids Res* **49**, 636–645 (2020).

59. Bertero, A. *et al.* Dynamics of genome reorganization during human cardiogenesis reveal an RBM20-dependent splicing factory. *Nat Commun* **10**, 1538 (2019).

60. Hinkle, E. R. *et al.* Stretching muscle cells induces transcriptional and splicing transitions and changes in SR proteins. *Commun Biol* **5**, 1–15 (2022).

61. Wada, T. & Becskei, A. Impact of Methods on the Measurement of mRNA Turnover. *Int J Mol Sci* **18**, 2723 (2017).

62. Ingolia, N. T., Ghaemmaghami, S., Newman, J. R. S. & Weissman, J. S. Genome-Wide Analysis in Vivo of Translation with Nucleotide Resolution Using Ribosome Profiling. *Science* **324**, 218–223 (2009).

CHAPTER 8

SUMMARY

SAMENVATTING

RESUMEN

SUMMARY

Alternative splicing is a crucial step in gene expression that expands the coding potential of the human genome. By including or excluding particular exons, multiple RNA sequences can be created from a single gene. In the heart, this process is essential to create the cardiac isoforms that give mechanical, electrical, and metabolic characteristics to cardiomyocytes. Through cardiac development and disease, changes in splicing factors adapt the splicing program of cardiomyocytes to adapt heart function. This thesis examines the mechanisms controlling alternative splicing in the heart.

In **chapter 2,** we studied the cardiac-enriched splicing factor quaking (QKI) in the developing and adult heart. To do so, we employed the Cre-Lox system to generate two cardiomyocyte-specific knock-out mouse models of QKI. Cardiomyocyte-specific deletion of QKI was embryonically lethal (E14.5). Adult mice with tamoxifen-inducible QKI deletion rapidly developed heart failure, with severe disruption of sarcomeres. RNA sequencing revealed that QKI regulates the alternative splicing of over 1000 genes, including sarcomere and cytoskeletal components, calcium handling regulators, and (post-)transcriptional factors. We found that many of these splicing changes corresponded to the loss of muscle-specific isoforms in the heart in the absence of QKI. Forced overexpression of QKI in cultured rat ventricular myocytes increased the expression of some of these isoforms and enhanced their contractility. We concluded that QKI is an important regulator of the muscle-specific alternative splicing program in embryonic and adult hearts.

In **chapter 3**, we investigated the role of QKI in the regulation of circular RNAs (circRNAs) formation in the heart. By analyzing the QKI knock-out mouse model that we established in chapter 2, we found that 17% of the circRNAs expressed in the mouse heart are differentially expressed in the absence of QKI. The results also showed a connection between linear splicing and back-splicing, as 58% of the QKI-regulated circRNAs were derived from mRNAs that underwent QKI-dependent splicing. In addition, we compared our results with the circRNAs regulated by another major splicing factor expressed in the heart, RBM20. We compared the QKI KO model with an RBM20 KO model and we found that QKI and RBM20 regulate the formation of a distinct but partially overlapping set of circRNAs. Strikingly, virtually all *Ttn*-derived circRNAs controlled by QKI and RBM20 were regulated in an opposite manner. Our study pinpoints QKI as a central regulator of circRNA formation in the heart.

In **chapter 4**, we aimed to get a get a broader picture of alternative splicing regulation in the heart by comparing splicing factor knock-out mouse models reported in literature in the last decades. We re-evaluated existing RNA-sequencing data from eight mouse models where splicing factors were genetically deleted (HNRNPU, MBNL1/2, QKI, RBM20, RBM24,

RBPMS, SRSF3, SRSF4). Our analysis revealed a significant overlap between the splicing networks of these factors, with some key splicing events requiring the action of multiple splicing factors simultaneously (i.e. *Camk2d*, *Ryr2*, *Tpm1*, *Tpm2*, *Pdlim5*). The highest of overlap was found between the splicing networks of MBNL, QKI, and RBM24. Additionally, our analysis of RNA-sequencing from a large cohort of 128 heart failure patients showed that the expression levels of MBNL1, QKI, and RBM24 correlated with changes in splicing of downstream targets, suggesting that these splicing factors may play a role in heart failure.

In **chapter 5**, we turned our attention to an unusual class of introns, namely minor or U12-dependent introns. Although minor introns are enriched in specific gene families crucial for cardiomyocyte function (e.g. voltage-gated sodium and calcium channels), the relevance of minor splicing in the heart is still unknown. In this chapter, we knocked down the essential minor spliceosome component U6atac in neonatal rat ventricular myocytes. Loss of U6atac caused the retention of minor introns, including those within *Scn5a* and *Cacna1c*. This led to decreased levels of $Na_v1.5$ and $Ca_v1.2$ proteins, and to reduced sodium and L-type calcium currents. In conclusion, we showed that minor intron splicing can modulate the expression and function of voltage-dependent ion channels in cardiomyocytes, which may be relevant in disease.

In **chapter 6**, we commented on a study about the role of the long non-coding RNA (lncRNA) triadin-antisense (*Trdn-as*) in the regulation of cardiac splicing. lncRNAs are a heterogeneous family of transcripts with versatile and broad functions, including the regulation of alternative splicing. The lncRNA *Trdn-as* expression correlates with the expression of the spliced isoforms of triadin, a molecular component of the calcium release unit of the cardiomyocyte. By creating a *Trdn-as* knockout mouse model and performing *in vitro* experiments, the role of *Trdn-as* as regulator of triadin splicing was uncovered.

In conclusion, the results presented in this thesis expand our comprehension of the role of alternative splicing in the heart and highlight its significance as a regulatory mechanism of cardiac function.

NEDERLANDSE SAMENVATTING

Alternatieve splicing is een cruciale stap in genexpressie. Het is tevens een mechanisme dat verantwoordelijk is voor het vergroten van het coderingspotentieel van het menselijk genoom. Door bepaalde exonen op te nemen of uit te sluiten in het mRNA, kunnen uit één enkel gen meerdere RNA-sequenties ontstaan. In het hart is dit proces essentieel om eiwit isovormen te creëren die de mechanische, elektrische en metabole eigenschappen van cardiomyocyten vormgeven. Tijdens de ontwikkeling, maar ook als gevolg van ziekte van het hart, wordt door aanpassingen in de expressie van splicing factoren het splicing programma van cardiomyocyten aangepast. Dit proefschrift onderzoekt de mechanismen die ten grondslag liggen aan alternatieve splicing regulatie in het hart.

In **hoofdstuk 2** hebben we de rol van de splicing factor quaking (QKI) onderzocht in het ontwikkelende en volwassen hart. Met behulp van het Cre-Lox systeem hebben we twee cardiomyocyt-specifieke knock-out muismodellen van QKI gegenereerd. Cardiomyocyt-specifieke deletie van QKI was lethaal tijdens de embryonale ontwikkeling (E14,5). Volwassen muizen met een tamoxifen-induceerbare QKI-deletie ontwikkelden snel hartfalen, met ernstige verstoring van sarcomeren. RNA-sequencing liet vervolgens zien dat QKI alternatieve splicing van meer dan 1000 genen regelt, waaronder sarcomeer- en cytoskeletale componenten, calcium handling regulatoren en (post-)transcriptionele factoren. Het bleek dat veel van deze QKI geïnduceerde splicing veranderingen overeenkwamen met het verlies van spier-specifieke eiwit isovormen. Overexpressie van QKI in gekweekte ventriculaire neonatale myocyten van ratten verhoogde de expressie van sommige van deze isovormen en verhoogde de contractiliteit van de cellen. We concluderen dat QKI een belangrijke regulator is van het spier-specifieke alternatieve splicing-programma in embryonale en volwassen harten.

In **hoofdstuk 3** onderzochten we de rol van QKI bij de vorming van circulaire RNAs (circRNA's) in het hart. Door RNA-sequencing en bioinformatische analyse van het QKI knock-out muismodel dat we in hoofdstuk 2 hebben gegenereerd, vonden we dat 17% van de circRNA's die in het muizenhart tot expressie komen, differentieel tot expressie komen in de afwezigheid van QKI. De resultaten toonden verder een verband aan tussen lineaire splicing en back-splicing, aangezien 58% van de door QKI gereguleerde circRNA's afkomstig waren van mRNA's die QKI-afhankelijke splicing ondergingen. Daarnaast hebben we onze resultaten vergeleken met de circRNA's die gereguleerd worden door een andere belangrijke splicing factor die in het hart tot expressie komt, namelijk RBM20. Vergelijking van QKI en RBM20 KO modellen liet zien dat QKI en RBM20 de vorming van een verschillend, maar gedeeltelijk overlappende set circRNA's regelen. Opvallend is dat vrijwel alle van *Ttn* afgeleide circRNA's die door QKI en RBM20 worden gereguleerd, op een tegengestelde manier worden

gereguleerd. Onze studie wijst QKI aan als een centrale regulator van circRNA-vorming in het hart.

In **hoofdstuk 4** hebben wij getracht een breder beeld te krijgen van alternatieve splicing regulatie in het hart, door splicing factor knock-out muismodellen te vergelijken. Hiertoe hebben we bestaande RNA-sequencing data geanalyseerd van acht muismodellen waarin splicing factoren genetisch waren verwijderd (HNRNPU, MBNL1/2, QKI, RBM20, RBM24, RBPMS, SRSF3, SRSF4). Uit onze analyse bleek een aanzienlijke overlap aanwezig te zijn tussen de splicing netwerken van deze factoren (bijv. *Camk2d*, *Ryr2*, *Tpm1*, *Tpm2*, *Pdlim5*). De grootste overlap werd gevonden tussen de splicing-netwerken van MBNL, QKI en RBM24. Bovendien bleek uit RNA-sequencing analyse van een groot cohort van 128 patiënten met hartfalen, dat de expressieniveaus van MBNL1, QKI en RBM24 gecorreleerd waren met veranderingen in splicing van downstream targets, wat suggereert dat deze splicing factoren een rol kunnen spelen bij hartfalen.

In **hoofdstuk 5** hebben we onze aandacht gericht op een ongebruikelijke klasse van introns, namelijk de zogenaamde 'minor' of 'U12-afhankelijke' introns. Hoewel minor introns verrijkt zijn in specifieke families van genen (bv. natrium- en calciumkanalen), is de relevantie van minor splicing in het hart nog onbekend. In dit hoofdstuk hebben we de essentiële minor spliceosome component U6atac uitgeschakeld in gekweekte neonatale ventriculaire ratten myocyten. Verlies van U6atac veroorzaakte retentie van minor introns, waaronder die binnen het transcript van *Scn5a* en *Cacna1c*. Functioneel leidde dit tot lagere niveaus van $Na_v1.5$ en $Ca_v1.2$ eiwitten, en tot verminderde natrium- en L-type calciumstromen. Concluderend hebben wij aangetoond dat minor intron splicing de expressie en functie van ionenkanalen in cardiomyocyten kan moduleren, hetgeen relevant kan zijn bij ziekte.

In **hoofdstuk 6** hebben we commentaar gegeven op een studie waarin de rol van het long non-coding RNA (lncRNA) triadin-antisense (*Trdn-as*) in de regulering van cardiale splicing onderzocht is. LncRNA's behoren tot een heterogene familie van transcripten met veelzijdige functies, waaronder de regulering van alternatieve splicing. De expressie van de *Trdn-as* blijkt te correleren met de expressie van bepaalde splice isovormen van triadine. Door het creëren van een *Trdn-as* knock-out muismodel en het uitvoeren van *in vitro* experimenten werd de rol van Trdn-as als regulator van triadine splicing blootgelegd.

Concluderend kan worden gesteld dat de resultaten beschreven in dit proefschrift ons begrip van de rol van alternatieve splicing voor een goed functionerend hart vergroot hebben.

RESUMEN

El empalme alternativo de genes es un proceso crítico en la expresión génica que amplía la capacidad de codificación del genoma humano. Mediante la inclusión o exclusión selectiva de exones, el empalme alternativo es capaz de crear múltiples secuencias de ARN a partir de un solo gen. En el corazón, este proceso es fundamental para crear las isoformas cardíacas que otorgan las características mecánicas, eléctricas y metabólicas a los cardiomiocitos (las células del corazón). A lo largo del desarrollo y la enfermedad cardíaca, el empalme alternativo adapta las isoformas expresadas en el corazón para modular su función. Esta tesis se centra en examinar los mecanismos que controlan el empalme alternativo en el corazón.

En el **capítulo 2** estudiamos el factor de empalme Quaking (QKI), el cual se encuentra altamente expresado en el corazón en desarrollo y adulto. Para llevar a cabo esta investigación, generamos dos modelos de ratón knock-out basados en el sistema Cre-Lox con el objetivo de eliminar QKI de manera específica en los cardiomiocitos. La deleción de QKI resultó letal durante el desarrollo embrionario (E14.5). En ratones adultos, la deleción inducida de QKI por tamoxifeno provocó insuficiencia cardíaca, con una grave alteración de los sarcómeros. A través de la secuenciación de ARN, se descubrió que QKI regula el empalme alternativo de más de 1000 genes, incluyendo componentes del sarcómero y del citoesqueleto, reguladores del control del calcio y factores (post)transcripcionales. Una gran parte de los cambios observados en ausencia de QKI se correspondieron con la pérdida de isoformas específicas del músculo cardiaco. Además, la sobreexpresión de QKI en miocitos ventriculares de rata *in vitro* incrementó la expresión de algunas de estas isoformas y aumento su contractilidad. Concluimos que QKI es un regulador esencial del programa de empalme alternativo del corazón.

En el **capítulo 3** investigamos el papel de QKI en la regulación de la formación de ARN circulares (ARNcirc) en el corazón. Al analizar el modelo de ratón knock-out establecido en el capítulo 2, encontramos que el 17 % de los ARNcirc expresados en el corazón del ratón se expresan de manera diferencial en ausencia de QKI. Los resultados también mostraron una conexión entre el empalme lineal y el empalme inverso, ya que el 58 % de los ARNcirc desregulados se derivaron de ARNm con otros defectos de empalme causados por la ausencia de QKI. También comparamos los ARNcirc controlados por QKI con los controlados por otro importante factor de empalme crucial para el corazón, RBM20. Al comparar el modelo KO de QKI con un modelo KO de RBM20 descubrimos que QKI y RBM20 regulan la formación de un conjunto distinto pero parcialmente superpuesto de ARNcirc. Sorprendentemente, prácticamente todos los ARNcirc derivados del gen titina (TTN) resultaron ser controlados por QKI y RBM20 manera opuesta. Nuestro estudio identifica a QKI como un regulador central de la formación de ARNcirc en el corazón.

En el **capítulo 4** buscamos obtener una perspectiva más amplia sobre la regulación del empalme alternativo en el corazón. Para ello, comparamos varios modelos de ratones knock-out de factores de empalme que se han descrito en la literatura científica durante las últimas décadas. Reevaluamos los datos de secuenciación de ARN de ocho modelos de ratones en los que se eliminaron genéticamente los factores de empalme HNRNPU, MBNL1/2, QKI, RBM20, RBM24, RBPMS, SRSF3 y SRSF4. Nuestro análisis reveló una superposición significativa entre las redes de empalme de estos factores. Algunos exones clave para la función cardiaca mostraron requerir la acción de múltiples factores de empalme de manera simultánea, como los presentes en *Camk2d*, *Ryr2*, *Tpm1*, *Tpm2* y *Pdlim5*. La mayor superposición se encontró entre las redes de empalme de MBNL, QKI y RBM24. Además, el análisis basado en la secuenciación de ARN de una cohorte de 128 pacientes con insuficiencia cardíaca mostró que los niveles de expresión de MBNL1, QKI y RBM24 correlacionan con el empalme alternativo de los exones controlados en ratón, lo cual sugiere que estos factores de empalme puedan desempeñar un papel en la insuficiencia cardíaca.

En el **capítulo 5** redirigimos nuestra atención a una clase inusual de intrones, a saber, los intrones menores o dependientes de U12. Aunque los intrones menores están más presentes en familias de genes cruciales para la función de los cardiomiocitos (p. ej., canales de sodio y calcio dependientes de voltaje), aún se desconoce su relevancia en el corazón. En este capítulo, inhibimos el componente del spliceosoma menor U6atac en los miocitos ventriculares de rata. La pérdida de U6atac provocó la retención de intrones menores, incluidos los de *Scn5a* y *Cacna1c*. Esto redujo los niveles de proteínas Nav1.5 y Cav1.2 y las corrientes iónica de sodio y calcio tipo L. En conclusión, demostramos que el empalme de intrones menores puede modular la expresión y la función de los canales iónicos dependientes de voltaje en los cardiomiocitos, lo que puede ser relevante en la enfermedad cardiaca.

En el **capítulo 6** comentamos un estudio sobre el papel del ARN largo no codificante (ARNlnc) triadina antisentido (*Trdn-as*) en la regulación del empalme cardíaco. Los ARNlnc son una familia heterogénea de transcritos con una gran variedad de funciones, entra las que se incluye la regulación del empalme alternativo. La expresión de *Trdn-as* se correlaciona con la expresión de las isoformas de triadina, un componente molecular de la unidad de liberación de calcio del cardiomiocito. Mediante la creación de un modelo de ratón knock-out para *Trdn-as* y la realización de experimentos *in vitro*, los autores demostraron el papel de *Trdn-as* como regulador del empalme de triadina.

En conclusión, los resultados presentados en esta tesis contribuyen a nuestra comprensión del empalme alternativo en el corazón y destacan su importancia como un mecanismo fundamental en la regulación de la función cardíaca.

APPENDIX

PHD PORTFOLIO

PhD student: Pablo Montañés Agudo
PhD period: October 2018 - March 2023
Promotor: prof. dr. Y.M. Pinto
Co-promotor: dr. E.E.J.M. Creemers

		ECTS
1. PhD TRAINING		
Courses		
2019	Introduction to Laboratory Animal Science (Doctoral School)	1.5
2019	Species-specific course on mice and rats (Doctoral School)	1.5
2019	Advanced qPCR (Doctoral School)	1.1
2019	Scientific writing (Experimental Cardiology)	0.3
2019	Practical biostatistics (Doctoral School)	0.6
2020	Project Management (Doctoral School)	0.6
2020	Mouse Morphology, Function and Genetics (Doctoral School)	1.5
2022	Basics in Electrophysiology (Experimental Cardiology)	0.3
Seminars, workshops and master classes		
2018 - 2023	Weekly department meeting (Experimental Cardiology)	6.0
2018 - 2023	Weekly progress report	6.0
2018 - 2020	Weekly Journal Club (Experimental Cardiology)	2.0
2021	Master class by C. Bezzina: Basics of GWAS (Experimental Cardiology)	0.1
2021	Master class by Y. M. Pinto: General principles of heart failure (Experimental Cardiology)	0.1
Conferences		
2019	EMBO/EMBL Symposium: The Non-Coding Genome (Heidelberg Germany) *Attendee*	0.9
2019	10th Rembrandt Symposium (Noordwijkerhout) *Poster presentation*	0.3
2020	25th Annual Meeting of the RNA Society (online) *Poster presentation*	0.9
2020	11th Rembrandt Symposium (online) *Poster presentation*	0.3
2021	Dutch German Joint Meeting (online) *Poster presentation*	0.3
2021	Annual Amsterdam Cardiovascular Sciences symposium, Amsterdam (The Netherlands) *Oral presentation*	0.3

PhD portfolio (continued)

		ECTS
2021	12th Rembrandt Symposium (online) *Oral presentation*	0.3
2022	Dutch RNA conference (Leiden) *Attendee*	0.3
2022	2nd Olympiad in Cardiovascular Medicine International Symposium on Experimental & Clinical Cardiology (Heraklion, Greece) *Poster presentation*	1.1
2022	XXIV World Congress International Society for Heart Research (Berlin, Germany) *Poster presentation*	1.1
2022	6th DCVA/NLHI Translational Cardiovascular Research Meeting (Utrecht) *Poster presentation*	0.3
2022	Amsterdam Cardiovascular Sciences symposium: Heart failure and Arrhythmias (Amsterdam) *Oral presentation*	0.1
2. TEACHING		
2021	MSc Internship - Eva Schepers (MSc Biomedical sciences, UvA) Project: Quaking regulates cardiac sarcomere maintenance by controlling striated muscle-specific splicing.	2.0
3. PARAMETERS OF ESTEEM		
Grants		
2022	ISHR Travel grant award	

4. LIST OF PUBLICATIONS

Montañés-Agudo, Pablo, Yigal M. Pinto, and Esther E. Creemers. "Splicing factors in the heart: Uncovering shared and unique targets." Journal of Molecular and Cellular Cardiology (2023): in press

Montañés-Agudo, Pablo, Simona Aufiero, Eva N. Schepers, Ingeborg van der Made, Lucia Cócera-Ortega, Auriane C. Ernault, Stéphane Richard et al. "The RNA-binding protein QKI governs a muscle-specific alternative splicing program that shapes the contractile function of cardiomyocytes. *Cardiovascular Research* (2023).

Montañés-Agudo, Pablo, and Yigal M. Pinto. "Triadin-Antisense: An lncRNA in the Backstage of Cardiac Alternative Splicing. *Circulation* 146, no. 9 (2022): 715-717.

PhD portfolio (continued)

Ernault, Auriane C., Arie O. Verkerk, Jason D. Bayer, Kedar Aras, **Pablo Montañés-Agudo**, Rajiv A. Mohan, Marieke Veldkamp et al. "Secretome of atrial epicardial adipose tissue facilitates reentrant arrhythmias by myocardial remodeling. *Heart rhythm* 19, no. 9 (2022): 1461-1470.

Ernault, Auriane C., Makiri Kawasaki, Benedetta Fabrizi, **Pablo Montañés-Agudo**, Shirley Amersfoorth, Rushd FM Al-Shama, Ruben Coronel, and Joris R. De Groot. "Knockdown of Ift88 in fibroblasts causes extracellular matrix remodeling and decreases conduction velocity in cardiomyocyte monolayers. *Frontiers in Physiology* (2022): 2442.

Montañés-Agudo, Pablo, Simona Casini, Simona Aufiero, Auriane C. Ernault, Ingeborg van der Made, Yigal M. Pinto, Carol Ann Remme, and Esther E. Creemers. "Inhibition of minor intron splicing reduces Na+ and Ca2+ channel expression and function in cardiomyocytes. *Journal of Cell Science* 135, no. 1 (2022): jcs259191.

Submitted

Montañés-Agudo, Pablo, Ingeborg van der Made, Simona Aufiero, Anke J. Tijsen, Yigal M. Pinto, and Esther E. Creemers. QKI regulates back-splicing in cardiomyoyctes

CONTRIBUTING AUTHORS

In alphabetical order

Simona Aufiero	Amsterdam UMC, location University of Amsterdam, Departments of Experimental Cardiology, and Clinical Epidemiology, Biostatistics and Bioinformatics; Amsterdam (The Netherlands)
Simona Casini	Amsterdam UMC, location University of Amsterdam, Department of Experimental Cardiology; Amsterdam (The Netherlands)
Vincent M. Christoffels	Amsterdam UMC, location University of Amsterdam, Department of Medical Biology; Amsterdam (The Netherlands)
Lucía Cócera-Ortega	Amsterdam UMC, location University of Amsterdam, Department of Experimental Cardiology; Amsterdam (The Netherlands)
Esther E. Creemers	Amsterdam UMC, location University of Amsterdam, Department of Experimental Cardiology; Amsterdam (The Netherlands)
Auriane C. Ernault	Amsterdam UMC, location University of Amsterdam, Department of Experimental Cardiology; Amsterdam (The Netherlands)
Diederik W.D. Kuster	Amsterdam UMC, location Vrije Universiteit Amsterdam, Physiology; Amsterdam (The Netherlands)
Ingeborg van der Made	Amsterdam UMC, location University of Amsterdam, Department of Experimental Cardiology; Amsterdam (The Netherlands)
Yigal M. Pinto	Amsterdam UMC, location University of Amsterdam, Department of Experimental Cardiology; Amsterdam (The Netherlands)
Carol Ann Remme	Amsterdam UMC, location University of Amsterdam, Department of Experimental Cardiology; Amsterdam (The Netherlands)
Stéphane Richard	McGill University, Department of Oncology and Departments of Biochemistry, Human Genetics and Medicine; Montréal (Canada)
Eva N. Schepers	Amsterdam UMC, location University of Amsterdam, Department of Experimental Cardiology; Amsterdam (The Netherlands)
Anke J. Tijsen	Amsterdam UMC, location University of Amsterdam, Department of Experimental Cardiology; Amsterdam (The Netherlands)

AUTHOR CONTRIBUTIONS

Chapter 2 - The RNA-binding protein QKI governs a muscle-specific alternative splicing program that shapes the contractile function of cardiomyocytes

Pablo Montañés-Agudo	Study design, data acquisition, analysis, interpretation, writing manuscript and revision of the manuscript.
Simona Aufiero	Data analysis, interpretation, revision and approval of the manuscript.
Eva N. Schepers	Data acquisition, analysis, interpretation
Ingeborg van der Made	Data acquisition, analysis, provided experimental resources, revision and approval of the manuscript.
Lucia Cócera-Ortega	Study design, analysis, provided experimental resources, revision and approval of the manuscript.
Auriane C. Ernault	Data acquisition, analysis, provided experimental resources, revision and approval of the manuscript.
Stéphane Richard	Provided experimental resources, revision and approval of the manuscript.
Diederik W.D. Kuster	Provided experimental resources, revision and approval of the manuscript.
Vincent M. Christoffels	Provided experimental resources, revision and approval of the manuscript.
Yigal M. Pinto	Study design, interpretation, provided experimental resources, revision and approval of the manuscript.
Esther E. Creemers	Study design, data acquisition, analysis, interpretation, provided experimental resources, writing, revision and approval of the manuscript.

Chapter 3 - QKI regulates back-splicing in cardiomyocytes

Pablo Montañés-Agudo	Study design, data acquisition, analysis, interpretation, writing manuscript and revision of the manuscript.
Ingeborg van der Made	Data acquisition, analysis, provided experimental resources, revision and approval of the manuscript.
Simona Aufiero	Data analysis, interpretation, revision and approval of the manuscript.

Chapter 3 - (continued)

Anke J. Tijsen	Provided experimental resources, revision and approval of the manuscript.
Yigal M. Pinto	Study design, interpretation, provided experimental resources, revision and approval of the manuscript.
Esther E. Creemers	Study design, data acquisition, analysis, interpretation, provided experimental resources, writing, revision and approval of the manuscript.

Chapter 4 - Insights into alternative splicing in the heart from knockout mouse models

Pablo Montañés-Agudo	Study design, data acquisition, analysis, interpretation, writing manuscript and revision of the manuscript.
Yigal M. Pinto	Data interpretation, revision and approval of the manuscript.
Esther E. Creemers	Study design, data acquisition, data analysis, interpretation, writing, revision and approval of the manuscript.

Chapter 5 - Inhibition of minor intron splicing reduces Na^+ and Ca^{2+} channel expression and function in cardiomyocytes

Pablo Montañés-Agudo	Study design, data acquisition, analysis, interpretation, writing and revision of the manuscript.
Simona Casini	Study design, data acquisition, analysis, interpretation, revision and approval of the manuscript.
Simona Aufiero	Data analysis, interpretation, revision and approval of the manuscript.
Auriane C. Ernault	Data acquisition, analysis, provided experimental resources, revision and approval of the manuscript.
Ingeborg van der Made	Data acquisition, analysis, provided experimental resources, revision and approval of the manuscript.
Yigal M. Pinto	Study design, interpretation, provided experimental resources, revision and approval of the manuscript.

Chapter 5 - (continued)

Carol Ann Remme	Study design, interpretation, provided experimental resources, revision and approval of the manuscript.
Esther E. Creemers	Study design, data acquisition, analysis, interpretation, provided experimental resources, writing, revision and approval of the manuscript.

Chapter 6 - Triadin-Antisense: a lncRNA in the Backstage of Cardiac Alternative Splicing

Pablo Montañés-Agudo	Writing and revision of the manuscript.
Yigal M. Pinto	Revision and approval of the manuscript.

ABOUT THE AUTHOR

Pablo was born on March 9th, 1993, in the city of Zaragoza, Spain, to his parents, José Antonio and María Jesus. After completing his primary and secondary education at Zalfonada public school and Avempace high school, Pablo decided to pursue a career in biological sciences. He enrolled at the University of Zaragoza to study a Bachelor's degree in Biotechnology, for which he graduated with honors in 2015. Throughout his undergraduate studies, he completed multiple internships in various laboratories at the University of Zaragoza and at the Spanish National Center for Cardiovascular Research in Madrid, which ignited his curiosity in understanding the molecular mechanisms underlying human disease.

In 2016, Pablo moved to Madrid to pursue a Master's degree in Genetics and Cell Biology at the Autonomous University of Madrid, in conjunction with Complutense University and Alcalá de Henares University. He completed his Master's thesis at the Spanish National Cancer Research Center, where he studied cell cycle dysregulation during tumorigenesis. Afterwards, he moved to Germany to continue his research in the field of oncology at the Max Planck Institute of Molecular Physiology and Duisburg-Essen University, investigating the role of cell proteases and chaperones in cancer.

Eventually, Pablo decided to shift his research focus back to the cardiovascular field. In 2018, he moved to The Netherlands to pursue a Ph.D. at the department of Experimental Cardiology at the Amsterdam Academic Medical Center, supervised by Dr. Esther E. Creemers and Prof. Dr. Yigal M. Pinto. His research focused on RNA splicing in the heart during development and disease. The results of his investigations are presented in this thesis.

ACKNOWLEDGMENTS

I wish to express my sincere gratitude to all the people who have supported me throughout the course of this thesis. Pursuing a PhD can be a challenging journey, but during these years, I have met many wonderful people who helped me overcome the difficulties and taught me valuable lessons about life and science. They also made my stay in Amsterdam an unforgettable and truly enjoyable experience.

First, I would like to expressing my special thanks to my promotors prof. dr. Yigal Pinto and dr. Esther Creemers.

Dear **Yigal**, thank you for welcoming me into your lab and for supporting me throughout these years. I learned a lot about science and medicine from you. Your valuable suggestions have been crucial to the success of my projects. Your straightforward thinking and vision for new ideas are truly inspiring. You embody what a wise man once said: "If you're going to try to embrace new worlds, you must try to embrace new ideas." Also, thanks for being the coolest supervisor ever. I will miss DJ YP at the parties.

Dear **Esther**, thank you for the invaluable guidance and for your support during these years. You have been a true mentor to me, teaching me many important lessons about research and academia. Whether the experiments were going well or not, you have always been there, providing new ideas, motivating me, and even lending a hand. I have enjoyed going to your office every 30 minutes to ask you questions, discuss science and papers, or just have a chat with you. I will miss that a lot. Let's not forget the enjoyable moments we had outside of the lab, specially at conferences and parties. I will miss going through poster sessions together and discuss science while enjoying a beer or some raki. I feel fortunate to have enjoyed your mentorship and friendship during these years. Thank you once again for everything, Esther.

I would also like to express my sincere appreciation to the members of my doctoral committee for their critical evaluation of this thesis. Thanks prof. dr. **Vincent Christoffels**, prof. dr. **Joris de Groot**, prof. dr. **Eva van Rooij**, dr. **Elisabeth Lodder**, prof. dr. **Anton Jan van Zonneveld** and dr. **Rick Wansink** for generously giving your time and effort.

Next, I want to thank my awesome paranymphs, **Dylan** and **Giovanna**. **Dylan**, my office neighbor and partner in crime, thank you for your friendship and for being my wingman in this PhD. You have always been there with your unconditional help, both inside and outside the lab. We have had so much fun together that I can't even recall everything - from taking siestas between talks in Crete to dancing the "Yigal move" at parties. You even made me suffer by dragging me to spinning, but I forgive you because you're a good friend. **Giovanna**,

Giovanissima, thank you for your friendship and your fiery spirit. It has been awesome to share this PhD journey with you. I will never forget all the nice aperitivos and dinners we had together. You showed me the way of La Dolce Vita, accompanied by sparkling Aperol Spritz and sweet Frangelico. Your sense of justice and your complaining skills are also outstanding - you would make a great lawyer! I wish both of you the best of luck finishing the last sprint in your PhDs. I'm looking forward to having dinner soon with Dr. D. de Vries and Dr. G. Nasilli.

I also want to give many thanks to my colleagues in the YP group. **Lucia**, muchas gracias por tu apoyo y amistad estos años. Aún recuerdo la primera vez que hable contigo cuando estaba haciendo la entrevista en el lab. Te convertiste inmediatamente en mi amiga y siempre fuiste un gran apoyo moral y científico durante estos años. Con todo tu esfuerzo te has ganado el puesto de co-promotora de mi corazón. Voy a echar de menos todos los buenos momentos que hemos pasado juntos en el lab, de conferencias, de fiesta y en mil sitios más. Te quiero un montón y te deseo lo mejor en tus aventuras de postdoc. **Anke**, thank you for all the scientific discussions and your valuable feedback. You have been a great help in brainstorming my projects during our meetings and you have always offer to help whenever you could. **Simona A.**, thanks for your hard work. Your wonderful bioinformatics skills have played a significant role in this thesis. Without your contribution, Esther and I would have been lost and this work would not have been possible. **Inge**, thank you for all of your support. Not only are you a black belt in Judo, but also in the lab. You have assisted me greatly with my experiments and taught me many lab techniques. I also had a lot of fun sharing our weird sense of humor together and fighting together in the corridor. **Eva**, it was a pleasure to have you in the lab for your master's project. You are hard worker and smart, and you became an integral part of the team very quickly. I thank you because I learned a lot while working with you and you provided many valuable insights for the QKI project. I wish you all the best in your future career. **Daria**, thank you for all your energy. You are an unstoppable woman, and I foresee a great PhD journey for you. Also, thank you for all the delicious sweets (including vodka) you brought to us all the time. To the (not so new) fresh blood in the lab: **Najoua**, **Robin**, **Anoek**, and **Dante**, may your experiments and life be as successful as a Western blot that runs perfectly on the first try with clear and significant bands. Also, cheers to the people who already left the lab, **Yolan**, **Federica**, and **Viviana**.

Cheers to my lab fellows of Experimental Cardiology. My PhD would not have been the same without all of you! **Benedetta**, fell you good? You are a truly good friend, and I really enjoy doing things together with you. By the way, I still think that you were Operator 10 all the time, but let's forget about it. Just give me a call whenever you want to play tennis and trivial, and cook some delicious fresh pasta together. **Lixia**, my PhD sister, we both started our PhD on the very same day, and we are finishing now. I am super happy that we both made it! I

am going to miss doing hotpot and preparing dumplings with you. But get ready because as soon as I can, I will visit you in China. **Caroline**, the coolest person in the lab. I have always been so impressed by how creative and organized you are, and I have always laughed so hard whenever we are together. Never forget our delicious Frühstück in Berlin, the "catchy-hand" dance move, and… PEEPAAAS!!! **Jaël**, a woman of action. We had so many adventures in Berlin, roller coasters, and even bouldering. I send you my blessings for good fortune with patch-clamping. **Molly**, the sunshine of the office, I am going to miss your over-enthusiastic good mornings. They really uplifted my mood every morning! And watch out with your neurons. **Jeanne**, since you left no one else starts a party as you do. It was wonderful to share so many funny moments with you and to be beer-AIOs together. **Mathilde**, your combination of a fantastic sense of humor, elegance, and a touch of sass is wonderful. Thank you for all the scientific (and gossip) knowledge you've shared. **Madelief**, you irradiate such good vibes and make such good questions. Magnificent!. **Fern**, pues eres bien chida y me lo he pasado padre contigo. Ándale y que te vaya bonito! **Dom**, my deficient English skills and your strong accent impeded the proper communication between us. But it was great having you around! **Alex**, you are the archetype of a gifted scientist full of curiosity. I will miss our philosophical conversations about water and the meaning of life. **Christian**, eres un tipo genial y te deseo lo mejor. And also thanks to **Gerard**, **Joost**, **Michele**, **Makiri**, **Pouja**, **Rushd**, **Edwin, Karolina, Raquel** and all the rest.

Many thanks to all the senior scientists in the lab. It really takes a village to raise a PhD, and you do so with your scientific expertise, your constructive criticism and your support. Thanks **Ruben**, **Bas**, **Veronique**, **Marieke**, **Connie**, **Roddie**, **Isabella**, and again, to **Elisabeth** and **Joris**. Special thanks to **Carol Ann** and **Simona**, because I really enjoyed working with you on minor introns and you taught me so many thinks about of electrophysiology and patch-clamp. Many thanks to the technicians. You are the fairy godmothers in the lab for all of us and you get the real job done. Thanks **Lisanne**, **Tanja**, **Leander**, and **Shirley**. An immense hug to **Marleen**, for your kindness and unconditional support to all the PhDs.

From the Medical Biology department, I want to thank **Vincent C.** for his support in the QKI paper and his contribution to my doctoral committee. Also to **Corrie**, because you taught me everything about histology and about how to get the perfect 4-chamber view of the heart. Also cheers to **Bjarke**, **Phil**, **Alex**, **Maurice**, **Quinn**, **Jettie**, **Monika**, **Rocco**, **Lieve**, **Michiel**, **Arnie**, **Max, Jianan**, **Geert**, **Karel**, **Lianne**, **Harsha**, **Alexandra**, **Jesus**, and all the rest.

I also want to send my love to my wonderful friends in The Netherlands. **Noelia**, gracias por enseñarme a sacar embriones, a bailar y a buscar trabajo. ¡Olé tú y olé Béjar! **Pedro**, gracias por enseñarme a hacer cerveza. A ver si nos llega pronto la jubilación para hacer más e irnos

juntos a andar por el monte y ver obras. Recuerdos para **Erik**. **Fransisca**, one of my first friends in the lab and also in Amsterdam. I will never forget eating delicious spicy food with you and blowing balloons together. Best wishes for you and **Daniel**. **Vincent P**, anywhere is hilarious wherever you are. The lab was never as funny as when you were around. Regards for **Ally** and the kids. Merci **Sandra**, d'être la personne la plus cool de cette planète. J'adore être malade avec toi et passer notre temps à faire des conneries, à regarder des films d'horreur ou à jouer aux cochons. Cheers to the French gang **Charlotte**, **Gueo**, **Elisabeth**, **Thomas**, **Marissa**, **Nico**, **Inch** and **Yohan**. Y muchas gracias a mis compañeros de CENL por hacer de Holanda un poco más como España. Gracias **Rodri** por ser un crack y por todo tu trabajo. Sin ti estaríamos perdidos. Y también para **Andrea**, **Paula**, **Jennifer**, **Carlos**, **Aitor** y a todos los demás.

Amor incondicional a mis amigos de Zaragoza. A mis amigos de toda la vida: **Jessi**, **Jorge**, **Papu** (¿eres tú mejor?), **Marta**, **Alex**, **Silvia**, **Elena**, **Laura**, **Adri**, **María**, os echo mucho de menos y … ¡Avempace siempre, leré, leré! A mis compañeros de biotecnología, con los que pase un años estupendos en la Universidad. **Sonia**, **Sara**, **Guille**, **Elena**, **Bea** y **Ángel**, a ver cuándo quedamos para echarnos la última en el Javis.

Gracias a mi hermano **Guille**, por soportarme tantos años y ayudarme en asuntos de diseño. Recuerdos a **toda mi familia**, porque aunque estéis en la distancia, os llevo siempre conmigo en el corazón. Muchos besos para mi **tía Chon**; para mis **tíos Carlos** y **Raquel**; para mis primos **Javier**, **Marina**, e **Irene**, y también **Carlos, Carlitos, Álvaro y Ana;** para mi tíos **Luis** y **Angelines**; para mi prima **Celia**, y para **Natalia** y **Judith**; para mi prima **Marta**, y para **Luis**, **Andrea** y **Sofía**; para mis tíos **Jesús** y **Nuria**, y para **Ángela** y **Laura**; para mi tío **Manolo** y para **Manu**, **Clara** y **Alba**; y para los que ya no están, mi tía **Elena**, mi tío **Miguel** y mis abuelos **Goyo**, **Pili**, **Ceci** y **Pepe**.

Merci également à ma famille française. Bisous à **Marie**, **Paulette**, **Louis**, et à tous les autres.

El mayor agradecimiento es para **mis padres**, y por eso esta tesis se la dedico a ellos. **Mamá**, **papá**, me lo habéis dado todo. Siempre habéis creído en mí y me habéis apoyado en los buenos y en los malos momentos. Me habéis enseñado el valor de ser uno mismo, a ser buena persona y a ser feliz. Aunque estemos lejos, siempre estáis a mi lado. Os quiero mucho.

This thesis concludes with the strongest pillar of my life: **Auriane**. Thank you for being with me throughout these challenging years. I honestly couldn't have done it without you. Our journey together began with our PhDs, and I will miss working with you in the lab and helping each other with our experiments, presentations, and papers. But I'm not worried because I envision a future full of joy and new adventures together. Life is much better by your side, I love you more and I hope we will live together happily ever after.